DEVELOPMENT OF HIGH PERFORMANCE CONCRETE UTILIZING INDIGENOUS INDUSTRIAL WASTE MATERIALS AND NANO-SILICA

BY

ANAS MOHAMMAD IBRAHIM ALKHATIB

A Dissertation Presented to the

DEANSHIP OF GRADUATE STUDIES

KING FAHD UNIVERSITY OF PETROLEUM & MINERALS

DHAHRAN, SAUDI ARABIA

In Partial Fulfillment of the

Requirements for the Degree of

DOCTOR OF PHILOSOPHY

In

CIVIL ENGINEERING

DECEMBER 2018

KING FAHD UNIVERSITY OF PETROLEUM & MINERALS

DHAHRAN- 31261, SAUDI ARABIA

DEANSHIP OF GRADUATE STUDIES

This thesis, written by **ANAS MOHAMMAD IBRAHIM ALKHATIB** under the direction of his thesis advisor and approved by his thesis committee, has been presented and accepted by the Dean of Graduate Studies, in partial fulfillment of the requirements for the degree of **DOCTOR OF PHILOSOPHY IN CIVIL ENGINEERING.**

Dr. Salah U. Al-Dulaijan
(Advisor)

Dr. Mohammed Maslehuddin
(Co-Advisor)

Dr. Shamsad Ahmad
(Member)

Dr. Ahmad S. Al-Gahtani
(Member)

Dr. Ali Algadhib
(Member)

Dr. Salah U. Al-Dulaijan
Department Chairman

Dr. Salam A. Zummo
Dean of Graduate Studies

20/12/14
Date

Dedicated to

My Beloved Parents

My Brothers

My Sisters

My Friends

My Holy Homeland Palestine

ACKNOWLEDGMENTS

In the beginning, I shall thank Allah (Glory be to Him) for giving me patience, good health, and ideas to fulfill the requirements of this study.

Acknowledgments are to my family, friends, and professors those who helped me to achieve the requirements of my thesis work. I want to pay thanks to The King Fahd University of Petroleum & Minerals for giving me the opportunity to achieve my dream through its labs, equipment and staff, and for supporting me through my graduate studies and funding my research.

I would like to thank my advisor Dr. Salah U. Al-Dulaijan for his encouragement, guidance and great efforts. Moreover, I acknowledge my gratitude to Dr. Mohammed Maslehuddin, the co-advisor, for his extensive guidance, insightful comments, immense knowledge, and personal involvement in the experimental work of this study. Thanks to the other committee members Dr. Shamsad Ahmad, Dr. Ahmad Al-Gahtani and Dr. Ali Algadhib for their informative comments and support. Thanks to the Research Institute at King Fahd University of Petroleum & Minerals for supporting this study.

Thanks to the laboratory engineers Eng. Mohammed Shameem, Eng. Omer, Eng. Syed Imran Ali and Eng. Najam for their help during my experimental work. I would like to pay thanks to the faculty members for their support and guidance.

I would like to show my great appreciation to my colleagues at the University for their friendship and support during my graduate studies. Special words of thanks are due to my family for their encouragement and unfailing support during the years of my study.

TABLE OF CONTENTS

LIST OF TABLES

LIST OF FIGURES

LIST OF ABBREVIATIONS

MWCNTs	:	Multi wall carbon nano-tubes
CKD	:	Cement kiln dust
EAFD	:	Electric arc furnace dust
LSP	:	Limestone powder
OA	:	Oil ash
NPZ	:	Natural pozzolan
NT	:	Nano TiO_2
NF	:	Nano Fe_3O_4
NA	:	Nano alumina
NC	:	Nano clay
GGBFS	:	Granulated ground blast furnace dust
SiC	:	Silicon carbide
TiC	:	Titanium carbide
NH	:	Nano hematite
SF	:	Silica fume
HPSCC	:	High performance self-compacted concrete
CSH	:	Calcium silicate hydrate
MS	:	Micro silica
RHA	:	Rice husk ash
SCC	:	Self-compacted concrete
CH	:	Calcium hydroxide
FA	:	Fly ash
SEM	:	Scan electron microscope
PCE	:	Polycarboxylate plasticizer
PP	:	Polypropylene fibre
FESEM	:	Field emission scan electron microscope
NP	:	Nano particles
ASC	:	Alite–sulphoaluminate cement

ABSTRACT

Full Name : ANAS MOHAMMAD IBRAHIM ALKHATIB

Thesis Title : Development of High Performance Concrete Utilizing Indigenous Industrial Waste Materials and Nano-Silica

Major Field : Civil Engineering

Date of Degree : December 2018

The properties of concrete can be enhanced by selecting appropriate quality and quantity of its constituents. Since the invention of concrete, there have been concerted efforts to improve its quality by the use of supplementary cementing materials (SCMs), such as silica fume, fly ash, blast furnace slag, natural pozzolan, etc. However, there also have been efforts to utilize other materials to improve the quality of concrete. Recently, nano-materials have also been used to improve the properties of concrete. The use of nano-materials has been reported to be beneficial in improving the properties of blended cement concretes prepared with the SCMs. Some industrial waste materials (IWMs) have also been used to improve the properties of concrete. The use of IWMs solves the problem of their disposal leading to environmental benefits. Consequently, there is a need to assess the possibility of utilizing IWMs in conjunction with nano-materials in to produce high performance concrete (HPC).

In the reported study, HPC was developed utilizing four IWMs, such as cement kiln dust, electric arc furnace dust, oil ash, and limestone powder, in conjunction with nano-silica (NS). The mechanical properties, durability and microstructure of the developed HPCs were evaluated. Though there was marginal improvement in the mechanical properties and durability of concrete prepared with the selected IWMs, the incorporation of NS in conjunction with the IWMs significantly improved the properties of the developed HPC. Since the selected IWMs and NS were used as partial replacement of cement the developed HPC will culminate in technical, economic and environmental benefits.

ملخص الرسالة

الاسم الكامل: انس محمد ابراهيم الخطيب

عنوان الرسالة: تطوير خرسانة عالية الأداء باستخدام مخلفات المصانع والنانو السيليكا

التخصص: الهندسه المدنيه/انشاءات

تاريخ الدرجة العلمية: كانون اول /2018

يمكن تعزيز خواص الخرسانة من خلال اختيار الكميه والنوعيه المناسبه لمكوناتها. منذ اختراع الخرسانة ، كانت هناك جهود متضافرة لتحسين جودتها باستخدام مواد التكثيف التكميلية (SCMs) ، مثل دخان السيليكا والرماد المتطاير وخبث أفران الصهر والبوزولان الطبيعي ، الخ. ومع ذلك ، هناك أيضًا جهود لاستخدام مواد أخرى لتحسين جودة الخرسانة. في الآونة الأخيرة ، تم استخدام مواد النانو أيضا لتحسين خصائص الخرسانة. وقد أفادت التقارير أن استخدام مواد النانو مفيد في تحسين خواص الخرسانة المحضرة باستخدام SCMs. كما تم استخدام بعض النفايات الصناعية (IWMs) لتحسين خصائص الخرسانة. ان استخدام IWMs يحل مشكلة التخلص منها مما يؤدي إلى العديد من الفوائد البيئية. وبالتالي ، هناك حاجة لدراسة إمكانية استخدام IWMs مع مواد النانو في إنتاج خرسانة عالية الأداء(HPC) .

في الدراسة المذكورة ، تم تطوير HPC باستخدام بعض IWMs ، مثل غبار قمائن الأسمنت ، غبار فرن القوس الكهربائي ، رماد الزيت ، مسحوق الحجر الجيري ، بالتزامن مع nano-silica (NS). تم فحص الخصائص الميكانيكية والديمومه والبنية الدقيقة للخرسانه المطوره. على الرغم من التحسن في الخواص الميكانيكية وديمومه الخرسانة التي تم إعدادها مع IWMs، فإن دمج NS مع IWMs أدى إلى تحسن ملحوظ في خصائص HPC. ان استخدام IWMs و NS كبديل جزئي للأسمنت في HPC المطور سوف يتوج بالفائدة التقنية والاقتصادية والبيئية.

CHAPTER ONE

INTRODUCTION

1.1 General

Concrete is a versatile composite material, which is used in a wide range of structures, such as buildings, dams, bridges, etc. The worldwide use of this material is due to its strength, durability, fire-resistance, and overall its ease of manufacture and low cost. The properties of concrete can be enhanced by selecting appropriate quality and quantity of its constituents. Since the development of concrete, its properties were successfully improved by incorporating several admixtures, notable among them being supplementary cementing materials (SCMs), such as silica fume, fly ash, blast furnace slag, and natural pozzolan.

The SCMs enhance the strength and durability of concrete through filling the micro pores thereby leading to a dense structure [1]. Other materials, such as natural pozzolan that have alumina and silica in their composition react with calcium hydroxide ($Ca(OH)_2$) to produce secondary calcium silicate hydrate (C-S-H) gel which decreases the size of the concrete voids. Decreasing or blocking the micro pores not only enhances the strength but also improves the durability of the concrete by preventing the diffusion of chloride, carbon dioxide, moisture, oxygen and sulfate in the concrete thereby minimizing its deterioration. SCMs affect the properties of fresh concrete, such as workability and setting time [2]. In

general, SCMs cause a reduction in the concrete strength and negatively affect the durability if their quantity exceeds certain quantity. The extra quantity of SCMs will weaken the interfacial zone between the mortar and the aggregates. Also, they increase the water content and decrease the workability. Exceeding a certain ratio of SCMS will produce a low strength concrete which can be used in different non-structural applications, like pavements, blinding concrete, blocks, filling materials, etc., which do not require high strength.

The particle size of SCMs exists in a nano- and a micro-scale. Therefore, the molecular structure of the SCMs can be improved with the use of nanotechnology [3]. In general, nanotechnology refers to the fundamental understanding, manipulation and development of material's nano- and micro-structure and their integration into macro constituent thereby introducing a new functionality. In construction industry, nanotechnology can be used to produce high-performance, durable and cost-effective SCMs. Figure 1.1 shows the particle size distribution and specific surface area of the constituents of concrete, including nano-materials. As is clear from this figure, the use of micro- and nano-materials is important to create a uniform size distribution of the materials such that the resulting concrete is dense and impermeable.

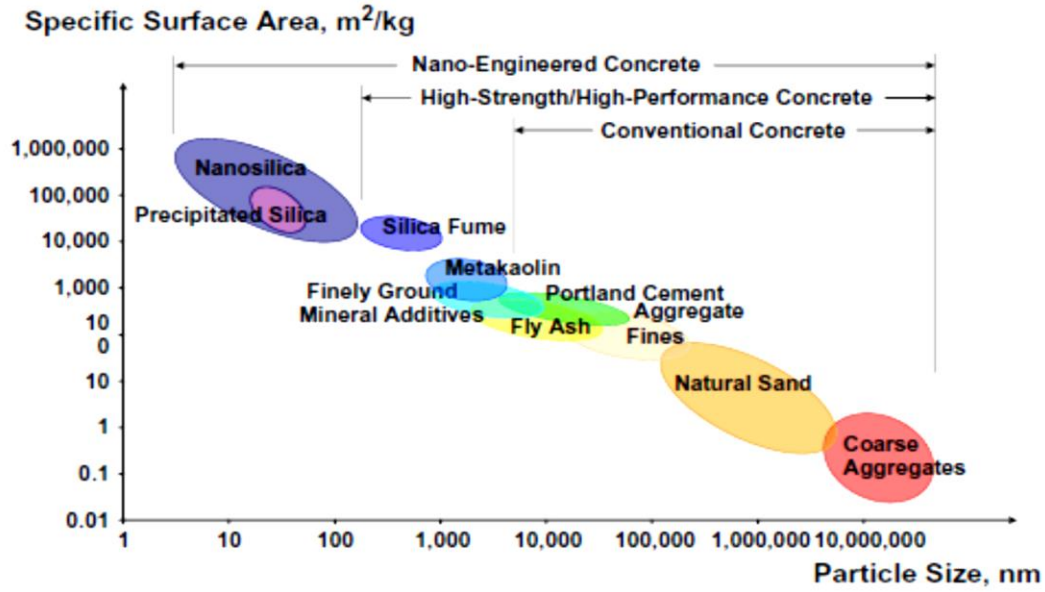

Figure 1.1: Particle size distribution and Specific surface area of concrete materials [4].

Recently, nano materials have been used to improve the mechanical properties and durability of concrete [5]. Nano materials affect the properties of hardened concrete by making its structure dense. A dense structure will delay the diffusion of chloride, carbon dioxide, moisture and sulfate in the concrete thereby minimizing its deterioration. Also, nano materials affect the properties of fresh concrete, such as workability and setting time. Significant research has been conducted on the use of SCMs in concrete. However, limited work has been conducted on the use of nano materials and industrial waste materials in the production of concrete. One of the significant potential advantages of using nano materials in conjunction to IWMs in concrete is the environmental protection leading to sustainable development. Also, it will result in a significant reduction in CO_2 emission by decreasing the need of large quantities of cement production which is a major contributor to the greenhouse gas emission.

One of the most efficient nano materials is nano-silica (NS) which influences the properties of concrete in different ways. It fills the C-S-H gel pores that makes the interfacial zone

stronger and denser. Further, it reacts with $Ca(OH)_2$ to produce stronger and denser C-S-H gel. A uniformly dispersed NS in the cement paste acts as a nucleus to bond with the hydration products. The nucleation effect controls the crystallization by limiting the growth of $Ca(OH)_2$. The growth limitation makes the cement matrix more compact.

In this study, a high performance concrete (HPC) with varying proportions of waste materials, such as cement kiln dust, electric arc furnace dust, oil ash, limestone powder and NS was developed. The mechanical properties, durability characteristics and the microstructure of the developed HPC were evaluated. The developed concrete culminated in economic and environmental benefits, due to the use of industrial waste materials.

1.2 Need of research

SCMs have been used in conjunction with nano materials to produce concrete with high strength and improved durability. However, there is a need to develop HPC with IWMs. A combination of IWMs and nano materials is advisable to enhance the properties of concrete. The development of such a concrete will lead to the following benefits: (i) reduction in the quantity of cement, leading to energy conservation and reduction in the greenhouse gas emission and (ii) resolution of the environmental and cost problems associated with the disposal of IWMs.

1.3 Research objectives

The overall objective of the proposed study was to develop high performance concrete utilizing indigenous industrial waste materials and nano silica. The specific objectives were the following:

i. Assess the mechanical properties of concrete prepared with varying dosages of CKD, EAFD, OA and LSP in conjunction with NS,
ii. Evaluate the durability characteristics of the developed HPC,
iii. Study the morphology and mineralogy of the developed high performance concrete., and
iv. Analyze the reduction in the greenhouse gas emission and predict the service life of the developed high performance concrete.

1.4 Research organization

The dissertation is divided into six distinct chapters. Each of the chapters is focused on a particular issue of the research work. The content in each chapter of this dissertation is as follows:

- Chapter 1 provides a general introduction and summary of the research, significance of work, research objectives and organization of the dissertation.

  1.1 General

  1.2 Need for the research

  1.3 Research objectives

  1.4 Research organization

- Chapter 2 presents a comprehensive literature review on the topic of this study.

  2.1 Description of nano-materials and their use in concrete

  2.2 Effect of nano-materials on fresh properties of concrete

  2.3 Effect of nano-materials on the mechanical properties of concrete

  2.4 Effect of nano-materials on durability of concrete.

  2.5 Effect of nano-materials on concrete micro structure.

- Chapter 3 discusses the details of the experimental work conducted to achieve the research objectives.

  3.1 Materials

  3.2 Concrete mix design

  3.3 Evaluation of macro level properties

  3.3.1 Compressive strength

  3.3.2 Flexural strength

  3.3.3 Shrinkage

  3.3.4 Reinforcement corrosion

  3.3.5 Rapid chloride permeability

  3.3.6 Chloride diffusion

  3.3.7 Sulfate attack

  3.4 Evaluation of micro level properties

  3.4.1 Morphology (SEM)

  3.4.2 Backscattered electron images (BEI)

  3.4.5 X-ray diffraction (XRD)

- Chapter 4 presents the test results and discussion for evaluation of macro and micro level properties of the developed concrete mixtures.
- 4.1 Tests results and discussion of CKD concrete properties
- 4.1.1 Macro properties of CKD concrete
- 4.1.2 Micro properties of CKD concrete
- 4.1.3 Discussion of CKD concrete properties
- 4.2 Tests results and discussion of EAFD concrete properties
- 4.2.1 Macro properties of EAFD concrete
- 4.2.2 Micro properties of EAFD concrete
- 4.2.3 Discussion of EAFD concrete properties
- 4.3Tests results and discussion of LSP concrete properties
- 4.3.1 Macro properties of LSP concrete
- 4.3.2 Micro properties of LSP concrete
- 4.3.3 Discussion the results of LSP concrete properties
- 4.4 Tests results and discussion of OA concrete properties
- 4.4.1 Macro properties of OA concrete
- 4.4.2 Micro properties of OA concrete
- 4.4.3 Discussion the results of OA concrete properties
- 4.5 Comparison between the effects of different IWMs on the properties of developed high performance concrete.
- Chapter 5 presents the reduction in the greenhouse gas emission and predicting the service life of the developed high performance concrete.

- Chapter 6 presents conclusions, recommendations emanating from the study and suggestions for future work.

CHAPTER TWO

LITERATURE REVIEW

2.1 Description of nano-materials and their use in concrete

In general, nanotechnology refers to the fundamental understanding, manipulation and development of material's nano- and micro-structure and their integration into macro constituent thereby introducing a new functionality. Nano technology has concerned substantial interest of researchers in recent years due to the significant role of materials with nanometer size (< 100 nm). The particle size of SCMs exists in a nano- and a micro-scale. Therefore, the molecular structure of the SCMs can be improved with the use of nanotechnology [3].

Concrete is a nano-structure, multi-phase, composite material. It is composed of an amorphous phase, nanometer to micrometer size crystals, and bound water. The amorphous phase, calcium–silicate–hydrate (C–S–H) is the ‘‘glue" that holds concrete together and is in itself a nanomaterial. The size of CSH sheet is less than 2 nm and the space between the sheets vary from 0.5 to 2.5 nm, while CH products are typically large with a width of about 1000 nm. The size of capillary voids range from 10 to 1000 nm. However, in a well hydrated paste with a low water-cement ratio the pore size is typically less than 100 nm. Since the hydration products are in the nano-scale, the enhancement in the concrete properties should be at the nano-scale

In construction industry, nanotechnology can be used to produce high-performance, durable and cost-effective SCMs. Figure 2.1 shows the particle size distribution and specific surface area of the constituents of concrete, including nano-materials. As is clear from this figure, the use of micro- and nano-materials is important to create a uniform size distribution of the materials such that the resulting concrete is dense and impermeable. A dense structure will enhance the mechanical properties of concrete and the durability through retarding the diffusion of aggressive species, such as chloride, sulfate, carbon dioxide, etc. Many researchers studied the effect of nano-particles (NPs) on the properties of concrete [6-8]. It was reported that utilizing NPs in concrete will improve its mechanical properties and durability. The improvement of concrete properties result from the following application of NPs:

- Nucleus-action: the uniformly dispersed NP in the cement paste acts as a nucleus to bond with the hydration products. Due to the high surface area of NP the hydration products will be deposited on the surface of NP during the hydration reaction, forming conglomeration consisting of NP as a nucleus [9].
- Enhance the formation of C-S-H: some nano materials like nano silica can react rapidly with $Ca(OH)_2$ due to its high surface area and produce stronger and denser C-S-H gel. The secondary gel will fill the pores especially in the interfacial transition zone (ITZ) making the cement matrix denser.
- Control the crystallization: if the cement has appropriate content of well dispersed NPs, the crystallization will be controlled by limiting the growth of $Ca(OH)_2$. The growth limitation will make the cement matrix more compact.

- Micro-filling effect: due to the small size of the NPs, they can fill the pores of C-S-H gel making the ITZ strong and dense.

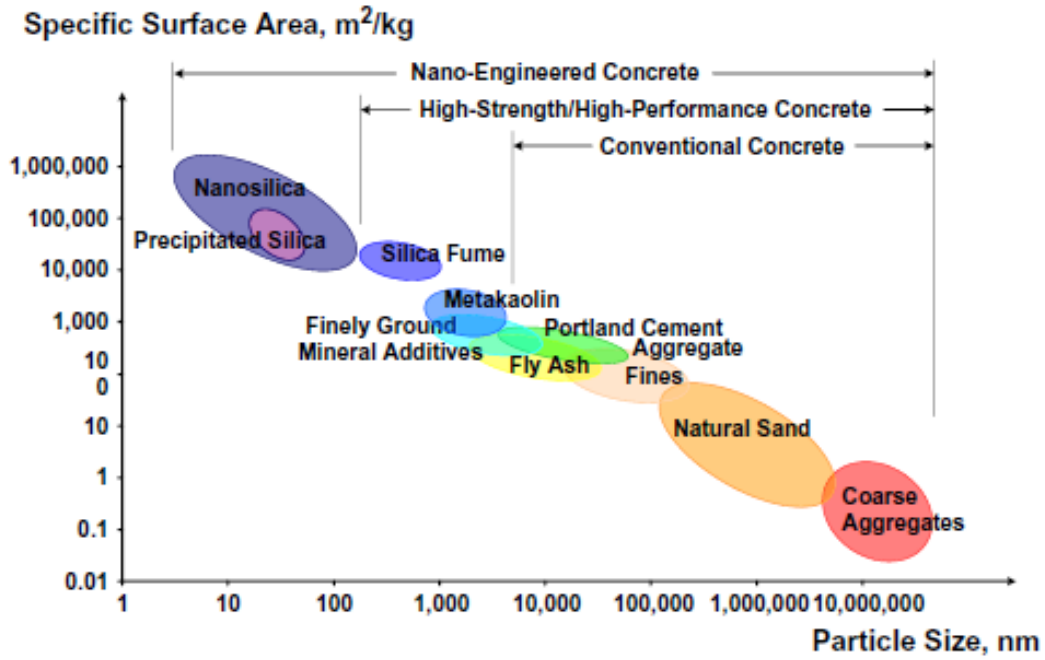

Figure 2.1: Particle size distribution and Specific surface area of concrete materials [4].

2.2 Effect of nano-materials on fresh properties of concrete

The nano-materials affect the fresh properties of concrete. Jayapalan et al. [3] studied the effect of adding micro- and nano-particles of limestone and TiO_2 on the properties of cement paste. The fillers (TiO_2 and limestone) were added to the cement with three different dosages, with different surface areas and with different agglomeration sizes. It was reported that the change in the rate of hydration was related to the size of TiO_2 and limestone particles. The hydration reaction was accelerated by 80, 180, and 280 minutes due to the addition of 10% of T_1, T_2, and T_3 as a partial replacement of cement, respectively, compared with that of the normal paste. The addition of 10% T_3 to the concrete showed the

ultimate rate of reaction and heat of hydration which was attributed to the well dispersed fine particles. The addition of 10% $L_{3,}$ as a partial replacement of cement, accelerated the hydration reaction by 125 min compared with that of normal paste, which was attributed to the dilution effect. A minor effect of limestone L_2 on the heat of hydration, while lime stone L_1 decreased the heat of hydration due to its coarse particle size.

Brghtson et al. [8] studied the workability of concrete prepared with nano-clay (NC). The NC was utilized in the concrete as a partial replacement of cement with a dosages of 0.5, 1, and 1.5%. It was reported that the workability decreased as the dosage of NC increased.

Khotbehsara et al. [10] investigated the properties of self-compacting mortar prepared with fly ash and nano-TiO_2 (NT). The percentages of NT used in the mortar were 1, 2, 3, 4, and 5% as a partial replacement of cement while the fly ash was used with a fixed dosage of 25%. The results showed that the diameter of the slump flow increased due to the addition of NT and the time of the funnel flow decreased. The specimens with 1% and 2% NT had the same flowability compared with the control specimens. The specimen with 5% NT had the lowest V-funnel time and the highest slump flow diameter.

Nazari et al. [11] investigated the setting time of cement paste with nano-TiO_2. The nano-TiO_2 with a size of 15 nm was added to the paste as a partial replacement of cement with different dosages (0.5%, 0.1%, 1.5%, and 2 %) by weight of cement. The results showed that the setting time decreased as the dosage of NT increased (Figure 2.2). The acceleration in the hydration reaction was attributed to the increase in the surface area which made the atoms unstable and active.

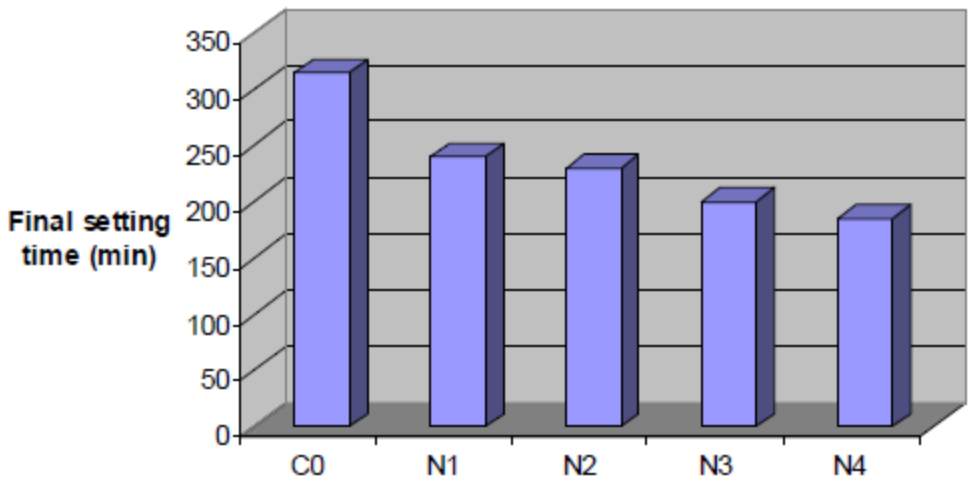

Figure 2.2: Influence of nano-TiO2 particles on the final setting time of cement paste (N1, N2, N3, and N4 are mixes with 1%, 2%, 3%, and 4% NT) [11].

Agarkar et al. [12] studied the workability of concrete with nano-Al_2O_3 particles. Nano Al_2O_3 with size of 15 nm was added to the concrete with four different percentages which were 0.5%, 1%, 1.5 %, and 2 % by weight of cement. The slump results showed that the slump decreased as the dosage of nano-Al_2O_3 was increased. The reduction in the slump was attributed to the high surface area of the nano-Al_2O_3 particles, which adsorb more water on their surfaces.

Hou et al. [13] studied the combined effect of fly ash and colloidal nano-silica (CNS) on the fresh properties of cement-based materials. Two types of fly ash were used in the study with dosages of 20%, 40%, and 60% by mass. Two dosages of CNS were added to the mortar with dosages of 2.25% and 5% by mass of the binder. The results showed that the CNS decreased the initial and final setting time while the fly ash increased the setting time. The effect of CNS on the setting time canceled the effect of fly ash in increasing the setting time. The initial and final sitting time of paste with 5% CNS and 40% fly ash replacement was similar to the plain cement paste. The reduction in the setting time of mortars with

CNS was attributed to the effect of CNS in accelerating the hydration reaction. The viscosity of the mortar with CNS was better than that with fly ash. The viscosity of plain cement paste with 5% CNS was 4.3 times that of 0% CNS, while the viscosity of fly ash cement paste with 5% CNS was 2.5 times that of 0% CNS. The fluidity decreased as the percentage of CNS increased, while the fluidity increased as the percentage of fly ash increased. The reduction in the flowability due to the presence of CNS was attributed to high surface area of CNS that increased the water demand.

Ltifi et al. [14] studied the fresh properties of cement mortar with nano-silica. The nano-silica was added to the mortar as 3 and 10% as a partial replacement of cement. The results showed that the flow time increased rapidly as the percentage of NS was increased. The reduction in the workability was attributed to the high surface area of NS which increased the water demand. Also, the reduction in the slump of NS concrete was due to the high solid to solid contact that resulted from the high volume of the hydration products.

Jalal et al. [15] investigated the effect of micro- and nano-particles of SiO_2 on the fresh properties of high performance self-compacting concrete (HPSCC). It was reported that utilizing NS and MS in the concrete increased the viscosity of the concrete. The visual inspection of the concrete through slump testing did not indicate bleeding and segregation. The workability of mixes with 2% NS was similar to that of normal concrete. However, the workability decreased due to the presence of 10% of MS in concrete. It was also reported that increasing the binder content in the mix increased the fluidity and decreased the segregation of the concrete (Figure 2.3).

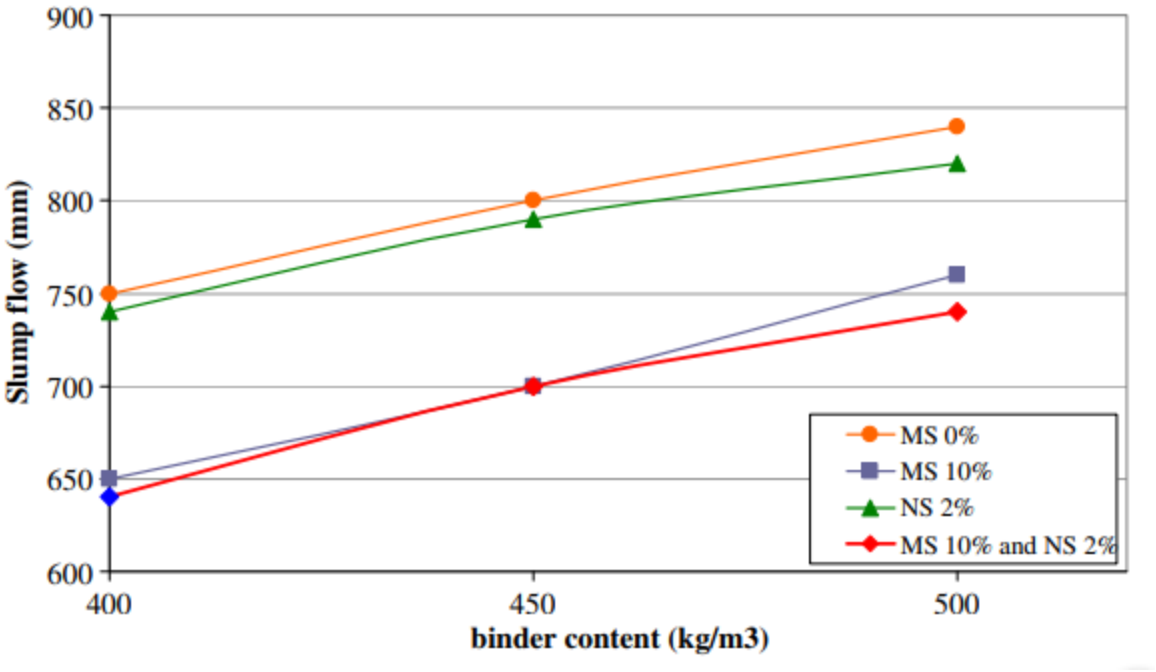

Figure 2.3: Results of slump flow test for different admixtures and binder contents [15].

Said et al. [16] investigated the effect of nano-silica (NS) on the properties of concrete. Fly ash (FA) and NS contents were the main parameters of the study. The results showed that the heat of hydration increased as the percentage of NS increased with or without FA. The ultimate temperature was obtained after about 10 hours of mixing. The early high temperature was due to the fact that the NS acts as a nuclei to the hydration products which accelerated the hydration reaction.

Rong et al. [17] investigated the heat of hydration of ultra-high performance concrete with nano-silica and fly ash. The results indicated that the heat of hydration increased as the dosage of NS increased up to a dosage of 3% NS then it decreased. The increase in the heat of hydration was due to the nucleation effect of NS, and due to the rapid consumption of $Ca(OH)_2$ by NS which has high surface area.

Quercia et al. [18] investigated the effect of nano-silica on fresh properties of self-compacted concrete (SCC). Two types of NS were utilized in the concrete, powder NS and colloidal suspension NS. The results showed that the CNS decreased the flowability, however it was within the flowability limit of SCC. The mixes with NS satisfied the requirement of V-funnel test, while the control mix did not. No segregation and bleeding were noted in any of the mixtures. The air content was high in the NS concrete due to the high surface area of NS. The mix with 3.8% NS showed similar flowability as the control mix.

Lin et al. [19] studied the influence of NS on properties of sludge mortar with fly ash. NS and fly ash were added to the mix with different ratios. The results showed that the consistency increased as the percentage of NS increased, which was due to the high surface area of NS. NS tended to integrate with water at early age of mixing caused by an increase in the consistency. The consistency also increased due to the optimum packing that resulted from the fly ash particles. It was indicated that the sludge/fly ash increased the initial and final setting time; however, the addition of NS decreased the setting time by accelerating the hydration reaction.

Qing et al. [20] investigated the effect of addition of nano-silica (NS) and micro silica (MS) on the properties of cement paste. The results showed that the effect of NS and MS on the setting time and the consistency were not the same. The NS acted as nuclei to the hydration products which accelerated the hydration reaction. Due to the high surface area of NS, the paste became thicker.

El-Baky et al. [21] studied the effect of nano-silica (NS) on the properties of cement-based mortar. The fresh properties of the mortar were measured. NS with size of 19 nm was added

to the cement mortar with a percentages of 1, 2, 3, 5, 7, and 10 % by weight of cement. The results showed that the workability of the cement mortar decreased as the percentage of NS increased up to a dosage of 7% NS then it started to increase. The reduction in the workability was due to the high surface area of NS which increased the water demand, while the increase in the workability of mixes with more than 7% NS was due to the lubrication effect of the unreacted NS.

Veerendrakumar et al. [22] investigated the properties of self-compacted mortar with high quantity of fly ash and NS. The dosages of NS were started from 0% up to 5 wt. % as a partial replacement of cement while the dosage of fly ash was 70%. The results showed that the NS negatively affected the workability of the mix due to its high surface area, therefore, superplasticizer was added to enhance the workability.

Najigivi et al. [23] studied the influence of two types of NS (N and M) with different ratios on the workability of concrete which was cured in two different curing media (water curing and lime solution curing). The results showed that the workability decreased as the percentage of both types of nano-particles increased. The reduction in the workability was due to the adsorption of water by NS which decreased the volume between the particles caused by high internal friction.

Fernández et al. [24] studied the individual and combined effect of nano-silica (NS) and polycarboxylate-ether (PCE) plasticizer on the fresh and hardened properties of lime mortars. The parameters of the study were the binder/aggregate ratio and the water/lime ratio. The results showed that the presence of NS increased the water demand of the mortar. The setting time was variably changed due to the presence of NS. In some mixes NS retards the setting time, while the addition of PCE accelerated the setting time.

2.3 Effect of nano-materials on the mechanical properties of concrete

Morsy et al. [25] investigated the mechanical properties of cement mortars with nano-clay and multi-wall carbon nanotubes (MWCNTs). The ratios of carbon nanotube were 0.005, 0.02, 0.05 and 0.1 wt. % of cement, while the ratio of nano-metakaolin was 6% by weight of cement. It was reported that the compressive strength increased as the percentage of MWCNTs increased up to 0.02% then it started to decrease (Figure 2.4). The increase in strength was attributed to the bond between the MWCNTs and the hydration products which acted against the micro cracks development. At higher ratios, MWCNTs agglomerated around the cement particles caused incomplete hydration which resulted in uncoated fibers. The uncoated fibers tended to slip causing micro cracks which caused a reduction in the compression strength. The compressive strength increased by 18% compared with the control mix due to the addition of nano-clay. The enhancement in the strength of nano-clay concrete was attributed to two strength mechanisms, first mechanism was void filling which resulted in a dense structure and the second mechanism was the formation of secondary C-S-H gel due to the pozzolanic reaction between the silica and calcium hydroxide.

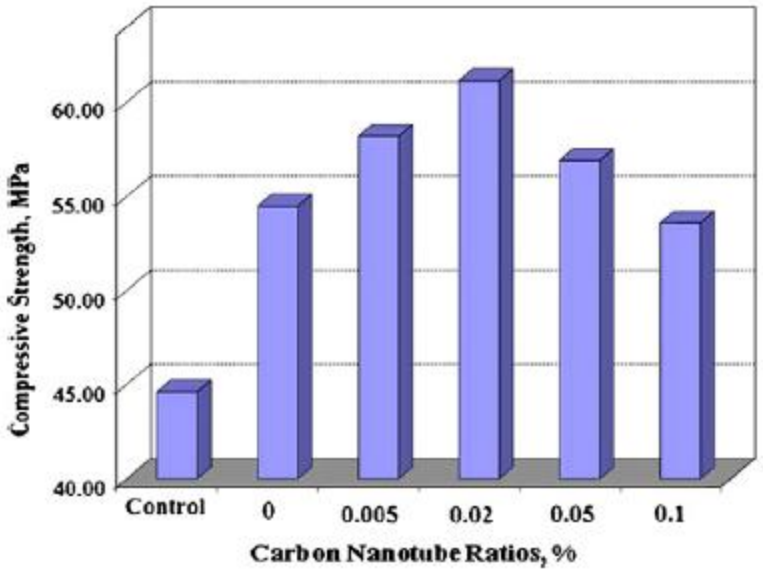

Figure 2.4: Compressive strength of blended cement mortar with CNTs after 28 days of curing [25].

Morsy et al. [6] studied the properties of cement mortar with nano-clay (NMK). The ratios of NMK were 0, 2, 4, 6, and 8% as a partial replacement of cement. The NMK was thermally treated for 2 hours at 750 □C in order to enhance its reactivity. The results showed that the compressive and tensile strength increased as the percentage of NMK was increased (Figure 2.5). When 8% of Portland cement was replaced with NMK, the compressive strength increased by 7% while the tensile strength increased by 49%. The enhancement in the strength was attributed to the filling action of NMK and the presence of secondary C-S-H gel from the pozzolanic reaction that resulted in a dense structure.

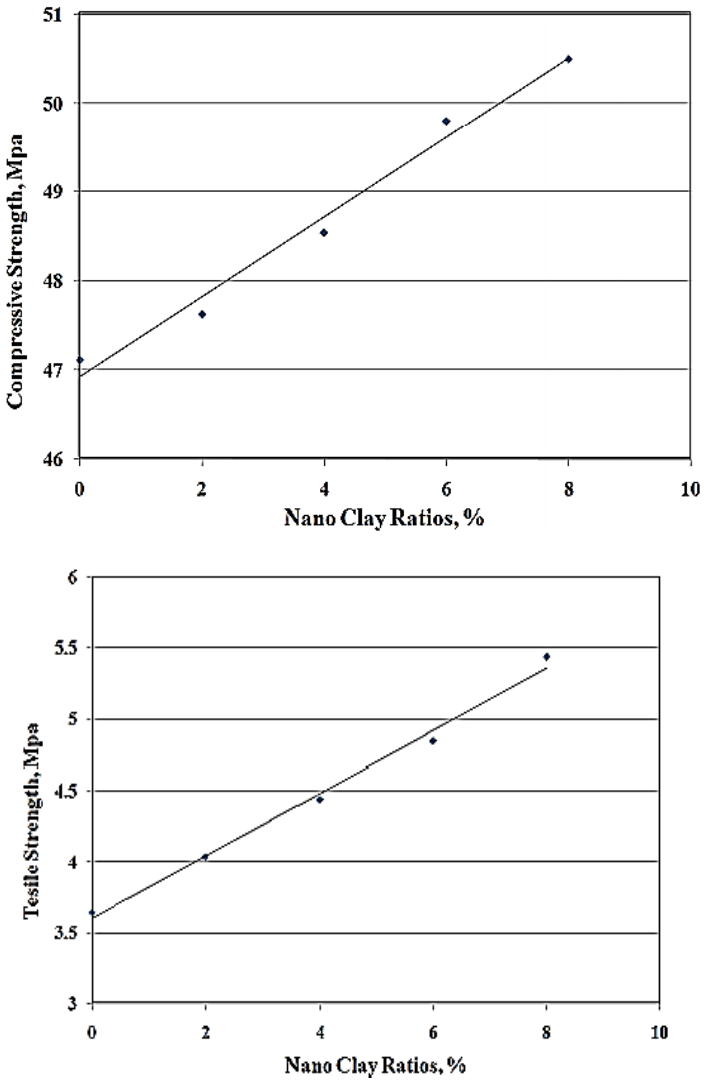

Figure 2.5: Compressive and tensile strength of NMK mortar hydrated for 28 days [6].

Shekari and Razzaghi [7] investigated the mechanical properties of high performance concrete with nanoparticles. Nano-ZrO_2 (NZ), Nano-Fe_3O_4 (NF), Nano-TiO_2 (NT) and Nano-Al_2O_3 (NA) were added to the mix as a partial replacement of cement with a constant ratio of 1.5%. Metakaolin was added to every mix with a percentage of 15% by weight of the cementitious material. The results showed that the compressive and the tensile strengths increased due to the use of nanoparticles in the concrete. The effect of NA in enhancing

the compressive strength was more than that of other nano-particles. The ultimate splitting tensile strength was noted in mixes with NA and NF particles.

Berghtson et al. [8] studied the influence of nano-clay on the mechanical properties of concrete. The nano-clay was used as a partial replacement of Portland cement with dosages of 0.5, 1, and 1.5%. The results showed that the compressive, tensile, and flexural strength increased as the nano-clay dosage was increased. The ductility of the nano-clay concrete improved compared with that of the control concrete.

Mohamed [26] studied the mechanical properties of concrete at different ages with nanoparticles. Nanoclay (NC) and nanosilica (NS) were used in the mix with different combinations and different percentages. The results showed that the enhancement in the compressive strength due to the addition of 0.75 % and 0.5 % NS at 28-days were 8.7% and 24.4%, respectively. The improvement was attributed to the pozzolanic reaction which produced more CSH gel and consumed more CH which is arrayed on the interfacial zone, and to the filling action that resulted in a dense structure. The 28-days flexural strength increased by 8.6 % due to the addition of 0.5% or 0.75% NS as a partial replacement of cement. The compressive and flexural strengths were increased as the percentage of the NS increased up to 0.75% then it started to decrease gradually. That was attributed to the agglomeration phenomenon that resulted in a non-uniform dispersion. The 28-day compressive strength increased due to utilizing 1% and 3% NC by 11.9 % and 47.1 %, respectively. The increase was due to the physical action of NC which resulted in a dense interfacial zone. The flexural strength was slightly improved due to the addition of NC, it improved by 8 % at 90 days. The combined effect of NS and NC on the mechanical properties of concrete was better than their individual effects. At 28- days, the compressive

strength of the concrete with 3 % nano-particles (0.75 NS and 0.25 NC) was more than that of the control mix and the NC mix by 56 % and 6.4 %, respectively.

Kinnaresh [27] studied the compressive strength of cement mortar with nano-clay (NC). NC was added to the mix as 1% and 2% replacement of cement. The results showed that the compressive strength increased as the percentage of NC increased. The increase in the 28-days compressive strength due to the addition of 1% and 2% NC were 310% and 200%, respectively.

Oltulu et al. [28] investigated the effect of nano-silica (NS), nano-Al_2O_3 (NA), and nano-Fe_2O_3 (NF) on the capillary pores and the compressive strength of mortars with fly ash (F). The dosages of the supplementary cementing materials were 0.5, 1.2, and 2.5% by weight of the binder. The results showed that the highest compressive strength was obtained when the nano-particles were added to the mix individually with a ratio of 1.25% by weight of the binder. The highest strength of binary concrete was obtained when both NS and NA added to the cement with a ratio of 1.25% by weight of the binder. The compressive strength of the binary concrete increased with age, the highest rate of strength development was at 28 days. The highest compressive strength of the ternary concrete was when NS, NA, and NF were added to the mix together with a ratio of 1.25%. The capillary pores decreased due to the addition of nano-particles.

Khotbehsara et al. [10] investigated the properties of self-compacting mortar with fly ash and nano-TiO_2 (NT). The percentages of NT were 1, 2, 3, 4, and 5% by weight of cement, as a partial replacement of cement while the fly ash was used with a fixed dosage of 25%. The results showed that the compressive strength increased as the percentage of NT was increased, the ultimate enhancement was 17% for specimen with 5 wt. % NT. The

enhancement in strength was attributed to the proper dispersion of the NT particles that restricted the growth of $Ca(OH)_2$ crystals which made the microstructure more compact and homogeneous.

Nazari et al. [11] investigated the flexural and the splitting tensile strength of cement paste with nano-TiO_2. Nano-TiO_2 measuring 15 nm was added to the cement with four different dosages of 0.5%, 1.0%, 1.5%, and 2 %, by weight of cement. The results showed that the split tensile and flexural strengths were increased due to the addition of NT up to a dosage of 2 % then it started to decrease. The reduction in the strength was attributed to the leaching of the extra silica that did not react with $Ca(OH)_2$. The reduction in the strength also was attributed to the bad dispersion of the NT particles.

Salami et al. [29] investigated the compressive strength of concrete with different nano particles. The nano-TiO_2 (NTC), nano-Fe_2O_3 (NFC), nano-Al_2O_3 (NAC), and nano-ZnO_2 (NZC) were added to the concrete with a percentage of 2% by weight of cement. The results showed that the compressive strength enhanced due to the addition of the nano-oxides while the ultimate enhancement in strength was 22.7% in concrete with 2% nano-TiO_2. The enhancement in the strength was attributed to the nucleation effect of the nano-particles which enhanced the hydration reaction, and also due to the filling action which resulted in a more compact structure.

Nazari et al. [30] investigated the strength of self-compacted concrete (SCC) with ground granulated blast furnace slag (GGBFS) and nano-Al_2O_3 particles. GGBFS was added to the mix with dosages of 15%, 30%, 45%, and 60% by weight of cement while the dosages of nano-Al_2O_3 particles was 1%, 2%, 3%, and 4% by weight of cement. The results showed that utilizing GGBFS in the mix enhanced the compressive, split tensile, and flexural

strengths up to a dosage of 45%, then the strength started to decrease. The reduction in strength was due to the reduction of CaO which was produced from GGBFS. The reduction in the quantity of CaO reduced $Ca(OH)_2$ and also the CSH gel. The compressive strength of the nano-concrete increased as the ratio of the nano-material increased up to a dosage of 3% then the strength started to decrease. The reduction in strength was due to the reduction in the quantity of lime that resulted in excess silica and also due to the improper dispersion of the nano-particles.

Mahawish et al. [31] studied the effect of silicon carbide (SiC) nano-particles and titanium carbide (TiC) nano particles on the properties of cement paste. Both types of nano-particles with size of 20 nm were added to the paste with six different dosages which were 1, 2, 3, 4, 5, and 6 wt. %. It was reported that the compressive, flexural, and the tensile strength of all specimens with nano-particles at all ages were more than that of the control specimens. The enhancement in strength was due to the filling action of the nano-particles that produced a compact structure. Also, the nano-particles accelerated the formation of C_3S, C_2S, and CH into C-S-H gel. The ultimate flexural and tensile strength was obtained in specimens with 5 wt % of nano-particles. The reduction in the compressive and flexural strength of the mortar with 6 wt% nano particles was related to the reduction in the quantity of lime which was not enough to react with the available nano-particles that resulted in free silica. The excess silica will leach out causing a reduction in the strength. The effect of TiC in enhancing the compressive strength was better than that of SiC that was due to the small particle size of SiC. The tensile strength increased as the quantity of nano-particles was increased.

Cao et al. [32] studied the quantity of leached uranium and sodium salts from cementitious paste with nano-hematite (NH) particles, and also they investigated the effect of NH particles on the physical properties of the cement mortar. The dosages of NH used were 1%, 2%, and 3% by weight of cement. The results showed that the compressive strength increased and the leaching decreased due to the addition of NH. The optimum physico-chemical and mechanical properties were obtained due to the addition of 1 wt. % NH. The presence of NH affected the degree and the rate of hydration which decreased the porosity and the permeability of the concrete. The reduction in uranium leaching was attributed to two mechanisms; first mechanism was due to the adsorption of uranium on the NH particles, while the second mechanism was due to the reduction of the transferred uranium through the dense structure.

Agarkar et al. [12] studied the compressive strength of concrete prepared with nano-Al_2O_3 particles. Nano-Al_2O_3 with particle size of 15 nm was added to the concrete with four different percentages, such as 0.5%, 1%, 1.5 %, and 2 %, by weight of cement. The results showed that the compressive strength increased as the dosage of nano-Al_2O_3 was increased up to a dosage of 1% then it started to decrease, although the strength of all specimens with nano-materials was more than that of the control specimen. The reduction in strength was due to the fact that the quantity of the available lime was less than the available nano-Al_2O_3, so an excess silica will not combine with lime. The excess silica will leach out causing a reduction in strength. Also, the reduction in strength may be attributed to the bad dispersion of the nano-Al_2O_3 particles. The enhancement in the strength was due to the filling action of the nano-Al_2O_3 particles that densified the concrete structure. Also, nano-

Al_2O_3 particles accelerated the hydration reaction which resulted in a rapid consumption of $Ca(OH)_2$.

Pathak et al. [33] studied the effect of nano-ZnO particles on the compressive strength of concrete. The ZnO-nano particles with size of 60 nm was partially replaced the cement content in three different dosages (0.5 %, 1 %, and 1.5 % wt.). The compressive strength increased due to the addition of nano-ZnO particles. The ultimate strength was increased by 18% when cement was replaced with 1 wt. % nano-ZnO. The nano-particles filled the pores that increased the density of the structure.

Hosseini et al. [34] studied the mechanical properties of ferrocement mortar. The parameters of the study were the ratios of nano-silica (NS) as a partial replacement of cement, the water to binder ratio, and the sand to binder ratio. The results showed that the compressive and flexural strengths improved as the percentage of nano-silica increased. The enhancement in the strength was due to the nucleation effect and filling action of NS. NS also reacted rapidly with $Ca(OH)_2$ and produced more CSH gel. The uniform dispersion of NS controlled the growth of $Ca(OH)_2$ crystals that resulted in a more uniform and dense structure.

Jo et al. [35] investigated the properties of cement mortars with nano-silica (NS). The dosages of NS were 3%, 6%, 10%, and 12% by weight of cement and the dosages of silica fume (SF) were 5%, 10% and 15% by weight of cement. The results showed that the compressive strength increased as the percentage of silica particles was increased. The enhancement in the strength was attributed to the pozzolanic reaction and the filling action of NS. The effect of NS in enhancing the properties of mortars was better than that of silica fume, which was due to its small particle size.

Ltifi et al. [14] studied the hardened properties of cement mortars with nano-silica. Nano-silica was added to the mortar as 3 and 10% partial replacement of cement. The results showed that the compressive strength increased as the NS content was increased. The enhancement in the strength was attributed to the production of secondary C-S-H gel from the pozzolanic reaction, and to the physical action of NS in filling the voids which produced a dense structure.

Saloma et al. [36] investigated the mechanical properties of concrete with nano-silica (NS). NS was added as a partial replacement of cement with dosages of 2.5%, 5%, 7%, and 10%, by weight of cement. The results indicated that the compressive strength increased as the percentage of NS was increased. The increase in the compressive strength at later ages was more than that at early ages, which can be attributed to the fact that the initial hydration reaction occurred between the cement and water only, while at later ages NS reacted with the free lime to produce secondary C-S-H gel. The modulus of elasticity enhanced due to the presence of NS in the paste. The reason of the high stiffness of the NS concrete was due to its dense structure and also due to the strong bond between the aggregate and the paste. The tensile strength increased as the percentage of NS increased.

Ozyildirim and Zegetosky [37] investigated the effect of nano-materials on the concrete strength. Nano-silica (NS), nano-clay (NC), silica fume, fly ash and slag were added to the cement in different ratios. The results showed that the compressive strength and the modulus of elasticity increased due to the addition of the nano-materials, the highest compressive strength was obtained in specimens with NS. Some types of NS had negative effect on the concrete performance.

Jalal et al. [15] investigated the effect of micro- and nano-particles of SiO_2 on the strength of high performance self-compacting concrete (HPSCC). The results showed that the compressive and tensile strength increased due to the presence of NS and MS in the concrete. The highest compressive strength was noted for ternary mixture (2% NS plus 10% MS). In the binary mixes, the concrete strength with 2% NS was more than that of concrete with 10% MS. The strength increased as the binder content was increased. The increase in the strength was attributed to the filling action and to the pozzolanic reaction of both NS and MS.

Nasution et al. [38] studied the effect of utilizing nano-silica (NS) as a partial replacement of cement on the mechanical properties of concrete. The results showed that the compressive strength improved due to the presence of NS in concrete. The improvement in the concrete properties was due to the consumption of $Ca(OH)_2$ in the pozzolanic reaction, the formation of secondary C-S-H gel, and due to the filling action of NS.

Nazari et al. [39] investigated the influence of nano-silica (NS) on the mechanical properties of high strength self-compacting concrete. The ratios of NS were 1%, 2%, 3%, 4%, and 5% by weight of cement. The results showed that the compressive strength, flexural strength, and tensile strength improved as the percentage of NS increased up to a dosage of 4 wt. % then, the strength decreased. Although, the strength of specimens with 5% NS was more than that of other specimens (except the specimens with 4% NS). The reduction in strength was due to the fact that the NS dosage was more than the available lime during the hydration process, which resulted in free silica. The free silica leached out causing a reduction in the strength. The high strength was related to the quick formation of

$Ca(OH)_2$ during the hydration reaction which reacted with the silica to produce secondary C-S-H gel. Further, the NS filled the pores and made the structure compact.

Said et al. [16] investigated the effect of NS on the properties of concrete. Fly ash (FA) and NS contents were the main parameters of the study. The results showed that the compressive and tensile strength of the concrete with and without fly ash increased as the percentage of NS was increased. The enhancement in the strength was attributed to the pozzolanic reaction and filling action of NS, which enhanced the density of the structure.

Sobolev et al. [40] investigated the mechanical properties of mortars with NS. The results indicated that the compressive strength improved during the early ages while it was negatively affected at later ages. The agglomeration of NS was the main reason for the reduction in strength, therefore; superplasticizers were added to enhance the strength. The compressive strength of concrete with NS and effective superplasticizer, enhanced by 20%. The performance of thermally treated NS was enhanced using ultra-sonification.

Rong et al. [17] investigated the mechanical properties of ultra-high performance concrete with nano silica and fly ash. Three dosages of NS were used in the mix (1%, 3%, and 5%) while the dosage of fly ash was 35%. Both NS and fly ash were used in the mix as a partial replacement of cement. The results indicated that the compressive strength and the flexural strength increased as the content of NS increased up to a dosage of 3%, then the mechanical properties slightly reduced. However the strength of specimens with 5% NS was more than that of specimens with fly ash only. The improvement in strength was attributed to the pozzolanic reaction. Also, NS acted as a nuclei of the hydration products. The strength of concrete with 5% NS decreased due to the agglomeration of NS particles. The agglomeration occurred due the high surface area of the NS.

Du et al. [41] studied the mechanical properties of concrete with nano-silica. The dosages of NS were 0.3% and 0.9% by weight of cement. The results showed that the compressive strength increased as the percentage of NS increased. The enhancement in the compressive strength of 0.3% NS and 0.9% NS specimens was 9% and 12%, respectively. The improvement in the strength was attributed to the effect of NS in refining the pore structure. Also, the enhancement was due to the pozzolanic reaction, which is the reaction between NS and $Ca(OH)_2$ to produce secondary C-S-H gel. The secondary C-S-H gel refined the structure and made it more dense and homogeneous.

Zahedi et al. [42] investigated the effect of nano-silica and rice husk ash (RHA) on the mechanical properties of cement mortars. The results showed that NS has significant effect on the performance of mortar while the RHA lowered the mortar strength at early ages. At later ages, RHA slightly enhanced the strength. The presence of both RHA and NS in the mix decreased the early age strength compared with that of NS concrete, while at later ages the strength was enhanced. The enhancement in the strength was attributed to the pozzolanic reaction and filling action of NS.

Beigi et al. [43] studied the effect of nano-silica on the concrete properties. The concrete was reinforced with different types of fibers, including steel, polypropylene, and glass fiber. The contents of NS were 2%, 4%, and 6% by weight of cement. The results showed that the mechanical properties enhanced as the dosage of NS increased up to a dosage of 4% then it started to decrease due to the agglomeration of the NS particles. The agglomeration resulted from the high surface area of the nano-particles. The increase in the strength was due to the pozzolanic reaction and the filling action of NS.

Quercia et al. [18] investigated the effect on nano-silica on self-compacted concrete (SCC). Two types of NS were utilized in the mix, powder-NS and colloidal suspension-NS. The results showed that the one-day strength was higher for the control specimen, while the strength of the powder-NS specimens was the lowest. At later ages, the highest compressive strength was for colloidal-NS concrete while the highest splitting tensile strength was for powder-NS concrete.

Jorge et al. [44] investigated the properties of Portland cement mortar with NS. The NS was added to the mix with percentages of 0%, 1%, 3%, 5%, and 10% as a partial replacement of cement. The results showed that the compressive strength increased as the percentage of NS increased. The 28-days compressive strength of 10% NS concrete enhanced by 80%. The enhancement in the strength was due to the filling action of the NS of the fine pores, and to the pozzolanic reaction which reduced the CH quantity and increased the secondary C-S-H gel.

Qing et al. [20] investigated the effect of nano-silica (NS) and micro-silica (MS) on the properties of cement paste. The results showed that the compressive strength increased as the percentage of NS and MS increased. The bond and the compressive strengths were higher in specimens with NS. The enhancement in strength was attributed to the filling action and to the pozzolanic reaction of NS. The strength of NS specimens was more than that of MS specimens, which was due to the better role of NS in the pozzolanic reaction and in filling the pores.

Rahel et al. [45] investigated the influence of high temperature on mortar with fly ash (FA) and nano-silica (NS). The main objective of the study was to produce high residual strength mortar after exposing the mortar to a temperature of 400 ˚C and 700 ˚C. The results showed

that high residual strength mortar was produced due to the addition of NS and FA. Up to 400 ˚C the cement-based materials showed stable microstructure, while after 400 ˚C dehydration occurred. X-ray diffractograms indicated that a reaction occurred between silica from the NS and the calcium silicate from calcium silicate hydrate which resulted in a new binder that caused high residual strength.

El-Baky et al. [21] studied the effect of nano-silica (NS) on the properties of cement-based mortar. NS with a size of 19 nm was added to the cement mortar with a percentages of 1, 2, 3, 5, 7, and 10% by weight of cement. The results showed that the compressive and the flexural strength increased as the quantity of NS was increased. The optimum dosage of NS in enhancing the compressive and flexural strength was 7 %. The scanning electron micrographs indicated that the enhancement in the strength was due to the reaction of NS with calcium hydroxide which resulted in the production of secondary CSH gel, the pores filled and the interfacial transition zone refined.

Elboghdadi et al. [46] studied the hardened properties of concrete with nano-silica (NS) and steel fibers (SF). The utilized dosages of NS were 1, 1.5, 2, and 4 wt. %, as a partial replacement of cement, while the SF was added as a volume substitution with a percentages of 0.45, 0.9, and 1.35%. The results showed that the compressive strength improved due to the addition of NS up to 2 wt. %, then it decreased due to the presence of agglomerated nano-particles. Adding 2 wt. % NS and 0.9 wt. % SF improved the modulus of elasticity by 94%. Utilizing 2 wt. % NS and 1.35% SF enhanced the flexural strength by 87.7% compared with the control specimen.

Veerendrakumar et al. [22] investigated the properties of self-compacted mortar with high quantity of fly ash and NS. The dosages of NS were started from 0 % up to 5 wt. % as a

partial replacement of cement with 70% fly ash. The results showed that the compressive strength of concrete with 5 wt. % NS and 70 % fly ash improved by 94 % compared with the mix with 70 % fly ash without NS. The enhancement in the strength was attributed to the pozzolanic reaction and filling action of NS.

Najigivi et al. [23] studied the influence of two types of NS (N and M) with different ratios on the compressive strength of concrete cured in two different curing media (water-curing and lime solution-curing). The compressive strength of concrete cured with water increased as the percentage of type N nano-particles increased up to a dosage of 1 wt. % then it started to decrease. The reduction in strength was due to the reduction in the lime quantity which resulted in excess silica. The strength reduction also resulted from the improper dispersion of the nano-particles. The enhancement in the strength was due to the consumption of CH in the pozzolanic reaction which is normally located at the interfacial zone between the mortar and the aggregate. Further, NS physically filled the pores within the structure. The ultimate compressive strength of concrete cured with lime solution was at replacement of 2 wt. % for both types of NS.

Abreu et al. [47] studied the influence of nano-silica (NS) on the mechanical properties of high performance concrete. Three different samples were prepared, a control sample, one with NS, and the other one with both micro- and nano-silica. The results revealed that the compressive strength and the modulus of elasticity increased due to the addition of NS. The ultimate results obtained when both nano- and micro-silica combined together, which was attributed to the reaction of silica with $Ca(OH)_2$ to produce extra gel and the physical effect of NS which resulted in optimum packing. The SEM results showed that the micro

structure of concrete with NS became finer and denser which agreed with the enhancement in the strength.

Fernández et al. [24] studied the individual and combined effect of the addition of nanosilica (NS) and polycarboxylate-ether (PCE) plasticizer on the fresh and hardened properties of lime mortars. The parameters of the study were the binder / aggregate ratio and the water / lime ratio. The results showed that the mechanical strength of lime mortar significantly enhanced due to the addition of NS. The enhancement resulted from the filling action of NS and the production of the secondary C-S-H gel from the pozzolanic reaction. The optimum mechanical properties were obtained when both NS and PCE were added to the mortar.

2.4 Effect of nano-materials on durability of concrete

Shekari and Razzaghi [7] investigated the durability of high performance concrete with nano-particles. Nano-ZrO_2 (NZ), Nano-Fe_3O_4 (NF), Nano-TiO_2 (NT) and Nano-Al_2O_3 (NA) were added to the concrete as a partial replacement of cement with a constant ratio of 1.5%. Metakaolin was added to the concrete with a percentage of 15% by weight of the cementitious material. The results showed that the water absorption and the chloride permeability decreased due to the addition of nanoparticles. The values of the water absorption in the specimens with nanoparticles were about 0.4 of water absorption in the control specimen (Figure 2.6). The chloride penetration reduced due to the addition of the nano particles (Figure 2.7). The reduction in the chloride permeability was in the range of 20 to 80% depending on the type of nano-material used.

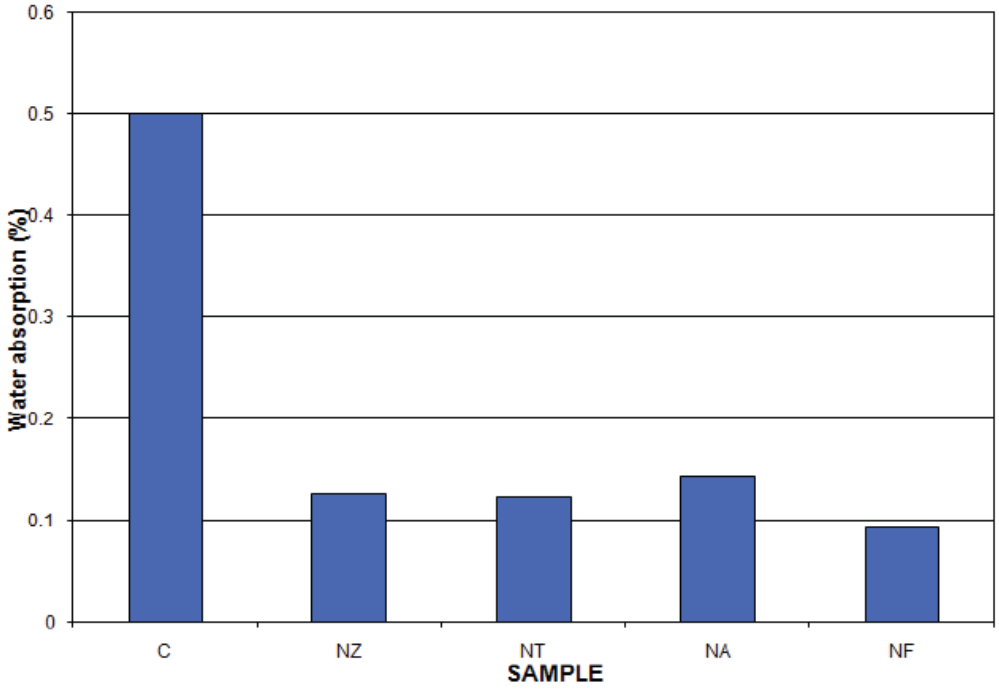

Figure 2.6: Water absorption of specimens [7].

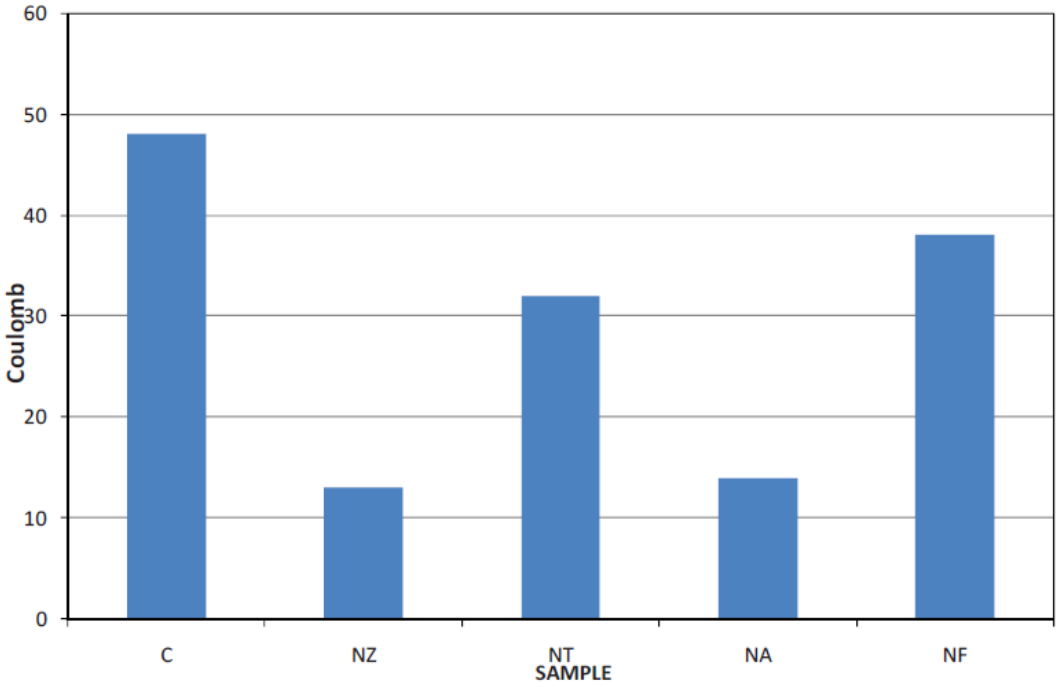

Figure 2.7: Chloride penetration in tested specimens [7].

Patel et al. [27] studied the permeability of cement mortar with nano-clay (NC). NC was added to the concrete with dosages of 1% and 2% by weight of cement. The results showed that the coefficient of permeability of the mortar specimens with 1% and 2% NC was 150% and 200%, respectively, more than that of the control specimen.

He and Shi [48] investigated the chloride permeability of cement mortar with different nano materials, such as Fe_2O_3, Al_2O_3, TiO_2, SiO_2 and nano-clays. The nanoparticles were added to the mortar with a ratio of 1% by weight of cement. The results of the electro-migration test reported that the chloride penetration resistance of the mortar improved due to the incorporation of the nano-materials. The significant enhancement was due to the use of NS and NC in the concrete. The effect of nano-materials in decreasing the chloride penetration was in the order of Clay-ho > Clay-hi >SiO_2 > TiO_2 > Al_2O_3 > Fe_2O_3, which represents the order of the surface area of these materials.

Zhang and Li [49] investigated the pore size and the chloride permeability of concrete with nanoparticles. The main parameters of the study were the content of TiO_2 and SiO_2 nano particles, and the quantity of polypropylene fiber (PP). The results showed that the micro structure of concrete was refined due to the addition of NS which decreased the chloride permeability. The effect of TiO_2-nanoparticle on the chloride permeability and pore size was better than the effect of same content of NS. The PP fibers reduced the chloride permeability and coarsened the microstructure. The combination of PP fibers and nano-TiO_2 negatively affected the chloride permeability and the pore size became coarser than that of concrete with PP fibers only.

Khotbehsara et al. [10] investigated the properties of self-compacting mortar with fly ash and nano-TiO_2 (NT). The percentages of NT used in the mortar were 1, 2, 3, 4, and 5% by

weight of cement as a partial replacement of cement content while the fly ash was used with a fixed dosage of 25%. The results showed that the water absorption decreased as the dosage of NT was increased. Minimum water absorption was measured in specimens with 4% NT. A marginal increase in the water absorption was noted in specimens with 5% NT which was attributed to the improper dispersion of the NT particles. The reduction in the water absorption due to the use of NT in the concrete was attributed to the dense microstructure that resulted from the physical action of NT in filling the voids. The electrical resistivity increased as the percentage of NT was increased, the optimum dosage of NT was 4%. It was reported that corrosion will not occur in specimens with 4% and 5% NT, while in the specimens with 1%, 2%, and 3% NT the corrosion rate ranged from low to moderate. The increase in the electrical resistivity was attributed to the compact structure of the cement paste. The chloride permeability decreased as the percentage of NT was increased. The chloride permeability of the NT concrete specimens was classified as low.

Salami et al. [29] investigated the water absorption of concrete with different nano materials. Nano-TiO_2 (NTC), nano-Fe_2O_3 (NFC), nano-Al_2O_3 (NAC), and nano-ZnO_2 (NZC) were added to the concrete with a percentage of 2% by weight of cement. The results showed that the water absorption decreased due to the addition of nano-materials. The reduction in the water absorption was due to the filling action of the nano-materials which resulted in a more dense structure.

Nazari et al. [30] investigated the water absorption of self-compacted concrete (SCC) with ground granulated blast furnace slag (GGBFS) and nano-Al_2O_3 particles. The GGBFS was added to the mix with different dosages (15%, 30%, 45%, and 60%) by weight of cement while the dosages of nano-Al_2O_3 particles were 1%, 2%, 3%, and 4% by weight of cement.

The results showed that the water absorption of the specimens with GGBFS increased as the quantity of GGBFS increased at the early ages, then at later ages it decreased. The water absorption of NGGBFS concrete after seven days was more than that of concrete with GGBFS only, while it was less at later ages. That was due to the fact that the hydration reaction for specimens with nano-particles became fast at early ages, so it needs more water. At later ages the structure became dense and the permeability decreased.

Mahawish et al. [31] studied the effect of silicon carbide (SiC) nano-particles and titanium carbide (TiC) nano-particles on the properties of cement paste. Both types of nano-particles with size of 20 nm were added to the paste with six different dosages which were 1, 2, 3, 4, 5, and 6 wt. %. The results showed that the water absorption of specimens with nano-materials was less than that of control specimens. The best enhancement in the water absorption was noted in specimens with 5% nano-material. The enhancement of the water absorption was due to the presence of nano-particles with high fineness, which blocked the pores within the matrix. At different replacement dosages and curing ages, the effect of SiC in enhancing the water absorption was better than that of TiC, because the particles of SiC were finer than TiC particles.

Ozyildirim and Zegetosky. [37] investigated the effect of nano-materials on the concrete permeability. Nano-silica (NS), nano-clay (NC), silica fume, fly ash, and slag were added to the cement with different ratios. The results showed that the permeability enhanced due to the presence of nano-materials in the concrete while the lowest permeability was noted in the silica fume mix.

Jalal et al. [15] investigated the effect of micro- and nano-particles of SiO_2 on the durability of high performance self-compacting concrete (HPSCC). The results showed that,

increasing the binder content from 400 to 500 kg/m^3 decreased the water absorption. The reduction in the water absorption of mixes with 2% NS and 10% MS was similar, while low water permeability was measured in the ternary mix (2% NS and 5% MS). The electrical resistivity of concrete increased due to the presence of SCMs. The probability of corrosion in mixes with 2% NS, 10% MS, and 2% NS + 10% MS was very low. The increase in the strength was attributed to the filling action and to the pozzolanic reaction of both NS and MS, which resulted in a compact structure with less pores.

Nasution et al. [38] studied the effect of utilizing nano-silica (NS) as a partial replacement of cement on the concrete properties. The results showed that the sulfate attack resistance improved and it was attributable to the presence of NS in concrete. The improvement in the concrete property were due to the consumption of $Ca(OH)_2$ in the pozzolanic reaction and the formation of secondary C-S-H gel, and due to the filling action of NS. Furthermore, the quantity of calcium aluminate decreased due to the addition of NS, which enhanced the sulfate resistance. The weight and strength loss in the specimens immersed in the sulfuric acid solution with NS was lower than that without NS.

Gaitero et al. [50] examined the effect of nano-silica (NS) on calcium leaching rate of cement paste using the accelerated degradation method. The results showed that NS at zero degradation stage increased the strength by 30% compared with the control specimen. The degradation of the control specimen was more than that of specimens with colloidal silica. The leaching of calcium hydroxide decreased after the addition of NS, resulted in low porosity. The improvement in the strength and the reduction in porosity and leaching were due to the changing of the calcium hydroxide to secondary C-S-H gel in the presence of

NS. Also, due to the filling action of NS which made the structure dense. The presence of NS in the mix densified the structure of C-S-H gel and increased its silicate chain length.

Nazari et al. [39] investigated the influence of nano-silica (NS) on the properties of high strength self-compacting concrete. The ratios of NS were 1%, 2%, 3%, 4%, and 5% by weight of cement. The results showed that the water absorption at two days was less than that of specimens with NS, while at later ages the water absorption decreased compared with the control specimens. The decrease in the water absorption was attributed to the fact that the NS accelerated the hydration reaction at early ages that increased the water demand. At later ages the structure became dense and the water permeability decreased.

Said et al. [16] investigated the effect of nano-silica (NS) on the properties of concrete. Fly ash (FA) and NS contents were the main parameters of the study. The results showed that the chloride permeability and the conductivity of the concrete enhanced due to the addition of NS. The enhancement in the permeability was attributed to the pozzolanic reaction and filling action of NS.

Du et al. [41] studied the durability characteristics of concrete with nano-silica. The dosages of NS were 0.3% and 0.9% by weight of cement. The results showed that the water penetration decreased due to the use of NS. The depth of penetration decreased by 56% in the mixes with 0.3% NS compared with that of control specimen. A slight increase in the water penetration of specimens with 0.9% NS was due to the agglomeration effect of NS particles. The chloride diffusion decreased as the dosage of NS was increased. A small reduction in the chloride permeability was noted in the specimens with 0.9% NS. The improvement in the durability was attributed to the effect of NS in refining the pores through the filling action, and due to the pozzolanic reaction, which is the reaction between

NS and $Ca(OH)_2$ to produce secondary C-S-H gel. The secondary silicate gel refined the structure and made it more dense and homogeneous.

Zahedi et al. [42] investigated the effect of nano-silica and rice husk ash (RHA) on the durability of cement mortars. The results showed that the NS has a significant effect on the performance of mortar while the RHA decreased the durability at early ages. The contribution of NS improved the durability, while the RHA enhanced the chloride resistance at later ages.

Quercia et al. [18] investigated the effect of nano-silica on self-compacted concrete (SCC). Two types of NS were utilized in the mix, powder NS and colloidal NS. The durability (chloride migration, conductivity, and freeze–thaw resistance and diffusion coefficients) improved due to the use of both types of NS in the mix. The durability was significantly enhanced due to the addition of 3.8% NS. The microstructure of the hardened concrete became homogeneous and denser due to the addition of NS, which was the reason for the enhancement in the durability properties.

Jorge et al. [44] investigated the properties of Portland cement mortar with NS. The NS was added to the concrete with percentages of 0%, 1%, 3%, 5%, and 10% as a partial replacement of cement. The expansion of mortars with 5 and 10 wt. % NS due to the immersion in 5% $MgSO_4$ solution after two years was reduced by 90% and 95%, respectively. The expansion decreased as the percentage of NS was increased. The capillary suction test showed that the absorption rate and absorption quantity decreased due to the presence of NS in the mix. The enhancement in the durability was due to the filling action of NS resulted in fine pores, and to the pozzolanic reaction that decreased the quantity of CH and increased the secondary C-S-H gel. Due to that, the concrete structure

became dense and more compact which prevented the ingress of $MgSO_4$ particles in the concrete.

2.5 Effect of nano-materials on micro structure of concrete

Morsy et al. [25] investigated the properties of cement mortars with nano-clay and multi-wall carbon nanotubes (MWCNTs). The ratios of carbon-nanotube were 0.005, 0.02, 0.05 and 0.1 wt. % of cement, while the ratio of nano-metakaolin was 6 % by weight of cement. Scanning electron microscope (SEM) showed that the microstructure of normal concrete was amorphous due to the presence of CSH. Further, the microstructure contained air voids and calcium hydroxide crystals (CH). Incorporating NMK in the mix produced more C-S-H and crystals of CH. Regarding the mix with both NMK and MWCNTs, the SEM images showed properly dispersed MWCNTs (Figure 2.8). When the ratio of the MWCNTs increased, the fibers slipped on each other causing weak bond between the fibers and the paste which decreased the strength.

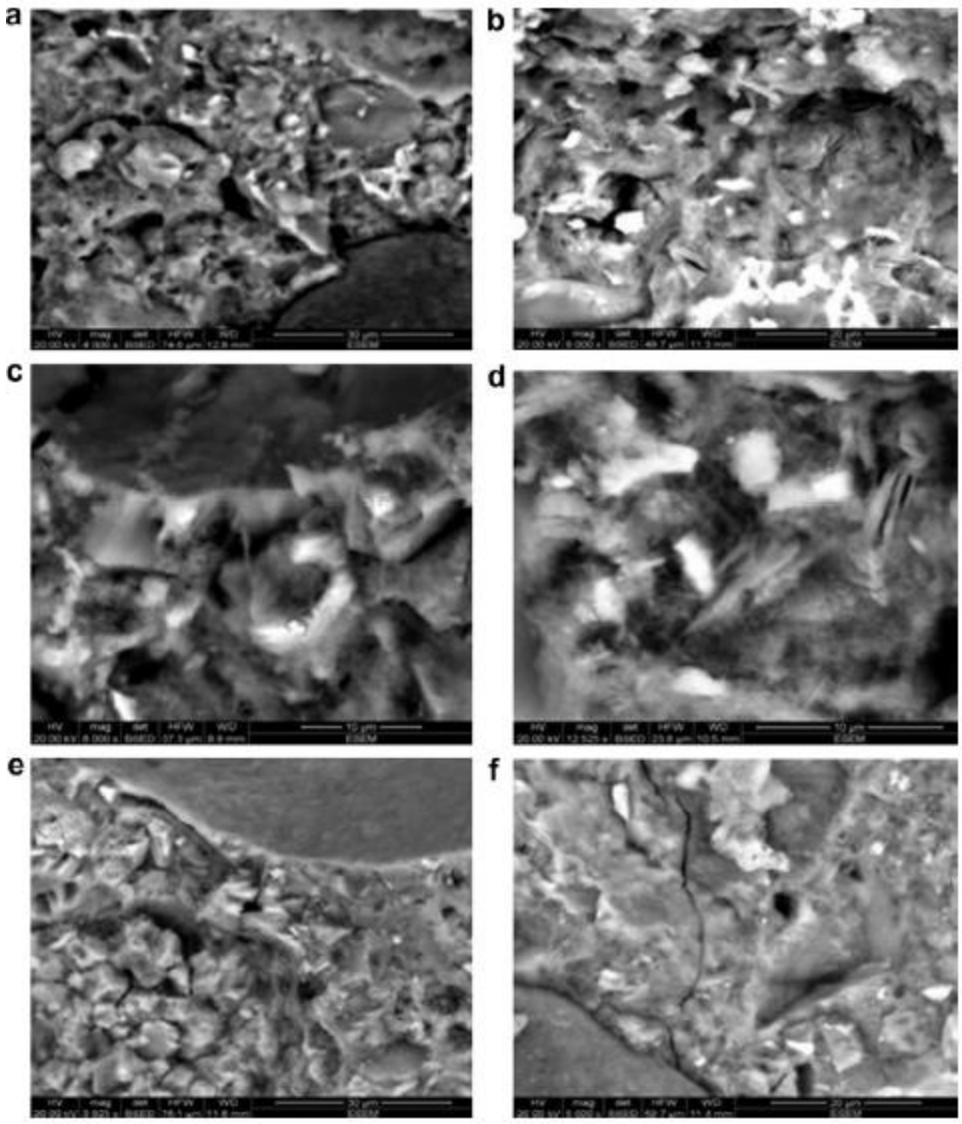

Figure 2.8: SEM of ordinary Portland cement mortar; (a) control mortar, (b) mortar containing 6% NMK, (c) mortar containing 6% NMK and 0.005% CNTs, (d) mortar containing 6% NMK and 0.02% CNTs, (e) mortar containing 6% NMK and 0.05% CNTs and (f) mortar containing 6% NMK and 0.01% CNTs [25].

Morsy et al. [6] studied the properties of cement mortar with nano-clay (NMK). The ratios of NMK used were 0, 2, 4, 6, and 8% as a partial replacement of cement. The SEM images showed that the microstructure of the normal paste consisted of standalone C-S-H which were connected together with a lot of needle hydrates and CH crystals (Figure 2.9a). Figure 2.9b and c represent the microstructure of mortar with 4% and 8% NMK. The micro-

structure was dense and more compact. The dense microstructure resulted from the nucleation effect of NMK on which the hydration products accumulated on the nano particles during the hydration reaction. Further, the NMK filled the voids in the CSH gel and prevented the CH from growing. The other particles in the concrete like aggregate, sand, etc. acted as a centro-plasm and the gel acted as a transmitter between them. So the effect of the NMK was noted not only on the paste but also on the interfacial zone between the paste and other particles.

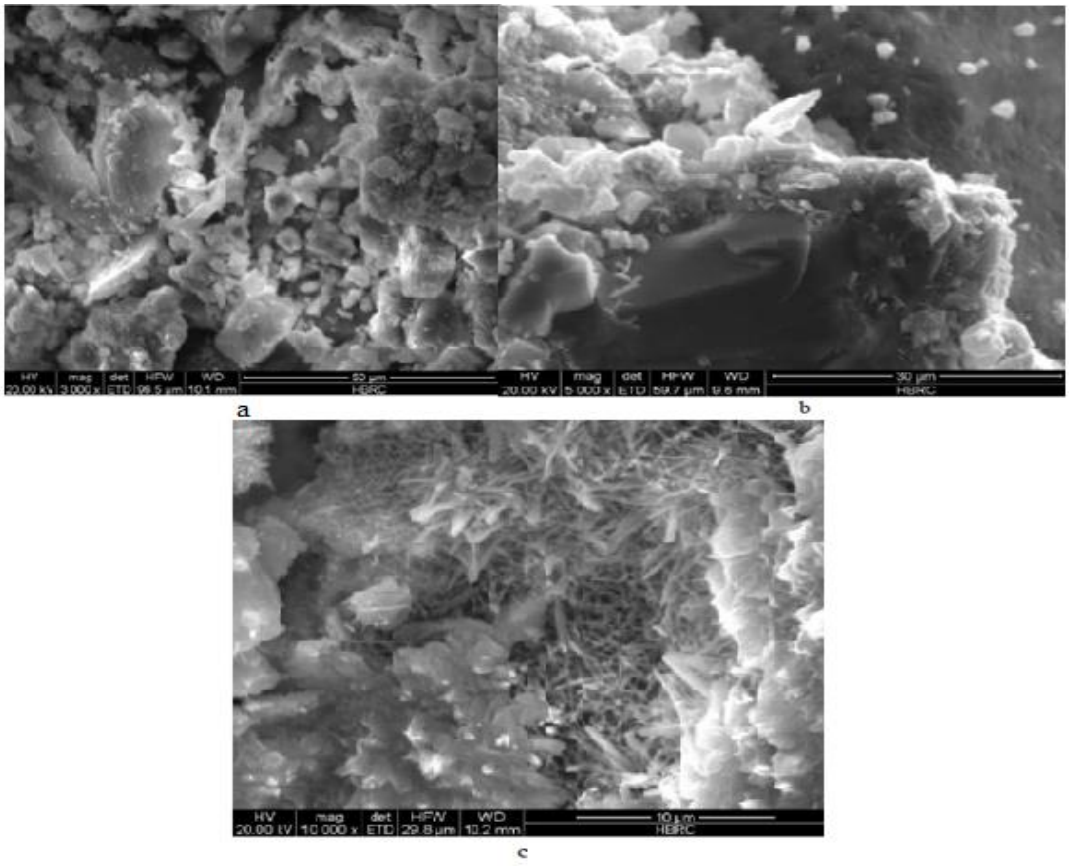

Figure 2.9: SEM micrographs of hydrated NMK mortar hydrated for 28 days, a) Cement mortar containing 0% NMK, b) Cement mortar containing 4% NMK, c) Cement mortar containing 8 % NMK [6].

He and Shi [48] investigated the microstructure of cement mortar with different nano-materials, such as Fe_2O_3, Al_2O_3, TiO_2, SiO_2 and nano-clays. The nano-particles were added to the mortar with a ratio of 1% by weight of cement. The field emission scanning electron microscopy (FESEM) showed that the morphology of the hydration products changed due to the addition of nanoparticles and the cement mortar became denser. The presence of the nano-materials limited the growth of $Ca(OH)_2$.

Khotbehsara et al. [10] investigated the properties of self-compacting mortar with fly ash and nano-TiO_2 (NT). The quantity of NT used in the mortar was 1, 2, 3, 4, and 5% by weight of cement as a partial replacement of cement, while fly ash was used with a fixed dosage of 25%. The SEM images showed that the microstructure with NT became denser and more uniform compared with that of the normal concrete. NT filled the voids and acted as kernels which restricted the growth of $Ca(OH)_2$. The enhancement in the strength and durability of the concrete with NT was attributed to the dense structure.

Mahawish et al. [31] studied the effect of silicon carbide (SiC) nano-particles and titanium carbide (TiC) nano-particles on the microstructure of cement paste. Both types of nano-particles with a size of 20 nm were added to the paste with six different dosages that were 1, 2, 3, 4, 5, and 6 wt. %. The microstructure of the control specimen was porous with many voids and with high quantity of $Ca(OH)_2$. The microstructure of specimens with nano-particles was more dense and uniform with small pores. Also, the quantity of $Ca(OH)_2$ was less, because it reacted with the nano-particles.

Hosseini et al. [34] studied the micro structural properties of ferrocement mortar. The parameters of the study were the quantity of nano-silica (NS) as a partial replacement of cement, the water to binder ratio, and the sand to binder ratio. The SEM images showed

large pores and high quantity of $Ca(OH)_2$ in the mortars without NS. The use of NS in the mortar decreased the pore size due to the filling action of NS. Also, NS consumed $Ca(OH)_2$ through the pozzolanic reaction which produced more C-S-H gel. The structure became dense and uniform.

Jo et al. [35] investigated the properties of cement mortars with nano-silica (NS). The dosages of NS were 3%, 6%, 10%, and 12% by weight of cement and the dosages of silica fume (SF) were 5%, 10% and 15% by weight of cement. The SEM micrograph of normal concrete shows isolated CSH surrounded with $Ca(OH)_2$. The microstructure of the mortar with NS was dense and uniform with small $Ca(OH)_2$ crystals. The dense structure resulted from the pozzolanic reaction and the filling action of NS.

Ozyildirim and Zegetosky. [37] investigated the roughness of concrete microstructure. Nano-silica (NS), nano-clay (NC), silica fume, fly ash, and slag were added to the cement with different ratios. The atomic force microscope (AFM) showed that the mortar with NS had uniform microstructure while the silica fume mortar microstructure was rough. The rough microstructure of silica fume mortar was due to agglomeration of silica fume particles.

Jalal et al. [15] investigated the effect of micro- and nano-particles of SiO_2 on the morphology of the microstructure of high performance self-compacting concrete (HPSCC). The SEM images indicated a uniform micro structure of mixes with NS, which was due to the uniformly dispersed nano-particles which acted as a kernel, on which the hydration products accumulated. The accumulation of the hydration products on the uniformly dispersed nano-particles decreased the voids in the microstructure and controlled the growth of $Ca(OH)_2$ crystals. The combined effect of NS and MS in compacting the

mortar microstructure was optimum. The SEM micrograph of normal concrete showed isolated CSH surrounded with needles of $Ca(OH)_2$.

Said et al. [16] investigated the effect of nano-silica (NS) on the properties of fly ash concrete. The SEM indicated that due to the addition of NS to the mix, the porosity of the micro-structure decreased and the structure became dense compared with the control microstructure. The improvement in the microstructure was attributed to the pozzolanic reaction and filling action of NS.

Rong et al. [17] investigated the microstructure of ultra-high performance concrete with nano-silica. The SEM showed that the microstructure of 3% NS concrete became dense with less micro pores and without plated $Ca(OH)_2$. The morphology of the microstructure showed perfect bond between the aggregate and the paste.

Du et al. [41] studied the microstructure of concrete with nano-silica. The dosages of NS were 0.3% and 0.9% by weight of cement. The SEM showed that the composition of the microstructure of normal concrete consisted of $Ca(OH)_2$ with a needle shape, amorphous CSH gel, and pores. Due to the addition of NS to the concrete, $Ca(OH)_2$ consumed in the pozzolanic reaction and extra CSH produced, that made the structure dense and homogeneous with tiny pores.

Lin et al. [19] studied the influence of NS on the micro structure of sludge mortar with fly ash. NS and fly ash were added to the mix with different ratios. The SEM showed that the addition of NS increased the hydrates of C-S-H and the mono-sulfoaluminate. Further, the crystallization resulted from NS and CH filled the pores of the structure.

El-Baky et al. [21] studied the effect of nano-silica (NS) on the microstructure of cement based mortar. The hardened and fresh properties of the mortar were measured. NS with size of 19 nm was added to the cement mortar at dosages of 1, 2, 3, 5, 7, and 10 % by weight of cement. The SEM images indicated that due to the reaction of NS with calcium hydroxide which resulted in producing secondary CSH gel, the pores filled, the interfacial transition zone was refined, the quantity of CH significantly reduced, and the microstructure became homogeneous and dense.

Sun et al. [51] investigated the effect of nano-silica (NS) on the early hydration properties of alite–sulphoaluminate cement (ASC). The dosages of NS were 1, and 3 wt. % used as a partial replacement of ASC. The results of the phase development composition analysis showed that NS did not have any influence on the type of the hydration products. At a dosage of 3 wt. % of NS, the porosity decreased by 54.09 % at three days. The SEM images showed that the microstructure became dense due to the addition of NS.

Niewiadomski et al. [52] studied the microstructure and the porosity of self-compacted concrete with nano-particles. SiO_2, TiO_2 and Al_2O_3 nanoparticles were added to the concrete with different quantities. The results showed that the microstructure of SCC enhanced and the porosity decreased. The addition of nanoparticles improved the hardness as well as the modulus of elasticity of SCC.

CHAPTER THREE

EXPERIMENTAL PROGRAM

3.1 Materials

A total of 22 concrete mixtures of high performance concrete were prepared in this study. The materials used in preparing these mixes were as follows:

3.1.1 Cement

Ordinary Portland cement (ASTM C 150 Type I) with a specific gravity of 3.15 was used in preparing the concrete specimens. Sufficient amount of cement was procured from a local supplier in Saudi Arabia. The chemical composition of cement is shown in Table 3.1.

Table 3.1: Chemical composition of OPC.

Component	Weight %
CaO	64.35
SiO_2	22.00
Al_2O_3	5.64
Fe_2O_3	3.80
K_2O	0.36
MgO	2.11
Na_2O	0.19
Equivalent alkalis	0.33
SO_3	2.10
Loss on ignition	0.70
C_3S	55.00
C_2S	19.00
C_3A	10.00
C_4AF	7.00

3.1.2 Industrial by-products

Four industrial wastes, namely electric arc furnace dust (EAFD), cement kiln dust (CKD), limestone powder (LSP), and oil ash (OA) were used in preparing the concrete specimens. A description of the selected industrial waste materials is as follows:

3.1.2.1 Electric Arc Furnace Dust (EAFD)

EAFD is generated during steel making process in an electric arc furnace. The EAFD consists mostly of iron oxide and zinc oxide. EAFD was obtained from Saudi Iron and Steel Company (HADEED). The chemical composition of EAFD is shown in Table 3.2.

Table 3.2: Chemical composition of EAFD.

Constituent	Weight %
Aluminium	0.7
Calcium	9.39
Cadmium	0.0004
Copper	0.06
Iron	33.6
Potassium	1.70
Magnesium	2.3
Manganese	1.8
Sodium	2.6
Nickel	0.01
Lead	1.31
Phosphorous	0.13
Silicon	2.38
Tin	0.03
Sulphur	0.57
Titanium	0.09
Zinc	10

3.1.2.2 Cement Kiln Dust (CKD)

CKD is a by-product of the cement manufacturing process. Cement clinker typically generates around 6 to 7% of CKD. The amount of alkalis, chloride and sulfate is considerably more in the CKD. CKD was sourced from a cement company in Jeddah, Western province of Saudi Arabia. The chemical composition of CKD is shown in Table 3.3.

Table 3.3: Chemical composition of CKD

Component	Weight %
CaO	49.300
SiO_2	17.100
Al_2O_3	4.240
Fe_2O_3	2.890
K_2O	2.180
MgO	1.140
Na_2O	3.840
P_2O_5	0.120
ZrO_2	0.011
Cr_2O_3	0.011
CuO	0.029
NiO	0.012
TiO_2	0.340
V_2O_5	0.013
Equivalent alkalis ($Na_2O + 0.658K_2O$)	5.270
$(SO_3)^{2-}$	3.560
Cl^-	6.900
Loss on ignition	15.800
BaO (µg/g (ppm))	78.200
ZnO (µg/g (ppm))	65.800

3.1.2.3 Oil Ash (OA)

OA is generated as a by-product in power generation plants through burning of oil to produce energy. OA was obtained from the Saudi Electricity Company power plant in Shayba, Saudi Arabia. It is a very fine material and most of it passes # 200 sieve. The main constituents of OA are carbon and sulfur. The chemical composition of OA is shown in Table 3.4.

Table 3.4: Chemical composition of oil ash

Constituents	Weight %
SiO_2	1.65
CaO	0.45
Al_2O_3	< 0.10
Fe_2O_3	0.47
MgO	0.48
K_2O	0.03
Na_2O	0.53
V_2O_5	2.65
Sulfur	9.6
$Na_2O + (0.658K_2O)$, %	0.55
Loss on ignition	60.6
Moisture %	5.9

3.1.2.4 Lime Stone powder

Limestone powder (LSP) is generated during the crushing of carbonate rocks. It was procured from a limestone quarry in Abu Hadriyah, Eastern Province of Saudi Arabia. The main component of the LSP is lime and silica. The chemical composition of LSP is shown in Table 3.5.

Table 3.5: Chemical composition of LSP

Component	Weight %
SiO_2	11.79
CaO	45.7
Al_2O_3	2.17
Fe_2O_3	0.68
MgO	1.8
K_2O	0.84
Na_2O	1.72
$Na_2O+(0.658K_2O)$	2.27
Loss on Ignition	35.1
Moisture	0.2

3.1.3 Nano material

Colloidal nanosilica, Cembinder 8, used in this research was procured by AkzoNobel Germany. The properties of nanosilica are shown in Table 3.6, as supplied by the manufacturer. Figure 3.1 and Figure 3.2 show the transmission electron microscopy (TEM) and XRD peaks of the colloidal nanosilica, respectively.

Table 3.6: Properties of colloidal nano-silica

Property	**Value**
Solid content (%)	50
Average particle size (nm)	35
Bulk density (g/cm^3)	1.4
Specific surface area (m^2/g)	80
Na_2O content (%)	0.2
Viscosity (cps)	<10
pH	9.5

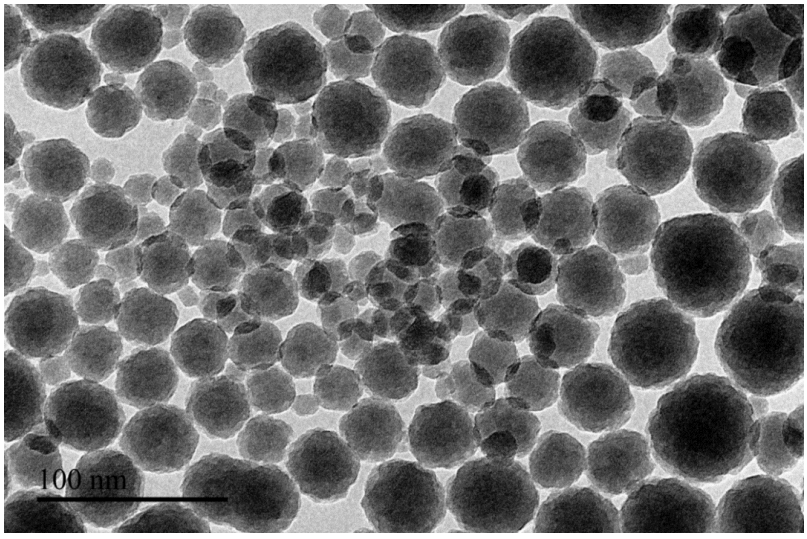

Figure 3.1: TEM of Colloidal Nano silica

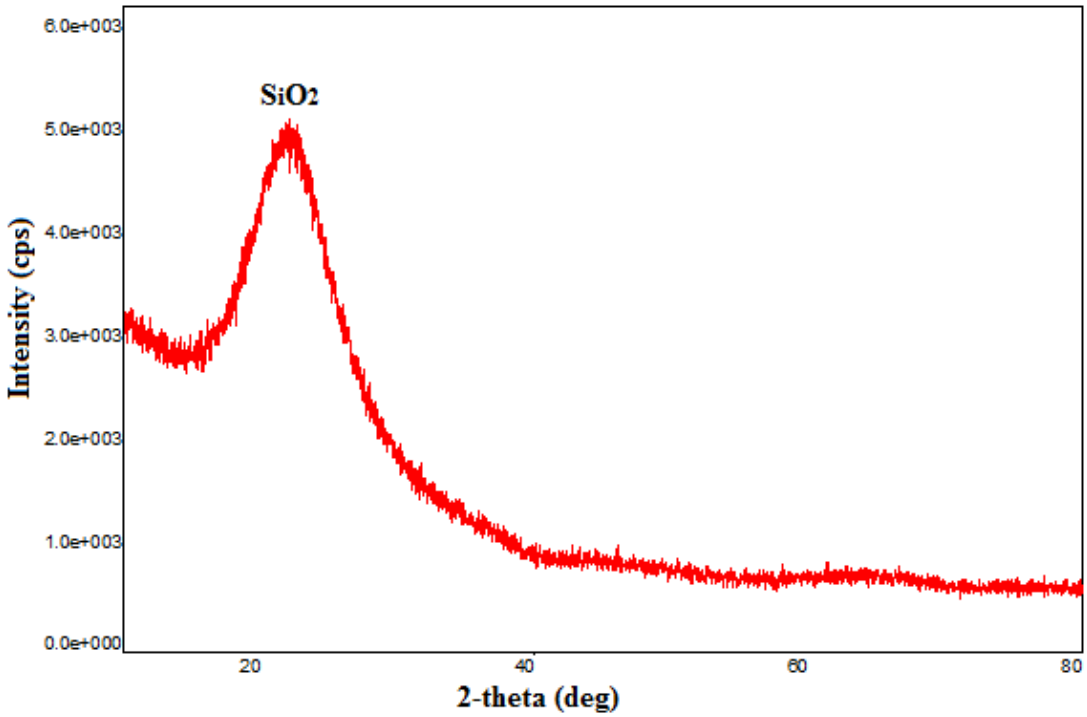

Figure 3.2: XRD diffractogram of colloidal nano-silica

3.1.4 Aggregates

The coarse aggregate used in this study was crushed limestone with a specific gravity of 2.6 and absorption of 1.1%. It was procured from a local quarry in Abu Hadriah, Eastern Province of Saudi Arabia. Four different sizes, namely ½ inch, 3/8 inch, 3/16 inch, and 3/32 inch were used in preparing the concrete specimens. Dune sand was used as a fine aggregate which is widely available in the Kingdom. The specific gravity and absorption of the fine aggregate were 2.56 and 0.6%, respectively.

3.1.5 Plasticizer

Glenium 51superplasticizer was used in preparing the concrete specimens. It was procured from a local supplier (BASF) in the Kingdom. Its technical data is shown in Table 3.7.

Table 3.7: Technical data of Glenium 51

Appearance	Brown liquid
Specific gravity @ 20°C	1.08±0.02 g/cm^3
pH-value @ 20°C	7.0±1.0
Alkali content	≤ 5.0
Chloride content	≤ 0.1 %

3.1.6 Casting and curing of concrete specimens

Specimens were prepared to assess the properties of the developed concretes (Table 3.8). After procuring all the needed materials, aggregates were sieved to get the required sizes. An electrically operated mixer was used in producing concrete. The coarse and fine aggregate were added first to the mixer and mixed under drying condition, then the powder (cement and industrial by-products) was added and mixed with the aggregate. After that, part of the water was added with the required additives. The NS was sonicated using an ultrasonic processor (Figure 3.3) and added to the mixer with the remaining volume of water. The materials were mixed until a homogeneous concrete was produced. The concrete was cast in molds of varying geometry and consolidated using a vibrating table (Figure 3.3). The molds were covered with plastic sheet for 24 hours, then they were demolded (Figure 3.3) and cured in water tank under laboratory temperature.

Table 3.8: Details of the test specimens

Property	Test standard	Test age	Specimen size	Number of specimens
Compressive strength	ASTM C 39	3, 7, 14, &28 days	100 mm cube	12
Flexural Tensile strength	ASTM C 78	28 days	40 × 40 × 160 mm	3
Drying Shrinkage	ASTM C 157	28 days cured, then measure at 3, 7, 14, 28, 56 , 90& 120 days	50 × 50 × 250 mm	3
Chloride permeability	ASTM C 1202	28 days	75 × 150 mm cylinder	1
Chloride diffusion	ASTM C 1556	28 days cured and then immersed in 5% $NaCl^-$ solution for 6 months	75 × 150 mm cylinder	1
Corrosion (rate & potential)	LPR Method	28 days cured and then partly submerged in 5% Cl^- solution	12 mm bar centered in a cylinder of 75 × 150 mm	3
Sulfate attack	ASTM C452	28 days cured and then immersed in 2.1% $MgSO_3$	50 × 50 × 50 mm mortar cube	3
		28 days cured and then immersed in 2.1% Na_2SO3	50 × 50 × 50 mm mortar cube	3
		Cured in water	50 × 50 × 50 mm mortar cube	3
		28 days cured and then immersed in 2.1% Na_2SO3	25×25×285 mm	2

Figure 3.3: (a) Casting of concrete specimens (b) Ultrasonic processor (c) Concrete specimens prepared for curing

3.2 Concrete mixture design

The concrete mixtures were prepared based on trial mixtures to control the water to binder ratio (w/b) and dosages IWMs, used as a partial replacement of the cement. The dosage of nano-silica was selected depending on a previous study conducted at KFUPM [53]. The results of that study showed that as the dosage of nano-silica increased the mortar compressive strength increased up to a dosage of 5% then it started to decrease (Figure 3.4). So, the NS dosage used in this study was restricted to 5% by weight of the binder which is

the optimum dosage. The proportions of the materials used in preparing the concrete mixtures are shown in Table 3.9.

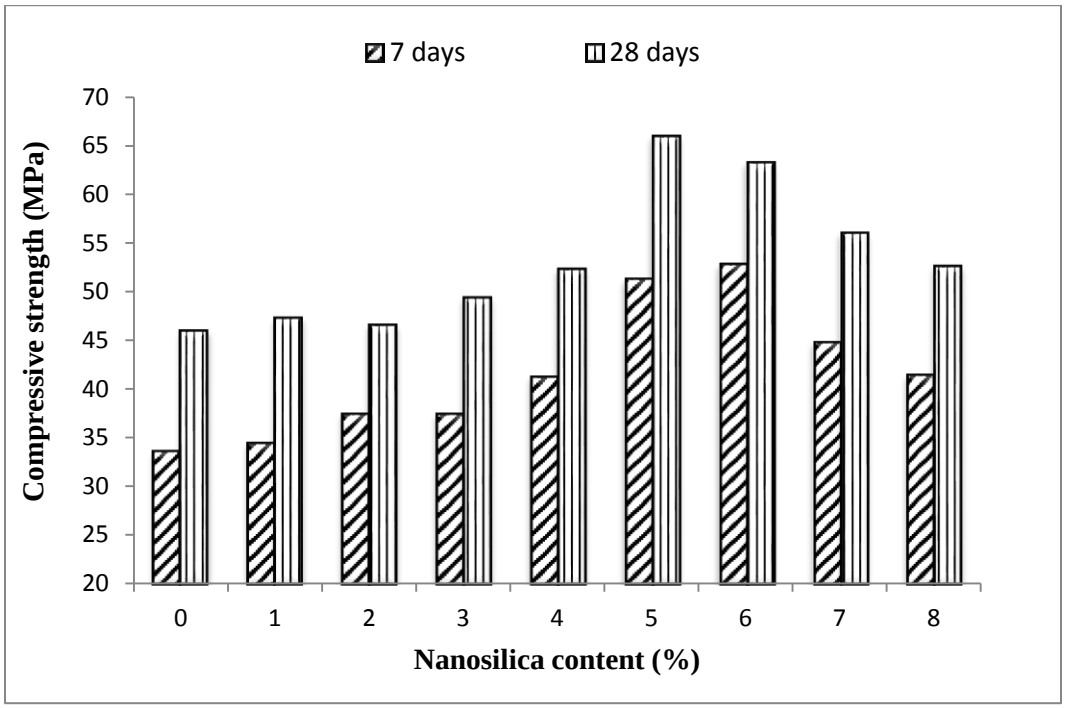

Figure 3.4: Compressive strength of mortar specimens at 7 and 28 days [53].

Table 3.9: Mixture proportions of concrete

IWM	Mix code	IWM content, %	Cement (kg/m^3)	NS (kg/m^3)	Coarse aggregate (kg/m^3)				Fine Aggregate (kg/m^3)	w/c
					$^1/_2$ in	$^3/_8$ in	$^3/_{16}$ in	$^3/_{32}$ in		
--	OPC	--	450	--	305.71	305.71	174.69	87.35	873.46	0.37
	OPC+5%NS	----	422.5	22.5	306.1	306.1	174.9	87.47	874.68	0.37
CKD	10%CKD	10	405	--	304.88	304.88	174.22	87.11	871.08	0.37
	15%CKD	15	382.5	--	304.46	304.46	173.98	86.99	869.9	0.37
	20%CKD	20	360	--	304.05	304.05	173.74	86.87	868.71	0.37
	10%CKD+5%NS	10	382.5	22.5	303.69	303.69	173.54	86.77	867.68	0.37
	10%CKD+5%NS	15	360	22.5	303.37	303.27	173.30	86.65	866.49	0.37
	20%CKD+5%NS	20	337.5	22.5	302.86	302.86	173.06	86.53	865.3	0.37
EAFD	5%EAFD	5	422.5	--	305.67	305.67	174.67	87.33	873.35	0.37
	10%EAFD	10	405	--	302.39	302.39	172.8	86.4	863.98	0.37
	5%EAFD+5%NS	5	405	22.5	304.48	304.48	173.99	86.99	869.94	0.37
	10%EAFD+5%NS	10	382.5	22.5	301.20	301.2	172.12	86.06	860.58	0.37
LSP	5%LSP	5	422.5	--	306.65	305.65	175.23	87.61	876.14	0.37
	10%LSP	10	405	--	304.35	304.35	173.91	86.96	869.56	0.37
	15%LSP	15	382.5	--	304.35	304.35	173.91	86.96	869.56	0.37
	5%LSP+5%NS	5	405	22.5	305.46	305.46	174.55	87.27	872.74	0.37
	10%LSP+5%NS	10	382.5	22.5	303.16	303.16	173.23	86.62	866.16	0.37
	15%LSP+5%NS	15	360	22.5	302.47	302.47	172.84	86.42	864.21	0.37
OA	5%OA	5	422.5	--	293.63	293.63	167.79	83.89	838.93	0.37
	10%OA	10	405	--	278.3	278.3	159.03	79.51	795.15	0.37
	5%OA+5%NS	5	405	22.5	292.43	292.43	167.11	83.55	835.53	0.37
	10%OA+5%NS	10	382.5	22.5	277.11	277.11	158.35	79.17	791.74	0.37

3.3 Evaluation of macro level properties

3.3.1 Compressive strength

The compressive strength of the developed concrete was determined using 100 mm cube specimens in accordance with ASTM C39 [54]. A hydraulic compression machine (MATEST) with capacity of 3,000 kN was used in the compression test (Figure 3.5). The load was applied at a constant rate of 1.5 kN/s until the specimen failed. Then, the ultimate load was recorded. The compressive strength was evaluated by dividing the ultimate load with the cross sectional area of the specimen. The concrete cubes were tested after 3, 7, 14, and 28 days of water curing. At each age, three specimens were tested, and the average compressive strength was reported.

Figure 3.5: Compressive strength testing machine

3.3.2 Flexural strength

The flexural strength of the developed concrete prisms was determined on 40×40×160 mm prismatic specimens using a four point loading test in accordance with ASTM C78 [55]. A universal testing machine (INSTRON 300K) with loading limit of 1000 kN was utilized in conducting the test. The applied load and the corresponding displacement at the mid span were recorded using a data logger, load cell and LVDT (Figure 3.6). The ultimate load was used in evaluating the flexural strength. The load was applied at a displacement rate of 0.5 mm/min. Three prisms from each mix were tested and the average flexural strength was calculated.

Figure 3.6: Flexural strength test set up.

3.3.3 Drying shrinkage

The drying shrinkage of concrete specimens measuring 50×50×250 mm was evaluated according to ASTM C157 [56]. The specimens were cured for 28 days then the initial length was measured after drying the surface moisture. The length of the specimens was thereafter measured after 3, 7, 14, 28, 56, 90 and 120 days. Three specimens were tested at each age and the average length was considered for calculating the drying shrinkage. A data logger, LVDT, and steel frame were used in measuring the length of the specimen (Figure 3.7).

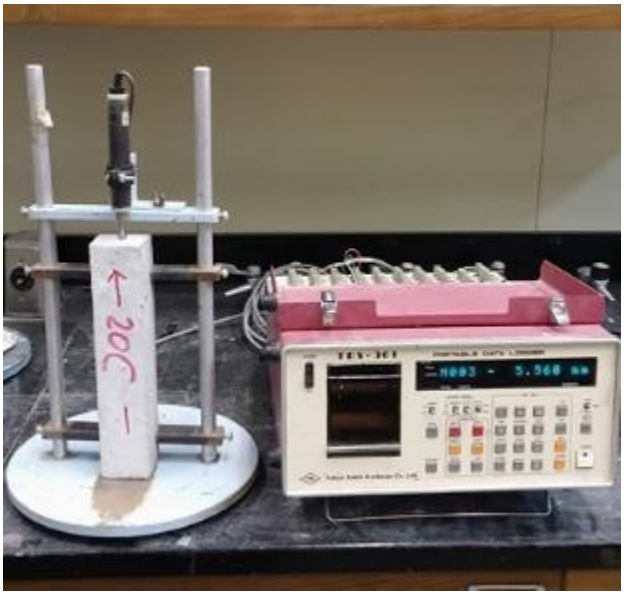

Figure 3.7: Drying Shrinkage test set-up

3.3.4 Rapid chloride permeability

The chloride permeability of concrete specimens was evaluated after 28 days of water curing according to ASTM C1202 [57]. Concrete cylinders measuring 75 × 150 mm were prepared from each mix and each cylinder was cut into three pieces. The side surfaces of the disks were coated with epoxy, then, the coating was cured according to the

manufacturer's instructions. Afterwards, the specimens was vacuum saturated using a vacuum desiccator. Then each concrete desk was clamped between two half-cells, one was filled with 3% NaCl solution while the other was filled with 0.3 N NaOH. A potential difference of 60 V DC was maintained across each cell and the current flowing between the two cells was monitored for a duration of six hours (Figure 3.8) and the total charge passed was calculated. The test was conducted on three disks and the average values are reported. The total charge passed was related to the chloride ion penetration.

Figure 3.8: Test set-up used to determine the Rapid Chloride Permeability.

3.3.5 Chloride diffusion

Concrete cylindrical specimens measuring 75×150 mm were prepared from each mix to determine the chloride diffusion according to ASTM C1556 [58]. The cylinders were cured for 28 days, then they were allowed to dry for seven days. The dry specimens were coated with epoxy, except one surface. The specimens were immersed in 5% sodium chloride solution for a period of six months and the diffusion of the chloride ions was ensured in one direction. Powder samples were taken from the specimens at five different intervals from the uncoated surface of the specimen.

To measure the free chloride concentration, five gm of the powder was dissolved in 50 gm of hot distilled water. After 24 hours, the sample was filtered with extra 50 gm of distilled water. Thereafter, 0.2 ml of the filtrated sample was added to 9.8 ml of distilled water. Thereafter, 2 ml of mercuric thiocynate and 2 ml of 0.25 M ammonium ferric sulfate were added to the solution. A small volume of the solution was analyzed using a spectrophotometer. The absorption reading was used to detect the chloride concentration which was plotted against the concrete depth. The resulting chloride profile was used to determine the coefficient of chloride diffusion according to Fick's second law of diffusion. Figure 3.9 shows some samples after filtration.

Figure 3.9: Some samples after filtration of digested chlorides

3.3.6 Corrosion measurements

Concrete cylinders measuring 75×150 mm were prepared with a 12 mm steel bar fixed at the center. Three cylinders were prepared from each mix. To avoid crevice corrosion, the 12-mm bars were coated with cement paste followed by an epoxy coating at the concrete-air interface and at the bottom of the bar. The concrete cylinders were cured with water for 28 days then they were partially immersed in 5% chloride solution. Reinforcement corrosion was evaluated by measuring corrosion potentials and corrosion current density.

Corrosion potentials: The corrosion potentials were measured using digital multimeter and a reference electrode. The positive terminal of the multimeter was connected to a saturated calomel reference electrode (SCE) while the negative terminal was connected to the steel bar (Figure 3.10). The difference in potential was measured for each specimens every two weeks and the average values are reported.

Corrosion current density: Reinforcement corrosion was also evaluated by measuring corrosion current density using linear polarization resistance method (LPRM). Three electrodes, reference electrode, working electrode (the steel reinforcement) and a reference electrode. The three electrodes were connected to a Potentiostat/Galvanostat. The steel was polarized to ±10 mV with respect to the reference electrode at a scan rate of 0.1 mV/s and the resulting current was measured (Figure 3.11). The slope of potential vs current curve represents the resistance of material to polarization (R_p). The corrosion current density was evaluated using the following formula:

$$I_{corr} = \frac{B}{R_p} \tag{3.1}$$

where:

I_{corr} = corrosion current density ($\mu A/cm^2$)

R_p = polarization resistance ($k\Omega.cm^2$)

$$B = \frac{\beta_a \beta_c}{(\beta_a + \beta_c)2.303} \tag{3.2}$$

β_a = anodic Tafel constant

β_c = cathodic Tafel constant

Figure 3.10: Test set-up for corrosion potential measurement

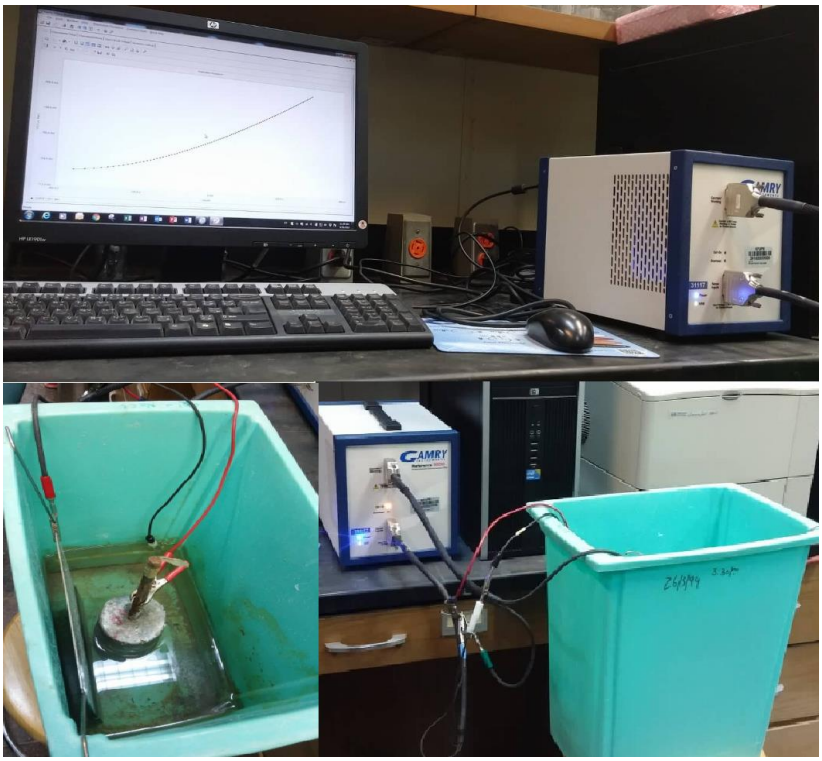

Figure 3.11: Test set-up for corrosion current density measurement

3.3.7 Sulfate attack

Two groups of specimens were prepared to evaluate the sulfate attack, the first group was beams (25×25×285mm) prepared with mortar while the other group was cubes (25×25×25 mm) prepared from paste. The beams were immersed in 2.1 % sodium sulfate solution while the cubes were divided into two groups, one group was exposed to 2.1% sodium sulfate solution while the other group was exposed to 2.1% magnesium sulfate solution. The sulfate attack was assessed through measuring the expansion of the beams and by inspecting the cubes visually. After 28 days of curing, the initial length of prisms were measured using the setup shown in Figure 3.12. Then, the specimens were immersed in 2.1% sodium sulfate solution. The length of each specimen was measured every month up to seven months of exposure to the sulfate solution.

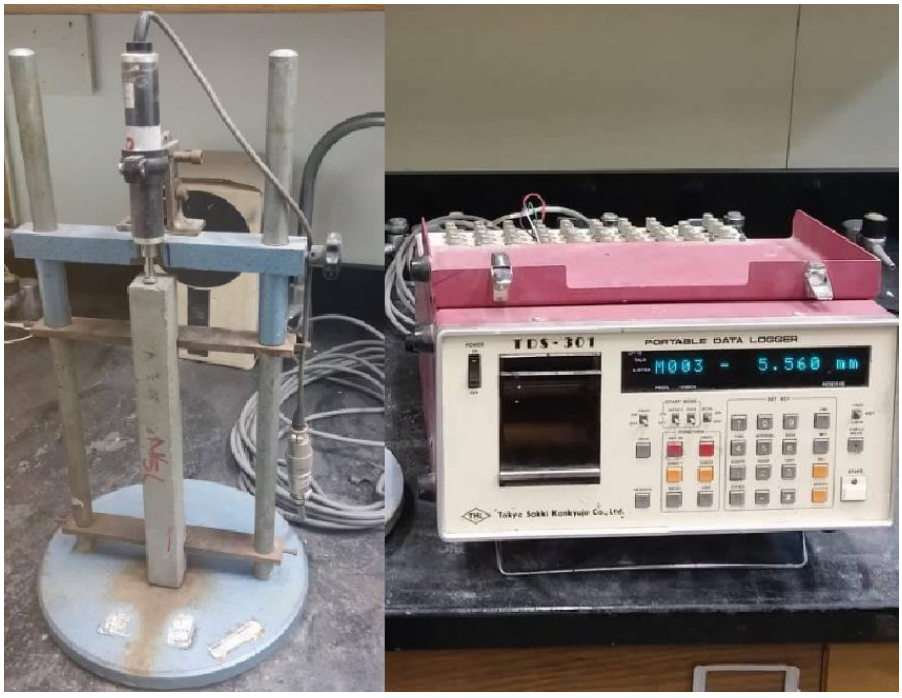

Figure 3.12: Test set-up used for expansion measurement of prism specimens

3.4 Evaluation of micro level properties

3.4.1 Morphology (SEM)

SEM is one of the electron microscope methods that produces images of samples by focusing a beam of electrons on the surface of the specimen. The morphology of the concrete specimens was studied using SEM. Morphology of concrete samples that were taken from concrete cubes tested for 28-days compressive strength and from cubes exposed to sulfate attack was evaluated. To enhance the resolution of the images, the concrete surfaces were coated with gold. The scanning electron microscope used in this study is shown in Figure 3.13.

Figure 3.13: Scanning electron microscope (SEM) used in the study.

3.4.2 Backscattered electron images

Backscattered electrons images (BEI) are electrons with high energy that can be applied for multiple elastic scattering events within a specimen. Compared to the SE image, the

greater energy used in BEI results in a larger interaction volume and lower spatial resolution. Also, the BEI is created depending on the composition of the different phases corresponding to their average atomic number and is classified by the brightness of different phases of the image. The concrete specimens and the machine (Figure 3.13) that were used in SEM were used also utilized for BEI.

3.4.3 Mineralogical composition

The mineralogical composition of the specimens was evaluated by utilizing X-ray diffraction (XRD) technique. X-ray diffraction provides chemical information about material constituents by characterizing the materials to different phases. In this study, the cement paste of different mixes were prepared and crushed after 28 days into fine powder. To characterize the constituents of the powder into different phases, the powdered samples were analyzed using Rigaku Ultima IV XRD equipment (Figure 3.14). The test was performed by changing the diffraction angle from 4^{o} to 80^{o} (2-theta). During the test, the samples were rotated according to the specified angles and the intensity of diffracted X-rays was recorded in counts per second (cps). The resulting data was analyzed to determine the different phases and their approximate percentage volume of the constituents.

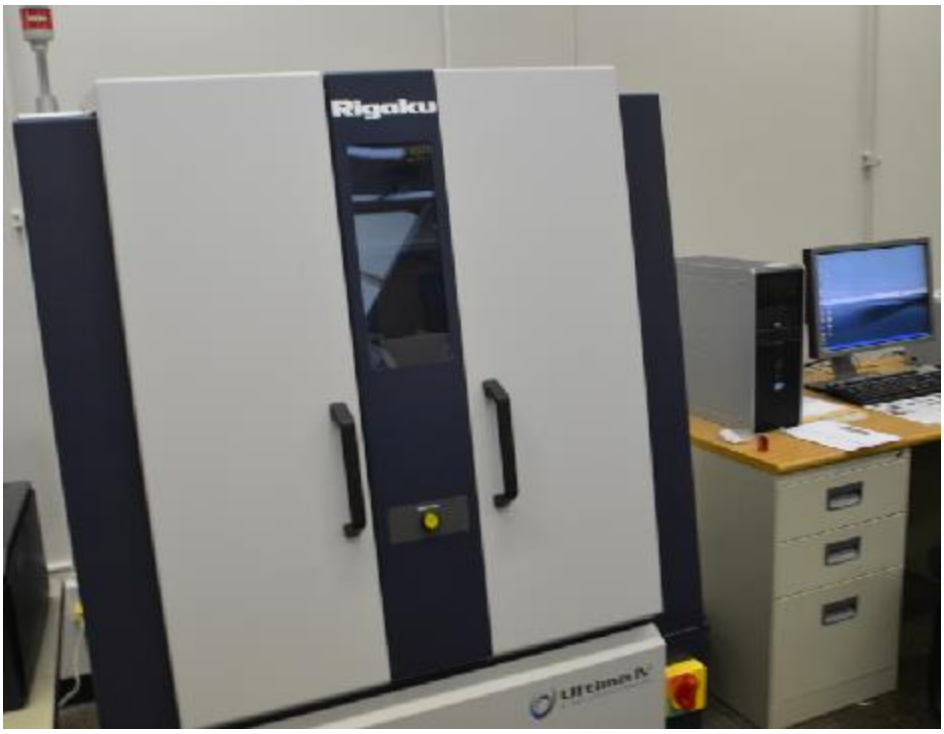

Figure 3.14: X-ray diffraction (XRD) machine used in the study.

CHAPTER FOUR

RESULTS AND DISCUSSION OF MACRO- AND MICRO-LEVEL PROPERTIES

4.1 Properties of OPC prepared with and without nano-silica

To evaluate the effect of NS on the properties of ordinary Portland cement (OPC) concrete, two groups of specimens were prepared. The first group was prepared with OPC only, while in the other group, 5% NS was used as a partial replacement of cement.

4.1.1 Macro properties

4.1.1.1 Compressive strength

Figure 4.1 depicts the compressive strength development of OPC concrete with and without NS. The compressive strength at different ages increased, the 28-day compressive strength of OPC and OPC+5%NS specimens was 58MPa and 72MPa, respectively, while the 3-day compressive strength was 35.6 MPa and 42.54 MPa, respectively. Due to utilizing 5%NS as a partial replacement of cement, the 28-day compressive strength increased by 24.1%.

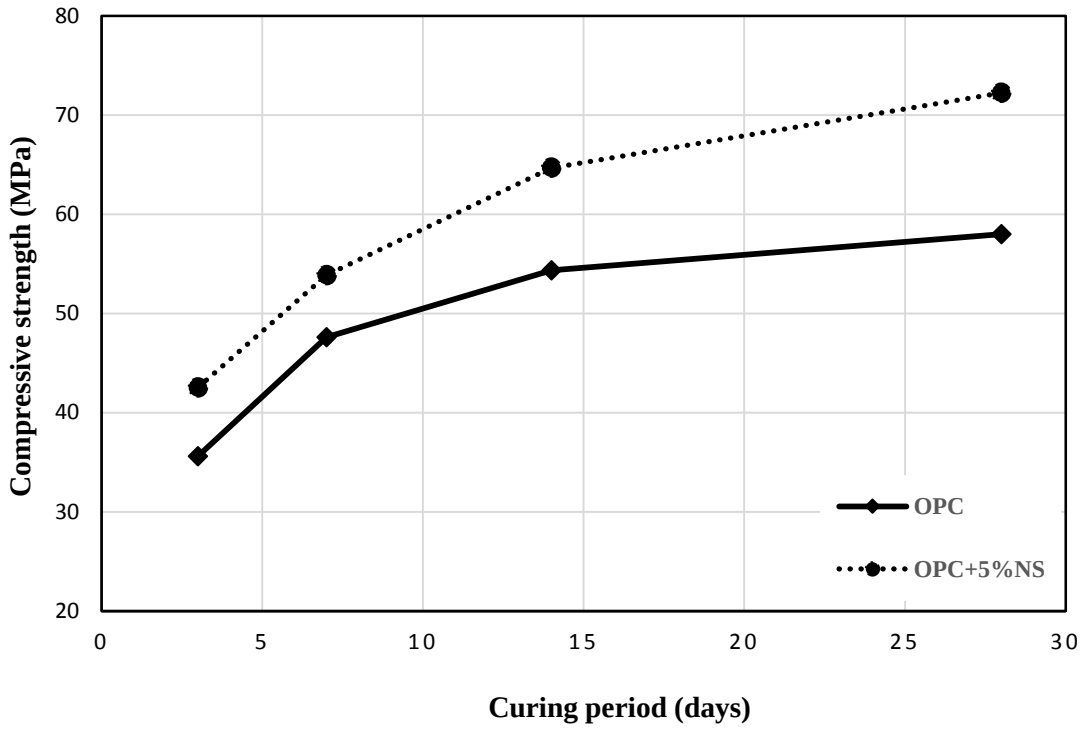

Figure 4.1: Compressive strength of OPC concrete with and without NS

4.1.1.2 Flexural strength

The 28-day flexural strength of OPC and OPC+5%NS specimens was 4.19 MPa and 5.81 MPa, respectively, (Figure 4.2). Incorporating 5%NS in the OPC concrete increased the flexural strength by 38.7%.

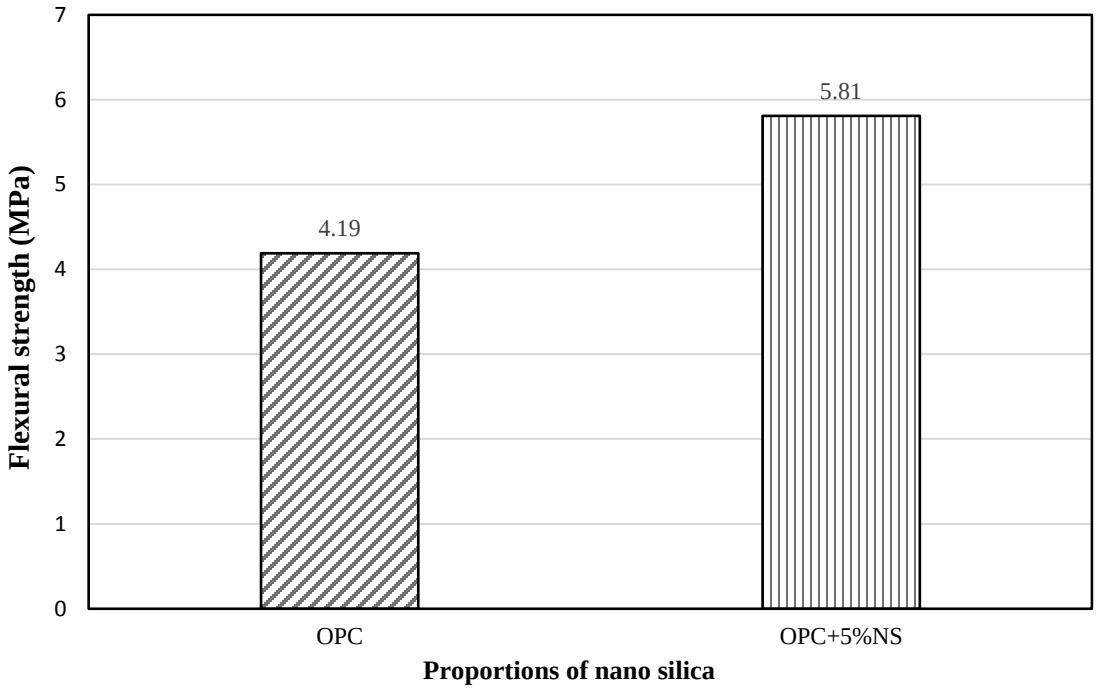

Figure 4.2: Flexural strength of OPC concrete with and without NS

4.1.1.3 Drying shrinkage

The drying shrinkage of OPC concrete specimens is depicted in Figure 4.3. It is clear that utilizing 5% NS in the concrete, as a partial replacement of cement, increased the drying shrinkage. However, the 7-day drying shrinkage of both mixes was less than 500 microns.

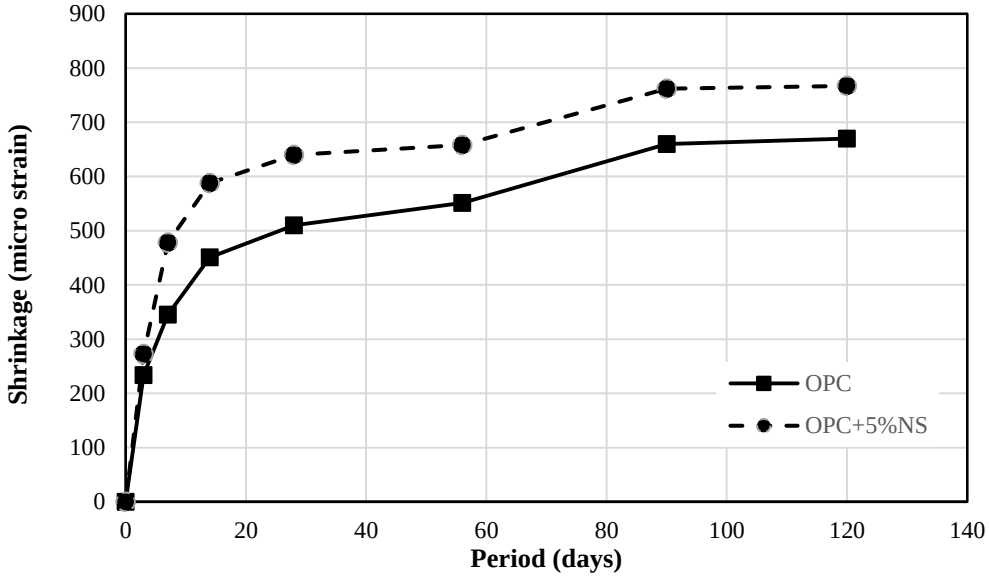

Figure 4.3: Drying shrinkage of OPC concrete specimens.

4.1.1.4 Chloride permeability

The total charge passed through the OPC specimens with and without NS is shown in Figure 4.4. The chloride permeability of OPC+5%NS specimens decreased significantly compared to that of only OPC.

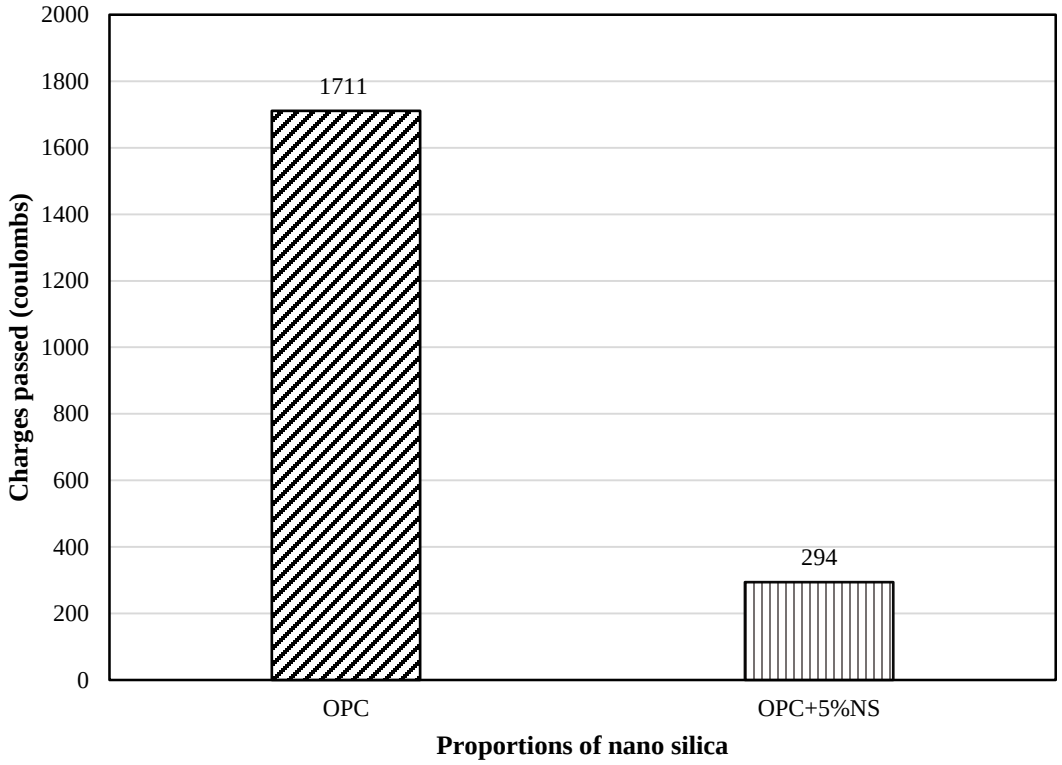

Figure 4.4: Rapid chloride permeability of OPC concrete specimens with and without NS.

4.1.1.5 Chloride diffusion

Figure 4.5 depicts the chloride concentration in the concrete specimens exposed to 5% sodium chloride solution for six months. The chloride concentration significantly decreased at all depths due to the use of 5% NS in concrete, as a partial replacement of cement. The slope of the chloride profile of OPC+5%NS concrete was more than that of OPC concrete, while at a depth of 40 mm the chloride concentration of the two specimens was similar. The resulting chloride profiles were utilized to determine the coefficients of chloride diffusion in accordance with Fick's second law of diffusion [59]. The coefficient of chloride diffusion of OPC and OPC+5%NS concrete was 16.2 and 6.21 × 10^{-8} cm^2/s,

respectively. It is clear that utilizing 5%NS in the concrete, as a partial replacement of cement, significantly decreased the coefficient of chloride diffusion.

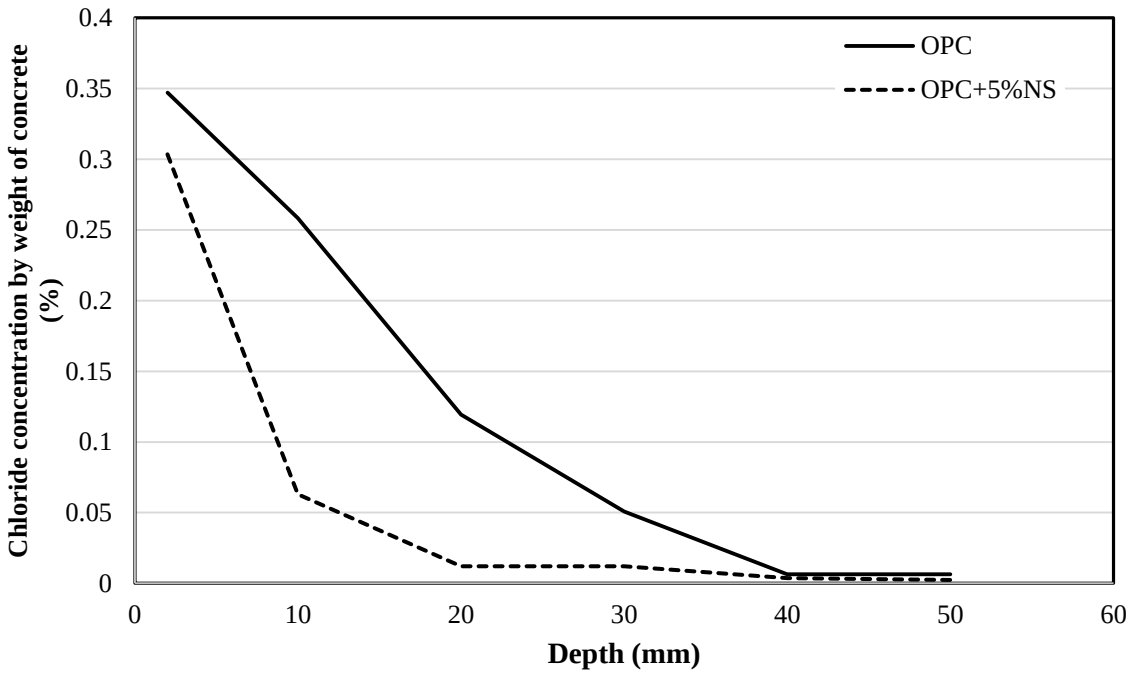

Figure 4.5: Chloride profile of OPC concrete with and without NS

4.1.1.6 Reinforcement corrosion

Corrosion Potentials: Three concrete cylinders with 12 mm steel bars were prepared from each mix and partially immersed in 5% chloride solution. The difference in potential was measured for each concrete cylinder with respect to a saturated calomel reference electrode (SCE) and the average potential difference was recorded. Figure 4.6 depicts the corrosion potential (E_{corr}) of concrete specimens prepared with and without NS. The potential values decreased due to the use of 5% NS in concrete.

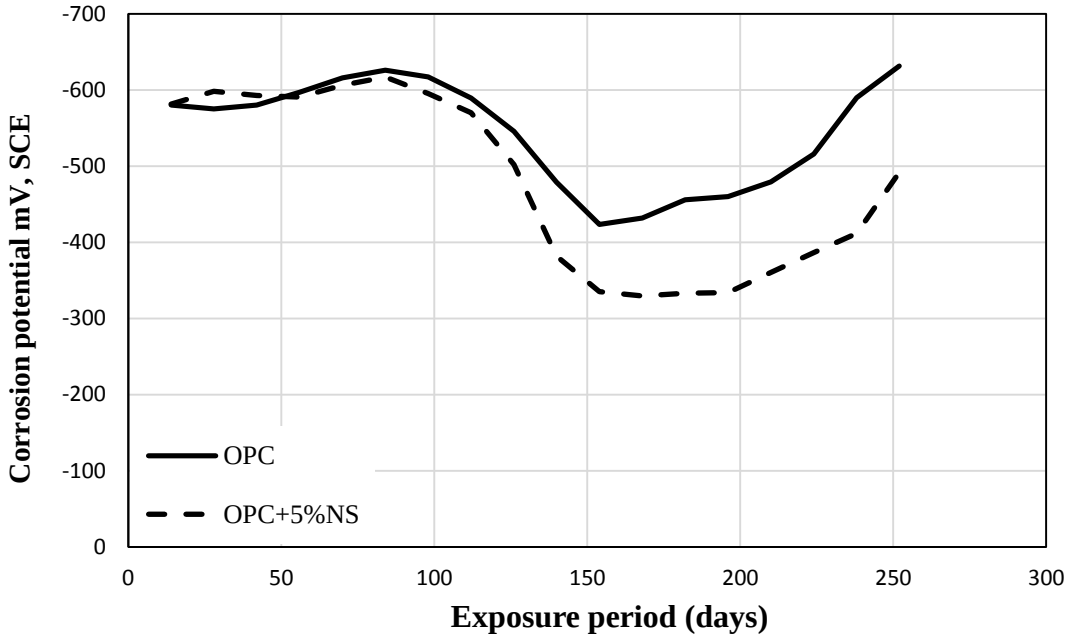

Figure 4.6: Corrosion potentials on steel in concrete with and without NS

Corrosion current density: The same concrete specimens prepared for measuring the corrosion potentials were used in evaluating the corrosion current density. Figure 4.7 shows the corrosion current density (I_{corr}) of concrete specimens with and without NS after 260 days of exposure. It is clear that utilizing 5% NS in the concrete caused a significant reduction in the I_{corr}.

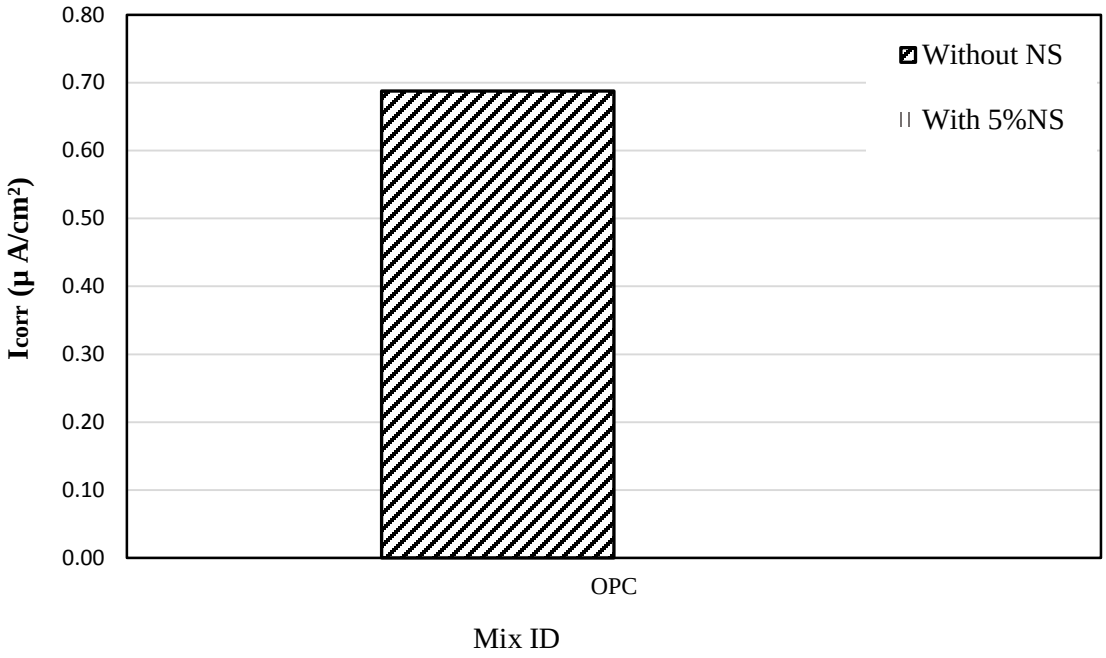

Figure 4.7: 260-day corrosion current density on steel in OPC concrete with and without NS

4.1.1.7 Sulfate attack

Two groups of specimens were prepared to evaluate the sulfate attack, the first group was mortar prisms (25×25×285mm) while the other group was cubes (25×25×25 mm) prepared from cement paste. The prisms were immersed in 2.1% sodium sulfate solution while the cubes were divided into two groups, one group was exposed to 2.1% sodium sulfate solution while the other group was exposed to 2.1% magnesium sulfate solution. The sulfate attack was assessed through measuring the expansion of the beams while the cubes were visually inspected. Figure 4.8 shows the expansion of OPC concrete specimens prepared with and without NS. It is clear that utilizing NS in the concrete, as a partial replacement of cement, significantly decreased the expansion due to sulfate attack. The edges of OPC cubes exposed in magnesium sulfate solution deteriorated while negligible

deterioration appeared on the surface of OPC+5%NS cube specimens (Figure 4.9). Deterioration was not noted in the specimens exposed to the sodium sulfate solution.

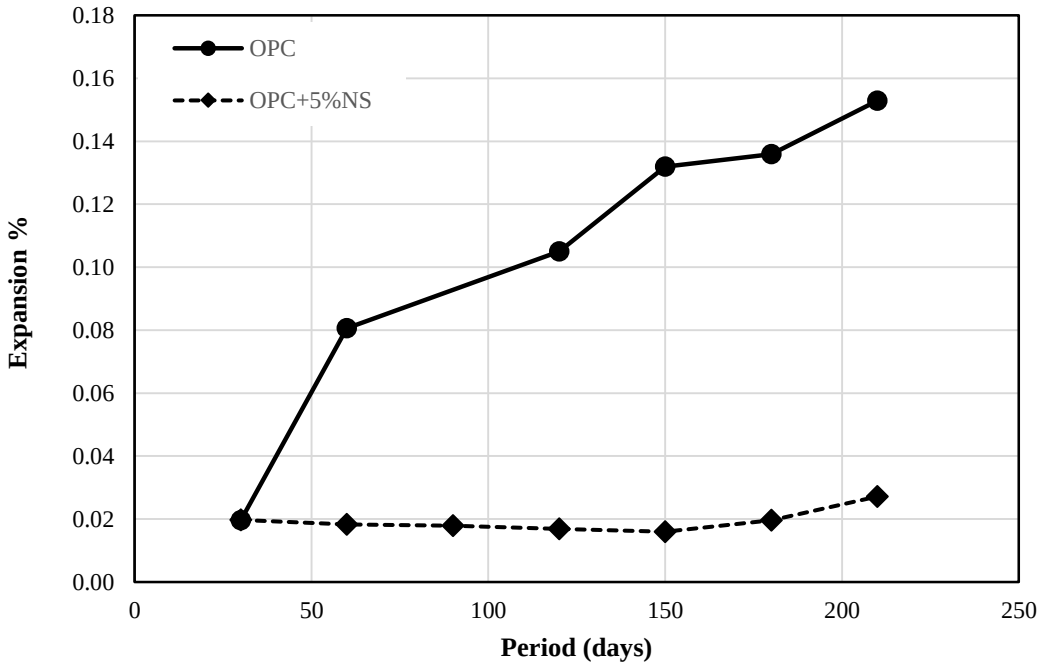

Figure 4.8: Expansion of OPC specimens prepared with and without NS

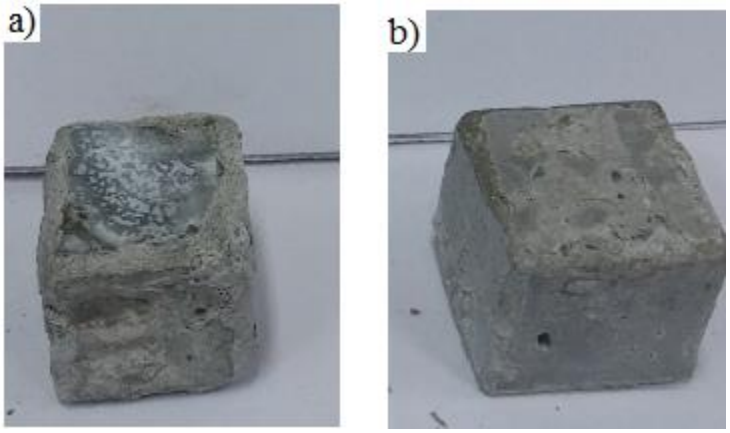

Figure 4.9: a) OPC cube and b) OPC+5%NS cube specimens exposed to magnesium sulfate solution.

4.1.2 Micro properties

4.1.2.1 Morphology

The scanning electron micrographs of OPC concrete specimens are shown in Figure 4.10. A normal morphology could be noted with the accumulation of calcium hydroxide (CH) at the interfacial zone between the paste and aggregates (Figure 4.10(a)). Further, a porous microstructure with cracks and CH is shown in Figure 4.10 (b and c). A dense microstructure could be noted in the OPC+5% NS specimen (Figure 4.11 (a)). More CSH gel and less CH appeared in the microstructure of OPC+5%NS specimen compared to that of OPC (Figure 4.11 (b&c)). The BEI images of OPC+5%NS showed better bond between the aggregate and paste compared to that of OPC specimens (Figure 4.11 (d) and Figure 4.10 (d)).

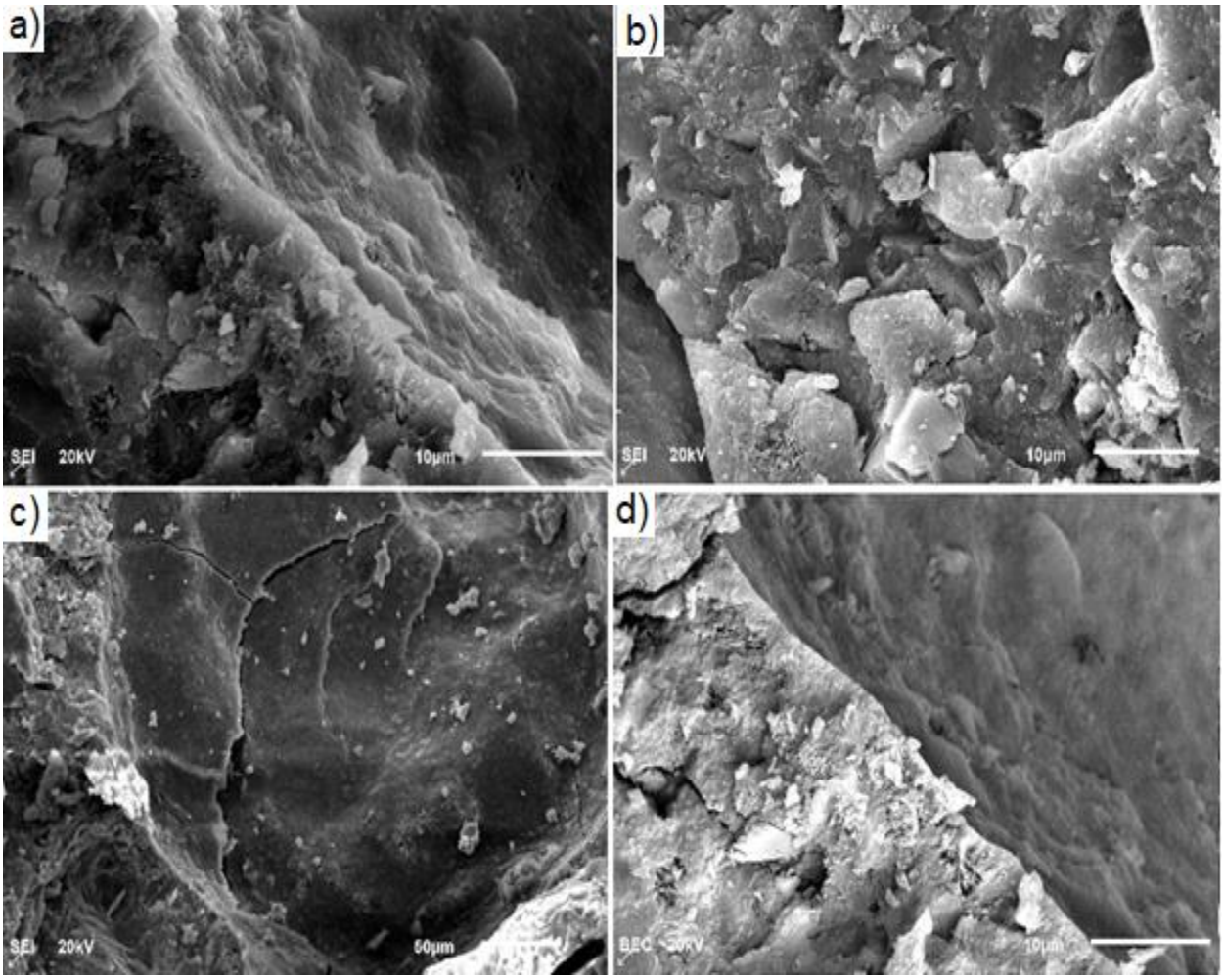

Figure 4.10: SEM and BEI images of OPC concrete specimen.

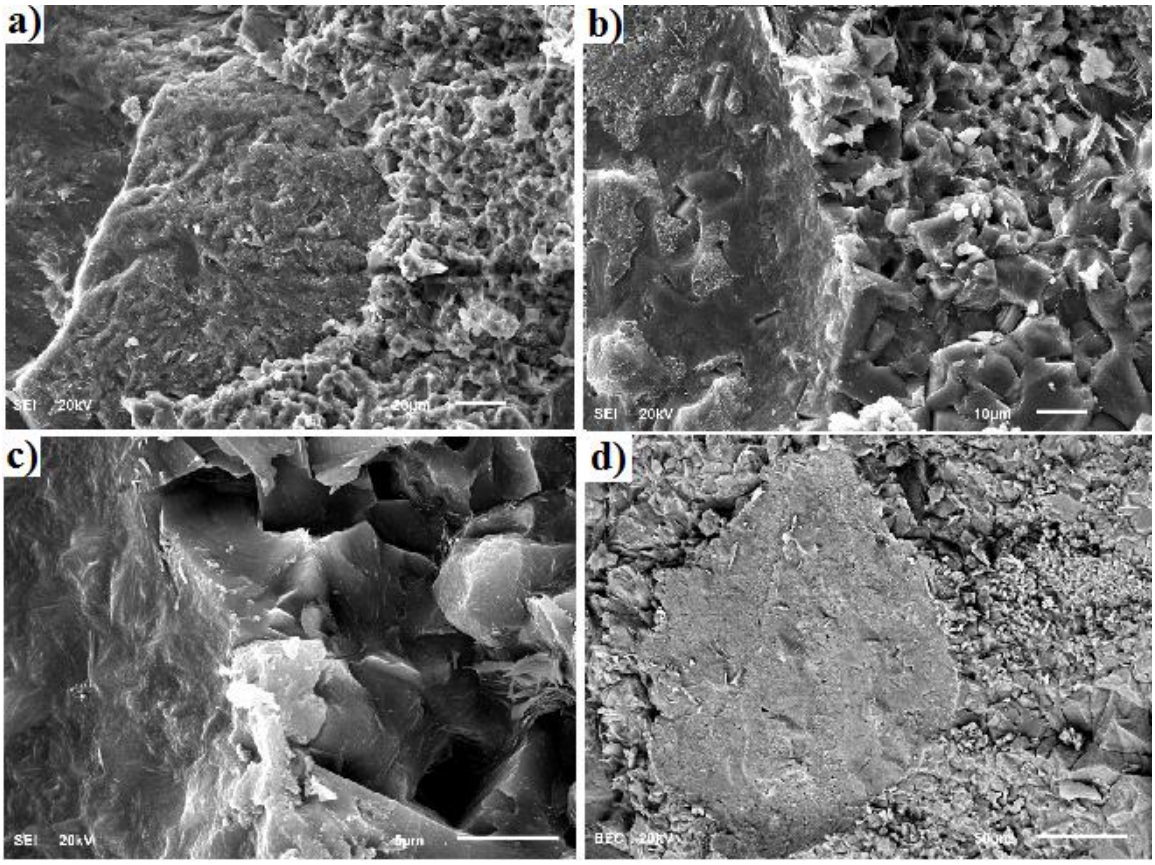

Figure 4.11: SEM and BEI images of OPC+5%NS concrete specimen

4.1.2.2 Mineralogical composition

The XRD spectra of OPC and OPC+5% NS are shown in Figure 4.12 and Figure 4.13, respectively. It is clear that utilizing NS in the concrete caused noticeable reduction in the calcium hydroxide peaks. Although 5% NS was added to the concrete, the quartz peaks did not change which proved that addition of 5% NS is the optimum dosage to be used. The XRD spectra of paste specimens exposed to the sodium sulfate solution is shown are shown in Figure 4.14. It can be noted that the intensity of the CH decreased, more gypsum was produced, and the secondary ettringite peak increased. Figure 4.15 depicts the XRD spectra for OPC+5%NS paste exposed to the magnesium sulfate solution. It is clear that the

gypsum peaks increased and CH further decreased compared to that of specimens cured in water.

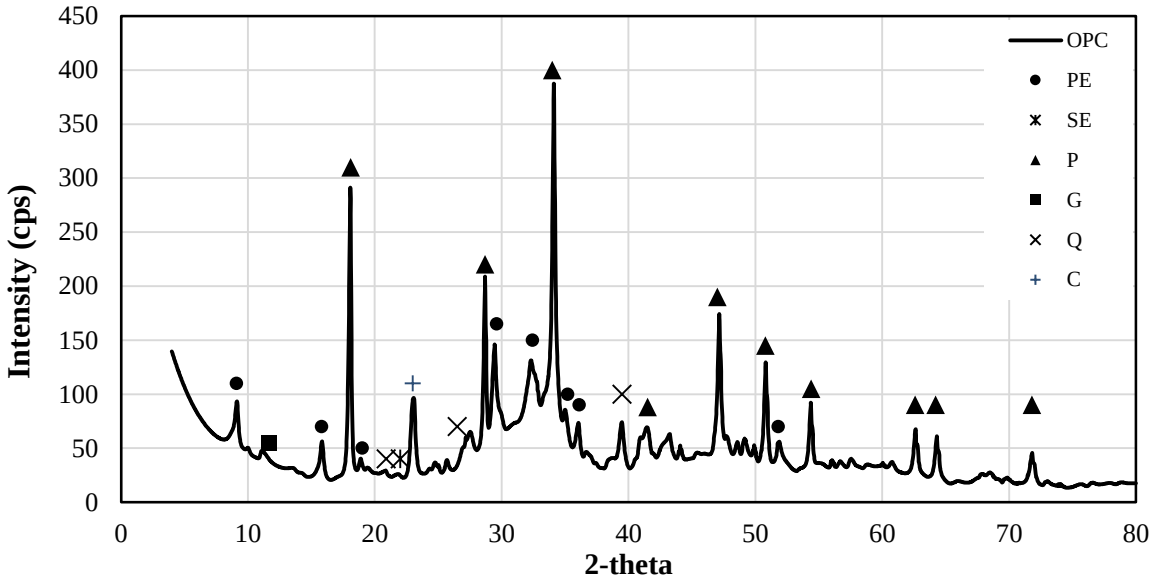

Figure 4.12: XRD spectra for OPC concrete specimens

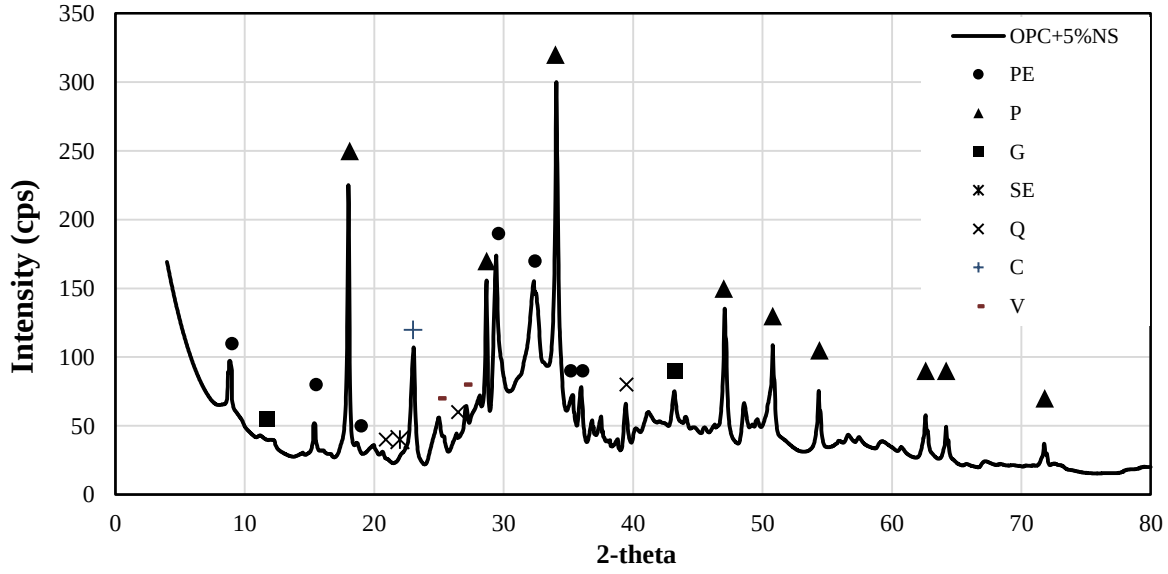

Figure 4.13: XRD spectra for OPC+5%NS specimens

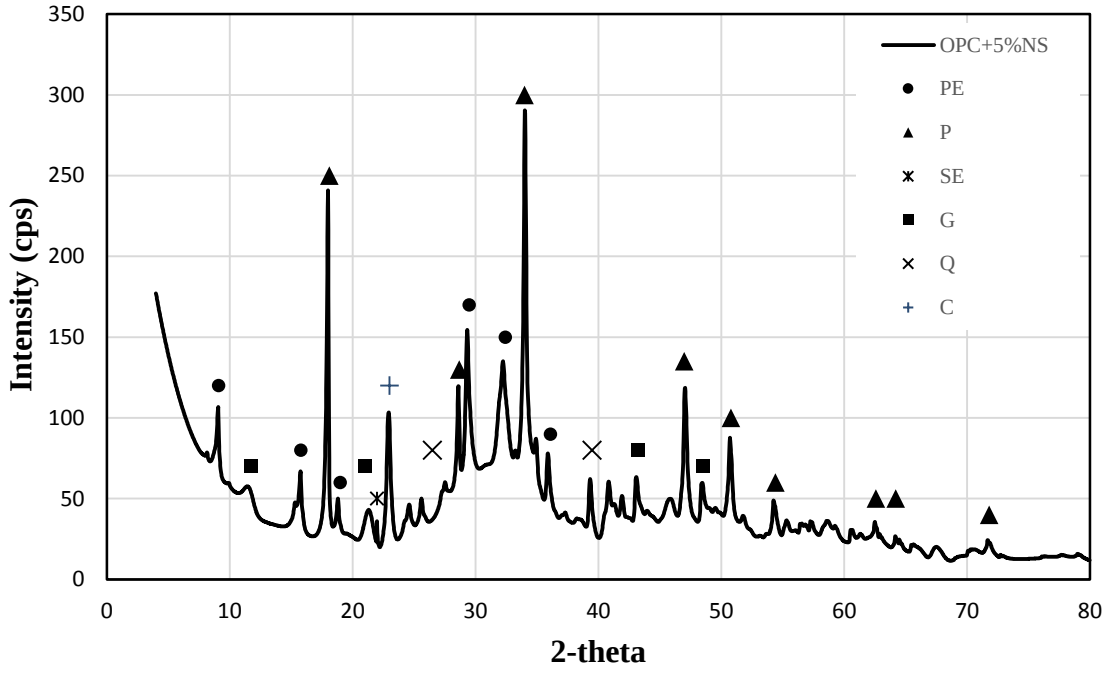

Figure 4.14: XRD spectra for OPC+5%NS specimens exposed to the sodium sulfate solution

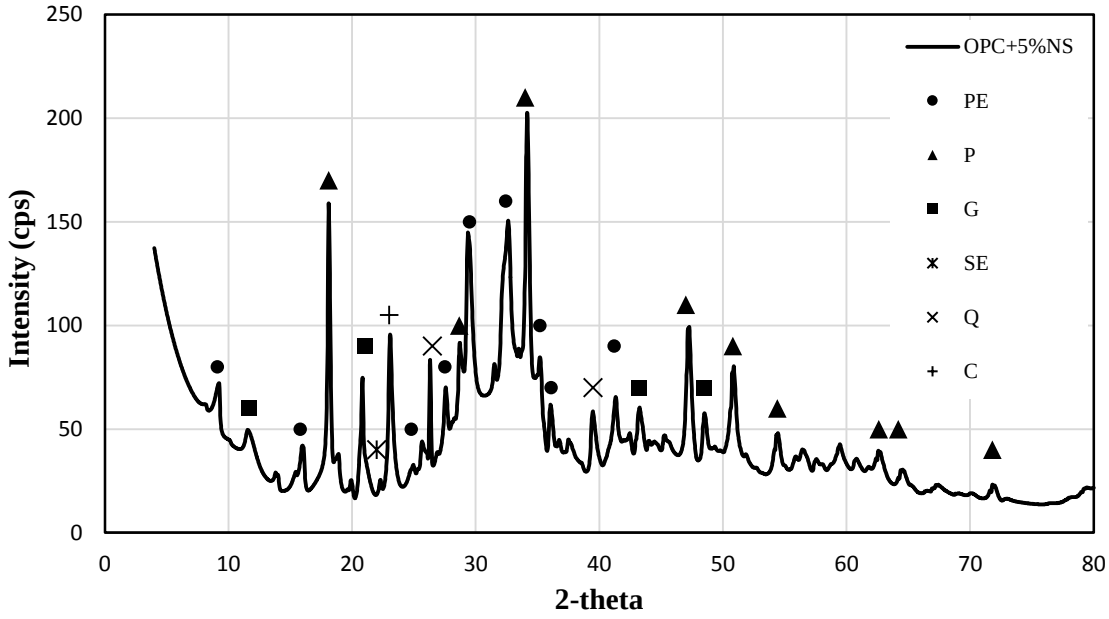

Figure 4.15: XRD spectra for OPC+5%NS specimens exposed to the magnesium sulfate solution

4.1.3 Discussion of results

Utilizing NS in OPC, as a partial replacement of cement, increased the strength. The enhancement in the compressive strength can be attributed to the formation of secondary C-S-H gel that was formed due to the pozzolanic reaction, which is the reaction between NS and CH and the physical action of NS, in which NS acts as a nuclei to the hydration products, fills the pores of CSH gel, and limits the growth of CH. The increase in the flexural strength due to the addition of NS may be attributed to the dense ITZ that resulted from the pozzolanic reaction, in which more CSH gel is produced and more CH was consumed which is normally accumulated at the ITZ making it weak. The XRD spectra of OPC+5%NS showed less CH compared to that in OPC which corroborates the chemical action of NS as well as the enhancement in the ITZ. SEM images of the OPC specimen with NS showed a compact micro structure with uniform and dense ITZ and a thin layer of CH at the ITZ. The dense microstructure and dense ITZ contributed to an increase in both the compressive and flexural strength of OPC concrete with 5%NS.

The drying shrinkage increased due to the use of 5%NS in the OPC concrete. The increase in the drying shrinkage of OPC+5%NS specimens may be attributed to the consumption of free water through the production of CSH gel and other hydration products. The dense structure of NS significantly decreased the chloride permeability and the chloride concentration at all depths. The dense structure delayed the diffusion of chloride ions, thereby decreasing the corrosion activity.

The presence of NS in concrete, as a partial replacement of cement, caused a significant reduction in concrete expansion due to sulfate attack which may be attributed to the consumption of CH in the reaction with NS. CH normally reacts with the available sulfate

ions to produce gypsum, which reacts with C_3A to produce ettringite. Due to a significant reduction in the quantity of CH in NS concrete, less ettringite is produced which decreased the concrete expansion. XRD spectra showed small peak of secondary ettringite in the OPC+5% NS specimens exposed in the sodium sulfate solution consequently there was a reduction in the expansion. The dense structure of NS concrete also delayed the diffusion of sulfate ions in to the specimens. Also, there was a reduction in the deterioration in the specimens. The reduction in the deterioration of the edges of OPC concrete may be attributed to the production of magnesium hydroxide from the reaction between magnesium sulfate and calcium hydroxide which caused reduction in the pH of the pore solution making CSH unstable. The negligible deterioration was noted in the OPC+5% NS specimen which may be attributed to the dense structure which delayed the diffusion of magnesium and sulfate ions. XRD spectra for the cube specimens exposed to the magnesium sulfate solution showed noticeable reduction in the CH and more gypsum. However, deteriorations was not noted in the specimens cured in the sodium sulfate solution which may be attributed to the short period of exposure.

4.2 Properties of CKD concrete prepared with and without NS

Three dosages of CKD (10%, 15%, and 20%) were used in preparing six different concrete mixes. Two mixes were prepared with same CKD dosages, one of them with 5% NS while the others were prepared without NS. Both CKD and NS were used in the concrete as a partial replacement of cement. The specimens were tested for the following macro- and micro-properties:

4.2.1 Macro properties

4.2.1.1 Compressive strength

Figure 4.16 depicts the compressive strength of CKD concrete specimens prepared without NS. The compressive strength of CKD concrete at different ages decreased compared with that of the control specimen (OPC). After 28 days, the compressive strength of specimens with 0%, 10%, 15% and 20% CKD was 58, 54.81, 54.08, and 53.08 MPa, respectively. The early strength of 10% CKD specimen was the highest compared with other CKD concrete specimens. The 3-day compressive strength of specimens with 0%, 10%, 15% and 20% CKD was 35.6, 41.04, 39.45, and 36.38 MPa, respectively. Due to the inclusion of NS in conjunctions with CKD, the compressive strength increased at all ages (Figure 4.17). At 28 days, the compressive strength of specimens with 10%, 15% and 20% CKD incorporating 5% NS was 70.23, 65.06, and 59.49 MPa, respectively. The presence of different dosages of CKD (10%, 15%, and 20%) in the mixes without NS caused a reduction in the 28-day compressive strength by 5.5%, 6.76%, and 8.48 %, respectively, compared with that of the control specimen (OPC). The use of 5% NS in the concrete with 10%, 15%, and 20% CKD improved the compressive strength by 21.09%, 12.17%, and 2.57%, respectively, compared to OPC (Figure 4.18). The use of 5% NS simultaneously with 10%, 15%, and 20% CKD concrete specimens, increased the 28-day compressive strength by 28.13%, 20.3%, and 12.08%, respectively (Figure 4.19).

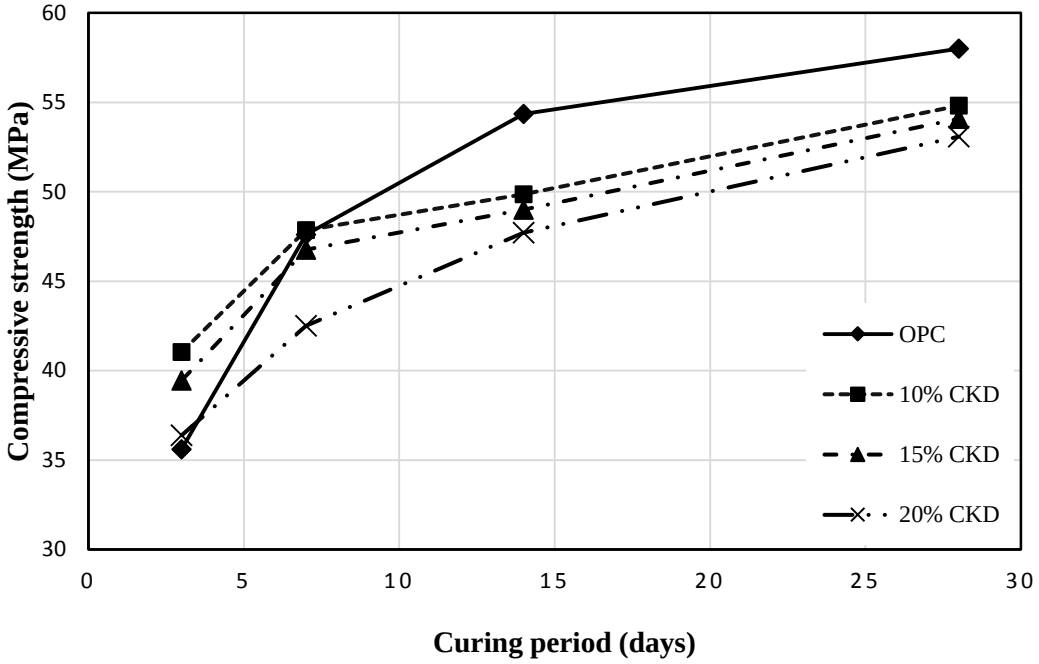

Figure 4.16: Compressive strength of CKD concrete without NS

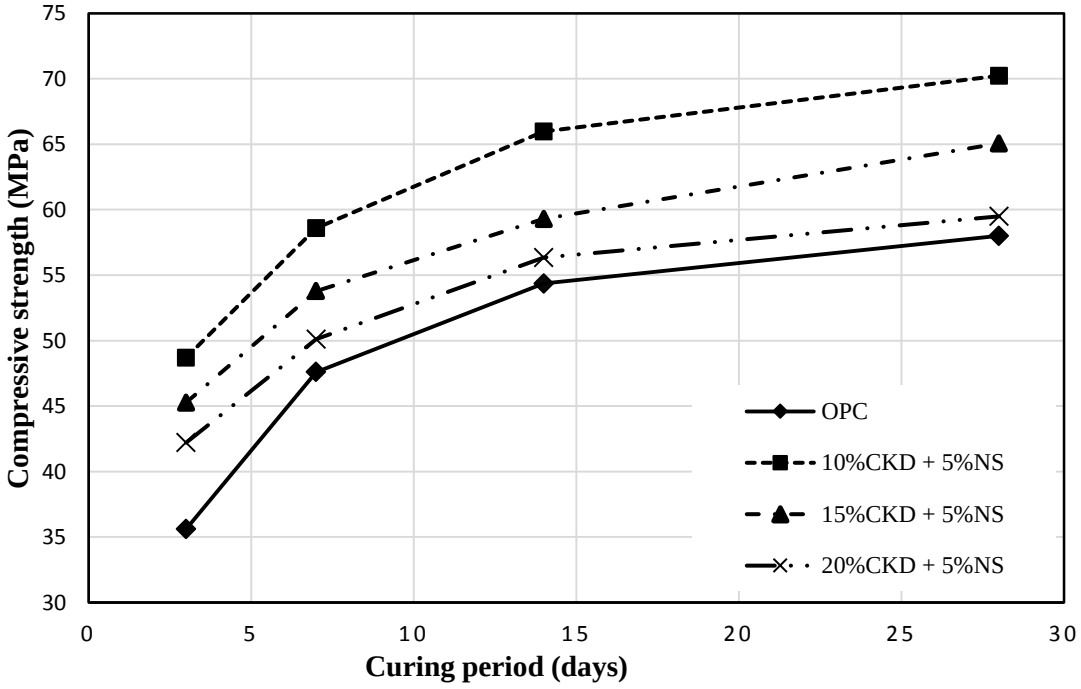

Figure 4.17: Compressive strength of CKD concrete with NS

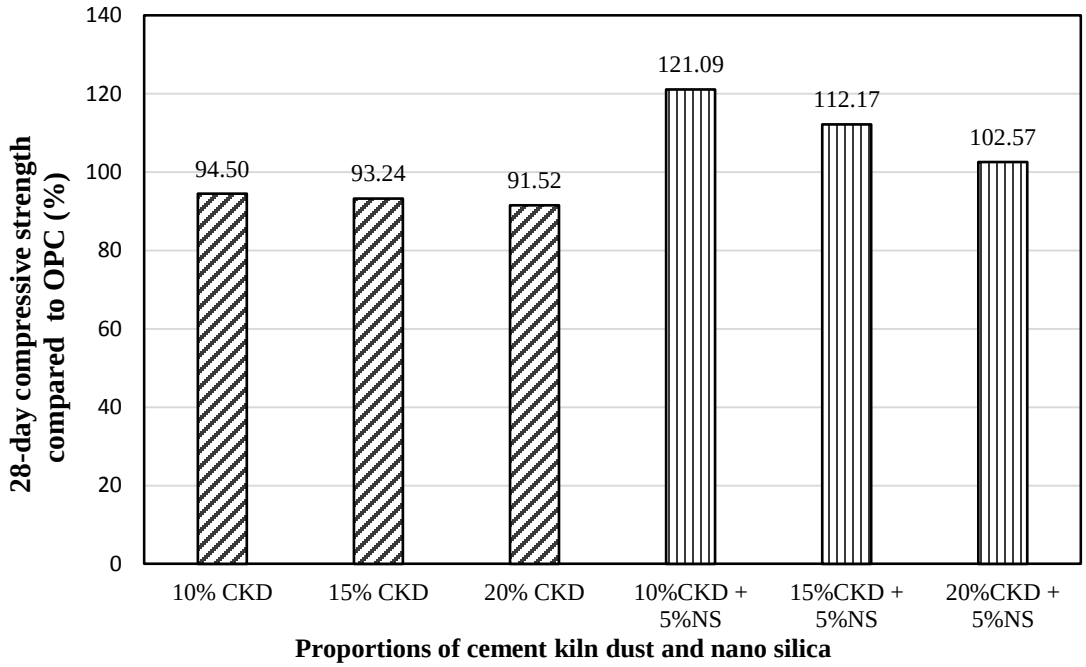

Figure 4.18: Change in 28-day compressive strength of CKD concrete specimens compared to OPC

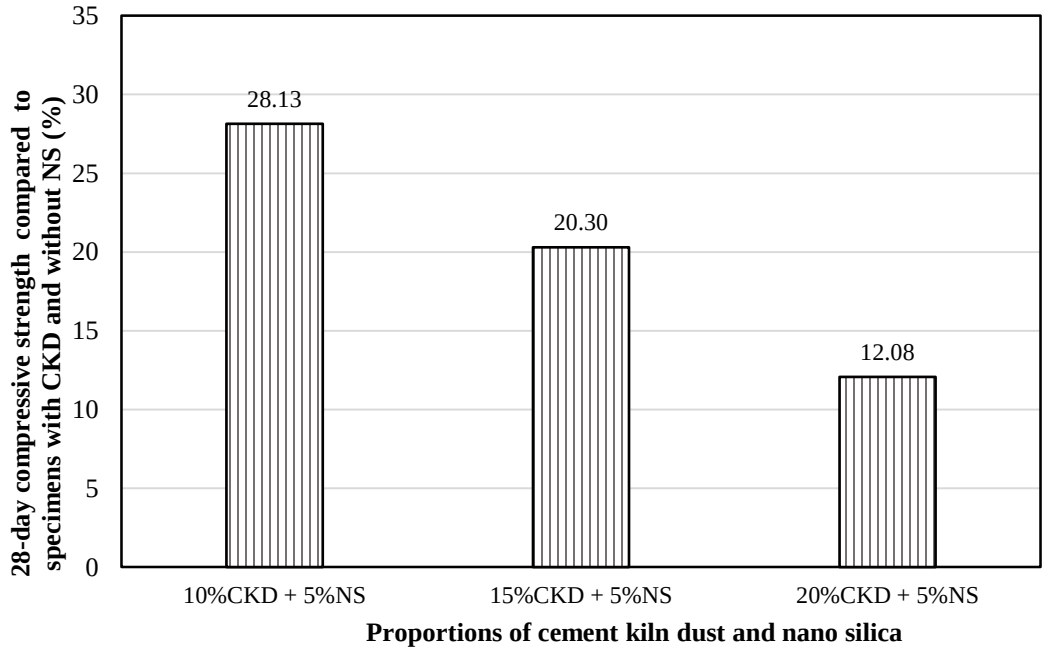

Figure 4.19: Effect of NS on the 28-day compressive strength of CKD concrete

4.2.1.2 Flexural strength

The flexural strength of CKD concrete specimens prepared with and without NS is shown in Figure 4.20. The flexural strength of specimens with 0%, 10%, 15%, and 20% CKD were 4.19, 3.95, 3.76, and 3.43 MPa, respectively. Due to utilizing 5% NS in conjunction with 10%, 15%, and 20% CKD, the flexural strength became 4.83, 4.51, and 3.9 MPa, respectively. As the percentage of CKD increased, the flexural strength decreased, it decreased, with respect to OPC by 5.8%, 10.26%, and 18.22% of specimens with 10%, 15%, and 20% CKD, respectively. The use of 5% NS in the concrete with 10% and 15% CKD, enhanced the flexural strength by 15.27% and 7.64% compared to OPC, respectively, while the strength of 20% CKD+5% NS was less than the strength of OPC by 6.92% (Figure 4.21). The increase in the flexural strength due to the addition of NS was 22.38%, 19.95% and 13.81% of specimens with 10%, 15%, and 20% CKD, respectively (Figure 4.22).

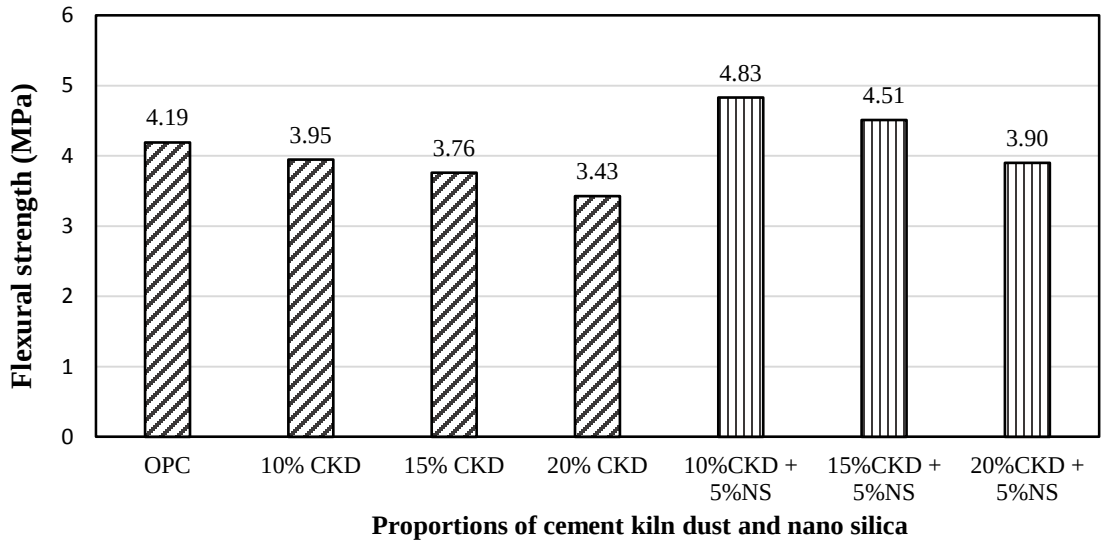

Figure 4.20: Flexural strength of CKD concrete specimens

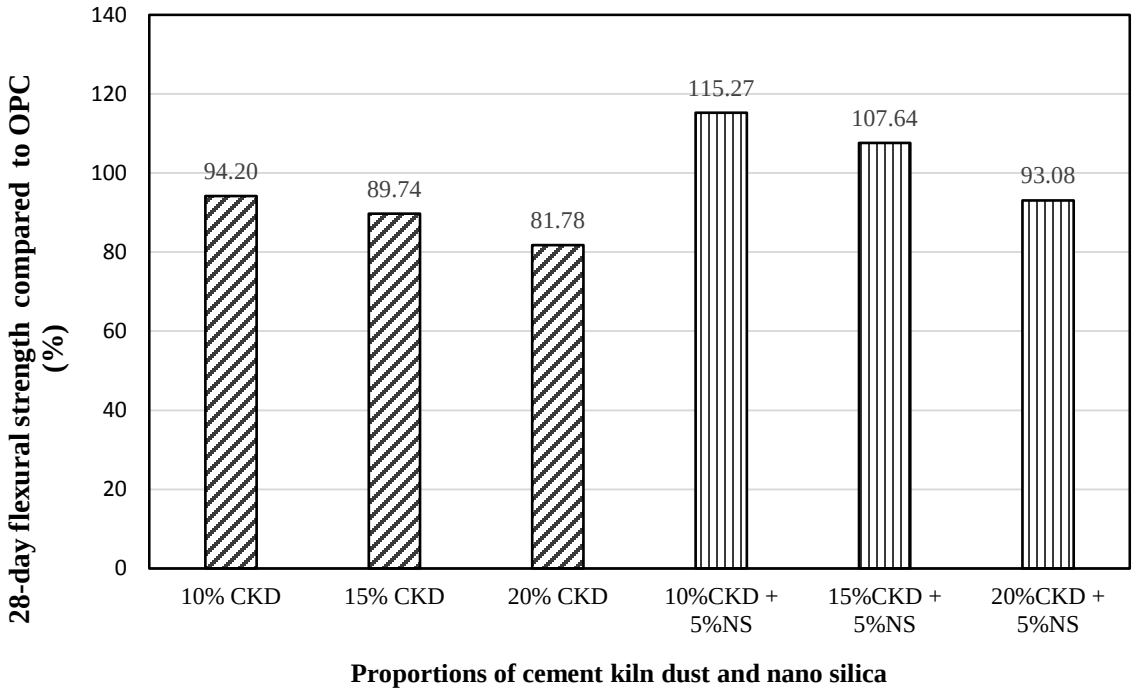

Figure 4.21: Change in the 28-day flexural strength of CKD concrete specimens with and without NS compared to OPC

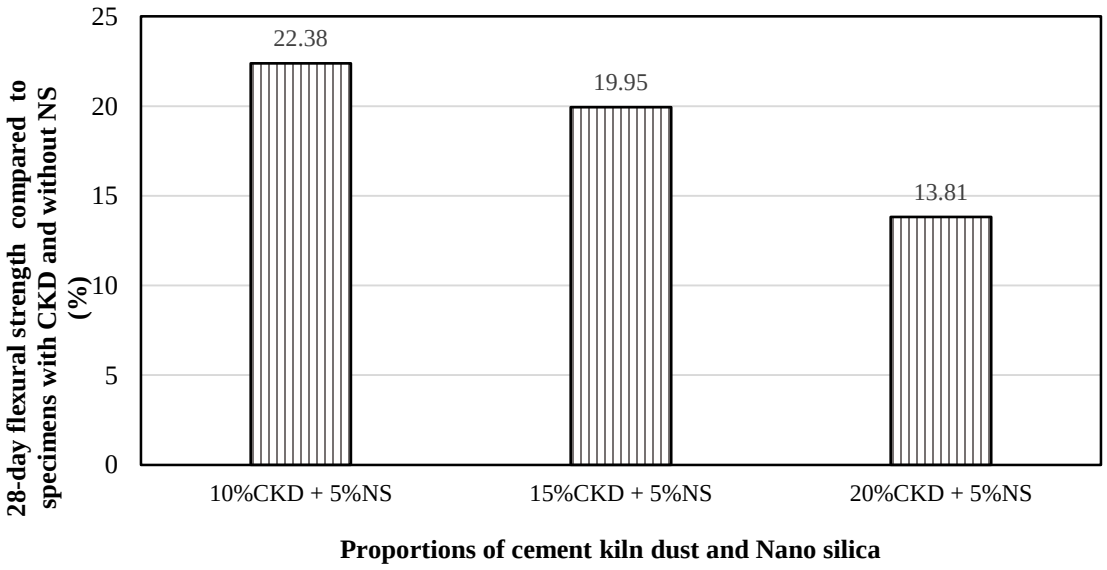

Figure 4.22: Change in the 28-day flexural strength of CKD concrete specimens due to the inclusion of NS

4.2.1.3 Drying shrinkage

The drying shrinkage of CKD concrete specimens increased as the dosage of CKD was increased, as depicted in Figure 4.23. The use of NS in the CKD concrete specimens increased the shrinkage further (Figure 4.24). However, the 7-day shrinkage of all the specimens was less than 500 µm, the threshold value considered to avoid failure due to drying shrinkage.

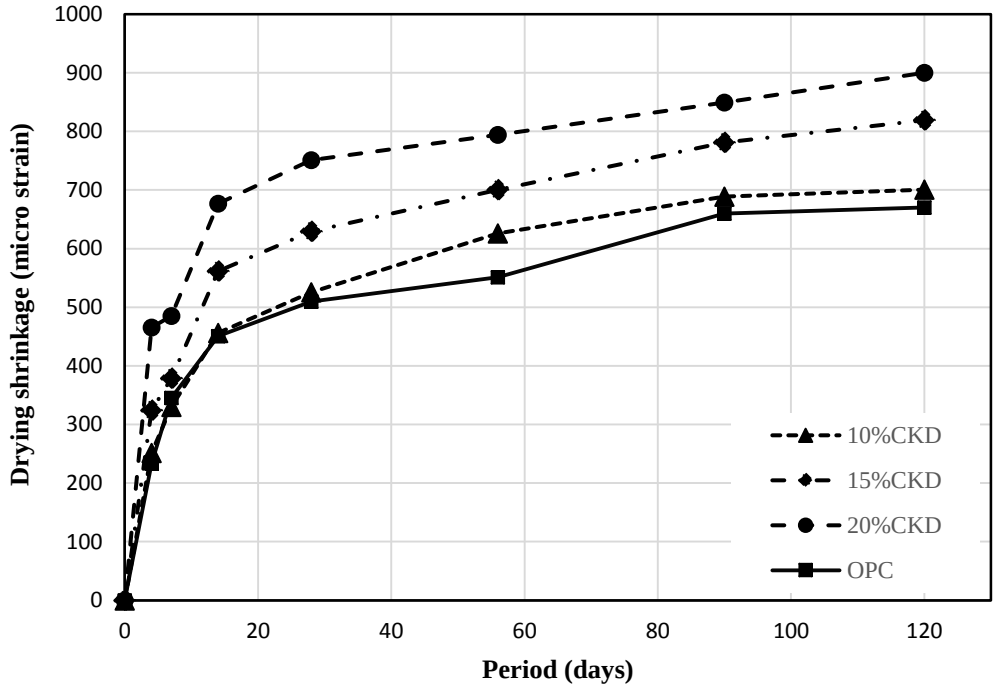

Figure 4.23: Drying shrinkage of CKD cement concrete specimens.

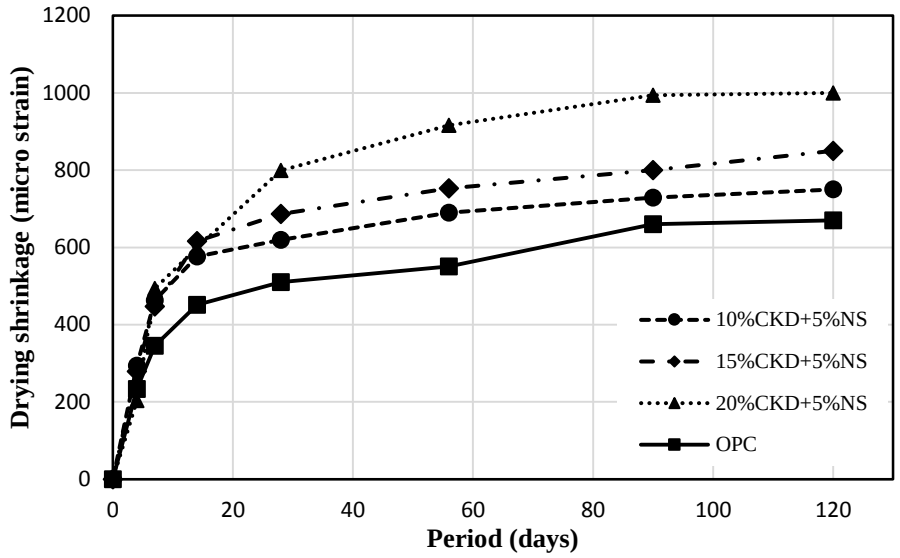

Figure 4.24: Drying shrinkage of CKD concrete incorporating NS.

4.2.1.4 Rapid chloride permeability

The chloride permeability increased due to the use of CKD in concrete. However, the use of NS in the CKD concrete significantly decreased its chloride permeability. The charge passed in coulombs through each specimen is shown in Figure 4.25.

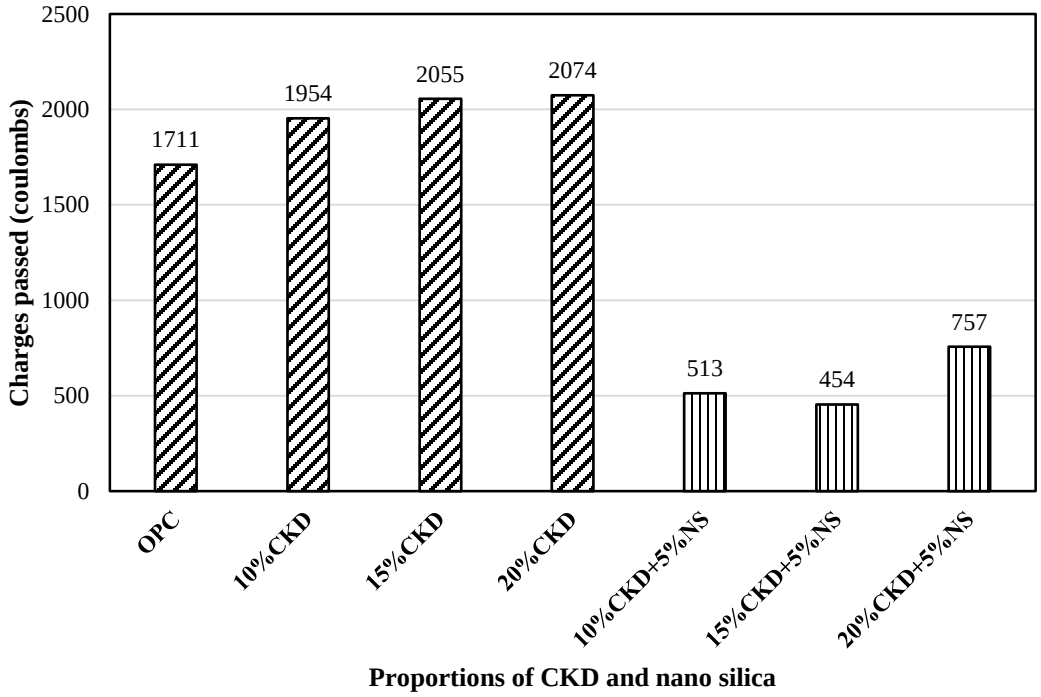

Figure 4.25: Rapid chloride permeability of CKD concrete specimens prepared with and without NS.

4.2.1.5 Chloride diffusion

The chloride profiles of CKD concrete with and without NS are shown in Figure 4.26, Figure 4.27, and Figure 4.28. It can be noted that the chloride concentration increased as the dosage of CKD increased at different depths. However, the chloride concentration decreased due to the use of 5%NS, as a partial replacement of cement. At depth of 40 mm the chloride concentration in all the CKD concrete specimens became almost equal but it was more than that in the OPC. The slope of the chloride profile of CKD concrete with NS was more than that of CKD concrete without NS. The resulting chloride profiles were utilized to determine the coefficients of chloride diffusion in accordance with Fick's second law of diffusion [59]. The coefficient of chloride diffusion of OPC, 10%CKD, 15%CKD, and 20%CKD concrete was 21.78, 24.8, and 29.86 $\times 10^{-8}$ cm^2/s, respectively, while it

decreased in specimens with NS, which was 14.87, 16.18, and 16.96 $\times 10^{-8}$ cm^2/s for 10%CKD+5%NS, 15%CKD+5%NS, and 20%CKD+5%NS concrete specimens, respectively (Figure 4.29).

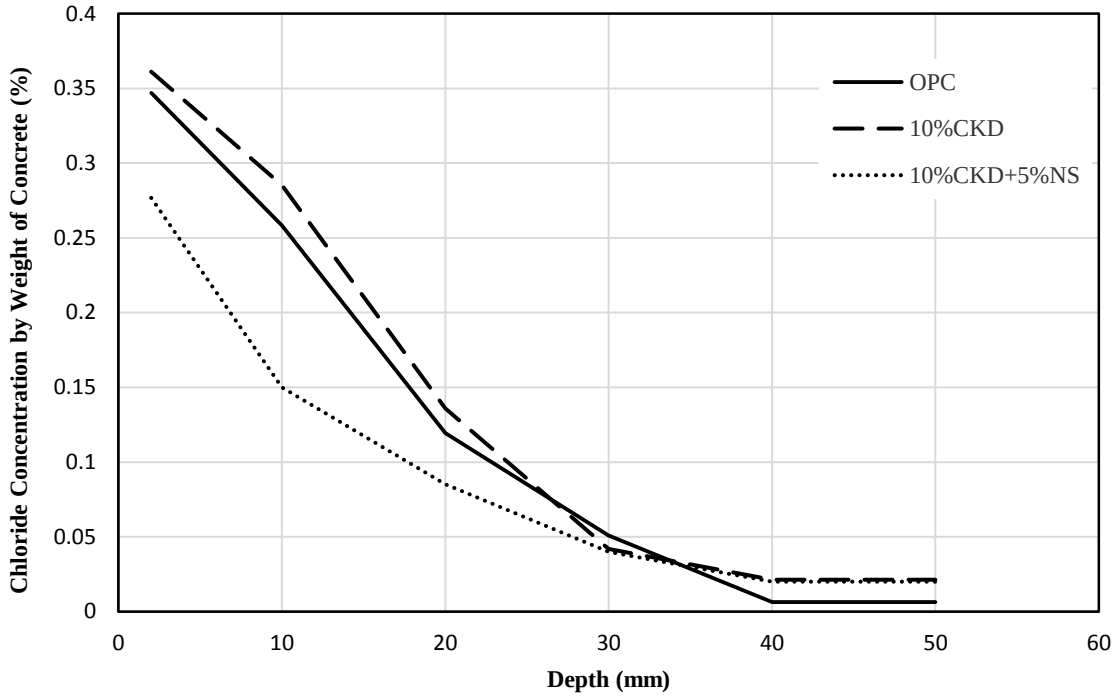

Figure 4.26: Chloride profile for 0% and 10% CKD concrete prepared with and without NS

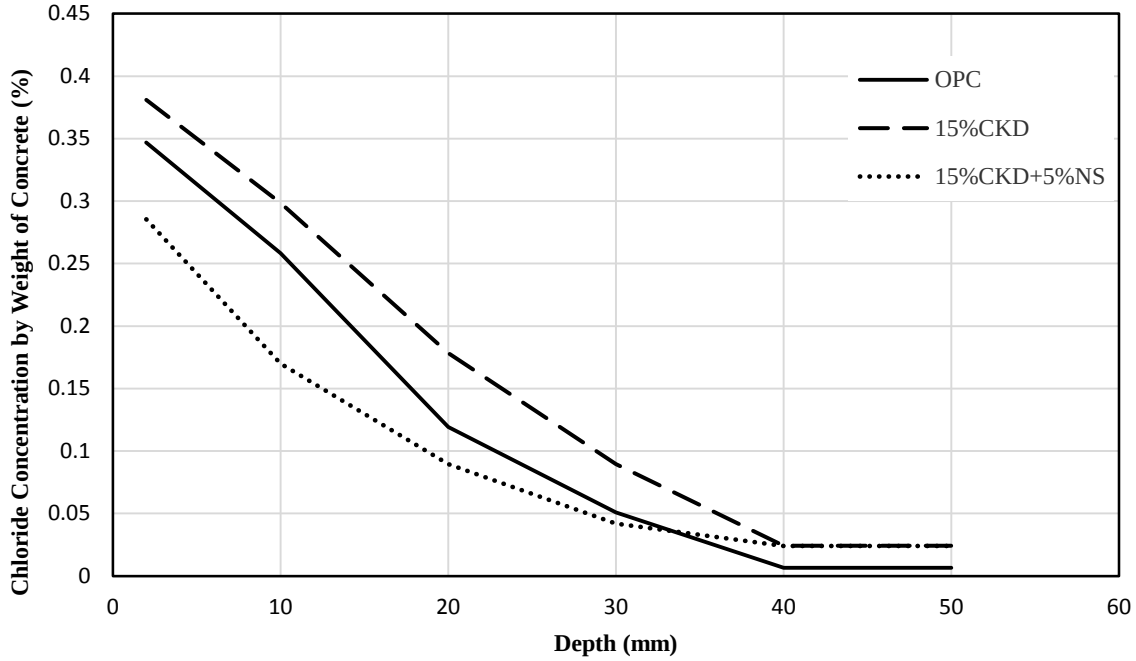

Figure 4.27: Chloride profile for 0% and 15% CKD concrete prepared with and without NS

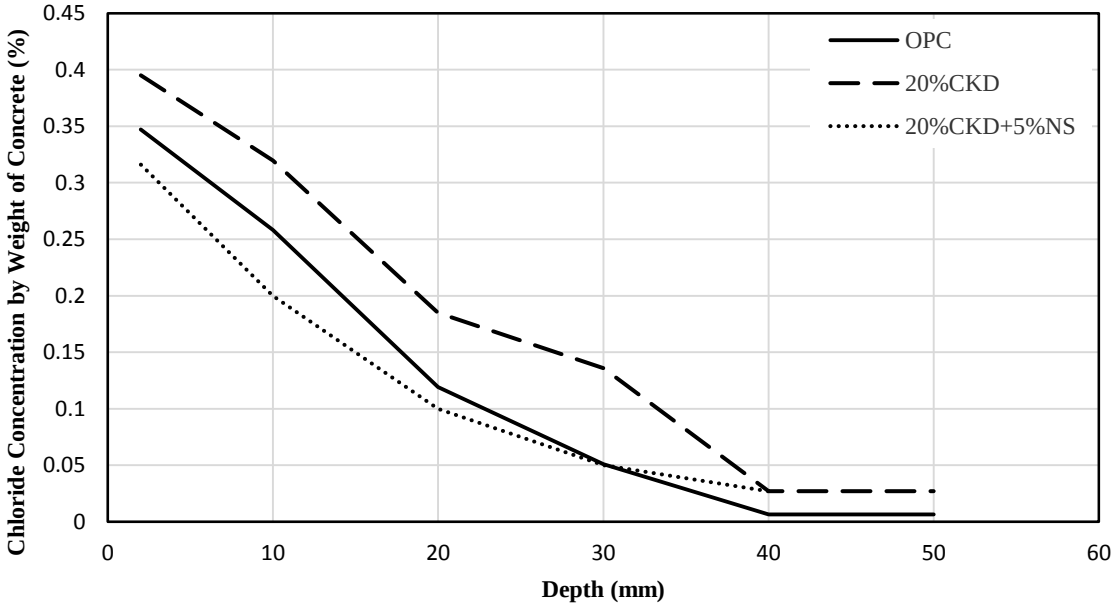

Figure 4.28: Chloride profile of 0% and 20% CKD concrete with and without NS

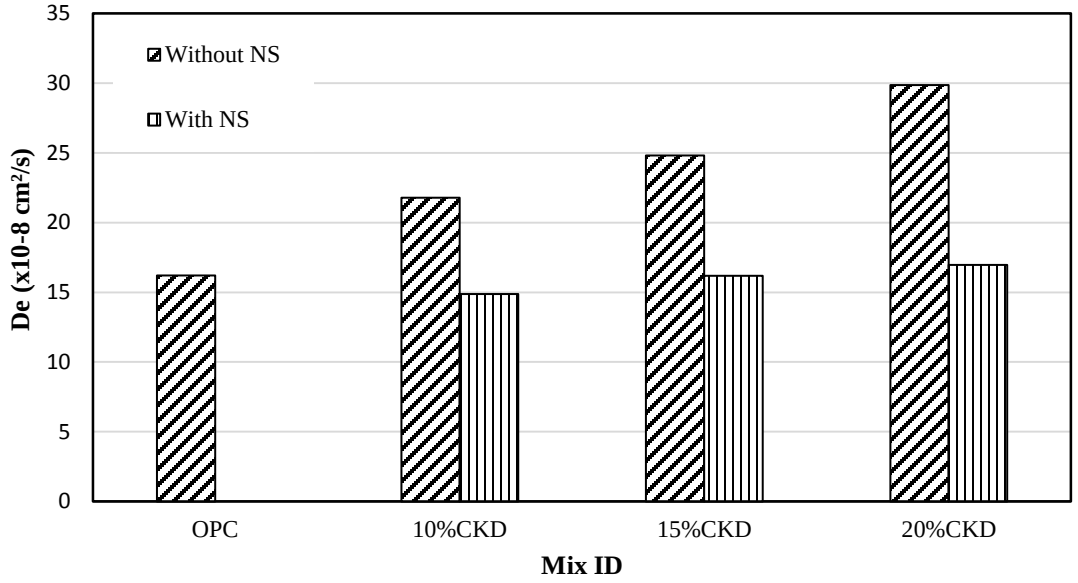

Figure 4.29: Chloride diffusion coefficients of CKD concrete prepared with and without NS

4.2.1.6 Reinforcement corrosion

Corrosion potentials: After 28 days of water curing, concrete cylinders with 12 mm steel bars, were exposed to 5% chloride solution for six months. Three cylinders were prepared from each mix. The difference in potential was measured for each concrete cylinder with respect to a saturated calomel reference electrode (SCE) and the average potential was recorded periodically. Figure 4.30, Figure 4.31, and Figure 4.32 depict the corrosion potential (E_{corr}) on steel in CKD concrete specimens prepared with and without NS. The potential values increased as the dosage of CKD was increased, while utilizing NS in the concrete decreased the corrosion potential. The corrosion potential of 10% and 15% CKD with NS was less than that of OPC, while the E_{corr} of 20%CKD concrete with NS was almost similar to that of OPC concrete.

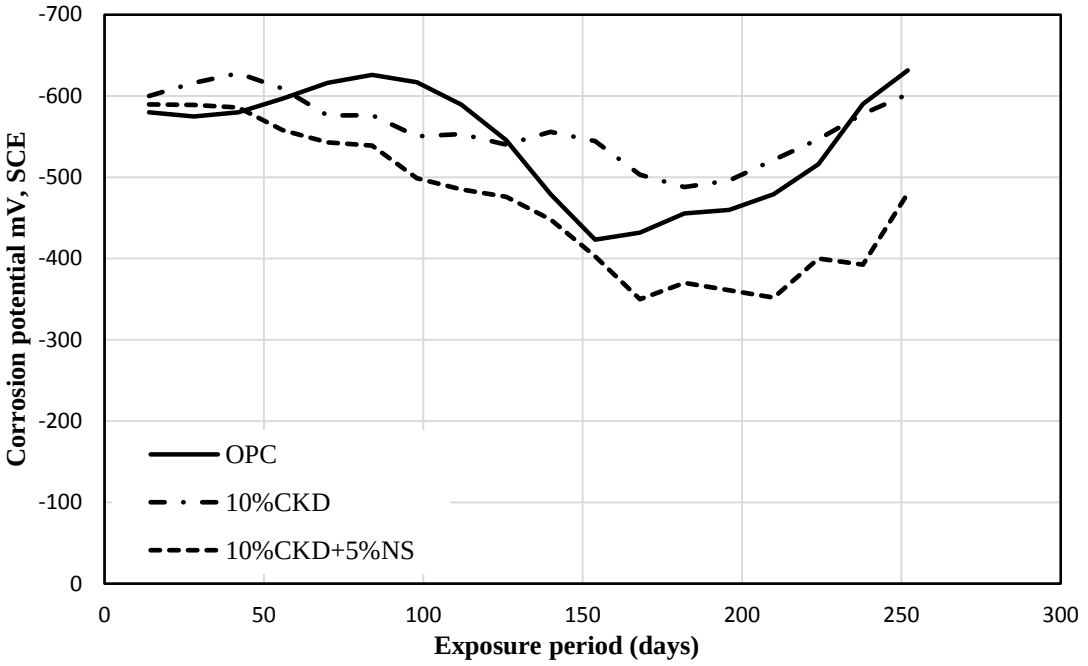

Figure 4.30: Corrosion potential on steel in 0% and 10% CKD concrete prepared with and without NS

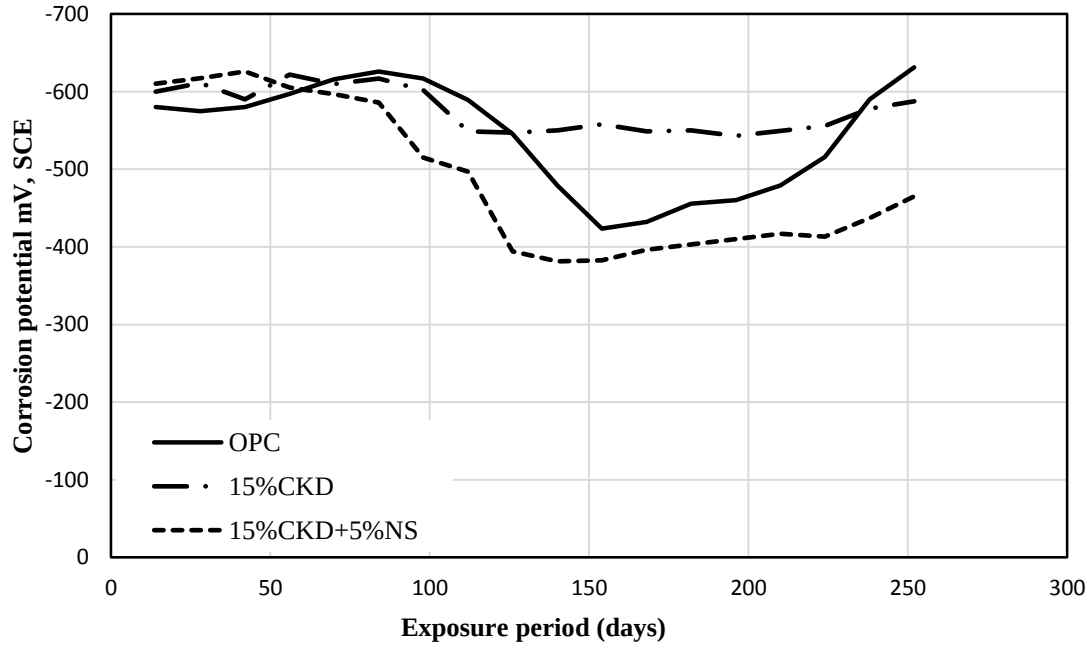

Figure 4.31: Corrosion potential on steel in 0% and 15% CKD concrete prepared with and without NS

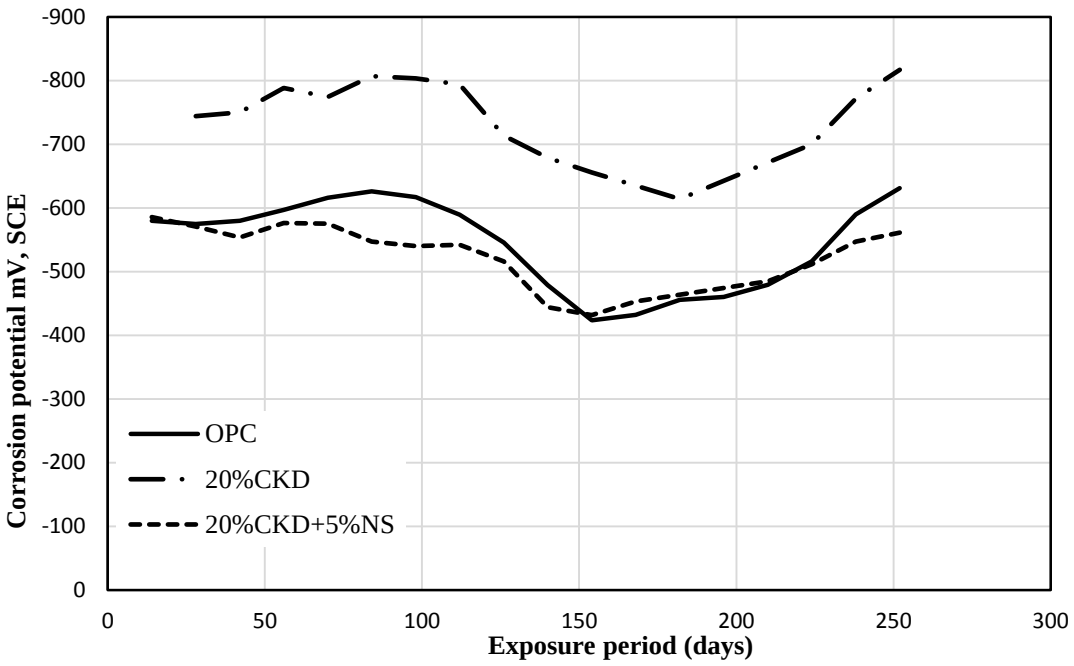

Figure 4.32: Corrosion potential on steel in 0% and 20% CKD concrete prepared with and without NS

Corrosion current density: After 260 days, the corrosion current density (I_{corr}) of the same concrete cylinders used for the purpose of measuring corrosion potentials was measured. Utilizing 15% and 20% CKD in the concrete as a partial replacement of cement increased the I_{corr} compared to that of OPC, while utilizing 10% CKD in concrete caused a slight reduction in the I_{corr}. Using 5% NS in conjunctions with CKD caused a significant reduction in the I_{corr} compared to that of CKD concrete without NS (Figure 4.33).

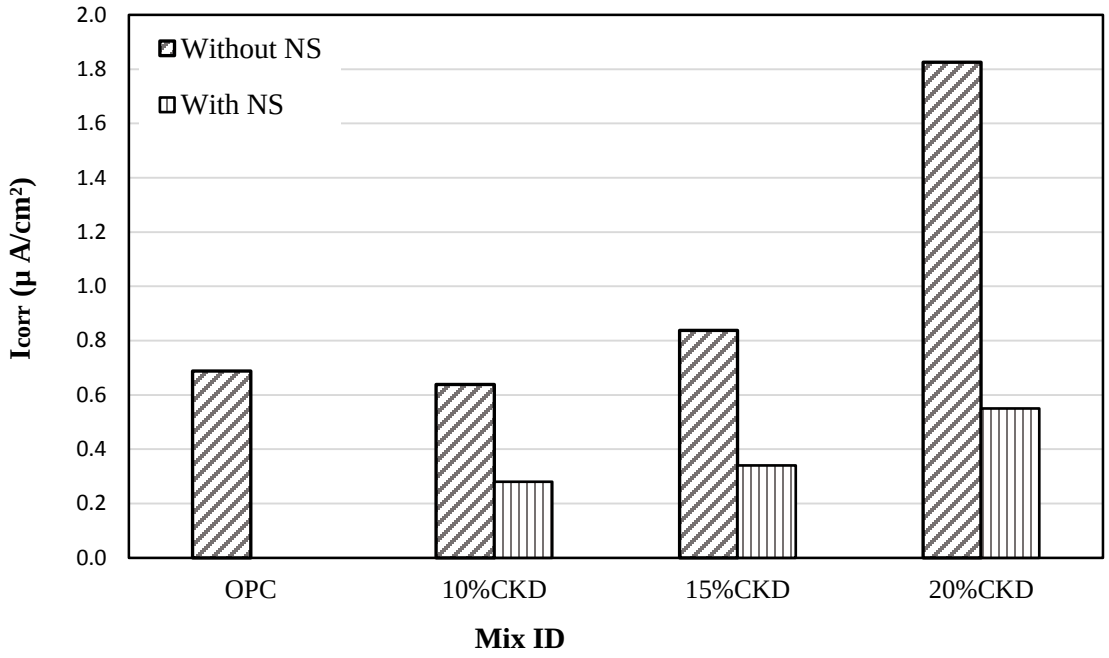

Figure 4.33: 260-day corrosion current density on steel in CKD concrete prepared with and without NS

4.2.1.7 Sulfate attack

The sulfate attack was assessed by measuring the expansion of the mortar prisms (25×25×285 mm) and by visual inspection of the deterioration of paste cubes (25×25×25 mm) cured in two different sulfate solutions. The prisms were immersed in 2.1 % sodium sulfate solution for six months while the cubes were divided into two groups, one group was exposed to 2.1% sodium sulfate solution while the other was exposed in 2.1% magnesium sulfate solution. Figure 4.34, Figure 4.35, and Figure 4.36 show the expansion of CKD concrete specimens with and without NS. It is clear that utilizing CKD in the concrete, as a partial replacement of cement, significantly increased the expansion, while utilizing NS in CKD concrete decreased the expansion compared to that of CKD concrete without NS. As the dosage of CKD increased, the expansion of the concrete with and without NS increased. The expansion of 10% and 15% CKD concretes with NS reduced

compared to that of OPC. The deterioration started at the edges of the CKD paste cubes cured in Magnesium sulfate solution (Figure 4.37, Figure 4.38, and Figure 4.39) while no noticeable deterioration was noted at the surface of NS paste cubes. Further, deterioration was not noted in the specimens exposed to the sodium sulfate solution.

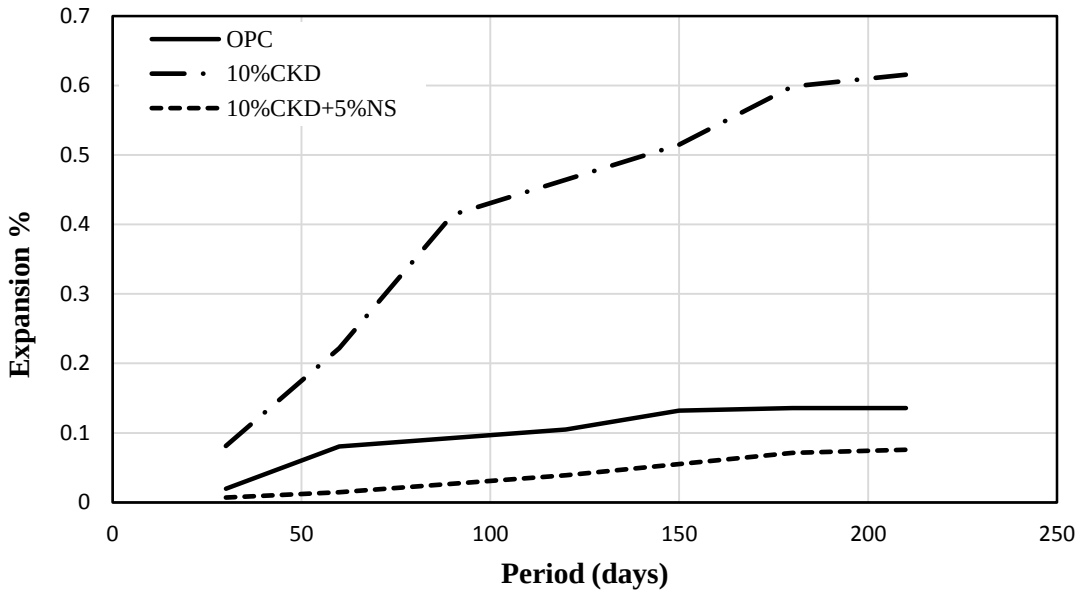

Figure 4.34: Expansion of 0% and 10% CKD concrete prepared with and without NS

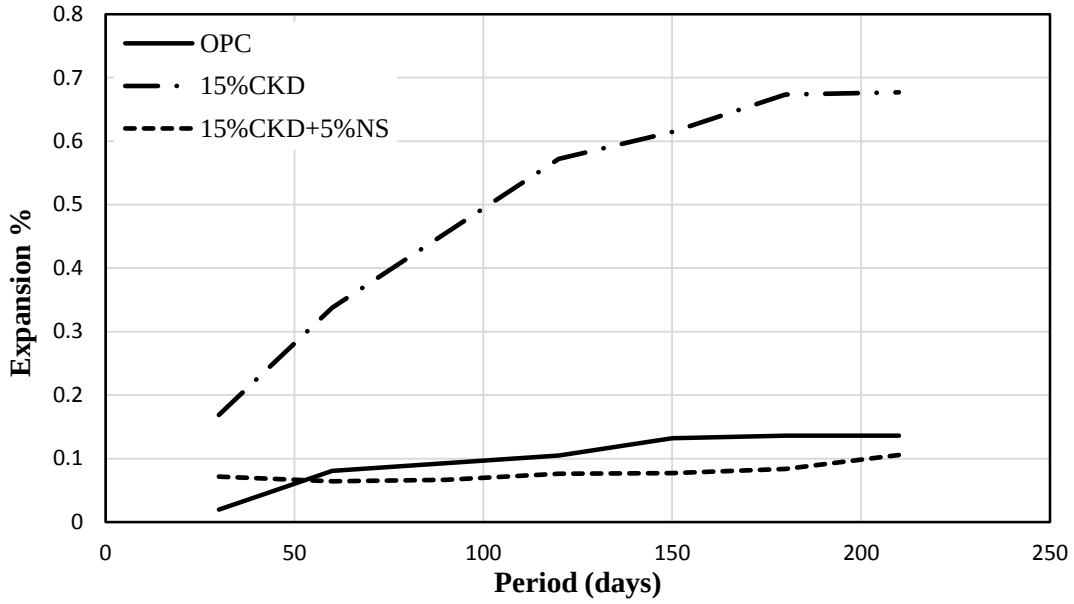

Figure 4.35: Expansion of 0% and 15% CKD specimens prepared with and without NS

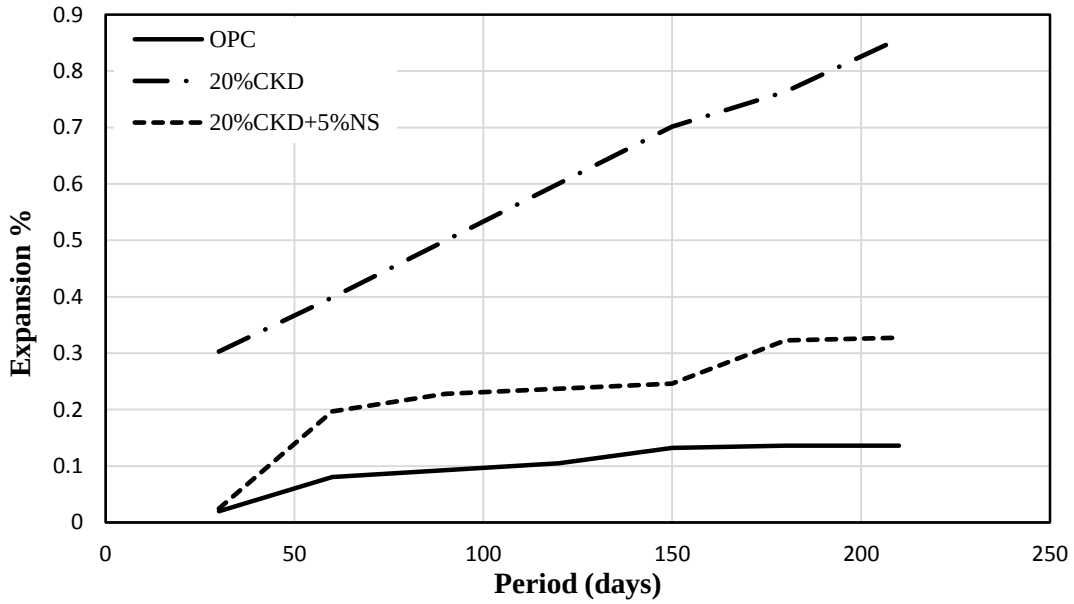

Figure 4.36: Expansion of 0% and 20% CKD specimens prepared with and without NS

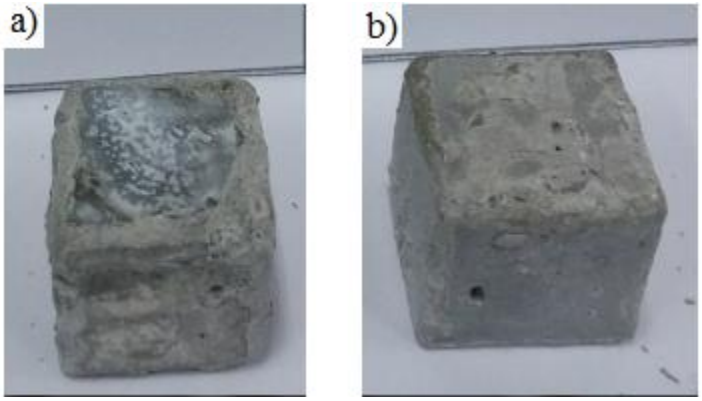

Figure 4.37: a) 10% CKD cube and b) 10%CKD+5%NS cube exposed to magnesium sulfate solution.

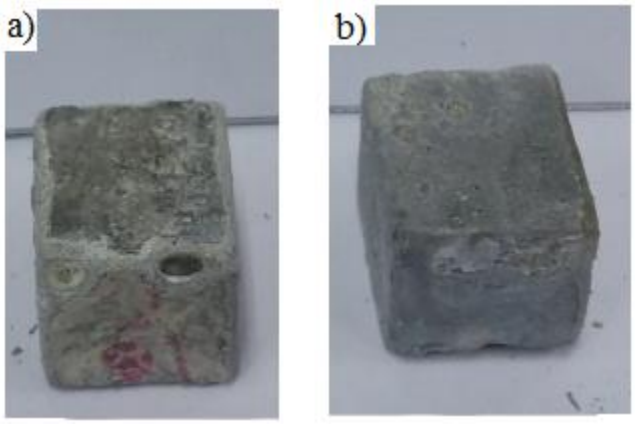

Figure 4.38: a) 15%CKD cube and b) 15%CKD+5%NS cube exposed to magnesium sulfate solution.

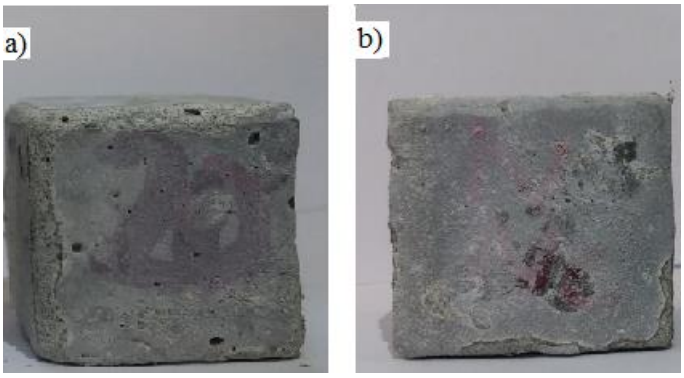

Figure 4.39: a) 20% CKD cube and b) 20%+5% NS cube exposed to magnesium sulfate solution.

4.2.2 Micro properties

4.2.2.1 Morphology

The scanning electron micrograph of 10% CKD specimen is shown in Figure 4.40. The morphology of 10%CKD concrete showed cracks at the interfacial transition zone between the aggregate and the paste (Figure 4.40(a)) as well as high quantity of CH is accumulated at the same zone (Figure 4.40(b &c)). The crystalline structure of CH and the ettringite needles appeared in the microstructure of 10% CKD specimens which make the micro structure porous (Figure 4.40(d)).

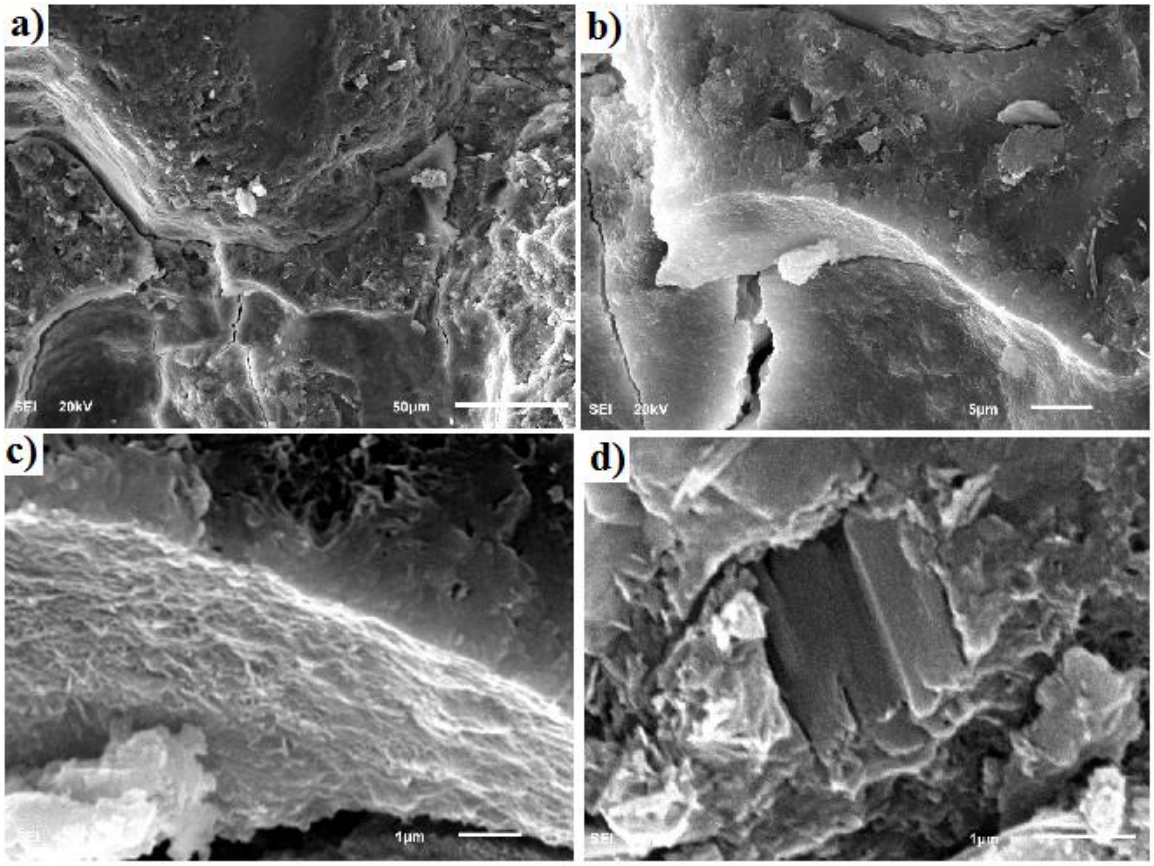

Figure 4.40: SEM of 10%CKD concrete specimen

The micrographs for the specimen with 10%CKD+5%NS show large quantity of C-S-H **(**Figure 4.41 (a)). Due to the pozzolanic action and filling action of NS, the ITZ became dense (Figure 4.41 (b) and (c)). The BEIs of concrete specimen with 10% CKD+5% NS showed good bond between the aggregate and the binder (Figure 4.41 (d) compared to that noted in the OPC concrete. A good bond between the aggregate and the paste was also noted in the speciemn with 20%CKD+5%NS but not as the bond noted in 10%CKD+5%NS specimen. More Cracks were noted in the microstructure of 20%CKD+NS specimen compared to that in 10%CKD+5%NS specimen (Figure 4.42).

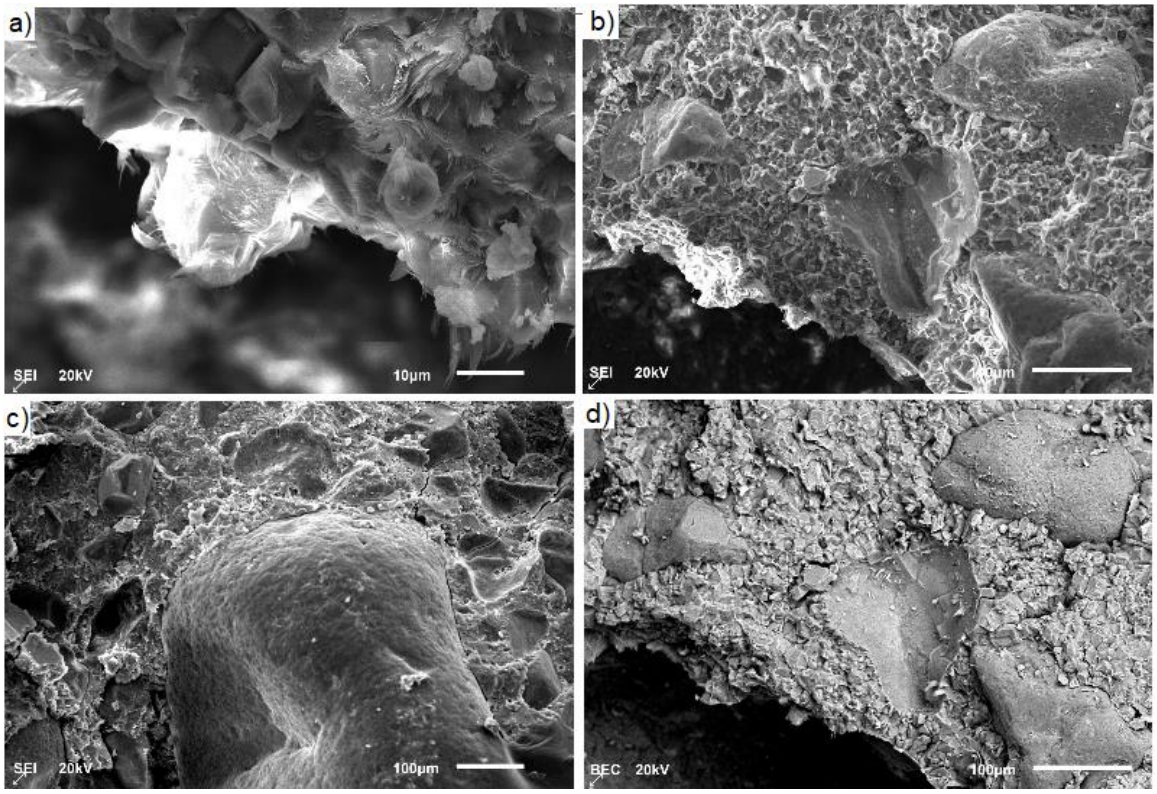

Figure 4.41: SEM and BEI images of 10%CKD+5%NS concrete specimen

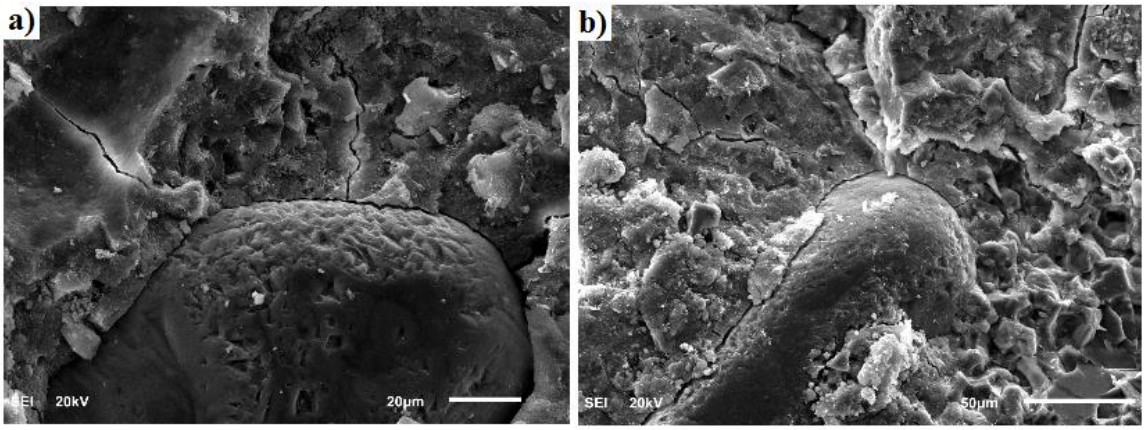

Figure 4.42: SEM images of 20%CKD+5%NS concrete specimen

4.2.2.2 Mineralogical composition

The XRD spectra of 10% CKD paste are shown in Figure 4.43. More secondary ettringite and gypsum can be noted in the spectrum of 10% CKD paste specimen compared to that of 0%CKD paste specimen. A reduction in CH peaks and production of more ettringite and quartz was noted in the spectrum of 10% CKD+5% NS paste specimen (Figure 4.44). As is clear in the XRD spectra of 10% CKD+5% NS paste specimen exposed to sodium sulfate solution, the CH further decreased and the secondary and primary ettringite increased (Figure 4.45). The spectra of 10% CKD+5% NS paste specimen exposed to the magnesium sulfate solution showed a significant reduction in the CH and a noticeable increase in the quantity of gypsum (Figure 4.46).

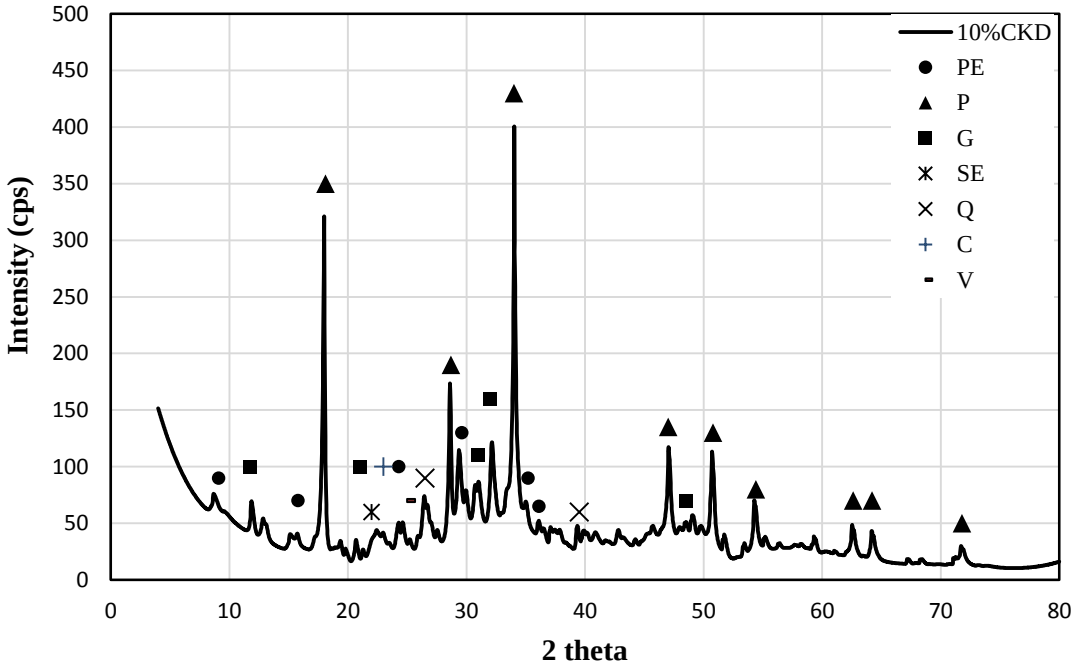

Figure 4.43: XRD spectra of 10% CKD concrete specimen

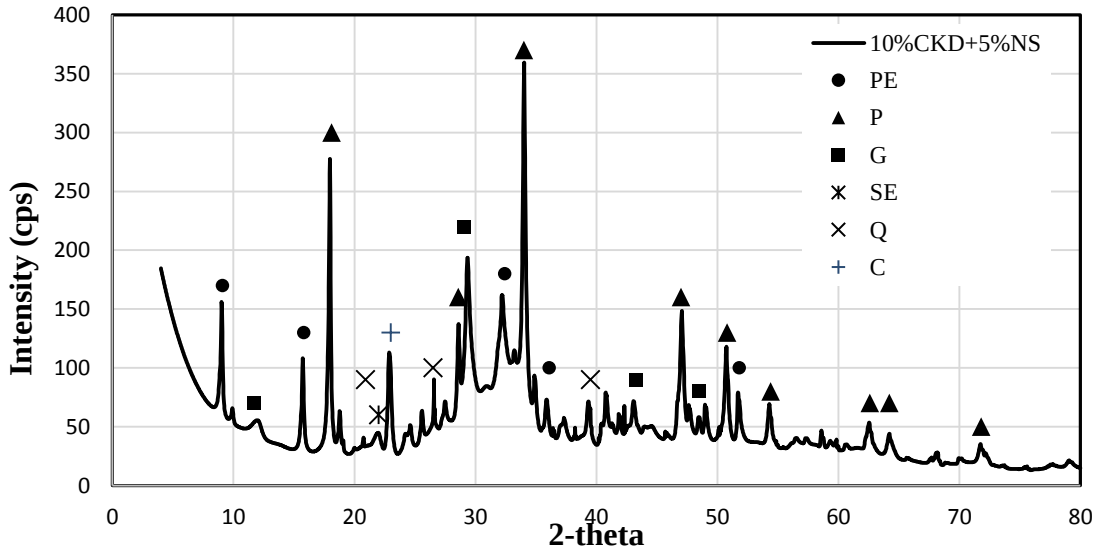

Figure 4.44: XRD spectra of 10%CKD+5%NS specimen

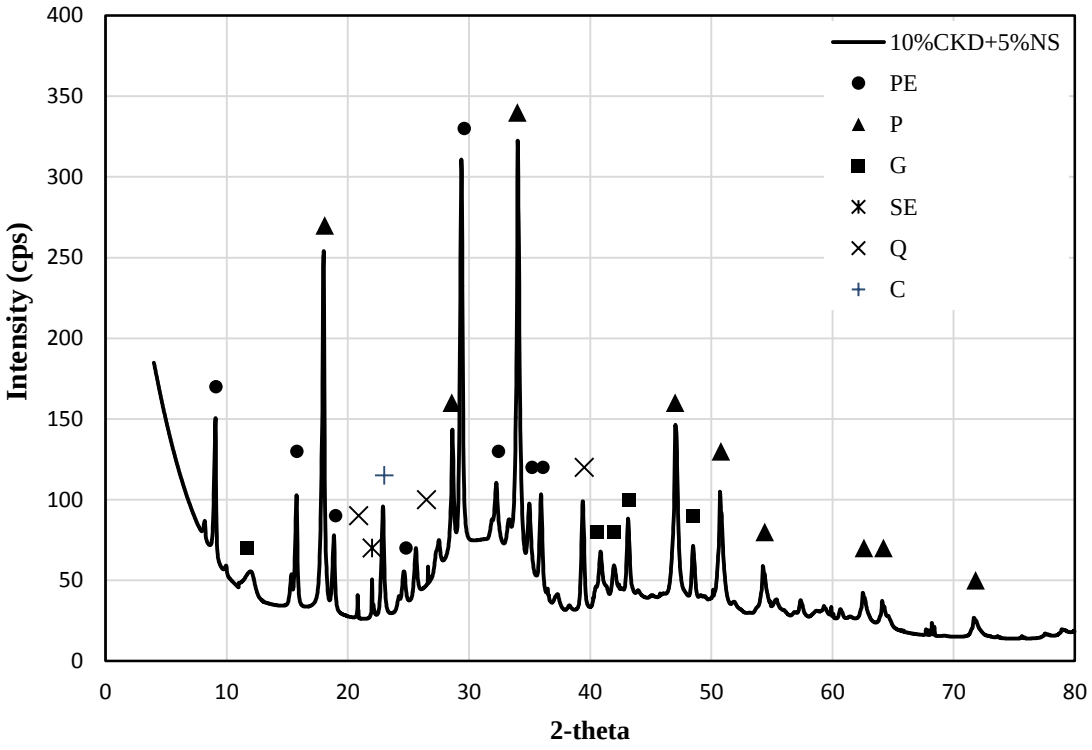

Figure 4.45: XRD spectra of 10%CKD+5%NS exposed to the sodium sulfate solution

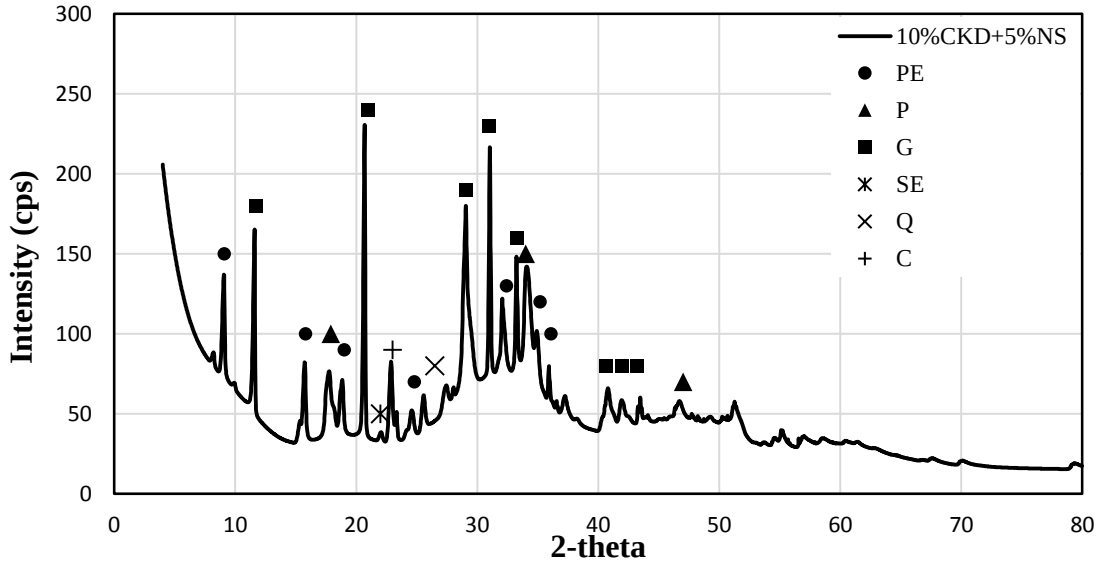

Figure 4.46: XRD results of CKD+5%NS cured in magnesium sulfate solution

4.2.3 Discussion of results

As stated earlier, two groups of CKD concrete specimens were prepared, the first group was prepared with three different dosages of CKD (10%, 15%, and 20%) as a partial replacement of cement, while in the second group, CKD (10%, 15%, and 20%) was utilized in the concrete in conjunctions with 5% NS. The compressive strength of CKD concrete without NS decreased as the dosage of CKD was increased. The reduction in the compressive strength may be attributed to a reduction in the cement content which resulted in a reduction in the quantity of C_2S and C_3S. CKD did not improve the compressive strength due to the low quantity of SiO_2 [60]. The reduction in the strength can also be attributed to an increase in the free lime content due to the presence of CKD which combined later with water to produce $Ca(OH)_2$ [61]. $Ca(OH)_2$ caused expansion in the paste due to its high volume which is almost twice the volume of lime and water molecules [62]. The XRD results showed more CH in the 10% CKD concrete compared to that of OPC. The SEM images of specimen with 10% CKD showed large quantity of CH accumulated at the interfacial zone. The role of sulfate as a constituents of CKD in lowering the strength can be summarized in forming gypsum due to the presence of calcium, forming sulfo-aluminate ($3CaO.Al_2O_3.CaSO_4.12H_2O$) which causes expansion in the paste [63], and the sulfate itself increased the porosity of concrete [64]. More gypsum and secondary ettringite was noted in the XRD spectra of CKD specimens. The chloride content in CKD caused reduction in strength through increasing the porosity by crystalizing the hydration products and through producing chloro-aluminate ($3CaO.Al_2O_3.CaCl_2.12H_2O$) which causes softening of the hydration products [65]. The interfacial zone became weak due to the presence of chloride, alkalis, and calcium hydroxide which caused a reduction in the

strength [66]. The morphology of 10% CKD specimen showed cracks at the ITZ between the aggregate and the mortar. Previous research [61] showed that as the CKD content increased, the chemically combined water decreased due to the low reactivity of CKD compared with OPC. The excess water enhanced the workability and improved the late strength by giving an opportunity to the formation of more C_2S and C_3S to react with water. The increase in free water and free lime as the CKD dosage increased clarify the small difference in the compressive strength of CKD concrete specimens. The increase in the early strength of the specimens with 10% and 15% CKD compared to that of OPC can be attributed to the appropriate alkalinity of the pore solution of concrete results in more CSH as a result of dissolution of silica ions [65].

The improvement in strength due to the inclusion of 5% NS in the CKD concrete may be attributed to the pozzolanic reaction between NS and $Ca(OH)_2$ which produced secondary CSH gel. The pozzolanic reaction not only produces extra gel but it also consumes $Ca(OH)_2$ which normally accumulates at the ITZ. The XRD spectra of CKD specimens with NS showed a noticeable reduction in the CH compared to that of specimens without NS. NS decreased the concrete porosity due to the production of CSH gel and enhanced the interfacial zone between the aggregate and the mortar. NS filled the pores in the hydration products and acted as a nuclei to it, which caused enhancement in strength. The dense micro structure and a dense interfacial zone, the absence of CH crystals and the production of more CSH from the pozzolanic reaction were clear in the morphology of 10%CKD+NS specimen. The ultimate strength was obtained in the specimen prepared with 10%CKD+5%NS due to the low quantity of free lime compared with other specimens. As the quantity of CKD increased the strength of the specimens with NS decreased which may

be attributed to the negative role of the free lime. The SEM images of specimen with 20%CKD+NS showed more cracks especially at the interfacial zone and less dense structure compared to the microstructure of 10% CKD specimen with same dosage of NS.

The flexural strength decreased as the dosage of CKD was increased. The reduction in the flexural strength of CKD concrete can be attributed to the high quantity of cement dust which offered low bond between aggregate and the mortar. The interfacial zone became weak due to the presence of chloride, alkalis, and calcium hydroxide [66]. The enhancement in the flexural strength of the specimens with NS can be attributed to the consumption of calcium hydroxide in the pozzolanic reaction and production of extra C-S-H gel which increased the bond between the aggregate and the matrix. NS acted as a nucli to the hydration products which densify the concrete structure and the interfacial zone. The ultimate flexural strength was obtained in the specimen of 10%CKD+5%NS. Then, as the dosage of CKD increased the flexural strength decreased. SEM images agreed with the flexural strength results. In 10%CKD+NS concrete, the ITZ was dense with no CH, while cracks appeared at the ITZ of 20%CKD+5%NS specimen. Regarding the specimen without NS, not only cracked ITZ appeared in the microstructure, but also large quantity of CH accumulated at the ITZ.

The optimum effect of NS in enhancing the compressive strength and flexural strength was obtained in 10%CKD+5%NS specimen. As the dosage of CKD increased the enhancement decreased. The positive chemical and physical effect of NS as well as CKD did not mask the negative effect of free lime, alkalis, sulfate, and chloride at higher dosages of CKD.

The drying shrinkage of CKD concrete specimens increased as the dosage of CKD was increased. The increase in the drying shrinkage may be attributed to a decrease in the free-

water due to the reduction in the cement content. A further increase was noted in the shrinkage of specimens with NS. This may be attributed to an increase in the hydration products mainly secondary C-S-H gel that consumes the mixing water. The increase in the drying shrinkage noted in the CKD concretes, indicates that appropriate preventive measures have to be adopted with these concretes to avoid shrinkage cracking.

Regarding the resistivity of the CKD concrete specimens against chloride permeability, a significant reduction in the charges passed through the specimens with NS was noted. Also, the chloride profile of CKD concrete with NS showed less chloride concentration at different intervals compared to that of CKD concrete. The reduction in the chloride permeability can be attributed to the dense structure formed due to the pozzolanic reaction between CH and NS, and to the physical action of NS, on which the nano particles acted as a nuclei to the hydration products which refined the micro structure and limited the growth of CH, furthermore NS filled the pores in the CSH.

The corrosion potential and corrosion current density increased as the dosage of CKD increased. However, the corrosion current density of 10%CKD concrete was slightly less than that of OPC. The increase in corrosion may be attributed to the negative role of CKD in lowering the density of the concrete as explained before. The increase in the corrosion current density in 10%CKD specimens may be attributed to the high alkalinity provided from CKD. The corrosion potential and corrosion current density decreased in CKD concrete with NS, which can be attributed to the enhancement in the concrete quality resulting from the physical and chemical action of NS. The dense, compact, uniform structure delayed the chloride diffusion, increased the concrete resistivity, and decreased the corrosion activity.

More expansion was noted in CKD concrete specimens due to sulfate attack which may be attributed to the high alkalinity of the pore solution of CKD concrete which promotes the production of more ettringite. Further, CKD has high sulfate content which reacts with CH to produce gypsum. Gypsum reacts with C_3A to produce ettringite which was noted in the XRD results. CKD has 6.35% C_3A, so replacing cement with CKD slightly decreased C_3A content. The use of NS in concrete as a partial replacement of cement significantly decreased the expansion. The chemical and physical action of NS increased concrete density and consumed CH which is essential in producing secondary ettringite. The deterioration of the edges of CKD concrete resulted from the production of magnesium hydroxide from the reaction between magnesium sulfate and calcium hydroxide which reduced the pH of the pore solution making CSH unstable. Negligible deterioration was noted in the CKD+5%NS specimens which may be attributed to their dense structure which delayed the diffusion of magnesium and sulfate ions. XRD spectrum of CKD+5% NS exposed to the magnesium sulfate solution showed more gypsum and less CH and ettringite. The production of magnesium hydroxide altered the formation of ettringite which is normally produced at high pH. However, deterioration was not noted in the specimens exposed to sodium sulfate solution which may be attributed to the short period of exposure.

4.3 Properties of EAFD concrete prepared with and without NS

To evaluate the properties of EAFD concrete, four concrete mixes were prepared in addition to concrete. Two mixes were prepared with 5% and 10% EAFD, while the other

two mixes were prepared with 5% NS in conjunctions with 5% and 10% EAFD. Both EAFD and NS were utilized in the concrete as a partial replacement of cement.

4.3.1 Macro properties

4.3.1.1 Compressive strength

The change in the compressive strength of EAFD concrete specimens due to the addition of OPC at different ages is shown in Figure 4.47. The 3-day compressive strength of OPC, 5% EAFD, 10% EAFD, 5% EAFD+5%NS and 10%EAFD+5%NS concrete specimens was 35.6, 34.6, 24.4, 43.03 and 39.04 MPa, respectively. The compressive strength of all the specimens increased with time. At 28 days, the compressive strength of OPC, 5% EAFD, 10% EAFD, 5% EAFD+5%NS and 10%EAFD+5%NS specimens was 58, 63.96, 56.13, 69.27, and 66.42 MPa, respectively. The 28-day compressive strength of all the specimens was more than that of OPC concrete, except that of 10% EAFD specimen. The increase in 28-day compressive strength due to the use of 5% EAFD was 10.28% with respect to OPC, while utilizing 10% EAFD in the concrete decreased the compressive strength by 3.2% (Figure 4.48). It was noted that utilizing 5% NS in the 5%, and 10% EAFD concrete improved the 28-day compressive strength by 19.43% and 14.53%, respectively, compared to that of OPC. The improvement in the compressive strength due to the use of 5% NS in the 5% and 10% EAFD concrete was 8.3% and 18.33%, respectively (Figure 4.49).

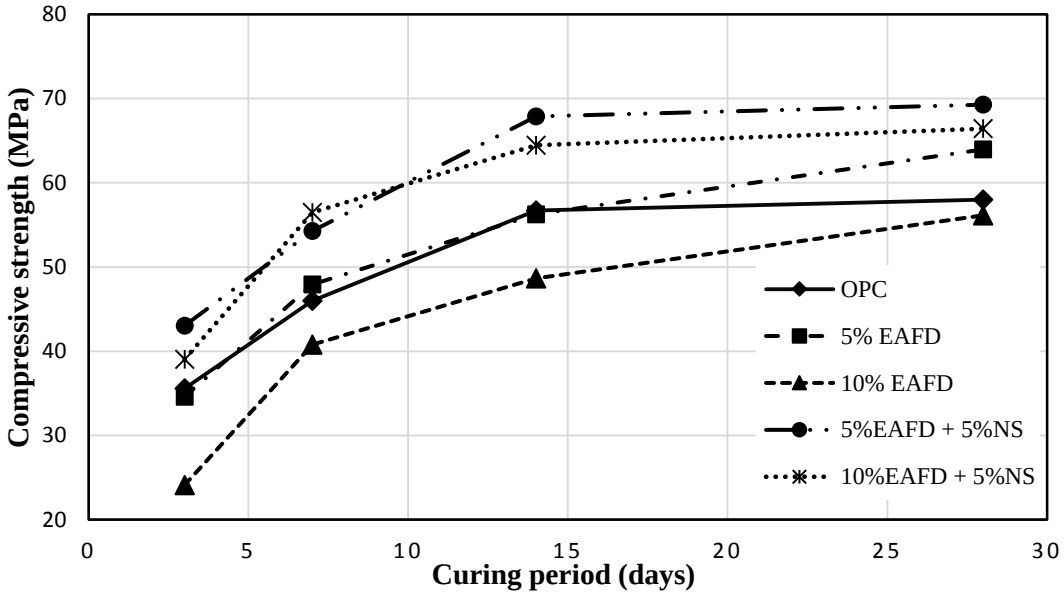

Figure 4.47: Compressive strength of EAFD concrete specimens

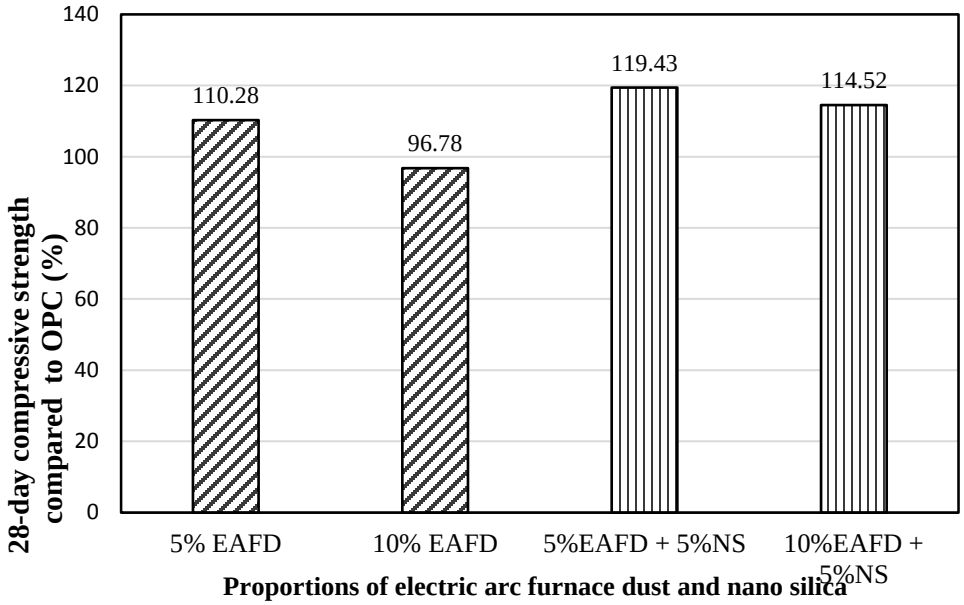

Figure 4.48: Change in the 28-day compressive strength of EAFD specimens compared to OPC

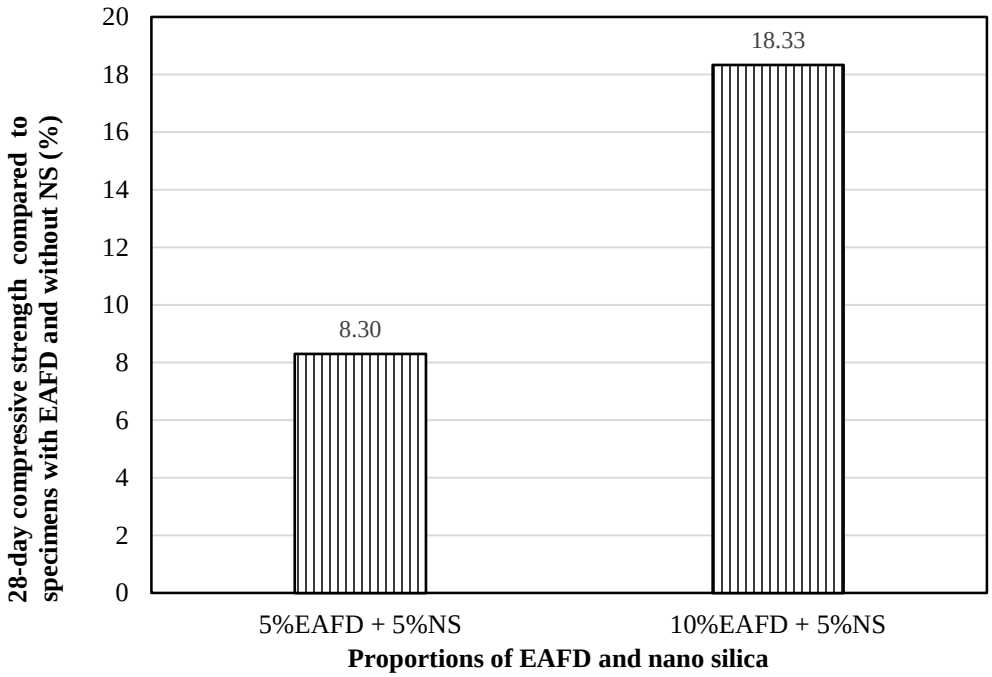

Figure 4.49: Effect of NS on the compressive strength of EAFD concrete specimens

4.3.1.2 Flexural strength

Figure 4.50 depicts the flexural strength of EAFD concrete specimens. The flexural strength of 5%EAFD, 10%EAFD, 5%EAFD+5%NS and 10%EAFD+5%NS specimens were 4.76, 4.58, 4.9, and 4.80 MPa, respectively. The use of 5% and 10% EAFD in the concrete increased the flexural strength by 13.6% and 9.3%, respectively, compared to OPC. Incorporating NS in EAFD concrete increased the flexural strength by 16.9% and 14.6% of 5%EAFD+5%NS and 10%EAFD+5%NS specimens, respectively (Figure 4.51). The increase in the strength of 5% and 10%EAFD due to the addition of NS was 2.9% and 4.8%, respectively (Figure 4.52).

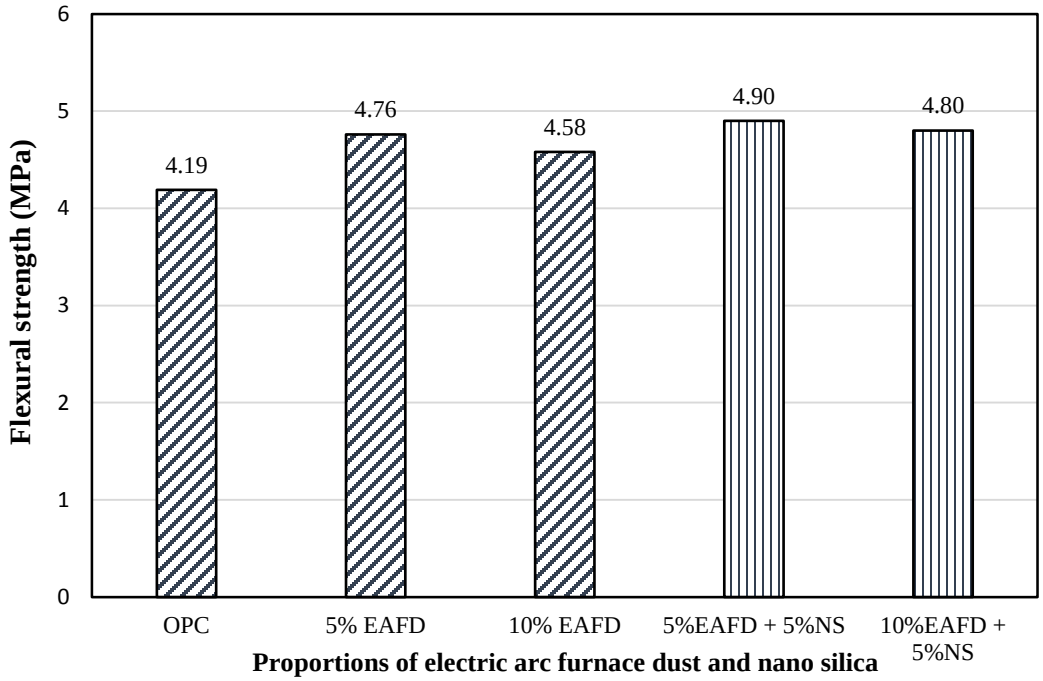

Figure 4.50: Flexural strength of EAFD concrete specimens

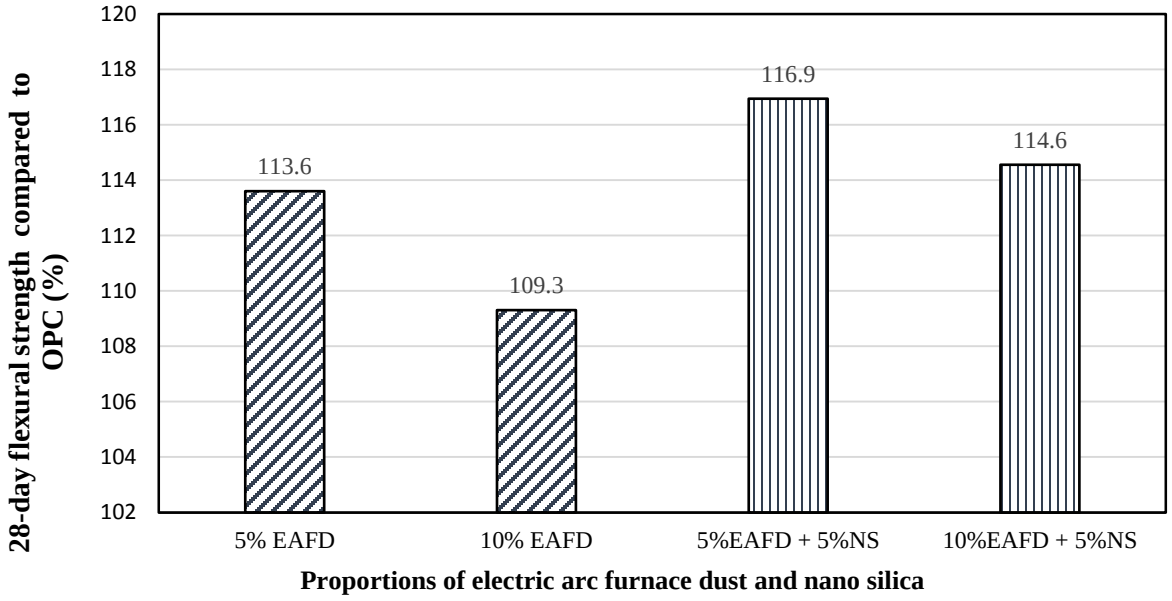

Figure 4.51: Change in the flexural strength of EAFD concrete specimens compared to OPC

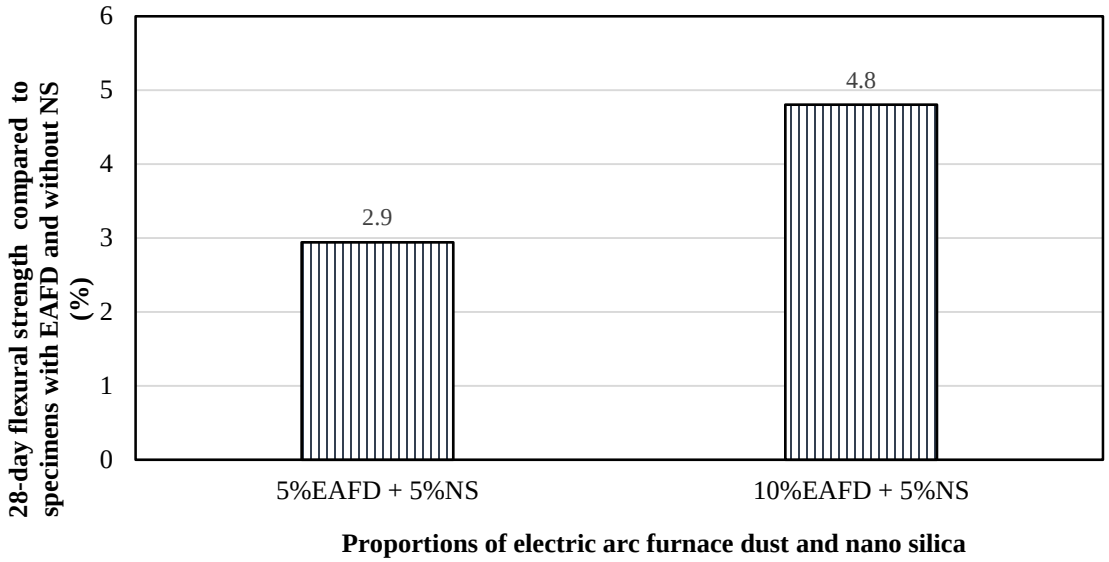

Figure 4.52: Effect of NS on the flexural strength of EAFD concrete

4.3.1.3 Drying shrinkage

The drying shrinkage of EAFD concrete specimens is depicted in Figure 4.53. A reduction in the drying shrinkage was indicated in 5% EAFD concrete specimens compared to that of control specimens, while the drying shrinkage of 10% EAFD specimens increased. However, the addition of NS in EAFD concrete further increased the shrinkage (Figure 4.53).

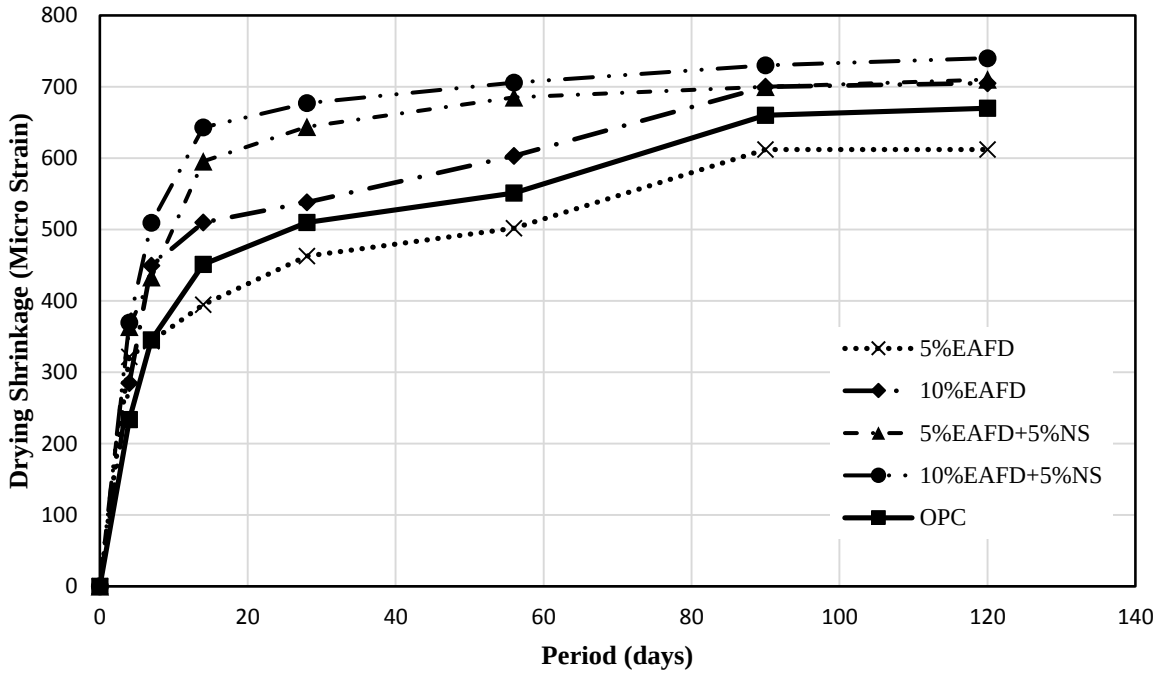

Figure 4.53: Drying shrinkage of EAFD cement concrete with and without NS.

4.3.1.4 Chloride permeability

Figure 4.54 depicts the total charge passed in coulombs passed through the EAFD specimens with and without NS. The total charge passed due to the use of EAFD in the concrete as a partial replacement of cement increased compared to that of OPC. The incorporation of NS in the EAFD concrete significantly decreased the chloride permeability.

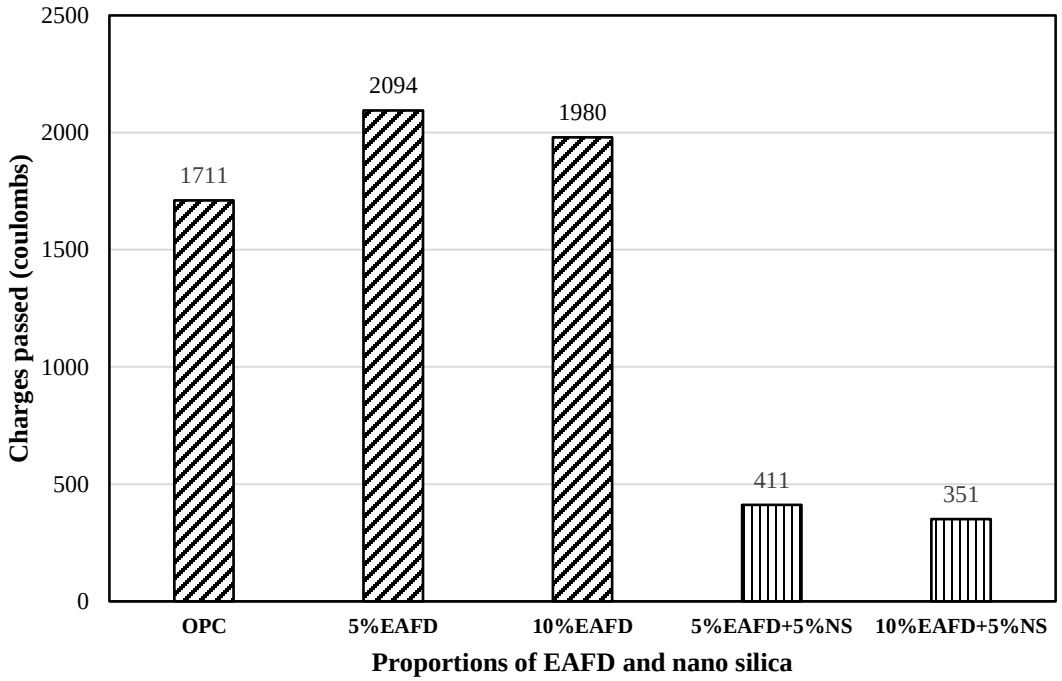

Figure 4.54: Rapid chloride permeability of EAFD concrete specimens with and without NS.

4.3.1.5 Chloride diffusion

The chloride concentration of EAFD concrete with and without NS at different depths are shown in Figure 4.55 and Figure 4.56. The chloride concentration increased as the dosage of EAFD increased. However, the chloride concentration of 5% EAFD at different depths was slightly less than that of OPC. The chloride concentration decreased due to the use of 5% NS as a partial replacement of cement. The difference in the chloride concentration of different EAFD concrete specimens with and without NS at a depth of 40 mm was negligible. The slope of the chloride profile of EAFD concrete with NS was more than that of EAFD concrete without NS.

The chloride profiles were utilized to determine the coefficient of chloride diffusion in accordance with the Fick's second law of diffusion [59]. The coefficient of chloride

diffusion of OPC, 5% EAFD, 10% EAFD, 5% EAFD+5%NS, and 10% EAFD+5%NS concrete was 16.2, 14.9, 16.8, 8.5, and 8.72 $\times 10^{-8}$ cm^2/s, respectively. It can be observed that using NS in EAFD concrete decreased the chloride diffusion (Figure 4.57).

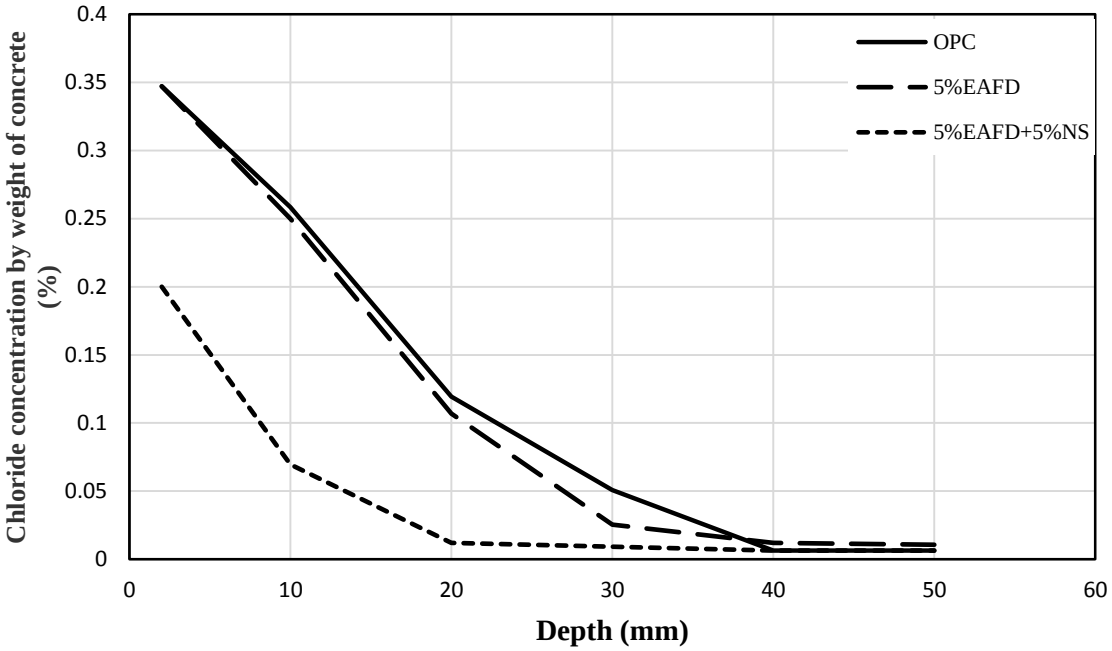

Figure 4.55: Chloride profile of 0% and 5% EAFD concrete with and without NS

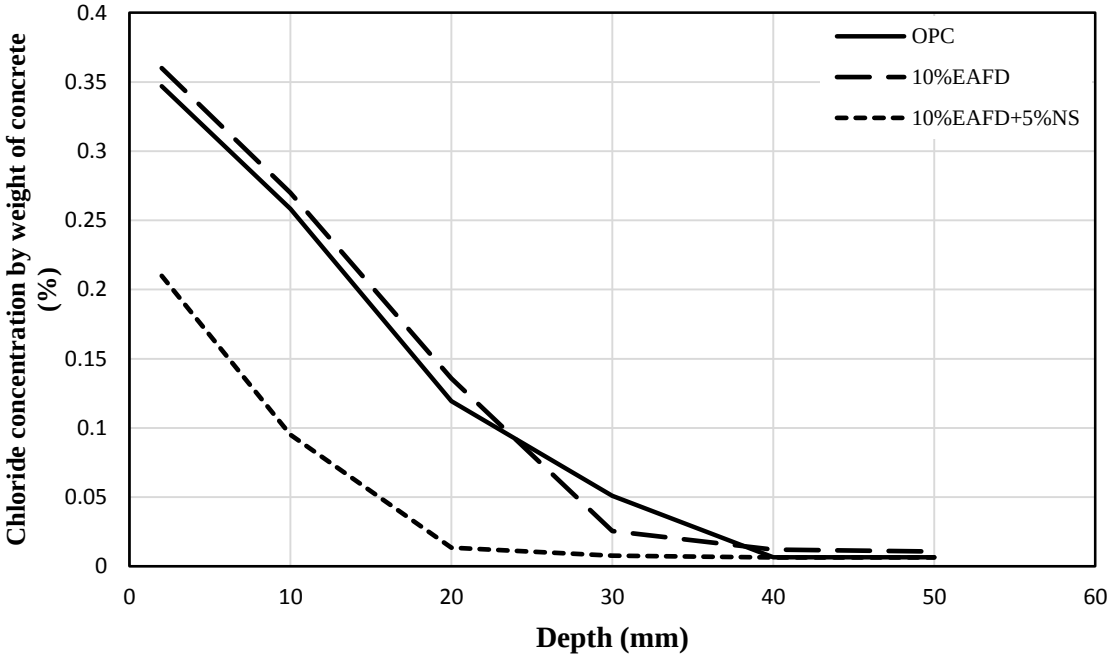

Figure 4.56: Chloride profile of 0% and 10% EAFD concrete with and without NS

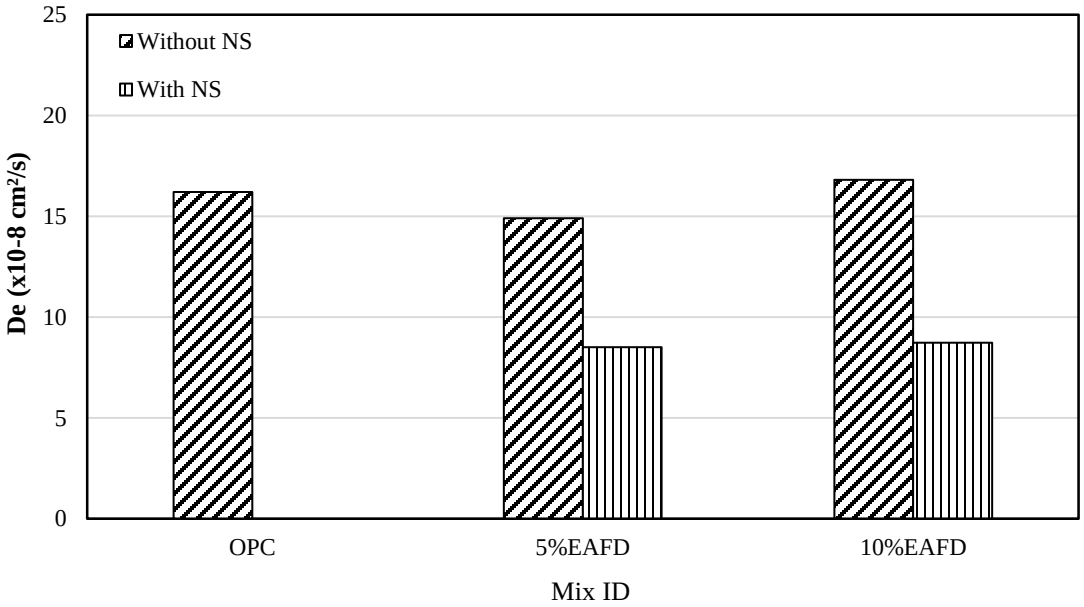

Figure 4.57: Chloride diffusion coefficients of different EAFD concrete with and without NS

4.3.1.6 Reinforcement corrosion

Corrosion potentials: The corrosion potentials were measured on concrete cylinders with 12 mm steel bars. The concrete cylinders were cured in water for 28 days, then they were partially exposed to 5% chloride solution. Three cylinders were prepared from each mix. The difference in the corrosion potential was measured for each concrete cylinder with respect to the saturated calomel reference (SCE) electrode and the average potential difference was recorded periodically. Figure 4.58 and Figure 4.59 depict the corrosion potential (E_{corr}) of EAFD concrete specimens with and without NS. The potential values decreased as the dosage of EAFD increased. However, the E_{corr} of specimens with 5% EAFD was almost similar to that of OPC, while it was lower in specimens prepared with 10% EAFD. The use of NS in the EAFD concrete decreased the corrosion potential compared to that of both EAFD concrete and OPC.

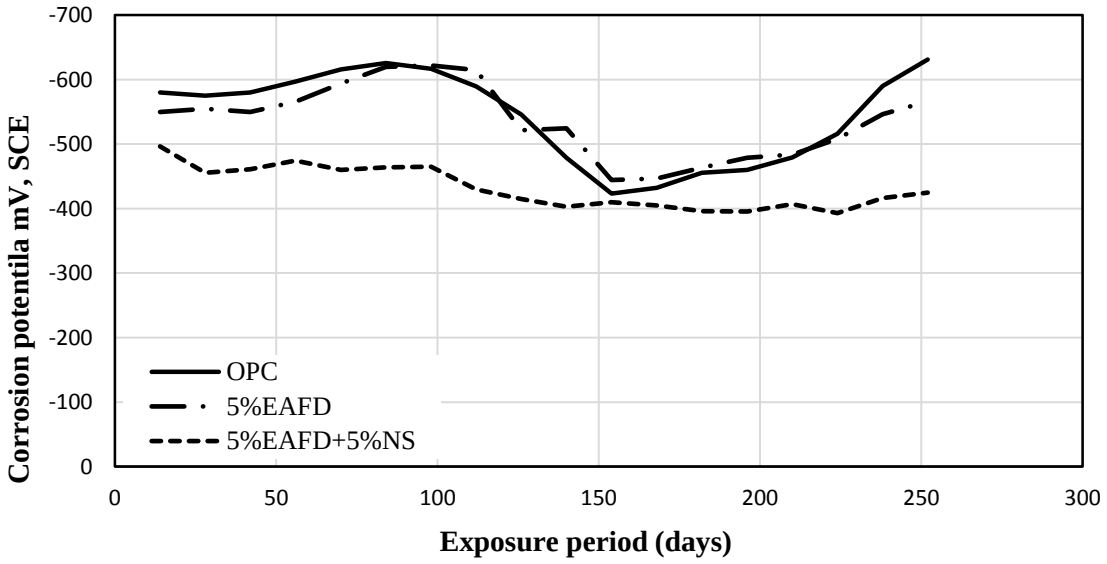

Figure 4.58: Corrosion potential of 0% and 5% EAFD concrete with and without NS

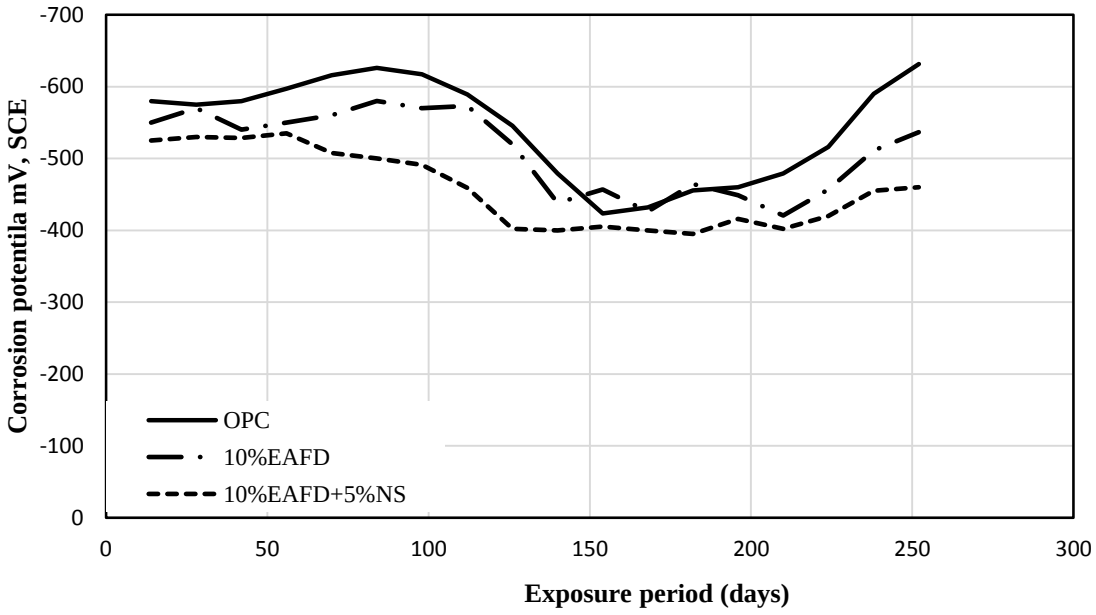

Figure 4.59: Corrosion potential of 0% and 10% EAFD concrete with and without NS

Corrosion current density: The corrosion current density after 260 days of exposure to 5% chloride solution was measured utilizing the same concrete cylinders used for assessing the corrosion potential. The use of 10% EAFD in the concrete, as a partial replacement of cement, decreased the I_{corr} compared to that of OPC, while the I_{corr} in the 5% EAFD concrete increased. The use of 5% NS in conjunctions with EAFD caused a significant reduction in the I_{corr} compared to that of EAFD concrete without NS (Figure 4.60).

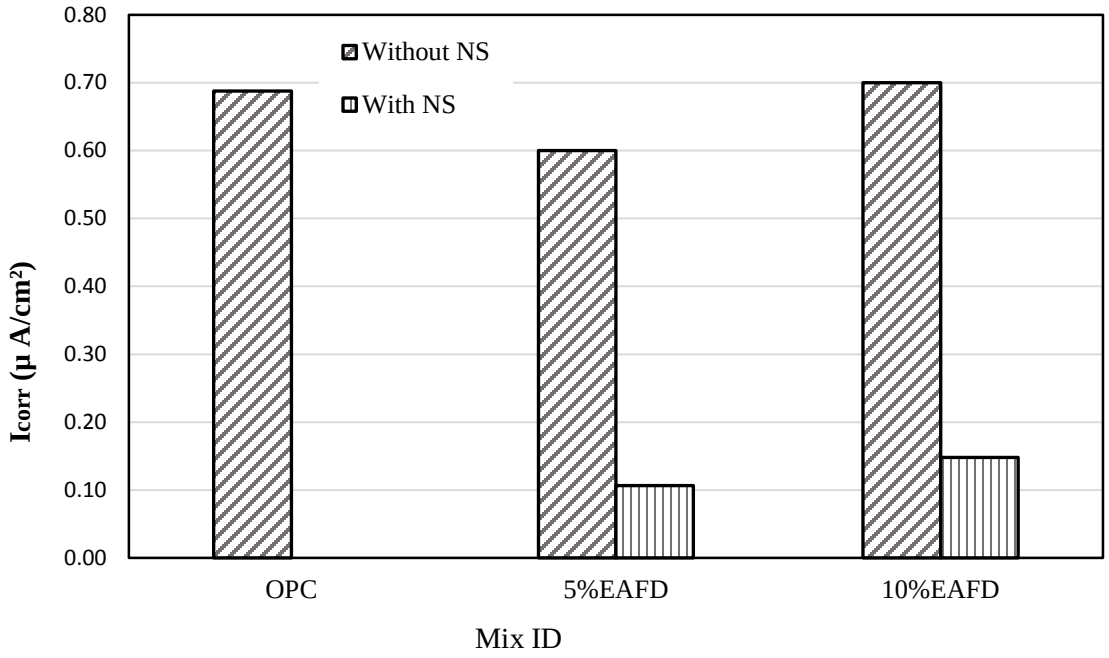

Figure 4.60: 260-day corrosion current density of EAFD concrete with and without NS

4.3.1.7 Sulfate attack

Figure 4.61 depicts the expansion of EAFD concrete specimens with and without NS due to sodium sulfate attack. It is clear that utilizing EAFD in the concrete as a partial replacement of cement decreased the expansion, while utilizing NS in the EAFD concrete caused a significant reduction in the expansion compared to that of EAFD concrete. As the dosage of EAFD was increased, the expansion of EAFD concrete decreased with and without NS. The deterioration started at the edges of EAFD paste cubes exposed to magnesium sulfate solution while negligible deterioration was noted on the surface of EAFD cubes incorporating NS (Figure 4.62 and Figure 4.63). Deterioration was not noted on the specimens exposed to the sodium sulfate solution.

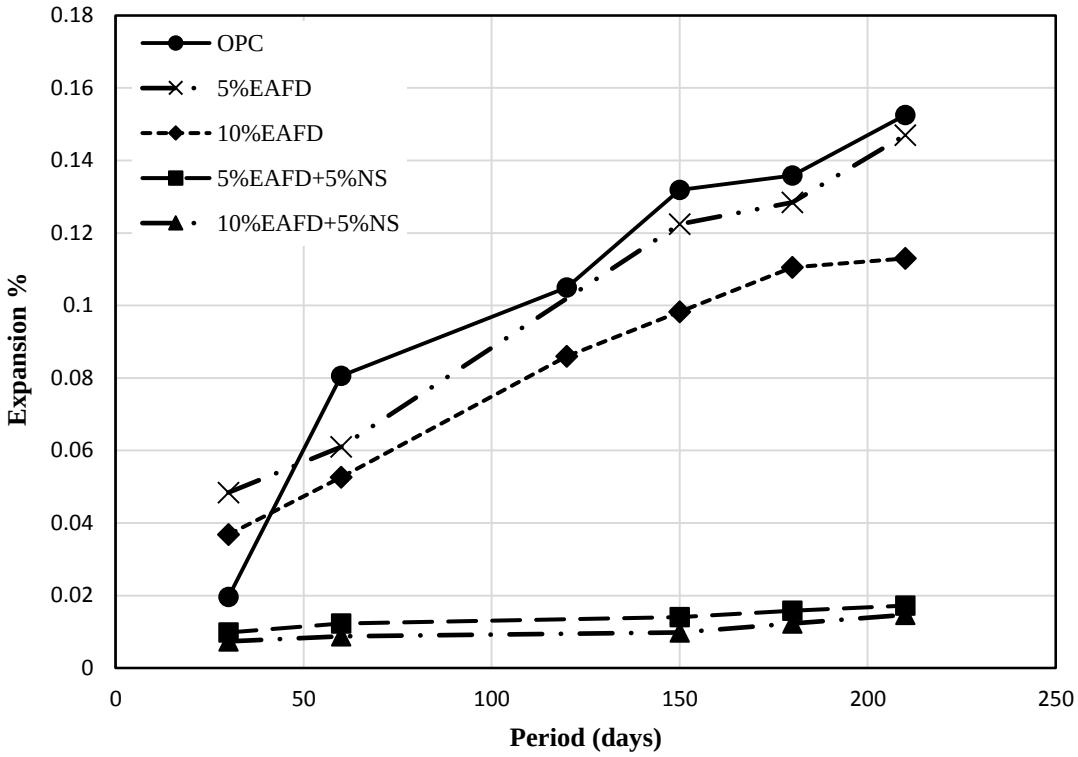

Figure 4.61: Expansion of EAFD concrete with and without NS

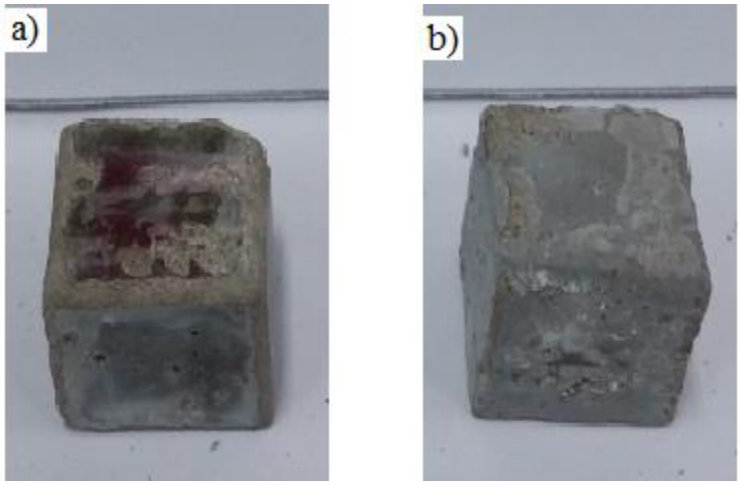

Figure 4.62: a) 5%EAFD cube and b) 5%EAFD+5%NS cube exposed to magnesium sulfate solution.

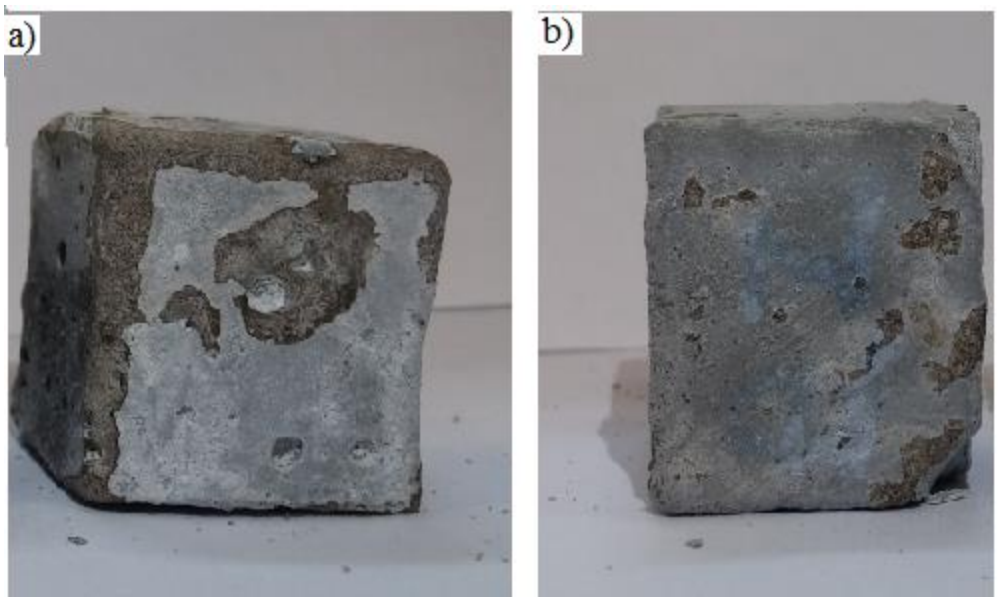

Figure 4.63: a) 10%EAFD cube and b) 10%EAFD+5%NS cube exposed to magnesium sulfate solution.

4.3.2 Micro properties

4.3.2.1 Morphology

The SEM of 5% EAFD specimen is shown in Figure 4.64. A porous microstructure with some cracks at the interfacial transition zone was noticed in this specimen. Due to the reaction between ZN and CH, low amount of CH was noted in the morphology of 5% EAFD concrete. A compact microstructure and dense interfacial zone was noted in the microstructure of 5% EAFD+5% NS (Figure 4.65(a, b, and c)). The BEI images showed a good bond between the aggregate and the paste (Figure 4.65(d)). A dense structure with high amount of CSH was noted in specimen with 10%EAFD and 5%NS (Figure 4.66).

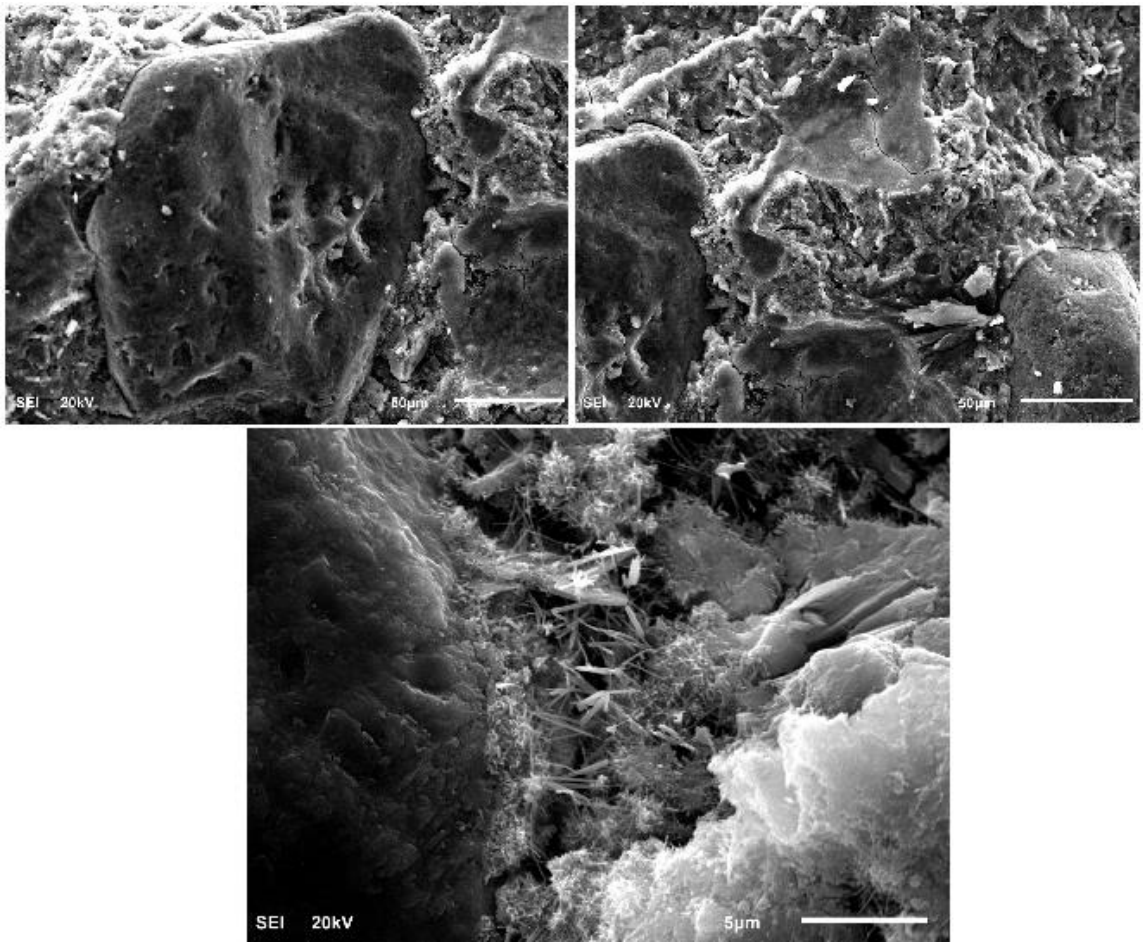

Figure 4.64: SEM of 5% EAFD concrete specimen.

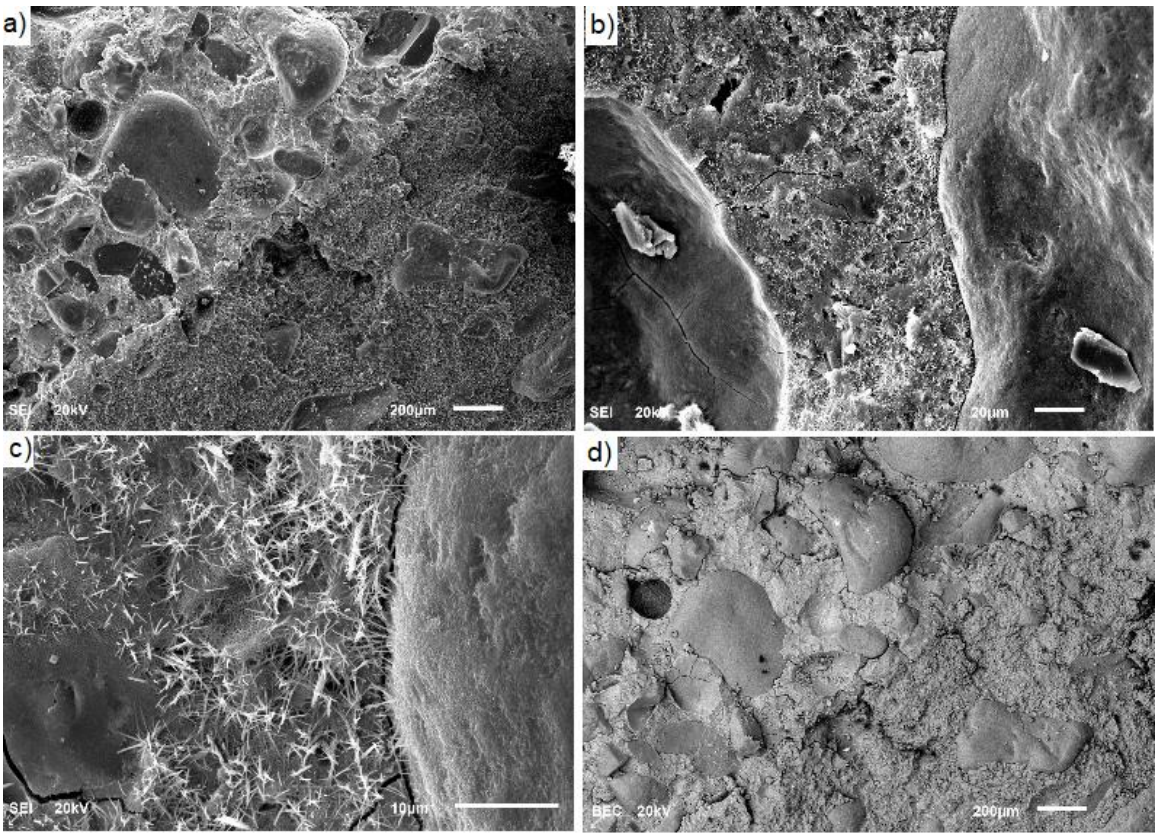

Figure 4.65: SEM and BEI images of 5% EAFD+5% NS concrete specimen.

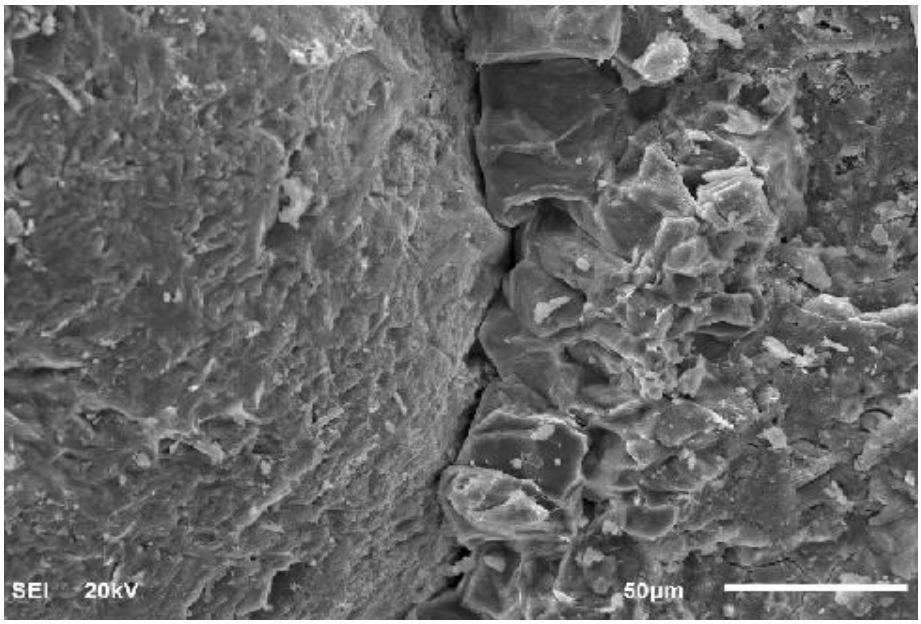

Figure 4.66: SEM of 10% EAFD and 5% NS concrete specimen.

4.3.2.2 Mineralogical composition

The XRD result of 5%EAFD showed reduction in CH peaks and noticeable reduction in ettringite compared to that of OPC (Figure 4.67). The use of 5% NS in 5%EAFD concrete further decreased the CH while ettringite increased significantly (Figure 4.68). The spectra for 5%EAFD+5%NS exposed to the sodium sulfate solution showed more secondary ettringite and less CH compared to that of specimen cured in water (Figure 4.69). A noticeable reduction in the CH peaks and a significant increase in the gypsum peaks was noted in the spectra for 5%EAFD+5%NS specimens exposed to the magnesium sulfate solution compared to similar specimens cured in water (Figure 4.70).

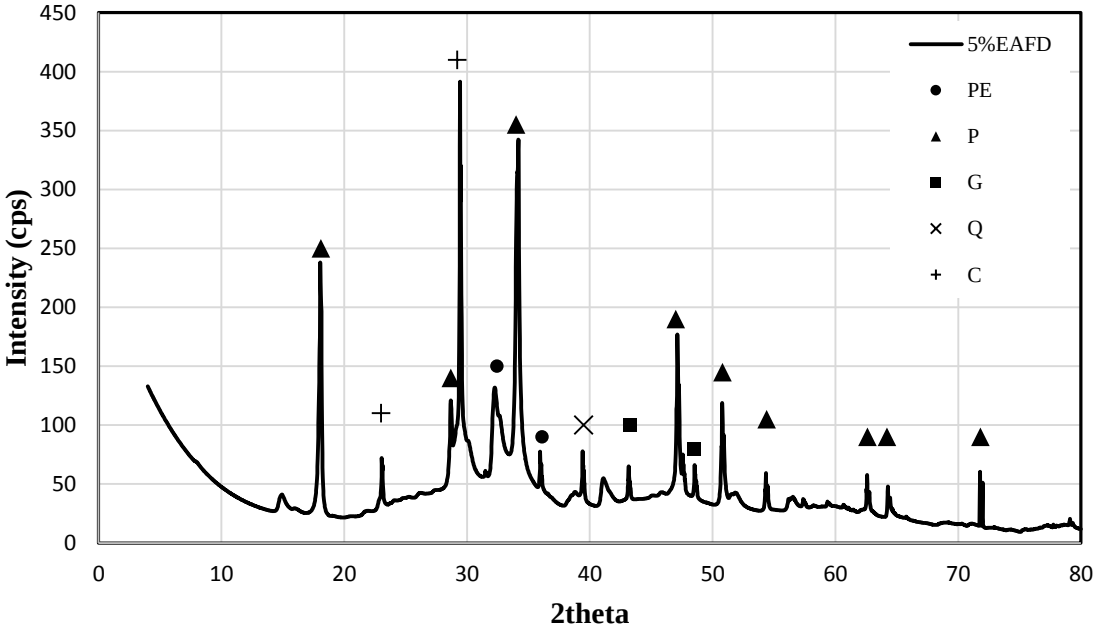

Figure 4.67: XRD spectra of 5%EAFD paste

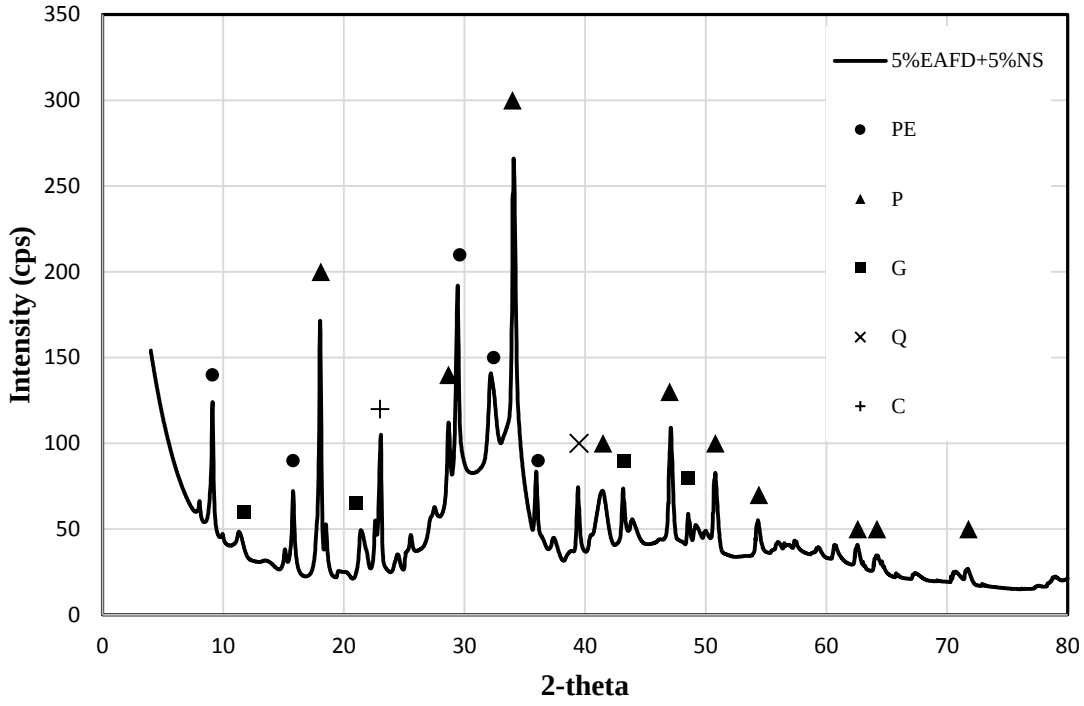

Figure 4.68: XRD spectra of 5%EAFD+5%NS paste

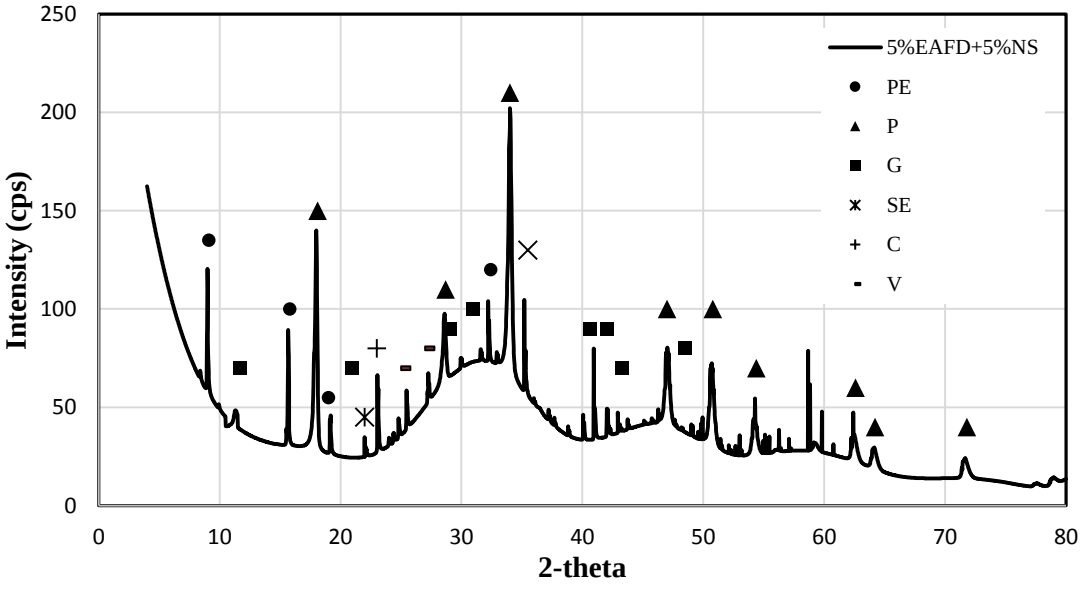

Figure 4.69: XRD spectra of 5%EAFD+5%NS paste exposed to sodium sulfate solution

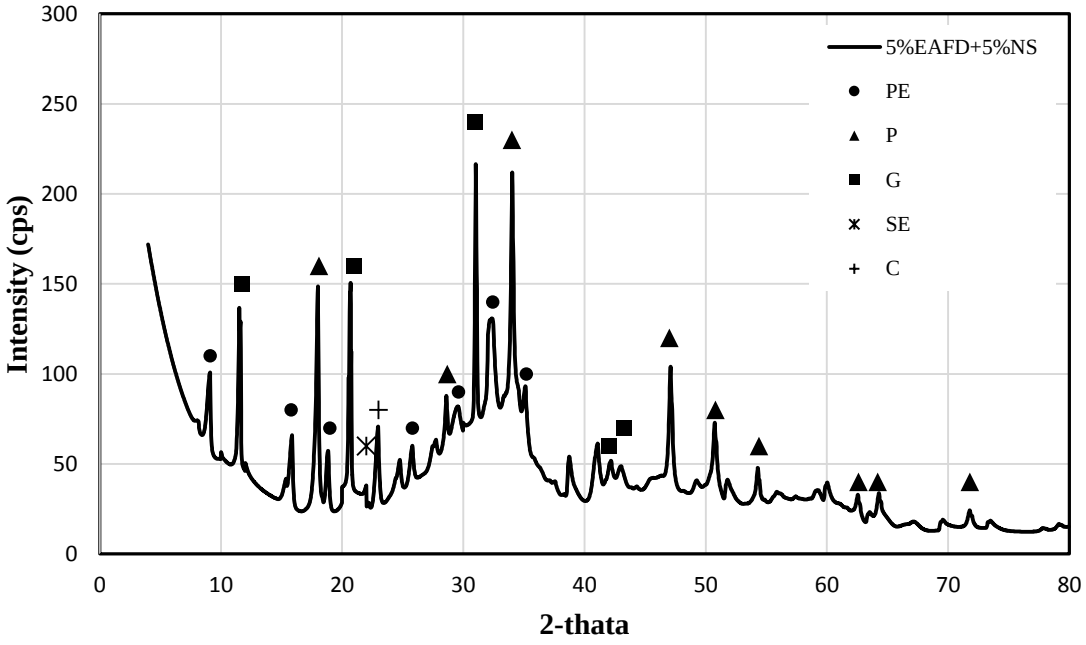

Figure 4.70: XRD spectra of 5%EAFD+5%NS exposed to magnesium sulfate solution

4.3.3 Discussion of results

Specimens of varying shape were prepared according to the test requirements to evaluate the properties of EAFD concrete with and without NS. EAFD was used in concrete with two different dosages (5% and 10%) as a partial replacement of cement. Two mixes were prepared with EAFD (5%EAFD and 10%EAFD) and the other two mixes were prepared with NS in conjunction with EAFD (5%EAFD+5%NS and 10EAFD+5%NS). The early age strength of EAFD concrete was low, which may be attributed to the effect of Zn, a constituent of EAFD, in retarding the hydration reaction. The XRD spectra showed less $Ca(OH)_2$ in the composition of EAFD concrete compared to OPC concrete, which was due to the reaction between $Ca(OH)_2$ and ZnO [67]. The absence of ettringite crystals in the EAFD concrete may be attributed to the reaction between Zn and C_3A to produce $CaZn_2(OH)_6.2H_2O$ [68]. Different studies represented different Zn layers that formed a

barrier around the cement particles. The $CaZn_2(OH)_62H_2O$ layer, made an impermeable barrier around the cement particles [69]. Other studies [67, 70-72] attributed the retardation effect of EAFD to the reaction between Zn and $Ca(OH)_2$ to produce $Zn(OH)_2$ which formed a barrier around the cement particles. This layer prevented the water molecules to react with cement particles, analogous to the effect of ettringite in retarding the hydration of C_3A. When the concentration of Ca^{++} and OH^- increased in the solution, the permeable layer of $CaZn_2(OH)_6.2H_2O$ formed and the hydration reaction proceeded again [67, 72]. It was indicated from the XRD results that different Zn compounds formed with time, on the first day, ZnO appeared in the structure, while on the fourth day, both ZnO and $CaZn_2(OH)_6.2H_2O$ formed and only $CaZn_2(OH)_6.2H_2O$ appeared on the seventh and fourteenth days of hydration [72]. Results of previous studies showed that the hydration reaction continued when $CaZn_2(OH)_6.2H_2O$ formed and the $Zn(OH)_2$ layer is an impermeable layer.

The 28-day compressive strength of 5% EAFD concrete improved by 10.28% while it decreased by 3.2% in the 10% EAFD specimens. The enhancement in the strength was attributed to the formation of Z-S-H as a result of the reaction between CSH and Zn which is stronger than CSH [69]. The formation of ZSH was described according to the surface layer theory [73] on which Ca^{++} ions surrounded the CSH layer forming a secondary layer. The Ca^{++} ions attracted the negative zincate ions that resulted in the formation of a third layer. Then due to the cation exchange, ZSH layer is formed. The reduction in the compressive strength of 10% EAFD concrete at 28-day compared to the control specimen was attributed to the high concentration of Zn ions which react with $Ca(OH)_2$ to produce CZH which has lower strength than CSH but a similar structure [73]. Regarding the

physical action of EAFD, it seems that the 5% EAFD is the optimum dosage and as the dosage increased the strength decreased. SEM images of 5% EAFD specimens showed porous and cracked microstructure but more compact compared with the morphology of OPC which agreed with the compressive strength results.

The use of NS in the EAFD concrete increased the rate of strength development. The enhancement in the early strength can be attributed to the consumption of $Ca(OH)_2$ by NS, that altered the formation of $Zn(OH)_2$ layer. The enhancement in the strength due to the addition of NS may be attributed to the pozzolanic reaction of NS which resulted in producing more gel. Also, due to the nucleation effect of NS in which NS acted as a nuclei to the hydration product. As stated earlier, Zn reacted with CSH producing ZSH which is stronger than CSH. Due to the production of more CSH from the pozzolanic reaction, ZSH content increased thereby increasing the strength. The strength enhancement in the 10% EAFD concrete due to the addition of NS was more than that of 5% EAFD+5% NS specimen, which can be attributed to the formation of more ZSH due to more Zn available from EAFD. Also, due to an increase in the hydration products, more EAFD can be incorporated as a filler. The role of NS (the physical and chemical actions) can also be noted in the SEM images of EAFD concrete with NS, which showed a compact microstructure and ITZ compared with that of EAFD concrete without NS. The morphology of 10%EAFD+5%NS specimens showed more CSH gel. XRD results showed less CH in the specimens with NS which may be attributed to the chemical action of NS with the CH.

The flexural strength increased due to the use of EAFD in the concrete. This may be attributed to the consumption of $Ca(OH)_2$ in the reaction with Zn that caused an

enhancement in the bond between the aggregate and the mortar. The effect of NS in enhancing the flexural strength was low which can be attributed to the absence of $Ca(OH)_2$ in the EAFD concrete with and without NS. The increase in the flexural strength may be attributed to the formation of extra CSH and ZSH and also to the filling action of NS which densified the ITZ.

The increase in the shrinkage of 10% EAFD concrete may be attributed to a decrease in the free-water in EAFD cement concrete. The decrease in the shrinkage of 5% EAFD concrete may be attributed to the filling action of EAFD particles that makes the structure dense and does not allow the free-water to evaporate. Thus, the use of 5% EAFD in concrete, as a partial replacement of cement, increased the strength and decreased the shrinkage. The increase in the drying shrinkage of EAFD concrete with NS may be attributed to an increase in the hydration products, mainly secondary C-S-H gel that consumes the mixing water. Consequently, precautions have to be taken to avoid shrinkage cracking of this type of concrete.

The total charge passed through the specimen's and the free chloride concentration significantly decreased due to the use of NS in conjunction with EAFD concrete. The enhancement in the chloride permeability resistance may be attributed to the dense, compact and uniform microstructure that resulted from the chemical and physical action of NS.

The corrosion potentials on steel in the concrete specimens with 5% and 10% EAFD was almost similar to that of OPC, which may be attributed to the physical effect of EAFD in densifying the concrete microstructure. The corrosion current density of 10% EAFD concrete was less than that of OPC which may be attributed to the optimum packing

obtained at this dosage. The corrosion current density further decreased due to the use of NS in concrete. Although NS consumes CH in the pozolanic reaction which reduces the pH of the pore solution, it produced more gel and filled the pores which compensated for the reduction in the alkalinity. The dense, compact, uniform structure delayed the chloride diffusion, increased the concrete resistivity, decreased the potential variation, and thereby decreased the rate of reinforcement corrosion.

The expansion due to the sulfate attack decreased due to the use of EAFD in the concrete, which may be attributed to a reduction in the quantity of C_3A. The use of NS in EAFD concrete, as a partial replacement of cement, significantly decreased the expansion. The chemical and physical action of NS enhanced the concrete density and consumed CH which is essential for producing gypsum and consequently secondary ettringite. The XRD spectra of EAFD+5% NS paste exposed to sodium sulfate solution indicated more secondary ettringite and less CH. The deterioration of the edges of EAFD paste specimens resulted from the production of magnesium hydroxide, which was produced due to the reaction between magnesium sulfate and calcium hydroxide. The magnesium hydroxide decreases the pH of the pore solution making CSH unstable. Negligible deterioration was noted in the EAFD+5% NS paste specimen. This may be attributed to its dense microstructure which delayed the diffusion of magnesium and sulfate ions in the specimen. The XRD spectra of EAFD+5% NS paste exposed to magnesium sulfate solution exhibited more gypsum and less CH. The production of magnesium hydroxide altered the formation of ettringite which is normally produced at high pH. However, deteriorations was not noted in the specimens exposed to sodium sulfate solution which can be attributed to the short period of exposure, i.e. six months.

4.4 Properties of LSP concrete prepared with and without NS

LSP was utilized in the concrete with three different dosages (5%, 10% and 15%) as a partial replacement of cement. Two groups of specimens were prepared, the first group prepared from three different mixes using different dosages of LSP (5%, 10% and 15%), while the second group was prepared from concrete with NS in conjunction with the different dosages of LSP. A total of six different groups of specimens were prepared to assess the properties of LSP concrete prepared with and without NS.

4.4.1 Macro properties

4.4.1.1 Compressive strength

The compressive strength of LSP concrete specimens is shown in Figure 4.71. The compressive strength of OPC, 5% LSP, 10% LSP, and 15% LSP specimens was 58, 58.2, 55.35 and 52.07 MPa, respectively. As the dosage of LSP increased, the compressive strength decreased. However, the strength of 5% LSP specimen was almost similar to that of OPC while the strength of 10% LSP, and 15% LSP specimens decreased compared to OPC by 4.27%, and 10.22%, respectively (Figure 4.73). The compressive strength increased due to the incorporation of 5%NS in the LSP concrete (Figure 4.72). At 28 days, the compressive strength of 5%LSP+5%NS, 10%LSP+5%NS, and 15%LSP+5%NS concrete was 63.45, 61.27, 58.32 MPa, respectively. Maximum strength was obtained in the 5%LSP+5%NS specimen. However, the strength decreased as the dosage of LSP was increased. Further, the strength of 15%LSP+5%NS was slightly more than that of OPC while the 28-day compressive strength of 5%LSP+5%NS, 10%LSP+5%NS specimens increased compared to OPC by 9.4% and 5.63%, respectively (Figure 4.73). The increase

in the compressive strength of LSP specimens due to the use of 5% NS was 9.03%, 10.34%, and 12% in specimens with 5%, 10%, and 15% LSP, respectively (Figure 4.74).

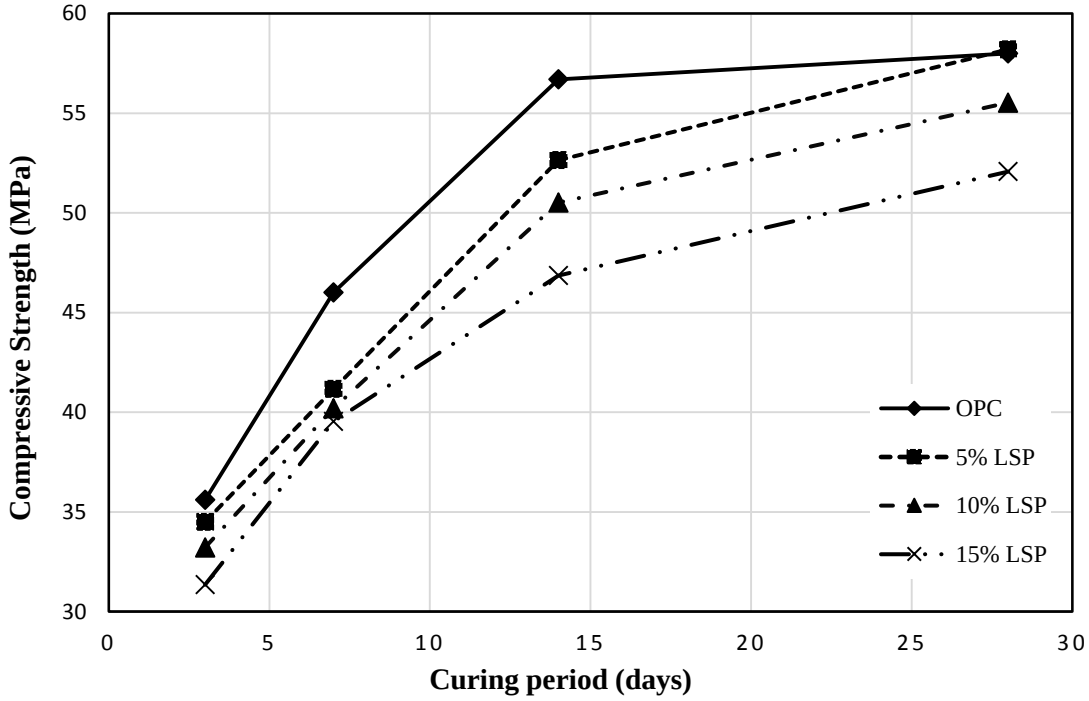

Figure 4.71: Compressive strength of LSP concrete specimens

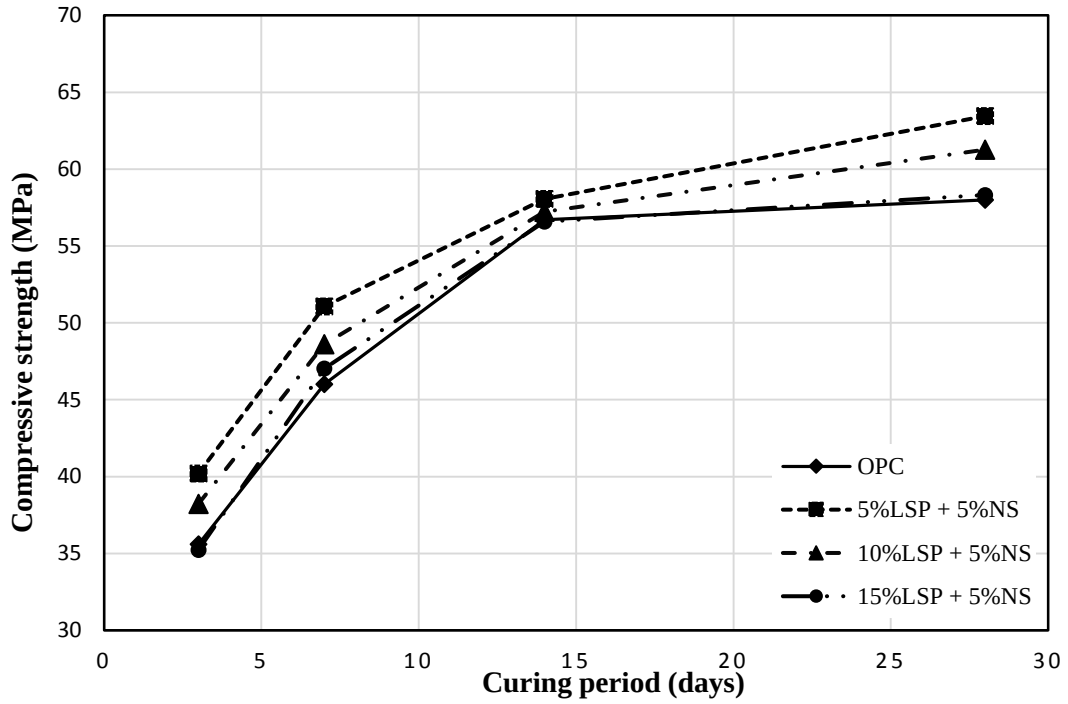

Figure 4.72: Compressive strength of LSP concrete with NS

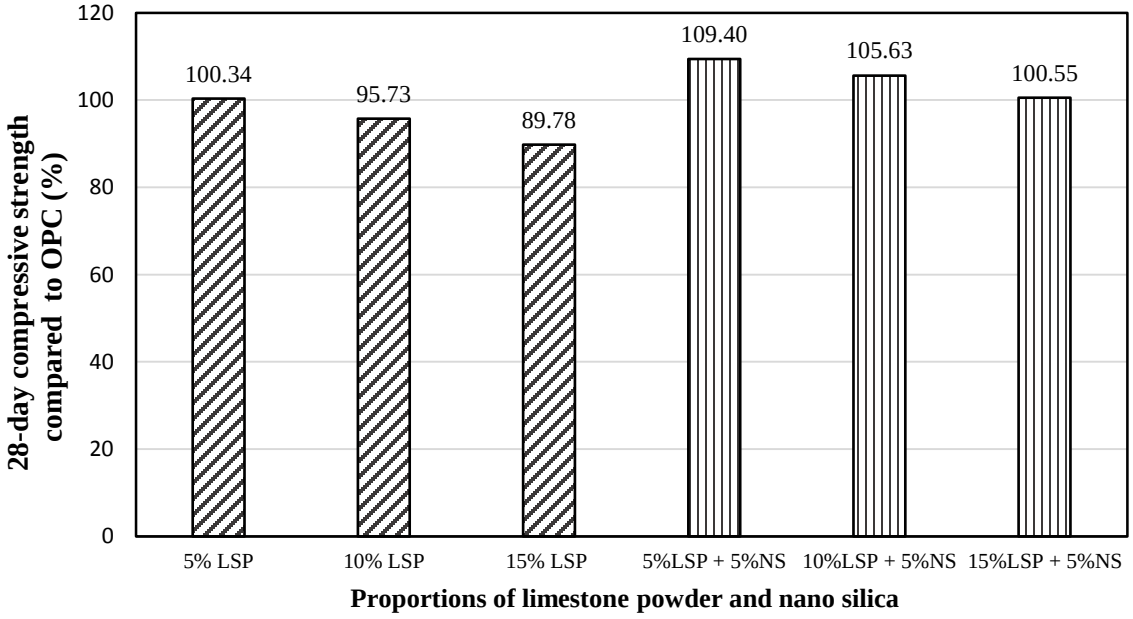

Figure 4.73: Change in 28-day strength of LSP concrete compared to OPC

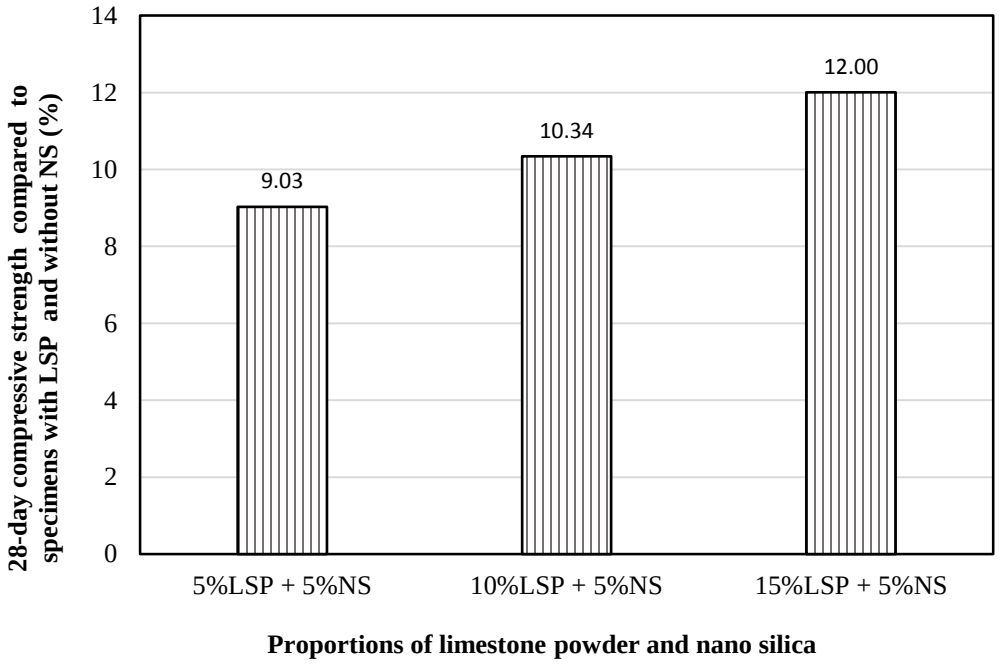

Figure 4.74: Change in 28-day compressive strength of LSP concrete with 5%NS

4.4.1.2 Flexural strength

A group of prisms were tested under four point loading to evaluate the flexural strength of LSP concrete. The 28-day flexural strength of OPC, 5% LSP, 10% LSP, 15% LSP, 5% LSP+5% NS, 10%LSP+5%NS, 15%LSP+5%NS was 4.19, 5.25, 5, 4.39, 5.81, 5.63, and 4.95 MPa, respectively (Figure 4.75). As the dosage of LSP increased, the flexural strength decreased. However, the strength of all the specimens was more than that of OPC. The use of LSP in the concrete increased the flexural strength by 25.3%, 19.33%, and 4.69%, of specimens with 5, 10, and 15% LSP, respectively, compared to OPC. The use of NS in conjunction with LSP enhanced the flexural strength by 38.66%, 34.37%, and 18.14% of 5%LSP+5%NS, 10%LSP+5%NS and 15%LSP+5%NS specimens compared to OPC, respectively (Figure 4.76). As a comparison between the LSP specimens with NS and those

without, the flexural strength of 5%LSP+5%NS, 10%LSP+5%NS, 15%LSP+5%NS specimens increased by 10.67%, 12.6%, and 12.84%, respectively (Figure 4.77).

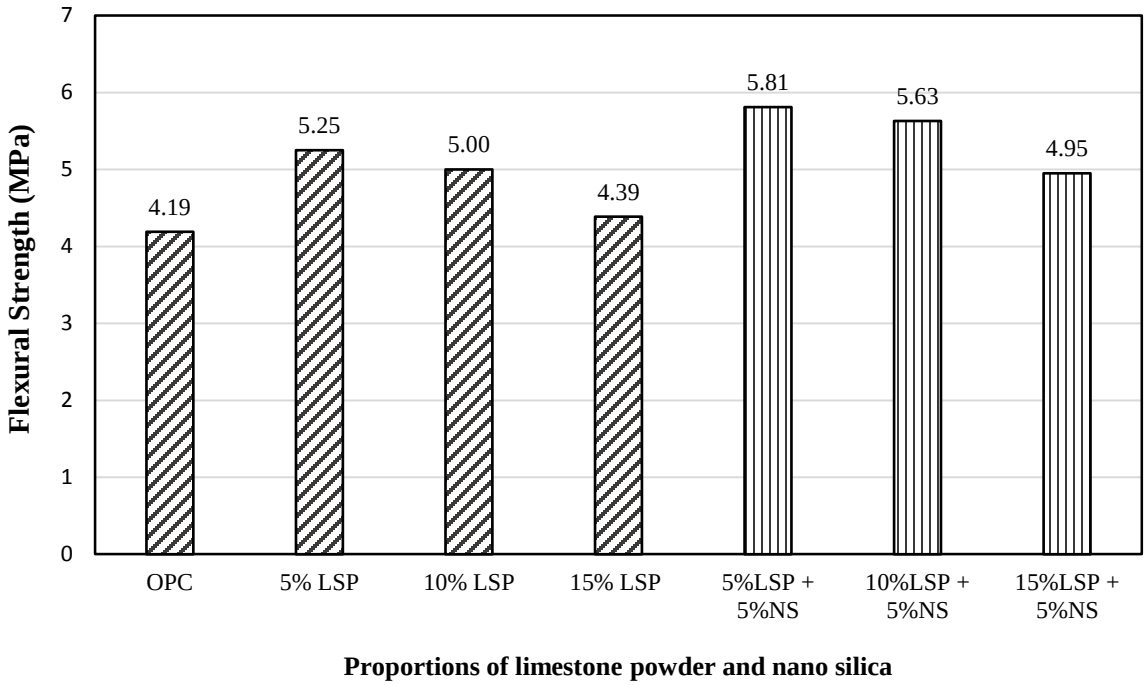

Figure 4.75: Flexural strength of LSP concrete specimens

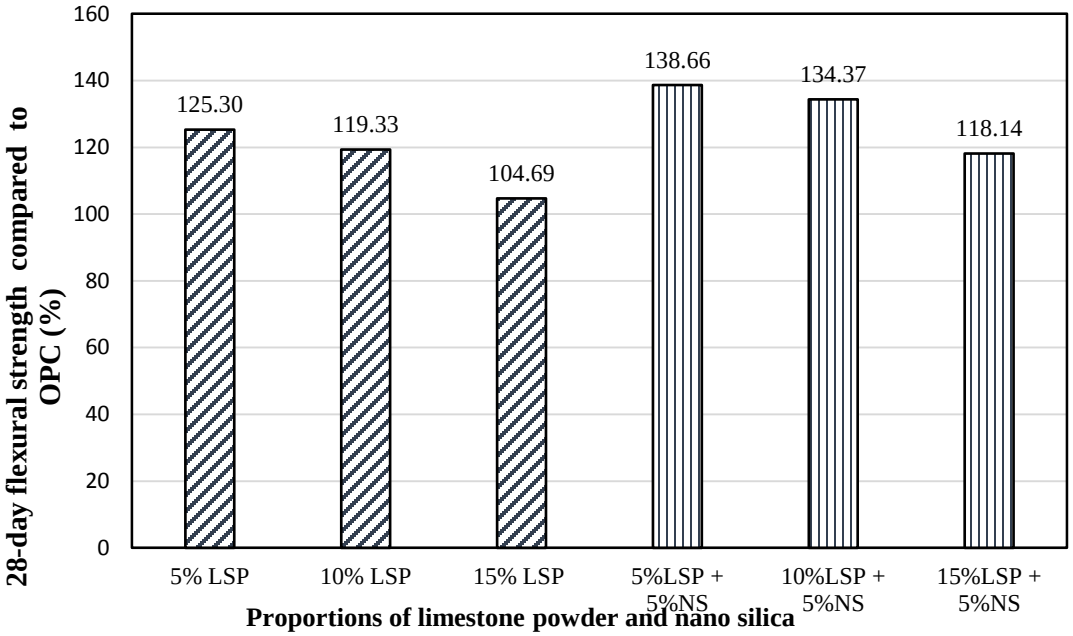

Figure 4.76: Change in compressive strength of LSP concrete specimens compared to OPC

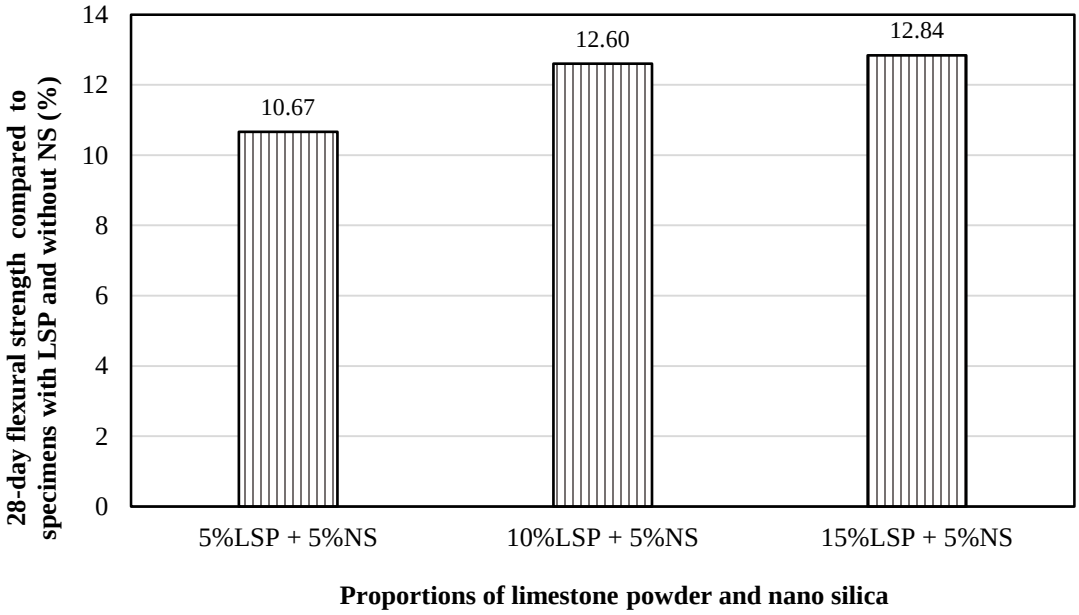

Figure 4.77: Change in the flexural strength of LSP concrete due to the addition of NS

4.4.1.3 Drying shrinkage

The drying shrinkage of LSP concrete with and without NS is depicted in Figure 4.78 and Figure 4.79. The drying shrinkage of 5%LSP specimen decreased, while the shrinkage increased as the dosage of LSP increased with respect to that of OPC (Figure 4.78). However, the shrinkage further decreased due to the incorporation of NS in the LSP concretes (Figure 4.79).

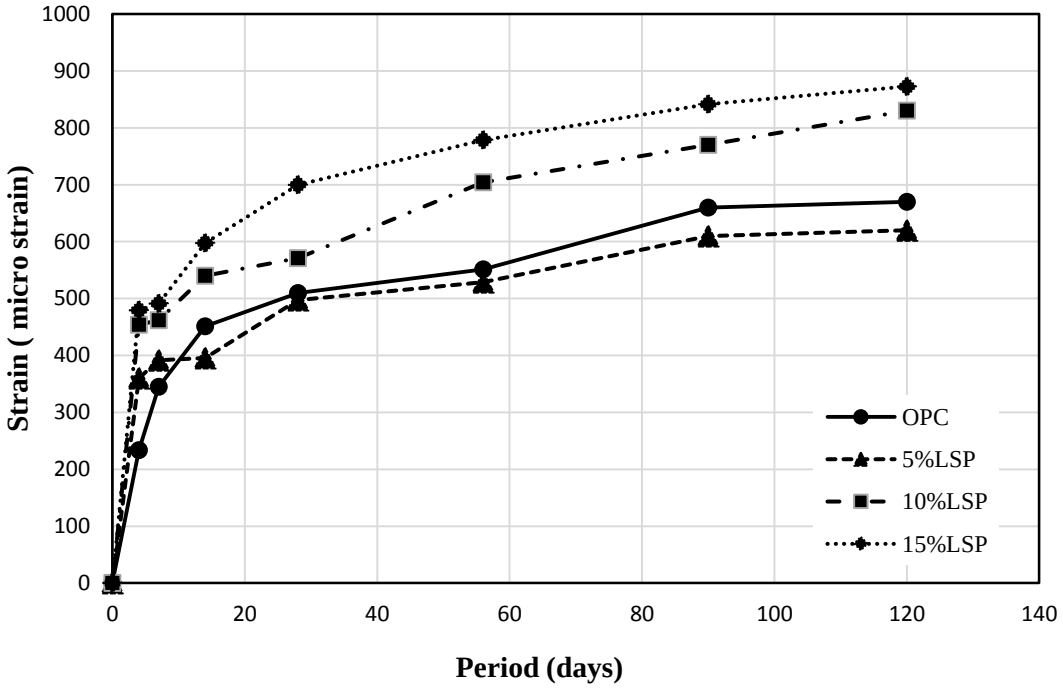

Figure 4.78: Drying shrinkage of LSP concrete without NS.

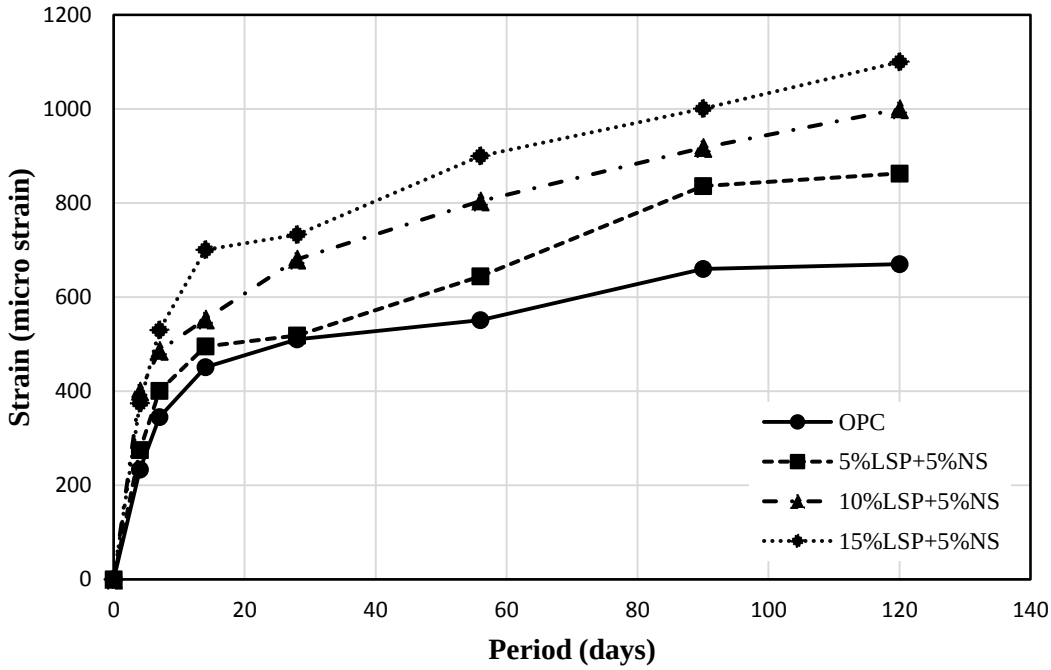

Figure 4.79: Drying shrinkage of LSP concrete with NS.

4.4.1.4 Chloride permeability

The total charge passed through the LSP concrete specimens with and without NS is shown in Figure 4.80. The chloride permeability increased as the dosage of LSP increased, while it significantly decreased in the LSP concrete with NS.

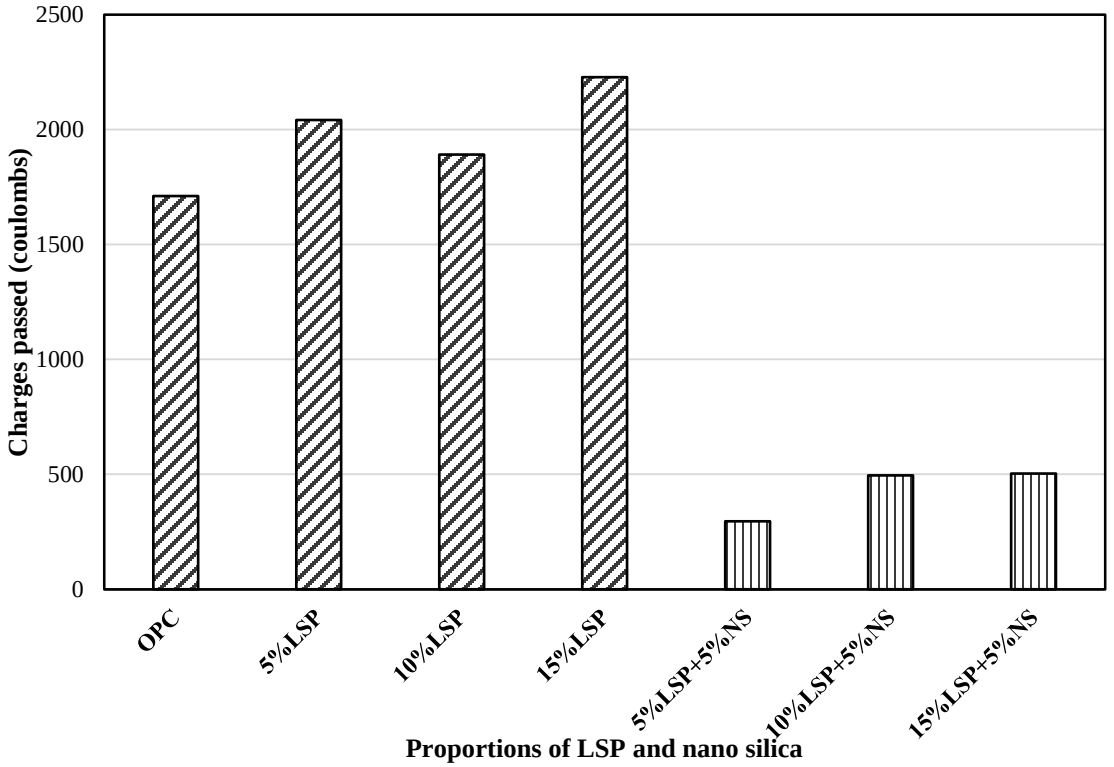

Figure 4.80: Rapid chloride permeability of the LSP concrete specimens with and without NS

4.4.1.5 Chloride diffusion

The chloride profiles of LSP concrete specimens prepared with and without NS are shown in Figure 4.81, Figure 4.82, and Figure 4.83. It can be noted that the chloride concentration increased as the dosage of LSP increased. However, the chloride concentration in 5%LSP concrete was less than that of OPC. The chloride concentration also decreased in the specimens with 5%NS. At depth of 40 mm, the chloride concentration of all LSP concrete specimens became almost equal. The slope of the chloride profile of LSP concrete with NS was more than that of LSP concrete without NS. The resulting chloride profiles were utilized to determine the coefficients of chloride diffusion in accordance with Fick's second law of diffusion [59]. The coefficients of chloride diffusion of OPC, 5%LSP, 10%LSP, and 15%LSP concrete were 16.2, 13.44, 17.41, and 19.7 $\times 10^{-8}$ cm^2/s, while they decreased in

the specimens with NS, which were 8.27, 8.95, and 10.07 $\times 10^{-8}$ cm^2/s in 5%LSP+5%NS, 10%LSP+5%NS, and 15%LSP+5%NS specimens, respectively (Figure 4.84).

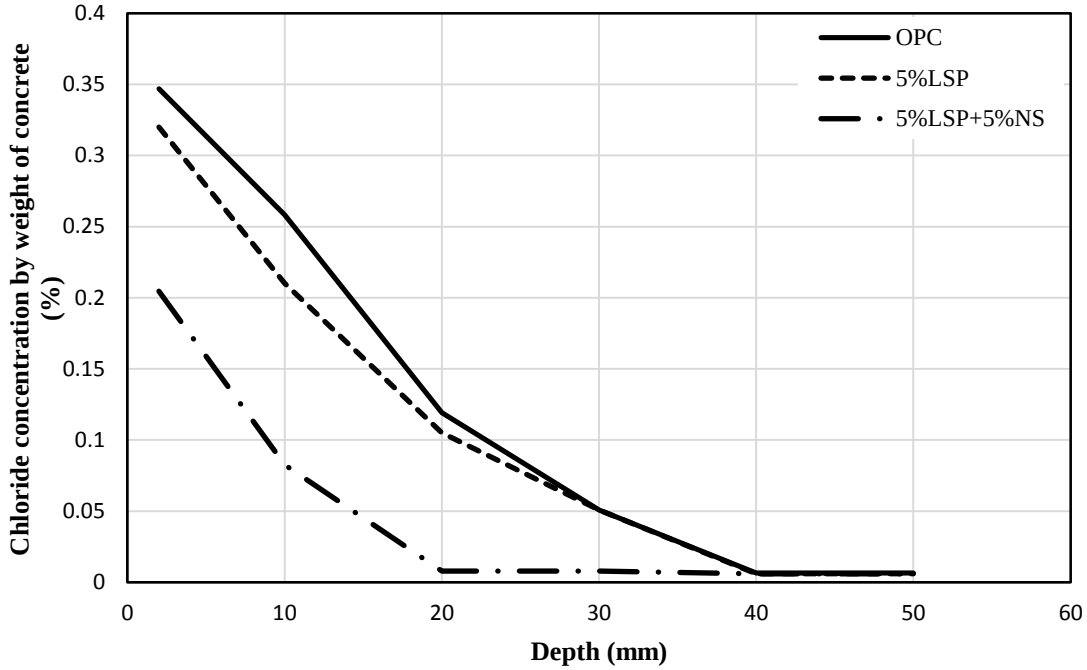

Figure 4.81: Chloride profile of 0% and 5%LSP concrete with and without NS

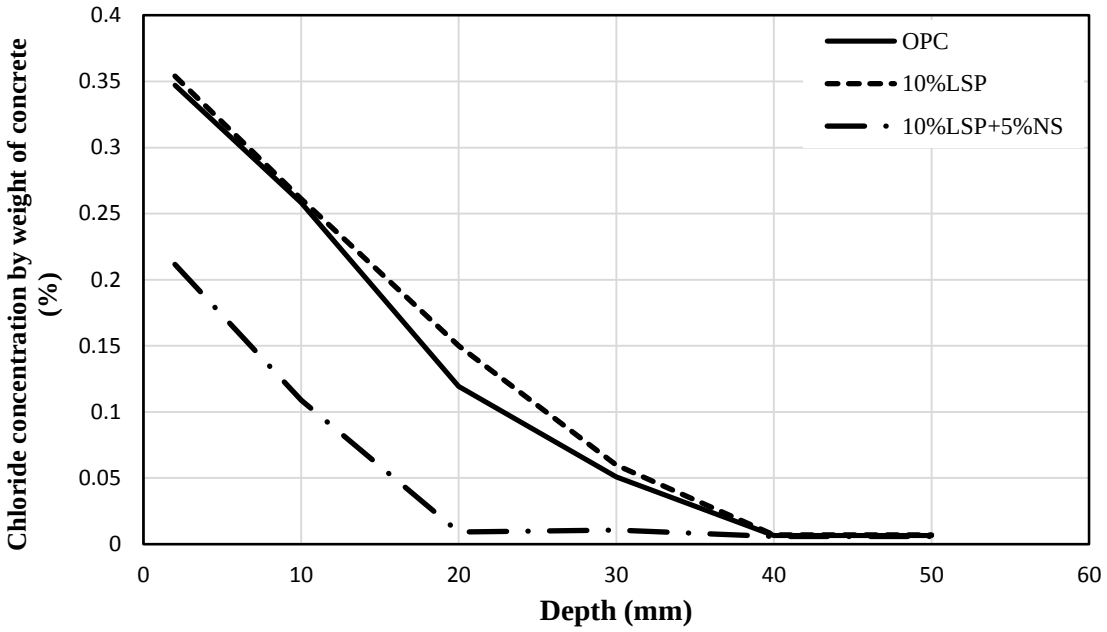

Figure 4.82: Chloride profile of 0% and 10%LSP concrete with and without NS

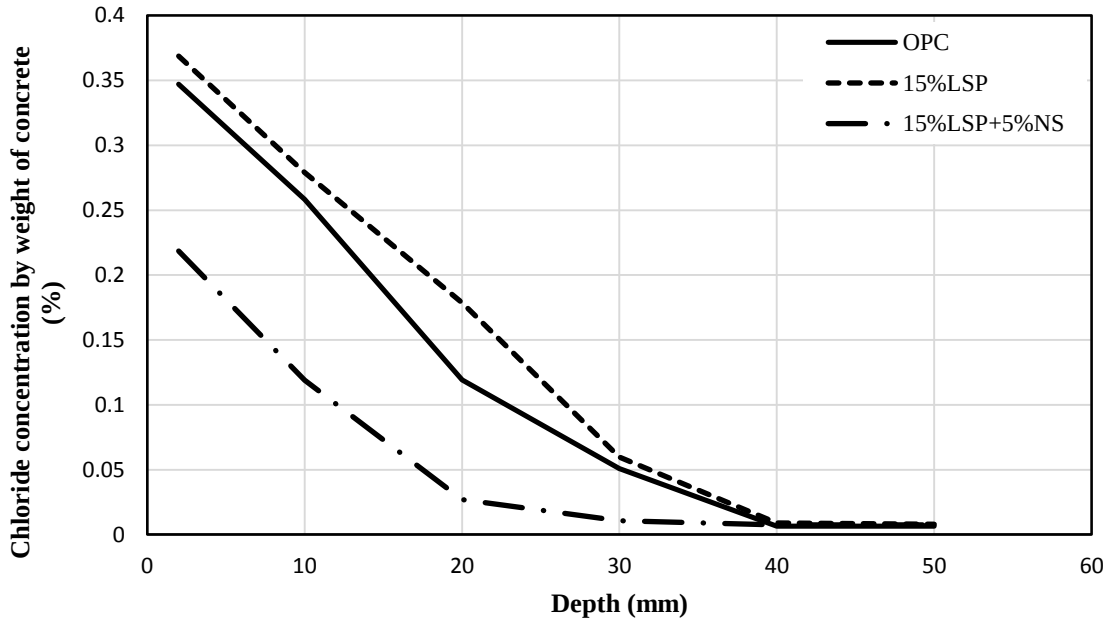

Figure 4.83: Chloride profile of 0% and 15%LSP concrete with and without NS

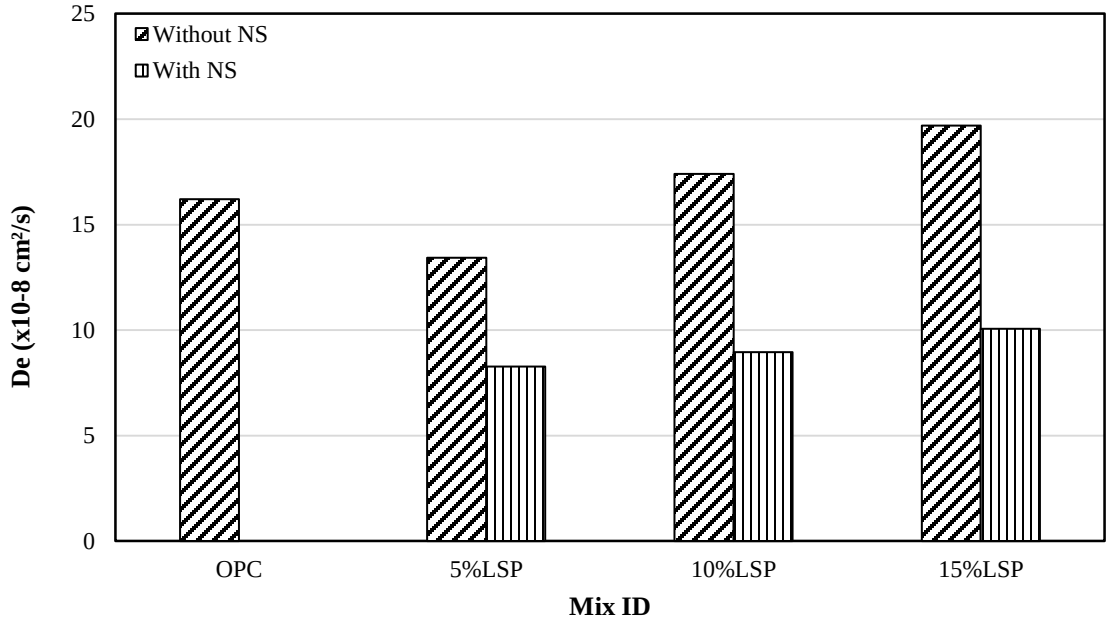

Figure 4.84: Coefficient of chloride diffusion in LSP concrete with and without NS

4.4.1.6 Reinforcement corrosion

Corrosion potentials: The measurements of corrosion potentials was conducted on concrete cylinders with 12 mm steel bars periodically. The corrosion potential was measured on each concrete cylinder with respect to a saturated calomel reference electrode (SCE) and the average value was recorded. Figure 4.85, Figure 4.86, and Figure 4.87 show the corrosion potential (E_{corr}) of LSP concrete with and without NS. The potential values increased as the dosage of LSP was increased, while utilizing NS in the concrete decreased the corrosion potentials compared to the LSP concrete. The corrosion potential of 5% and 10%LSP with NS was less than that of OPC while the corrosion potential of 15%LSP concrete was more.

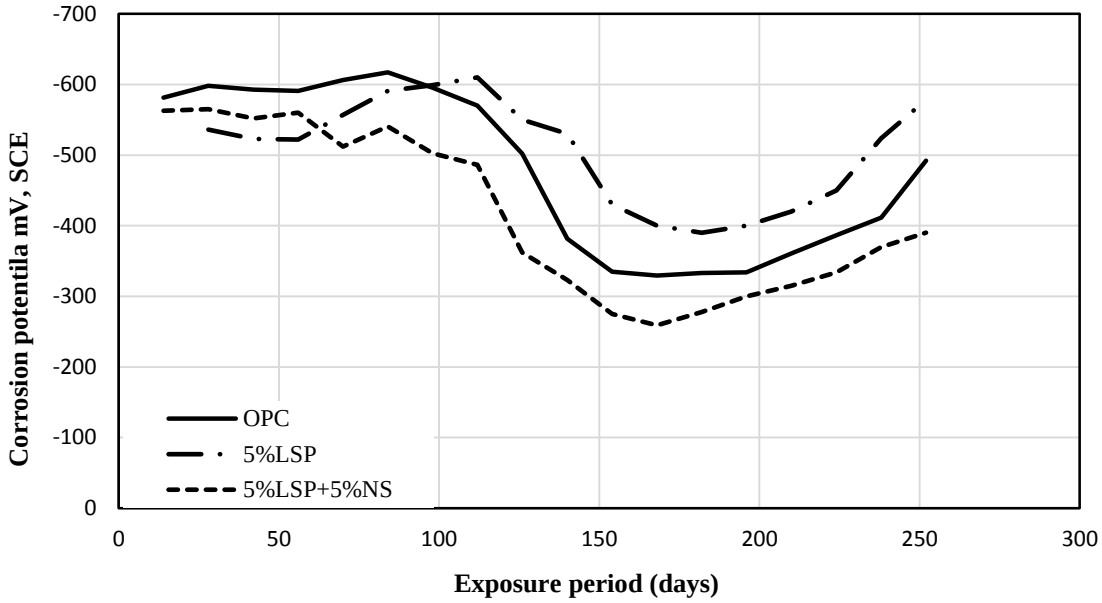

Figure 4.85: Corrosion potentials on steel in of 0% and 5% LSP concrete with and without NS.

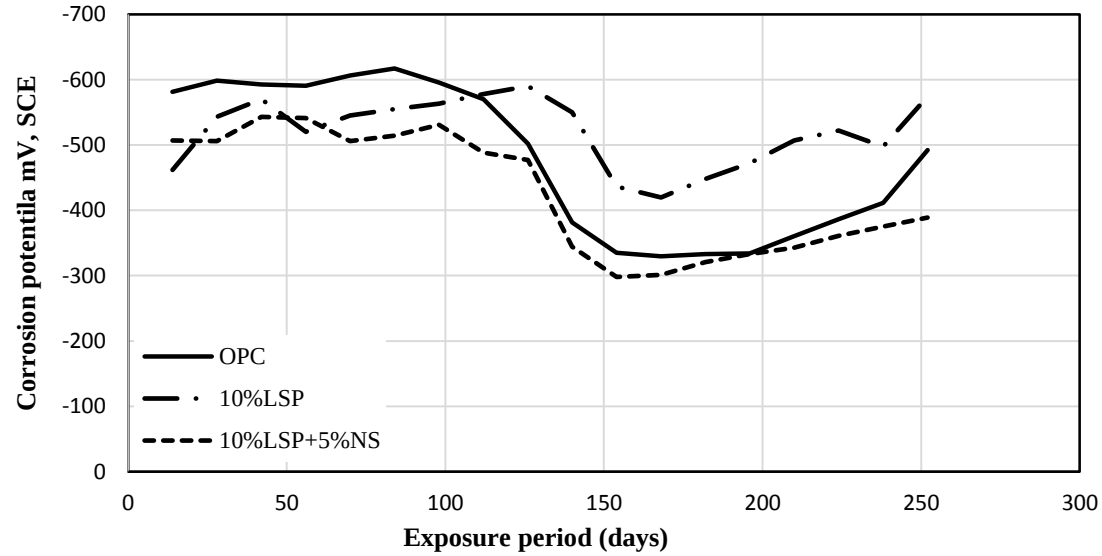

Figure 4.86: Corrosion potentials on steel in 0% and 10% LSP concrete with and without NS.

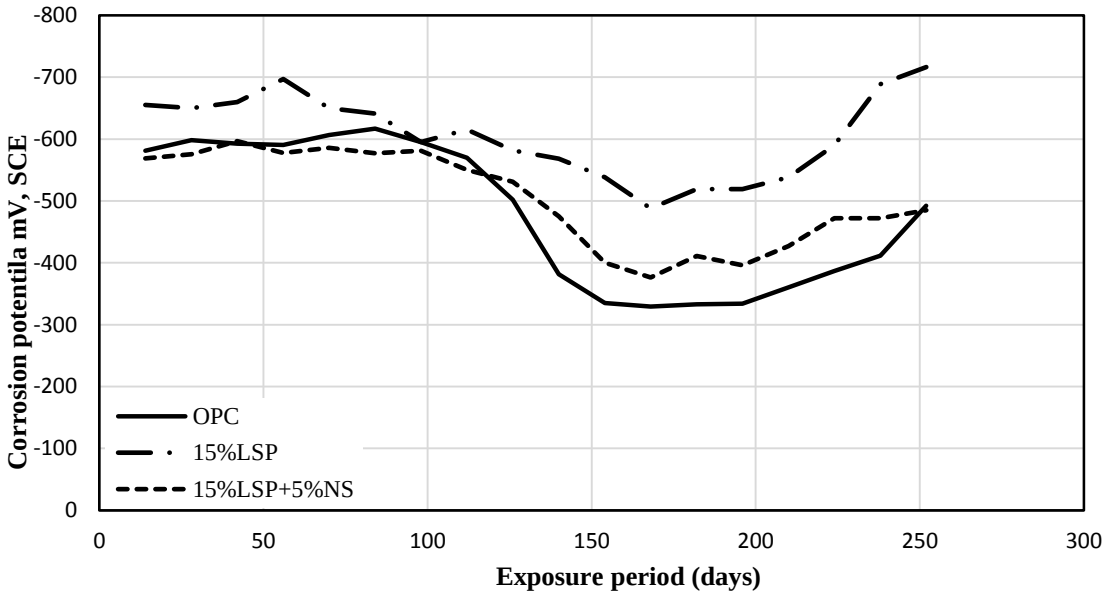

Figure 4.87: Corrosion potentials on steel of 0% and 15%LSP concrete with and without NS

Corrosion current density: The corrosion current density was measured utilizing the concrete specimens that were used for evaluating corrosion potentials. The use of 5% and 10% LSP in the concrete, as a partial replacement of cement, decreased the I_{corr} compared to OPC, while utilizing 15%LSP in the concrete increased the I_{corr} compared to that of OPC. The use of 5% NS in conjunction with LSP significantly decreased the I_{corr} compared to that of LSP concrete without NS (Figure 4.88).

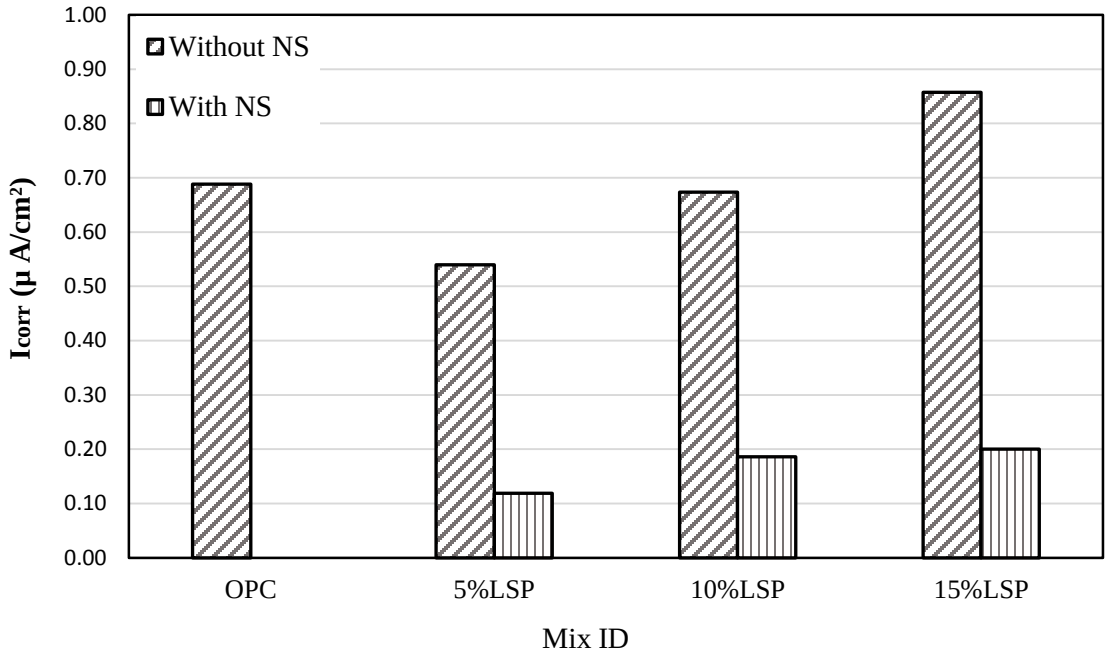

Figure 4.88: 260-day corrosion current density on steel in LSP concrete with and without NS

4.4.1.7 Sulfate attack

The sulfate attack was assessed by measuring the expansion of mortar beams (25×25×285mm) and by visual inspection of the deterioration of paste cubes (25×25×25 mm) exposed to two different sulfate solutions. The prisms were immersed in 2.1% sodium sulfate solution for six months while the cubes were divided into two groups, one group was exposed to 2.1% sodium sulfate solution while the other group was exposed to 2.1% magnesium sulfate solution. Figure 4.89, Figure 4.90, and Figure 4.91 show the expansion of LSP concrete specimens with and without NS. It can be noted that utilizing LSP in the concrete as a partial replacement of cement decreased the expansion compared to that of OPC. However, the expansion of 5%LSP concrete was almost similar to that of OPC. The use of NS in the LSP concrete further decreased the expansion compared to that of LSP concrete. As the dosage of LSP was increased the expansion of the concrete with and

without NS decreased. The deterioration started at the edges of the paste cubes cured in the magnesium sulfate solution, as shown in Figure 4.92, Figure 4.93, and Figure 4.94. The deterioration increased as the dosage of LSP was increased, while no deterioration was noted in the cubes containing NS and LSP. No signs of deterioration were noted in the cube specimens exposed to the sodium sulfate solution.

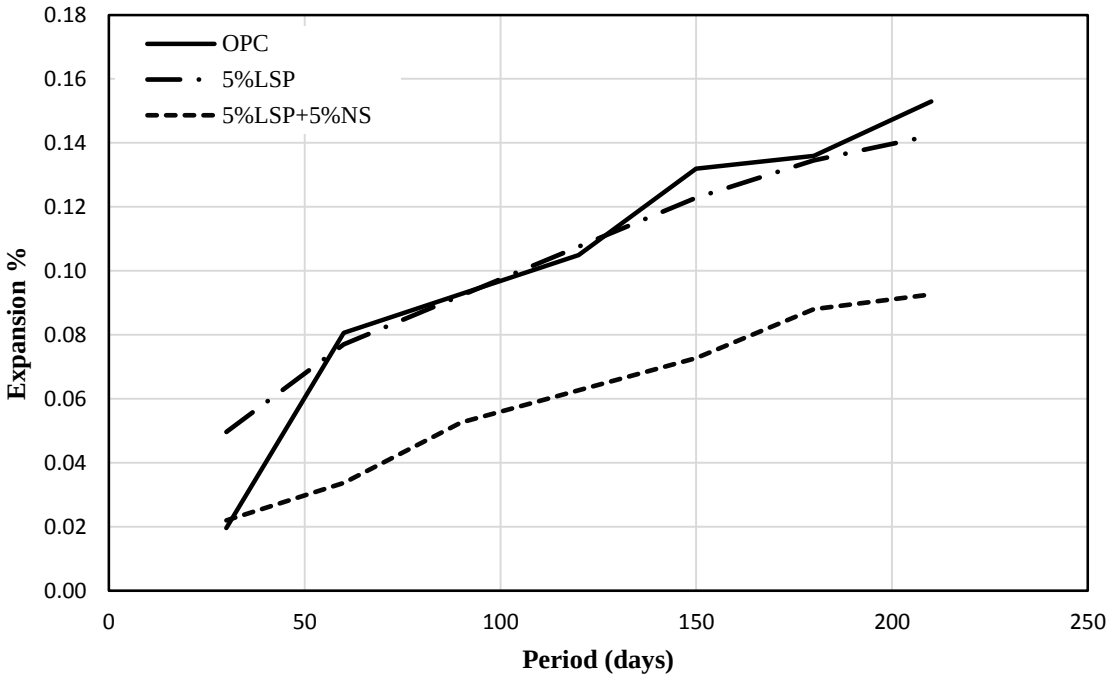

Figure 4.89: Expansion of 0% and 5% LSP concrete with and without NS

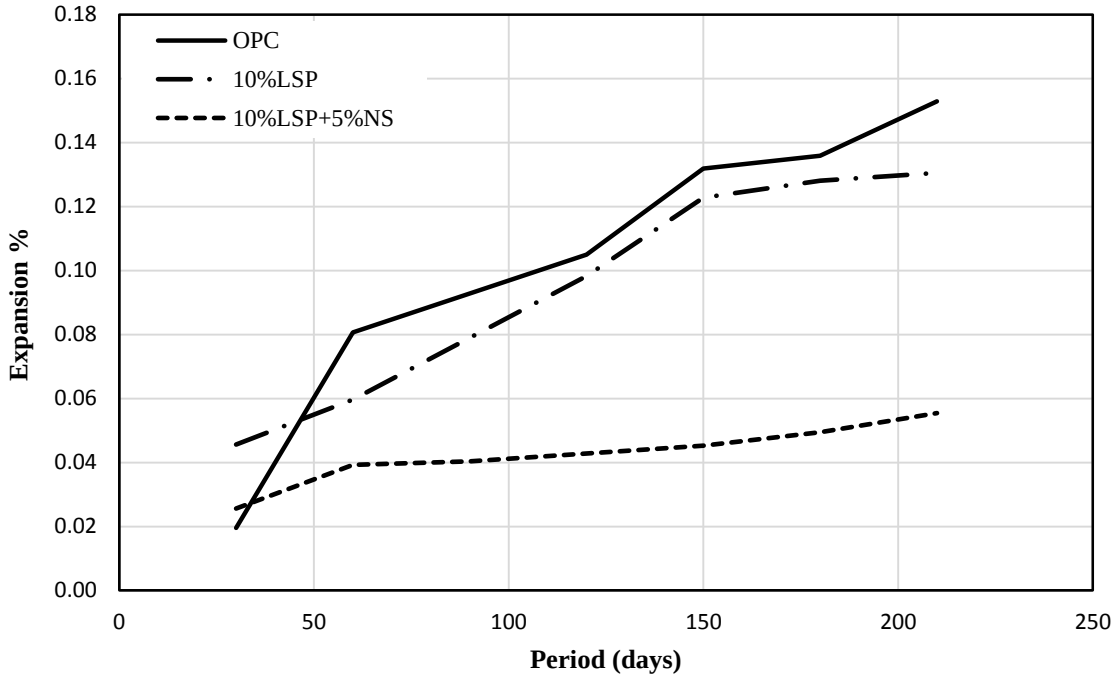

Figure 4.90: Expansion of 0% and 10% LSP concrete specimens with and without NS

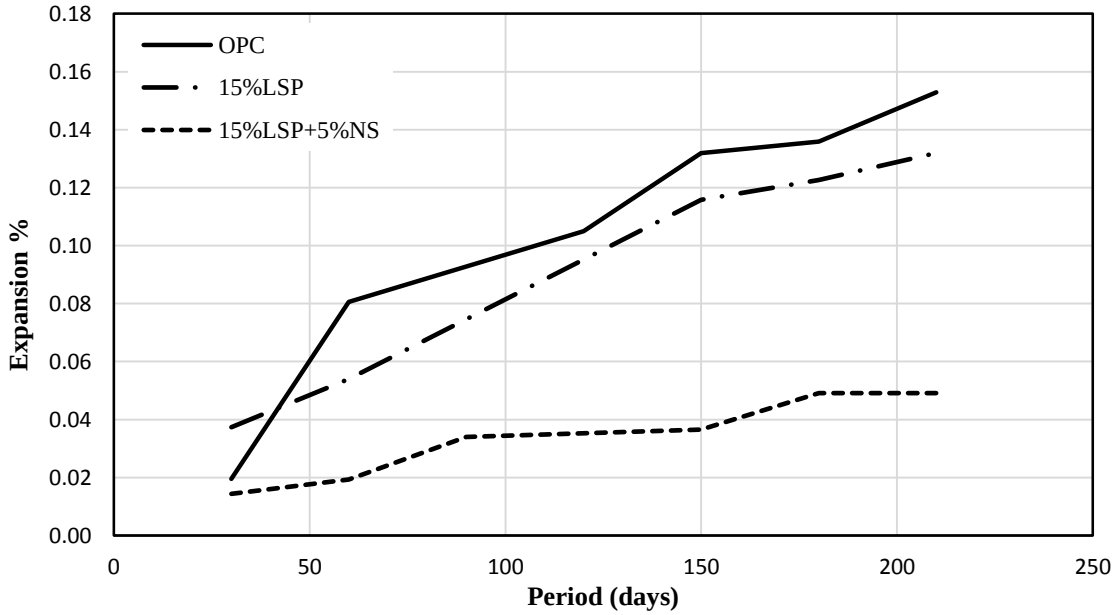

Figure 4.91: Expansion of 0% and 15% LSP concrete specimens with and without NS

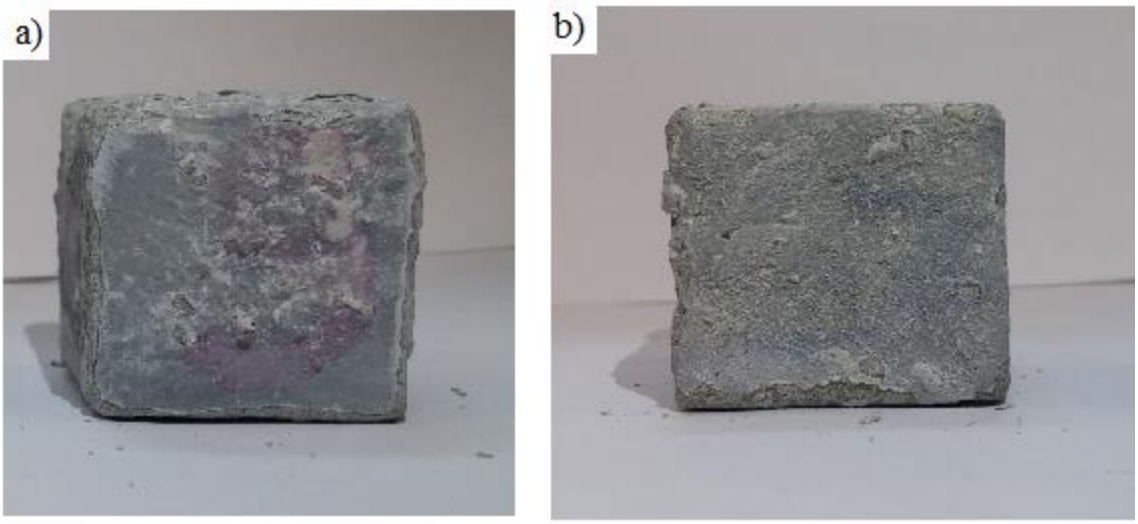

Figure 4.92: a) 5%LSP cube and b) 5%LSP+5%NS cube exposed to magnesium sulfate solution.

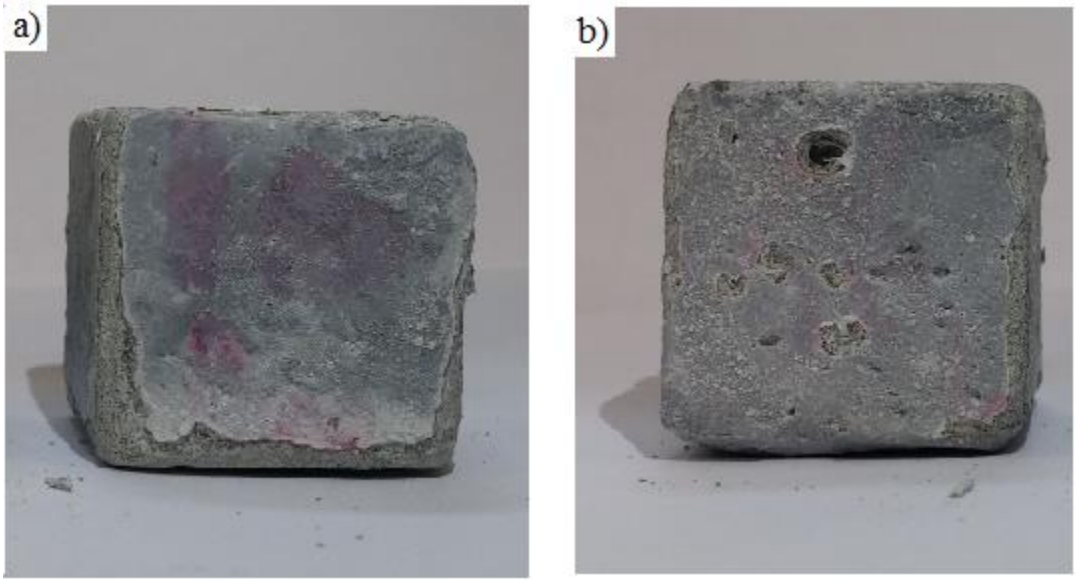

Figure 4.93: a) 10%LSP cube and b) 10%LSP+5%NS cube exposed to magnesium sulfate solution.

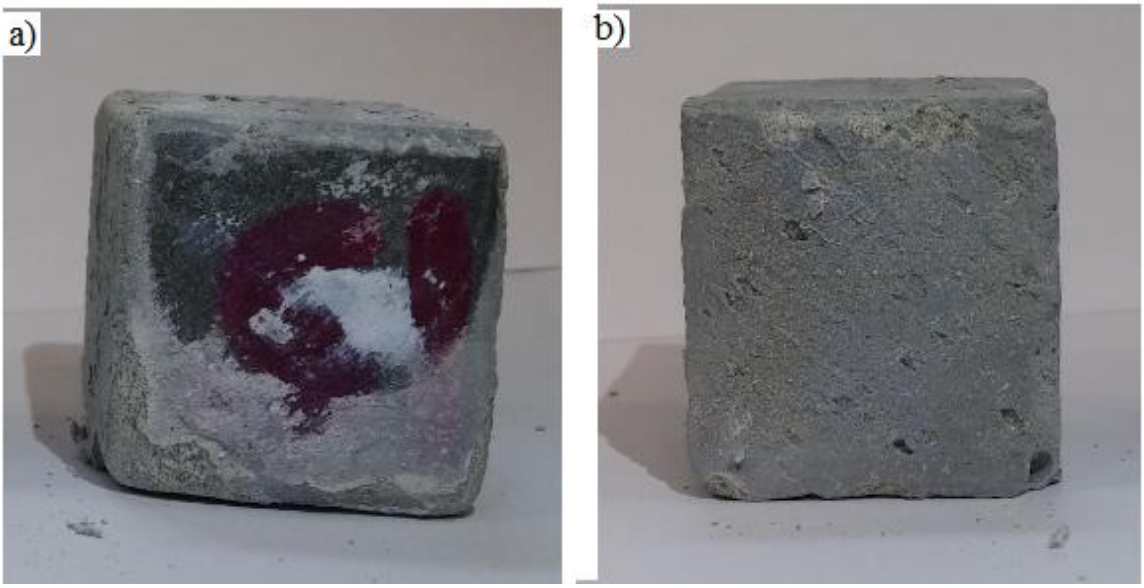

Figure 4.94: a) 15%LSP cube and b) 15%LSP+5%NS cube exposed to magnesium sulfate solution.

4.4.2 Micro properties

4.4.2.1 Morphology

Figure 4.95 shows the SEM of 5% LSP concrete specimen. A porous structure with cracks at the interfacial transition zone (ITZ) were noted in the morphology of 5%LSP (Figure 4.95 (a)). Low quantity of calcium hydroxide (with respect to the microstructure of OPC) and non-uniform CSH gel were appeared in the microstructure of 5%LSP (Figure 4.95 (b)). A more uniform and compact microstructure and dense ITZ with a thin CH layer were noted in the 5%LSP+5%NS specimen (Figure 4.96 (a& b)). Large amount of CSH gel was noted in the microstructure and at the ITZ of 5%LSP+5%NS specimen (Figure 4.96 (b& d). The BEI images of 5%LSP+5%NS showed good bond between the aggregate and the matrix (Figure 4.96(c)). The morphology of 15%LSP+5%NS specimen is depicted in Figure 4.97. The ITZ of 15%LSP+5%NS enhanced compared to that of specimen without NS but it is more porous than in 5%LSP+5%NS specimen (Figure 4.97

(a)). More CSH gel appeared in the microstructure of 15%LSP+5%NS specimen, but it was not as dense as in 5%LSP+5%NS. A thin layer of CH appeared at the ITZ of 15%LSP+5%NS specimen that is thicker than the layer appeared in the microstructure of 5%LSP+5%NS specimen (Figure 4.97 (a)).

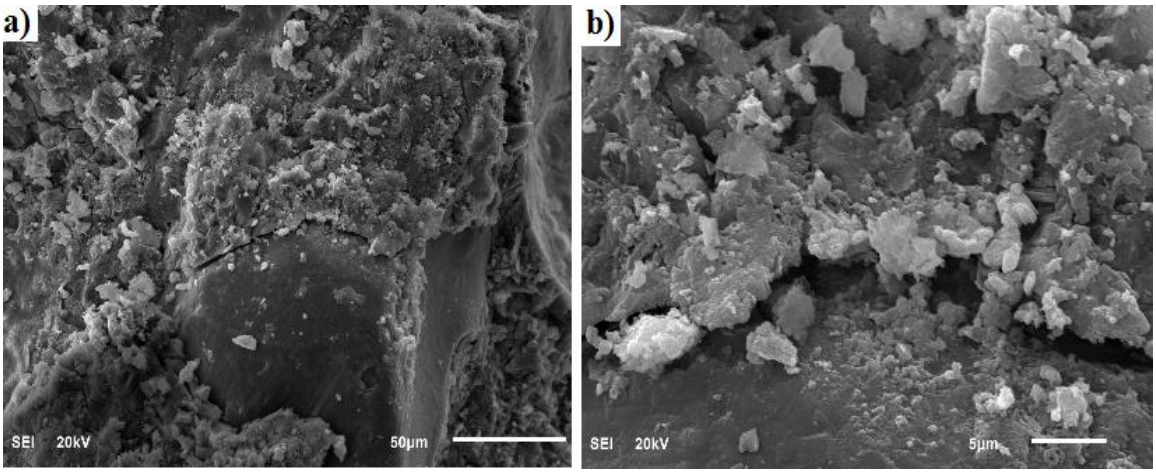

Figure 4.95: SEM of 5%LSP concrete specimen.

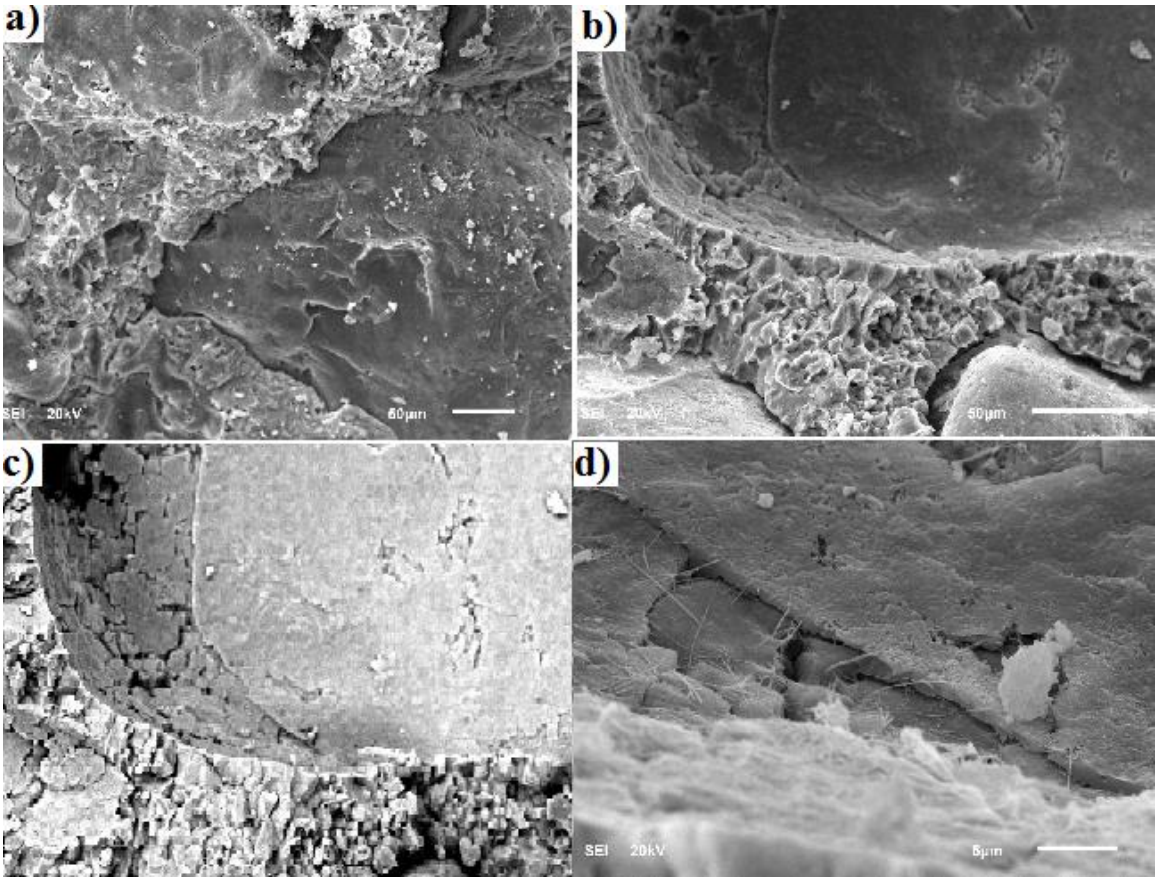

Figure 4.96: SEM and BEI images of 5%LSP+5%NS concrete specimen.

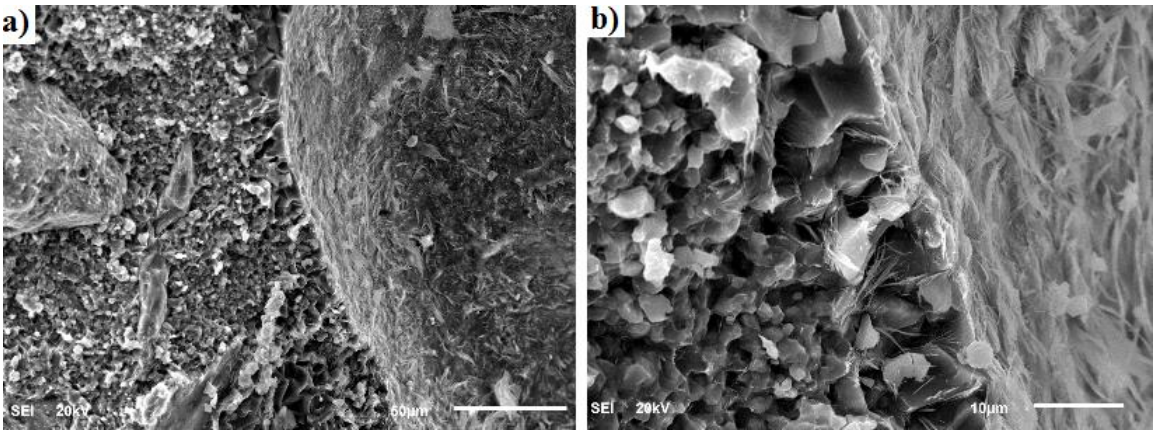

Figure 4.97: SEM of 15%LSP+5%NS concrete specimen.

4.4.2.2 Mineralogical composition

The XRD spectra for 5%LSP paste specimen is almost similar to that for OPC with a small reduction in the CH peaks (Figure 4.98). The use of 5%NS in the 5%LSP paste caused a reduction in the CH peaks (Figure 4.99). It was noted in the spectra of 5%LSP+5%NS paste exposed to the sodium sulfate solution that the CH peaks decreased and the secondary ettringite peak increased compared to that of the same specimen but cured in water (Figure 4.100). A significant reduction in the CH and more gypsum was produced in the specimen exposed to the magnesium sulfate solution, as shown in Figure 4.101.

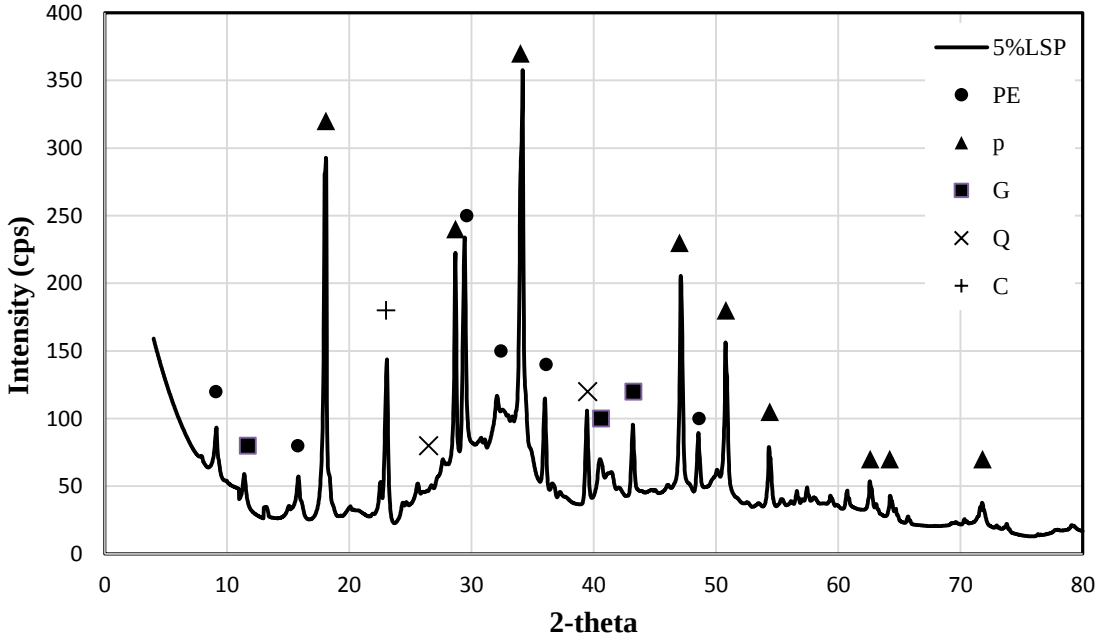

Figure 4.98: XRD spectra of 5%LSP paste specimen.

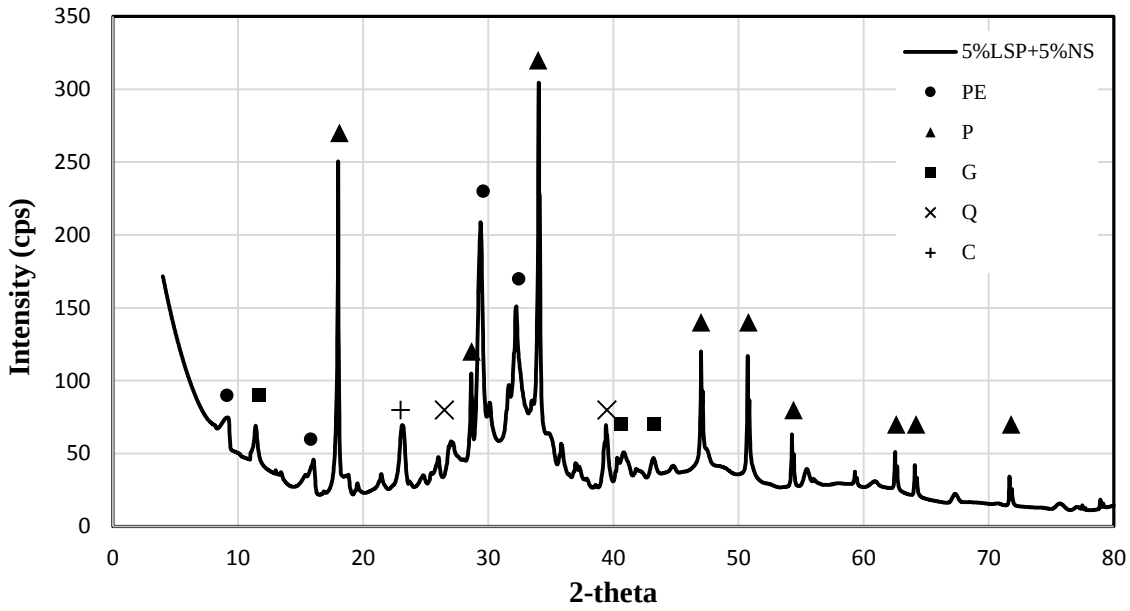

Figure 4.99: XRD spectra of 5%LSP+5%NS paste specimen.

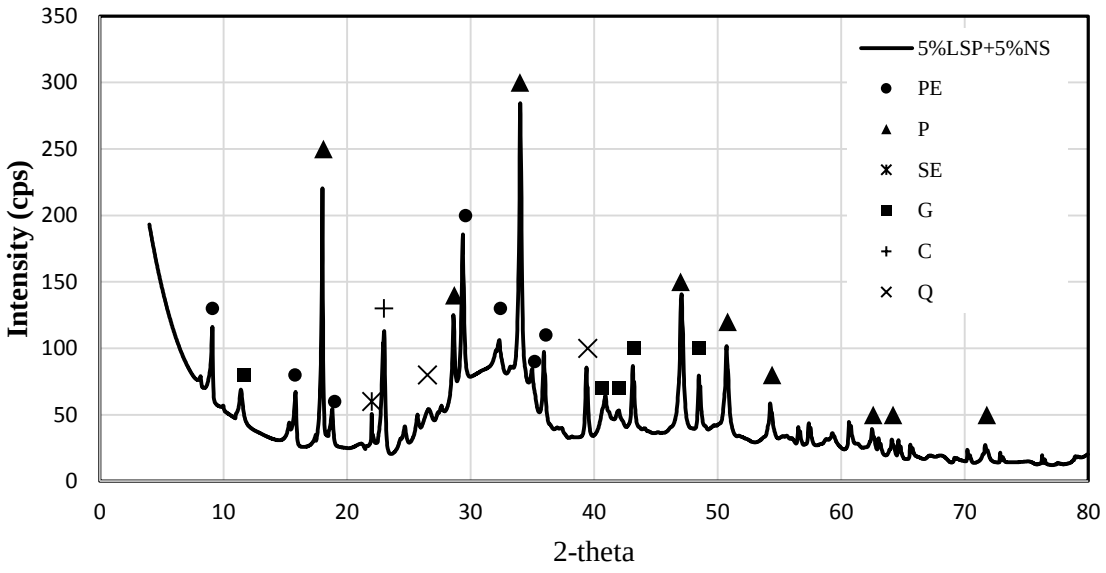

Figure 4.100: XRD spectra of 5%LSP+5%NS paste specimen exposed to the sodium sulfate solution.

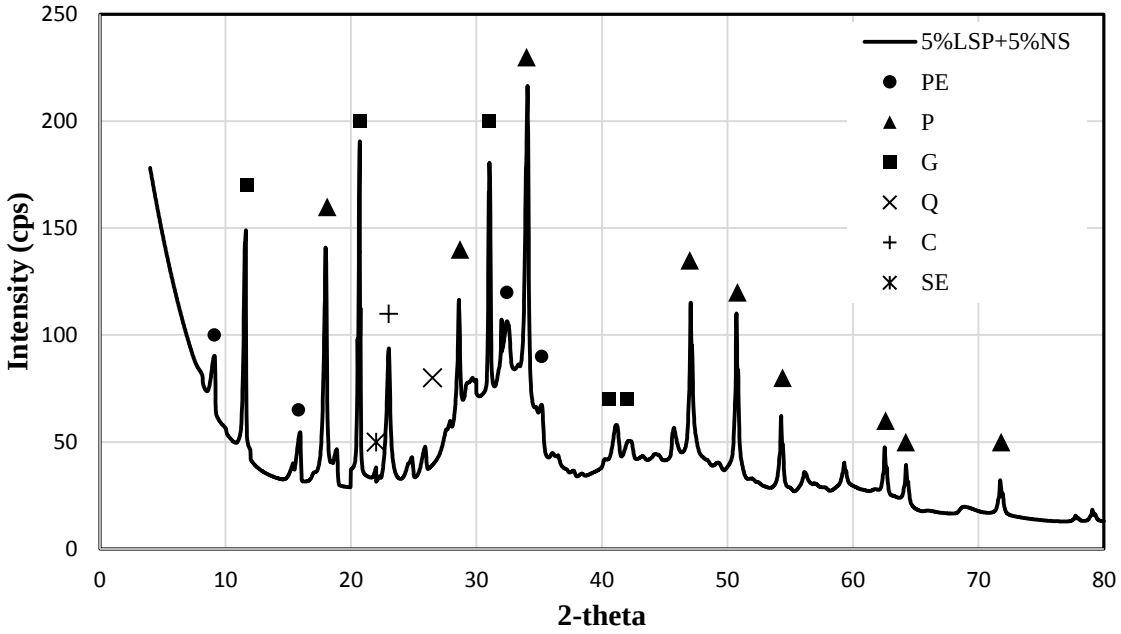

Figure 4.101: XRD spectra of 5%LSP+5%NS paste exposed to the magnesium sulfate solution

4.4.3 Discussion of results

The use of LSP in the concrete as a partial replacement of cement decreased the strength. However, the strength of 5% LSP specimens was almost similar to that of OPC. The reactivity of LSP was low compared to that of OPC, so the increase in the strength may be attributed to the nucleation effect of LSP, in which LSP acted as a nuclei to the CH crystals [74]. Also, LSP can contribute to the strength through its reaction with C_3A in cement to produce calcium hemi-carboaluminate, calcium monocarboaluminate and calcium tri-carboaluminate [74]. It was reported that a small quantity of LSP is utilized in CSH, forming carbonated hydrated calcium silicate compound [75, 76]. The reduction in the strength of LSP specimens may be attributed to the dilution of cement as well as to the reduction of the interfacial zone strength.

The compressive strength of LSP concrete specimens improved with the addition of NS at different ages, which can be attributed to the formation of secondary gel resulting from the pozzolanic reaction. Also, due to the physical action of NS, in which NS acted as a nuclei to the hydration products. As stated earlier, LSP reacts with CSH gel to produce carbonate hydrated calcium silicate compound, so its effect increased due to the extra gel produced. Due to the high CSH content, more was LSP utilized in the CSH reaction, that lead to the high strength enhancement of 15%LSP+5%NS specimen compared with other concretes. The maximum strength was obtained in 5%LSP+5%NS concrete specimens, which means that the best compaction was obtained when 5%LSP was utilized in the concrete. The reduction in the strength in specimens with NS was related to the same reasons mentioned for the specimens without NS. SEM images of LSP concrete with NS showed a compact micro structure with uniform and dense ITZ and a thin layer of CH accumulated at the ITZ. The dense structure resulted from the pozzolanic reaction and the physical action of NS and LSP particles. The denseness of the microstructure decreased as the dosage of LSP increased at the same dosage of NS, which strongly agreed with the reduction of the compressive strength as the dosage of LSP increased. XRD spectra showed a reduction in the CH due to the use of NS in the concrete, which agreed with the reduction in the CH layer at the ITZ, as shown in SEM images.

The flexural strength increased due to the use of LSP in concrete, which can be attributed to the role of LSP in enhancing the interfacial zone compared to OPC. CH normally accumulates at the interfacial zone which causes a reduction in the bond between the aggregate and the mortar which negatively affects the flexural strength. LSP acts as a nuclei to CH leading to an increase in the flexural strength [74]. As the dosage of LSP increased

the flexural strength decreased, however the lowest flexural strength of LSP concrete was more than that of OPC. The reduction in the flexural strength may be attributed to the dilution of cement, low pozzolanic reactivity of LSP, and to the effect of free-LSP in weakening the interfacial zone. The use of NS in the LSP concrete increased the flexural strength of all the specimens. This may be attributed to the secondary CSH gel resulting from the pozzolanic reaction and to the physical effect of both NS and LSP. SEM images of LSP concrete with NS showed a dense and untracked ITZ.

The reduction in the drying shrinkage of 5% LSP specimen may be attributed to the dense structure resulting from the filling action of LSP particles which minimizes the evaporation of the water. The dense structure does not allow the free water to evaporate. Thus, the use of 5% LSP in concrete, as a partial replacement of cement, did not decrease the strength and decreased the shrinkage. The drying shrinkage of concrete with 10% and 15% LSP increased, which can be attributed to the decrease in the free water resulted from the low reactivity of LSP compared to that of OPC since LSP used as a partial replacement of cement. The increase in the drying shrinkage of LSP concrete with NS may be attributed to the consumption of free water in the hydration reaction.

The porous structure of LSP concrete without NS was clear in the SEM images while a dense, compact, and uniform microstructure was noted in the microstructure of LSP concrete with NS. The dense microstructure resulting from the physical and chemical effect of NS decreased the decreased the diffusion of chloride ions and the chloride permeability.

The corrosion potentials and corrosion current density of specimens with 5% and 10% LSP was less than that of OPC, which may be attributed to the physical effect of LSP in improving the microstructure. The denseness of the microstructure further increased due

to the use of NS in the concrete. Although NS consumed CH in the pozzolanic reaction which reduced the pH of the pore solution, it produced more gel and filled the pores which compensate the reduction in the alkalinity. The dense, compact, uniform structure delayed the chloride diffusion, increased the concrete resistivity, decreased the potential variation, and thereby decreased the corrosion current density.

Less expansion was noted in LSP concrete due to sulfate attack which may be attributed to the reduction in C_3A content. The use of NS in LSP concrete, as a partial replacement of cement, significantly decreased the expansion. The chemical and physical action of NS increased the concrete density and consumed CH, which is essential for producing secondary ettringite. The deterioration of the edges of LSP paste resulted from the production of magnesium hydroxide which produced from the reaction between magnesium sulfate and calcium hydroxide which caused a reduction in the pH of the pore solution making CSH unstable. Negligible deterioration was noted in the LSP+5%NS specimens which may be attributed to their dense structure which delayed the diffusion of magnesium and sulfate ions in to the core of the specimens. Further, deterioration was not noted in the specimens exposed to the sodium sulfate solution which can be attributed to the short period of exposure. The XRD spectra showed an increase in the secondary ettringite peak in the spectra of 5%LSP+5%NS specimens cured in sodium sulfate solution, while more gypsum appeared in the spectra of specimens exposed to the in magnesium sulfate solution.

4.5 Properties of OA concrete with and without NS

The properties of OA concrete were evaluated by conducting different tests on concrete specimens. The specimens were prepared from four different mixes, in which OA was utilized in the mixes with two different dosages (5% and 10%). Two mixes were prepared with OA, while in the other two mixes NS was utilized in conjunction with OA. In all the mixtures OA and NS was used as partial replacement of cement.

4.5.1 Macro properties

4.5.1.1 Compressive strength

The compressive strength development is shown in Figure 4.102. The early-age compressive strength of the OA concrete specimens was less than that of OPC. At 3 days, the compressive strength was 22.92 and 13.29 MPa in 5%OA and 10%OA specimens, respectively. Due to the addition of NS in the OA concrete, the early-age strength increased noticeably, it became 43.37 and 36.49 MPa in 5%OA+5%NS and 10%OA+5%NS specimens, respectively. Further, the strength of OA concrete, with and without NS, increased with age. The maximum strength was obtained in 5%OA+5%NS specimen, then the strength decreased as the dosage of OA was increased. The 28-day compressive strength of 5%OA, 10%OA, 5%OA+5%NS and 10%OA+5%NS specimens was 61.35, 49.5, 71.05, and 62.52 MPa, respectively. The use of 5%OA in the concrete increased its strength by 5.78% compared to OPC, while the strength decreased by 14.66% when 10% of cement content was replaced with OA (Figure 4.103). The use of 5% NS in the mixes with 5% and 10% OA increased the strength by 22.5% and 7.79%, respectively, compared

to OPC. The effect of NS in increasing the compressive strength of 10%OA specimen was moer than that in 5%OA specimen, it was 26.32% and 15.81%, respectively (Figure 4.104).

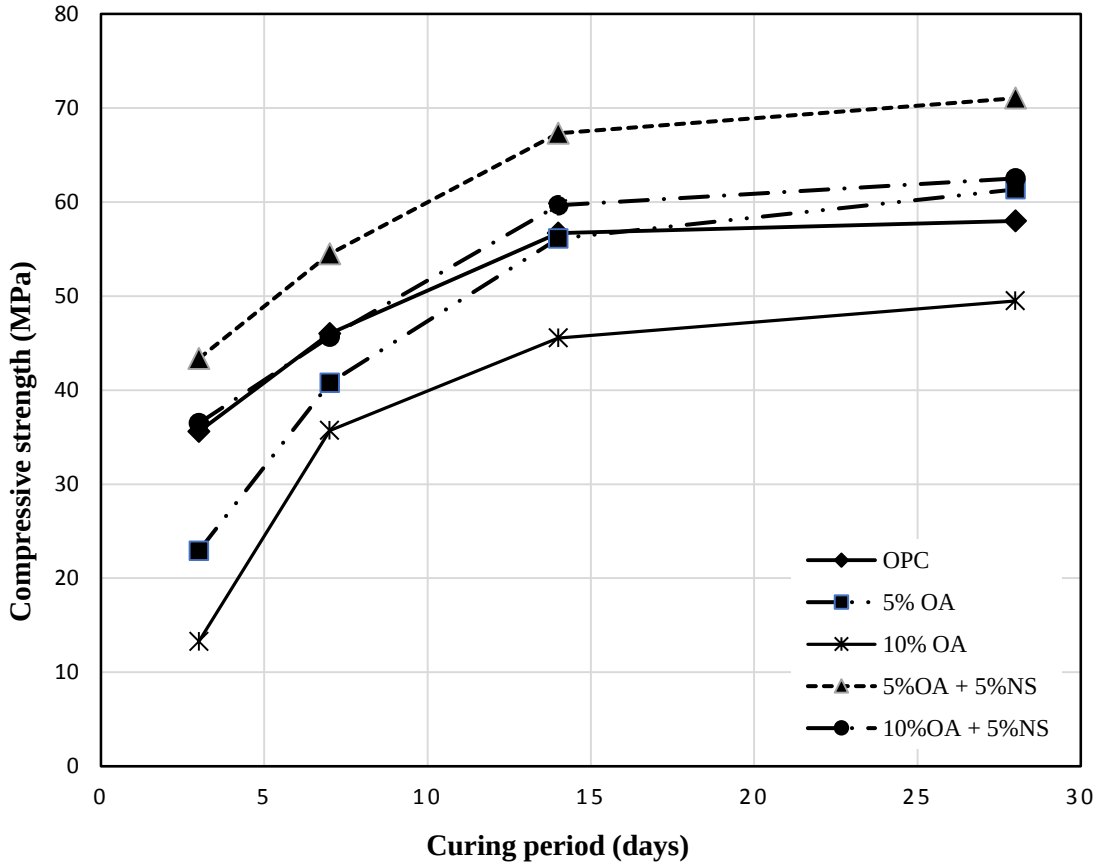

Figure 4.102: Compressive strength of OA concrete specimens

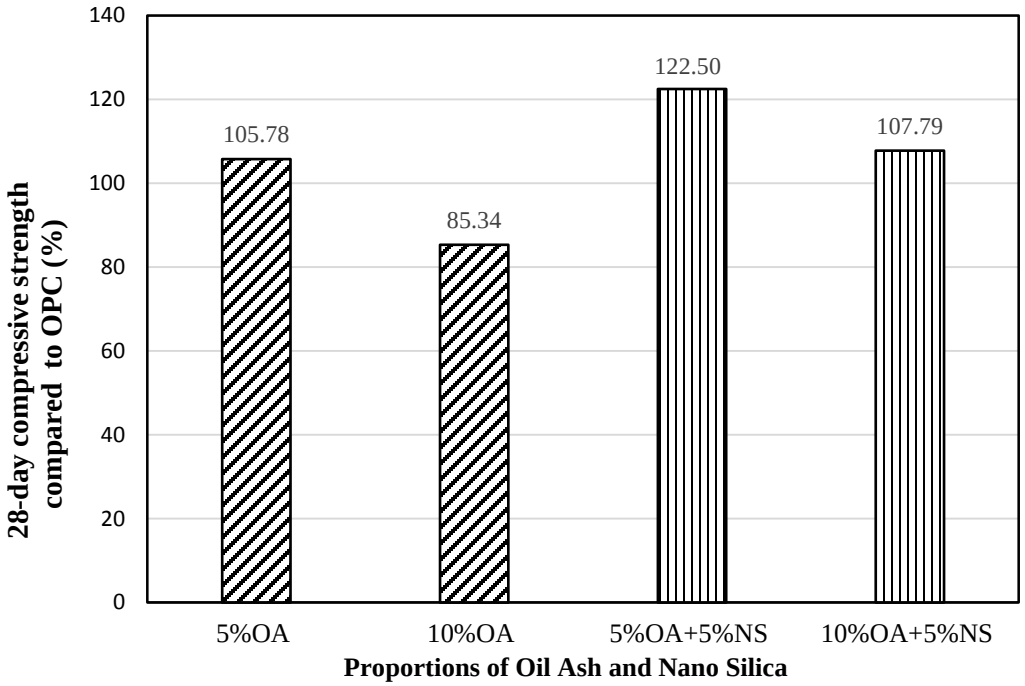

Figure 4.103: Change in 28-day compressive strength of OA concrete specimens compared to OPC

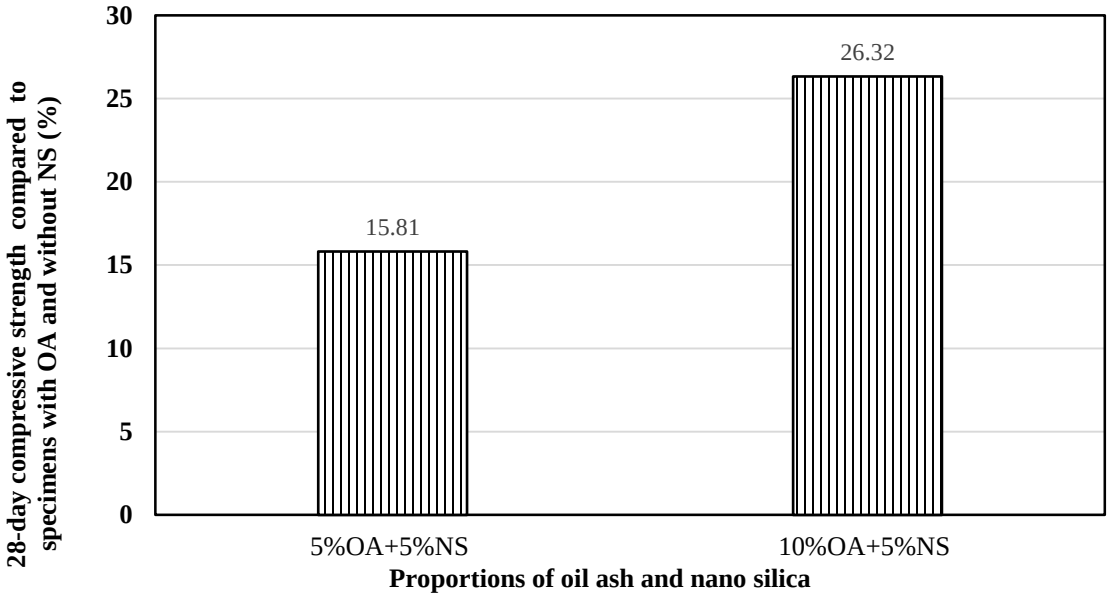

Figure 4.104: Percentage increase in the compressive strength due to the use of 5%NS in the OA concrete

4.5.1.2 Flexural strength

Figure 4.105 depicts the flexural strength of OA concrete specimens. The flexural strength of 5%OA, 10%OA, 5%OA+5%NS and 10%OA+5%NS specimens was 4.24, 3.39, 4.81, and 4.67 MPa, respectively. The use of 5%OA in the concrete increased the strength by 1.2% compared to OPC. When the dosage of OA was increased to 10%, the flexural strength decreased by 19.2% compared to OPC. The incorporation of NS in the concrete increased the flexural strength by 14.8% and 11.5% in the 5%OA+5%NS and 10%OA+5%NS specimens, respectively (Figure 4.106). The optimum OA dosage was 5% with and without NS, while the strength of 10%OA concrete, with and without NS, decreased. However, the strength of 10%OA+5%NS was higher than that of OPC. The increase in the strength in the specimens with 10%OA, due to the addition of NS, was more than that of specimens with 5%OA (Figure 4.107).

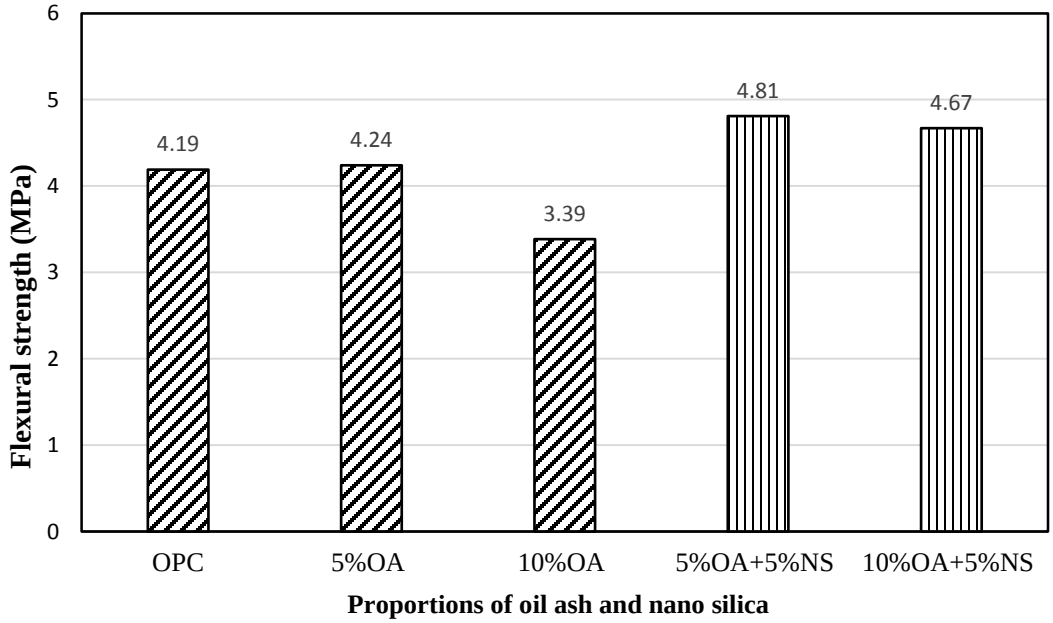

Figure 4.105: Flexural strength of OA concrete specimens

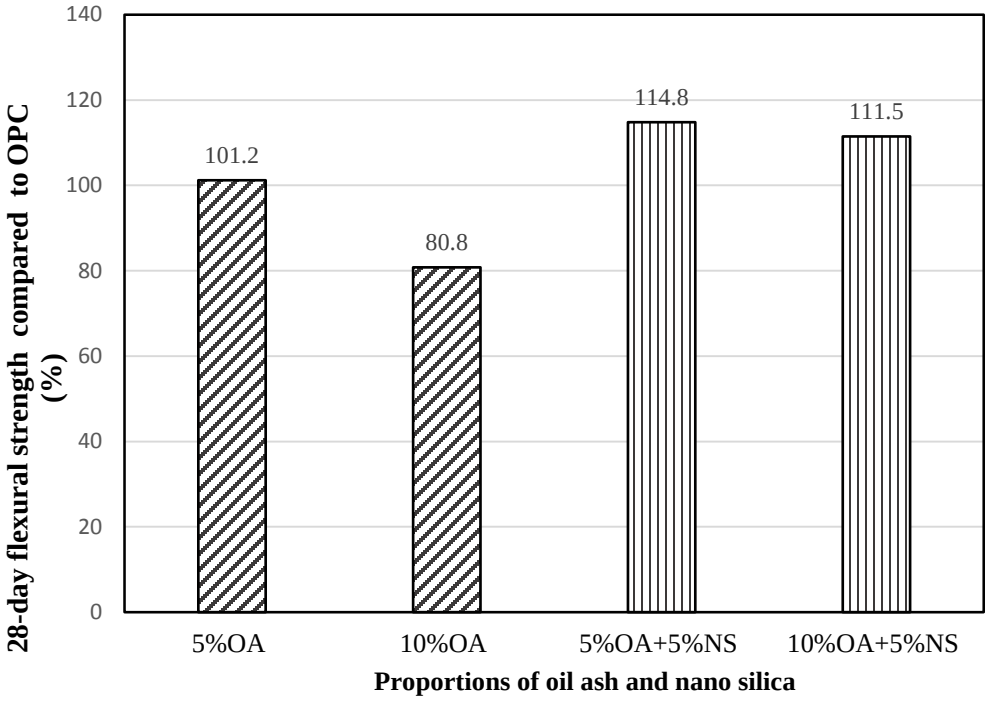

Figure 4.106: Change in the flexural strength of OA specimens compared to OPC

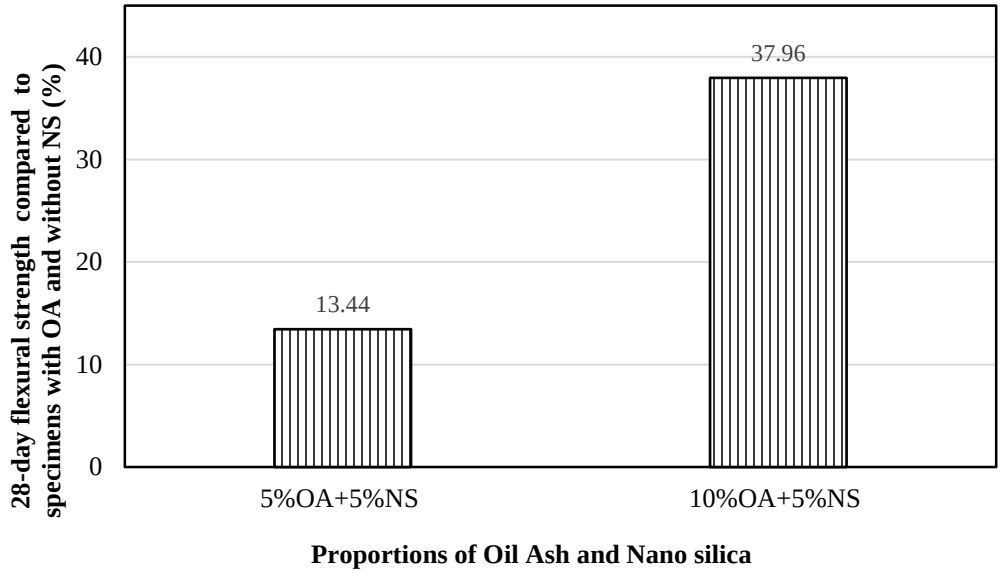

Figure 4.107: Effect of NS in enhancing the flexural strength of OA specimens

4.5.1.3 Drying shrinkage

Figure 4.108 depicts the drying shrinkage of OA concrete specimens. Replacing cement with 5%OA caused a reduction in the drying shrinkage, while increasing the dosage of OA up to 10%, increased the drying shrinkage. The incorporation of NS in the OA concrete further increased the drying shrinkage. As the dosage of OA was increased, the drying shrinkage of NS concrete also increased.

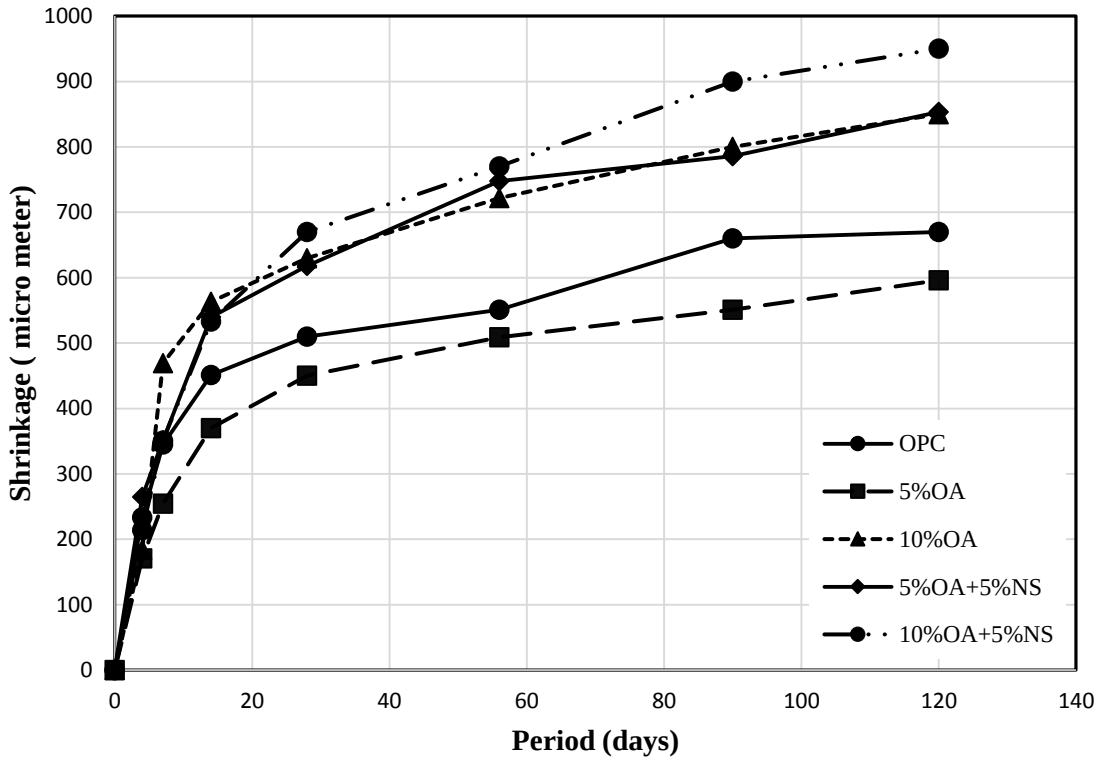

Figure 4.108: Drying shrinkage of OA cement concrete with and without NS.

4.5.1.4 Chloride permeability

The total charge passed through the OA specimens is depicted in Figure 4.109. The chloride permeability of 5%OA specimens decreased compared to that of OPC, while it

increased in the specimen with 10%OA. The incorporation of NS in the OA concrete caused a noticeable decrease in the chloride permeability.

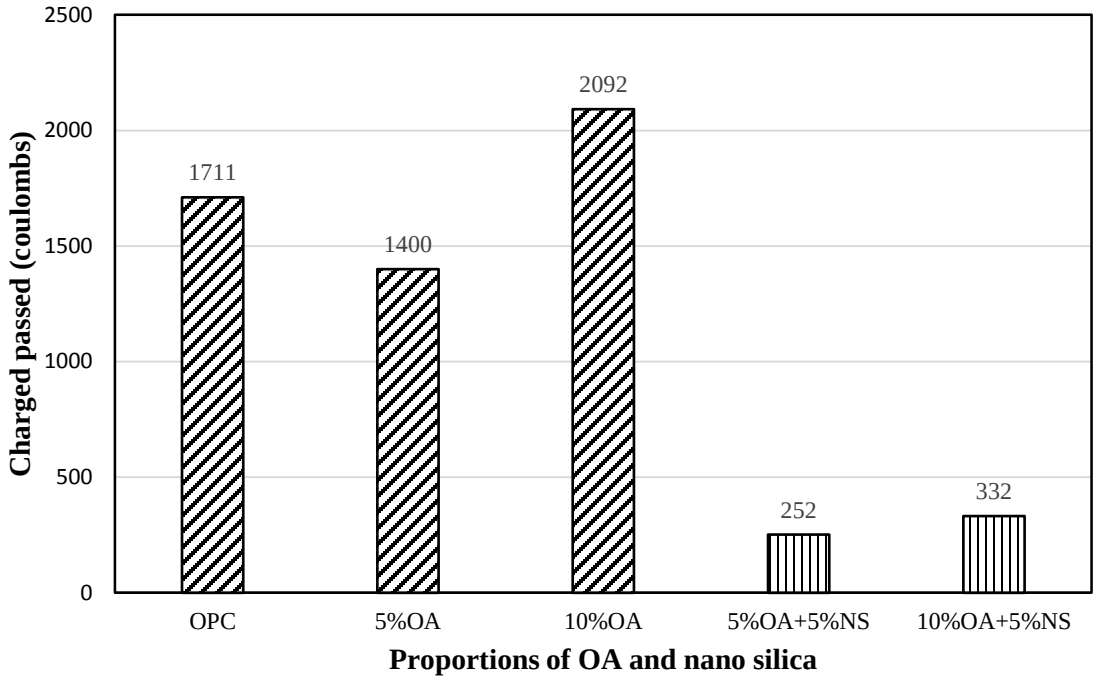

Figure 4.109: Rapid chloride permeability of OA concrete specimens prepared with and without NS.

4.5.1.5 Chloride diffusion

The chloride profiles of OA concrete specimens prepared with and without NS are shown in Figure 4.110 and Figure 4.111. The chloride concentration increased as the dosage of OA increased at different depths. However, the chloride concentration of 5%OA concrete at different depths was slightly less than that of OPC. Further, the chloride concentration decreased due to the incorporation of 5%NS, as a partial replacement of cement. The difference in chloride concentrations of different OA concrete specimens with and without NS at a depth of 40 mm was negligible. The slope of the chloride profile of OA concrete with NS were more than that of OA concrete without NS. The chloride profiles were

utilized to determine the coefficients of chloride diffusion in accordance with Fick's second law of diffusion [59]. The coefficient of chloride diffusion of OPC, 5%OA, 10%OA, 5%OA+5%NS and 10%OA+5%NS concrete was 11.95, 19.28, 8.29, and 7.62 $\times 10^{-8}$ cm^2/s, respectively. The use of NS in the OA concrete decreased the coefficient of chloride diffusion (Figure 4.112).

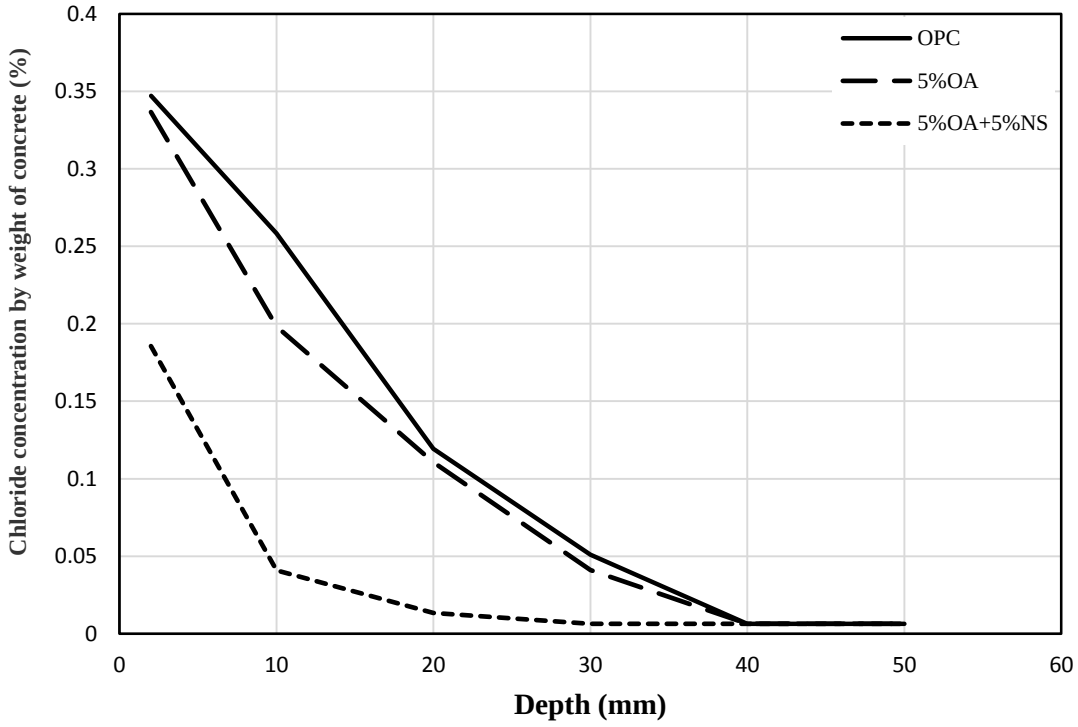

Figure 4.110: Chloride profile of 0% and 5% OA concrete with and without NS

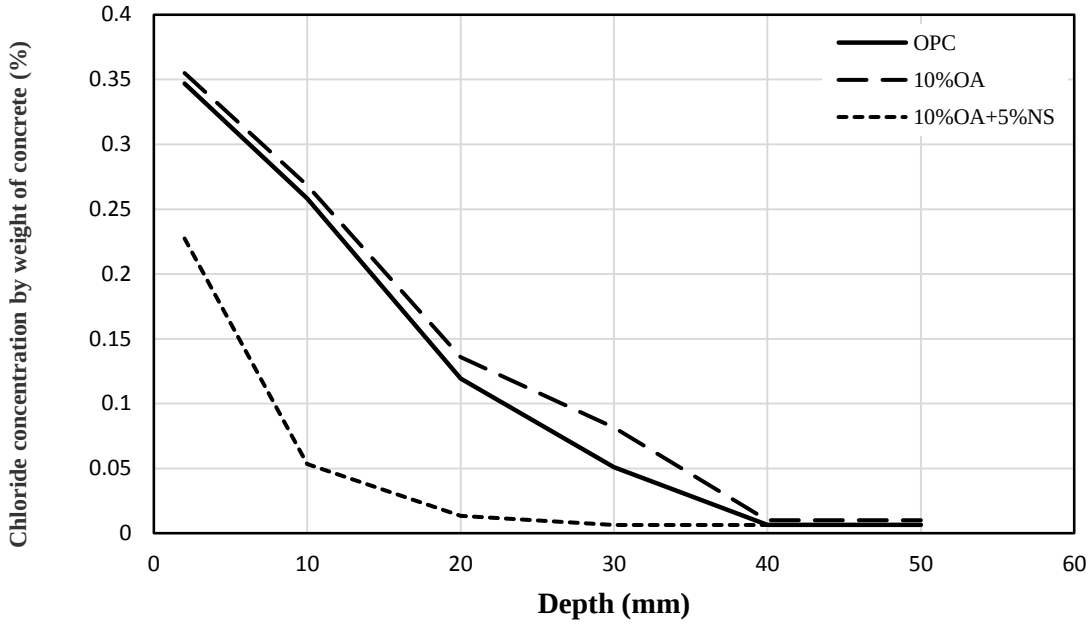

Figure 4.111: Chloride profile of 0% and 10% OA concrete with and without NS

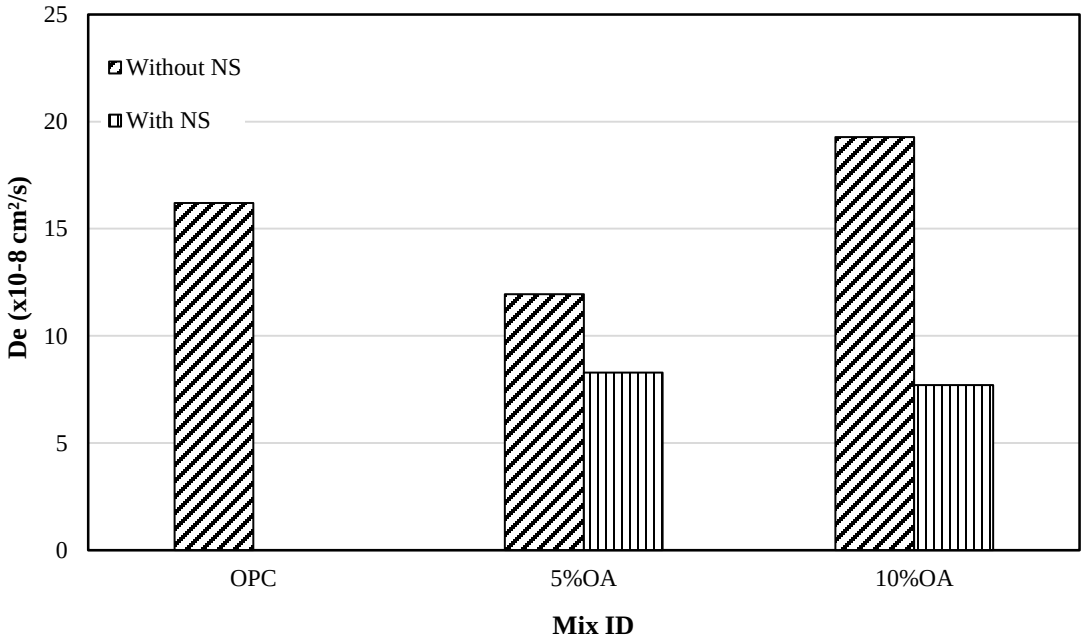

Figure 4.112: Coefficient of chloride diffusion for OA concrete with and without NS

4.5.1.6 Reinforcement corrosion

Corrosion potential: The corrosion potential were measured on concrete cylinders with 12 mm steel bars. Three concrete cylinders were prepared for each mix and cured in water for 28 days, then they were partially exposed to 5% chloride solution. The difference in potential was measured for each concrete cylinder with respect to saturated calomel reference (SCE) electrode and the average potential difference was recorded periodically. Figure 4.113 and Figure 4.114 depict the corrosion potential (E_{corr}) of OA concrete specimens with and without NS. The potential values increased as the dosage of OA was increased. However, the E_{corr} of specimens with 5%OA was almost similar to that of OPC. The use of NS in the OA concrete decreased the corrosion potentials compared to that of OA concrete.

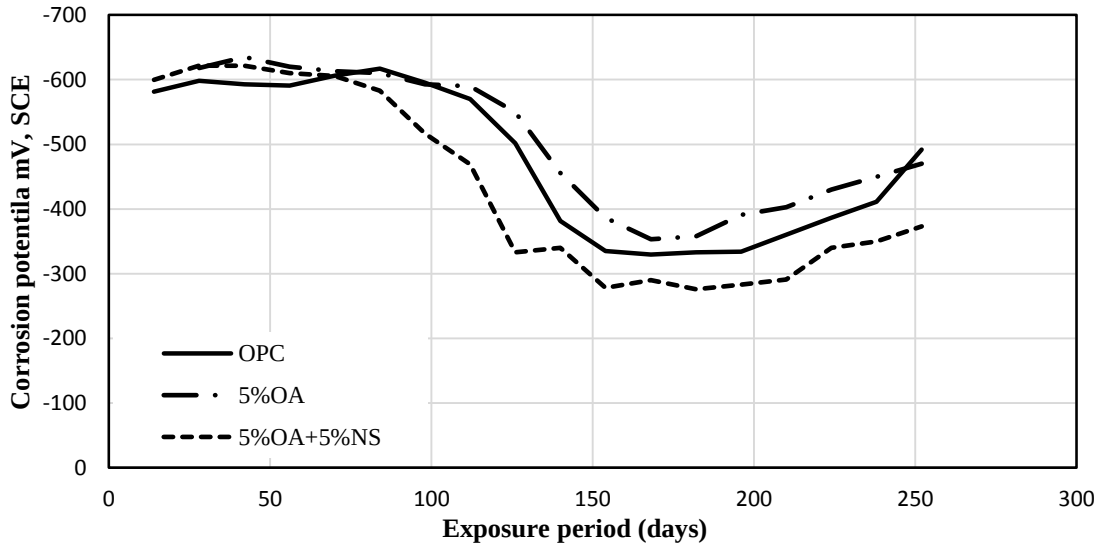

Figure 4.113: Corrosion potential of 0% and 5% OA concrete with and without NS

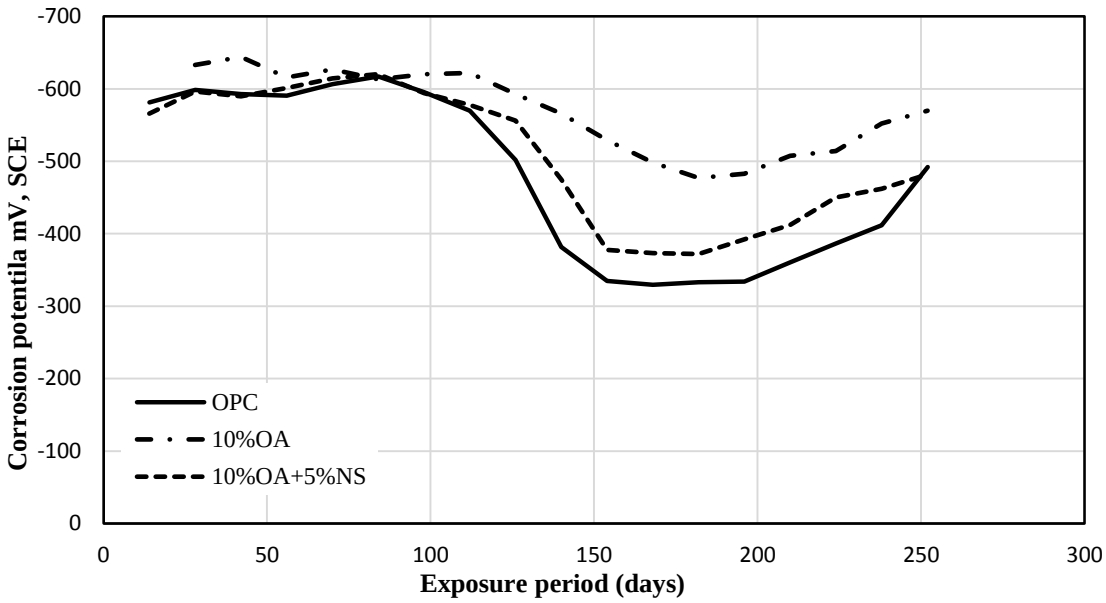

Figure 4.114: Corrosion potential of 0% and 10% OA concrete with and without NS

Corrosion current density: The corrosion current density after 260 days of exposure to 5% chloride solution were measured utilizing the same concrete cylinders used for assessing the corrosion potential. Utilizing 5%OA in the concrete as a partial replacement of cement decreased the I_{corr} compared to that of OPC, while the I_{corr} of 10%OA concrete increased. The use of 5% NS in conjunctions with OA caused a significant reduction in the I_{corr} compared to that of OA concrete without NS (Figure 4.115).

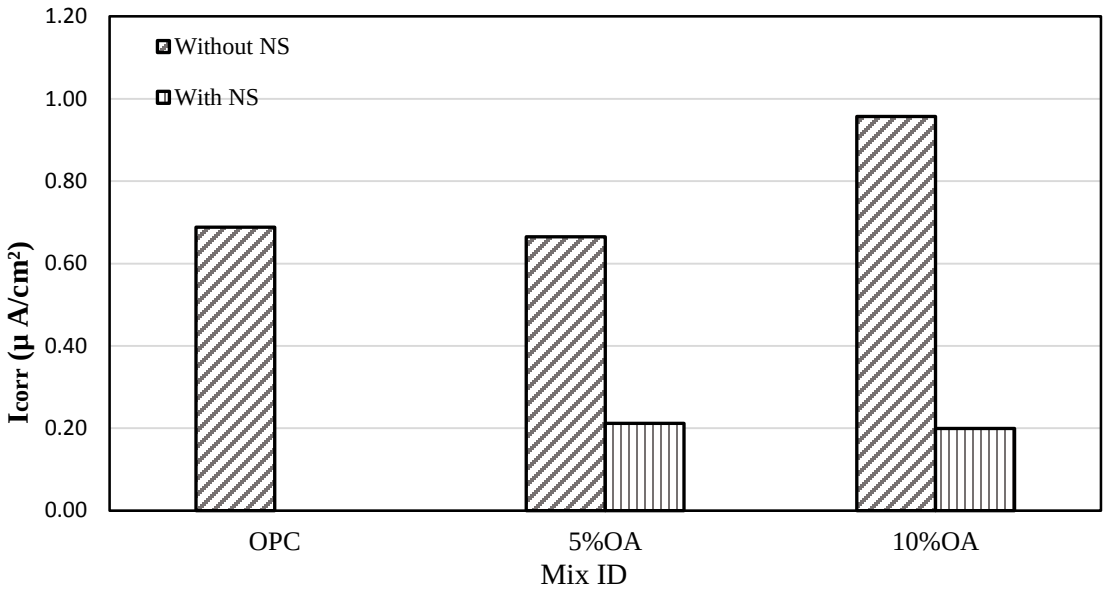

Figure 4.115: Corrosion current density on steel in OA concrete prepared with and without NS

4.5.1.7 Sulfate attack

Figure 4.116 shows the expansion of OA concrete specimens with and without NS. It is clear that utilizing OA in the concrete as a partial replacement of cement decreased the expansion, while utilizing NS in the OA concrete caused a significant reduction in the expansion compared to that of specimens without NS. As the dosage of OA was increased, with and without NS, the expansion decreased. The deterioration started at the edges of the OA paste cubes exposed to the magnesium sulfate solution while a negligible deterioration appeared on the surface of OA cubes with NS. Deterioration was not noted on the surface of specimens exposed to the sodium sulfate solution (Figure 4.117 and Figure 4.118).

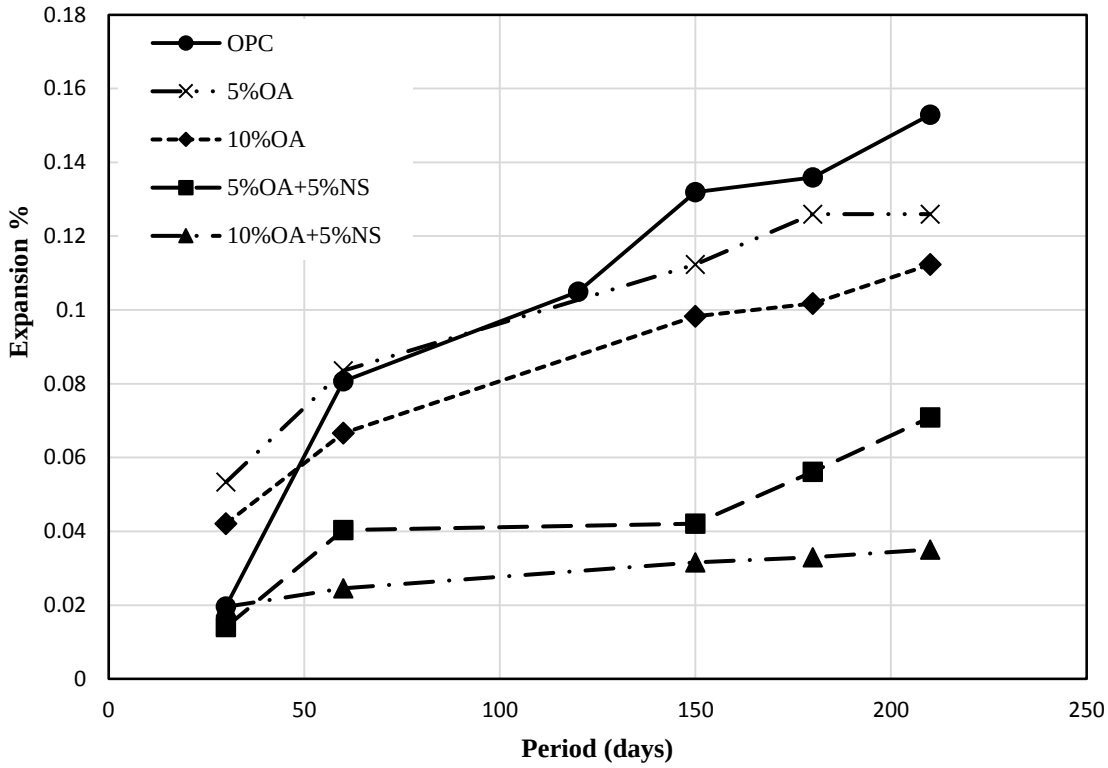

Figure 4.116: Expansion of OA concrete with and without NS

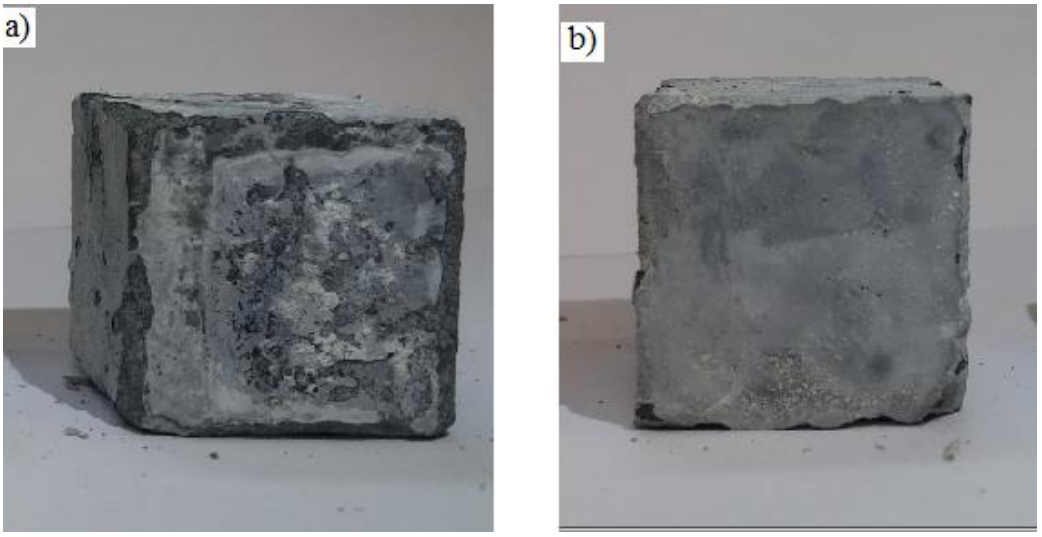

Figure 4.117: a) 5%OA cube and b) 5%OA+5%NS cube exposed to magnesium sulfate solution.

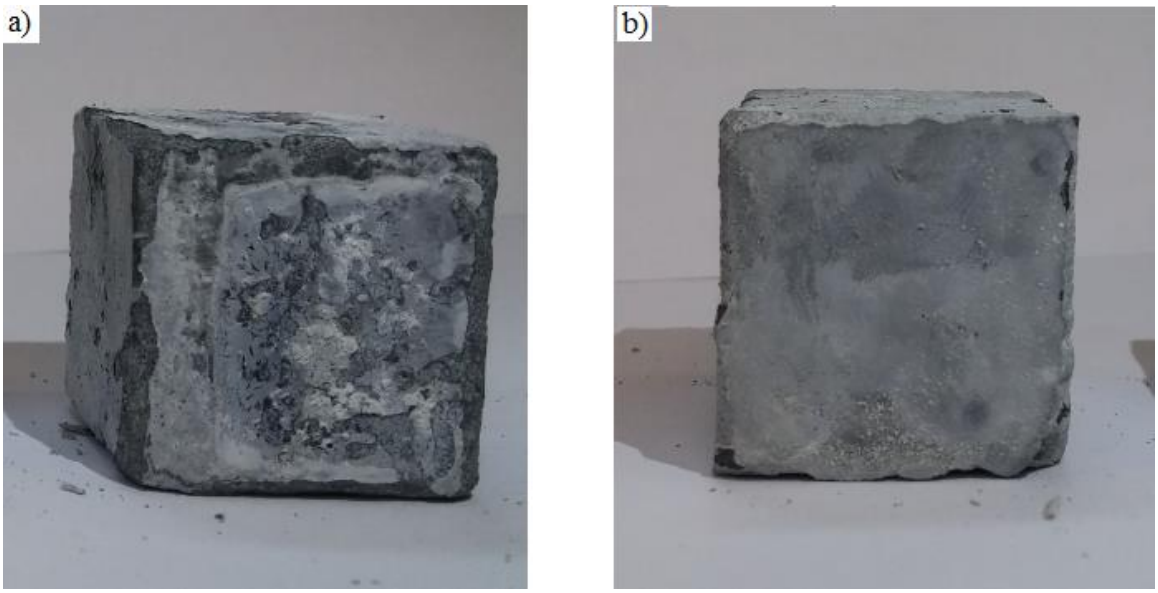

Figure 4.118: a) 10%OA cube and b) 10%OA+5%NS cube exposed to magnesium sulfate solution.

4.5.2 Micro properties

4.5.2.1 Morphology

The SEM micrograph of 5%OA specimen is shown in Figure 4.119. The morphology of 5%OA specimen showed clear cracks at the ITZ, non-uniform morphology, and a porous microstructure (Figure 4.119 (a)). At higher resolution, a porous and non-uniform CSH gel was evident (Figure 4.119(b)). The morphology became dense and more uniform and minor cracks appeared at the ITZ in the specimens prepared with 5%NS in conjunction with 5%OA (Figure 4.120(a)). At higher resolution, the CSH appeared denser and compact compared to that of 5%OA (Figure 4.120(b& d)). The BEI image showed excellent bond between the aggregate and the matrix (Figure 4.120(c)). Figure 4.121 shows the interfacial zone of 10%OA+5%NS which is dense, compact, and without cracks. A film of CH is noted at the ITZ of 10%OA+5%NS specimen (Figure 4.121 (b)).

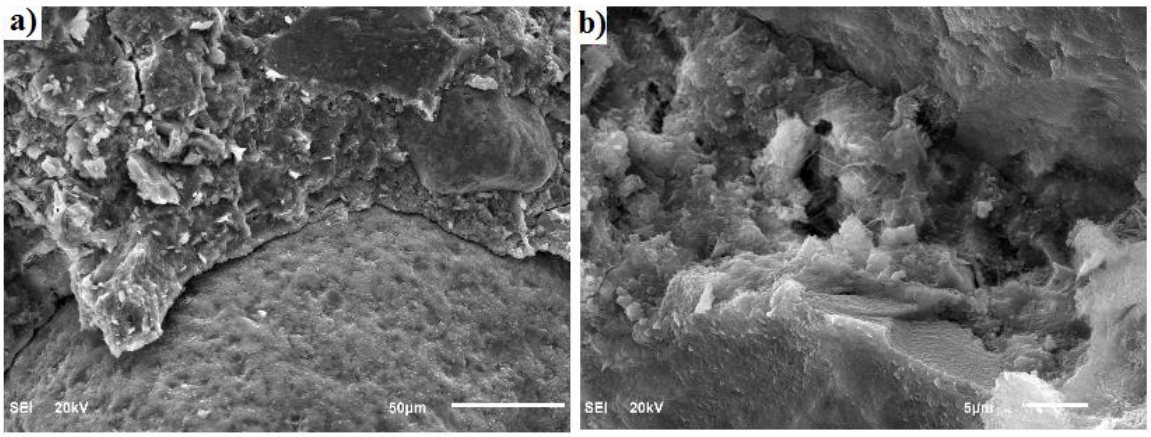

Figure 4.119: SEM of 5%OA concrete specimen.

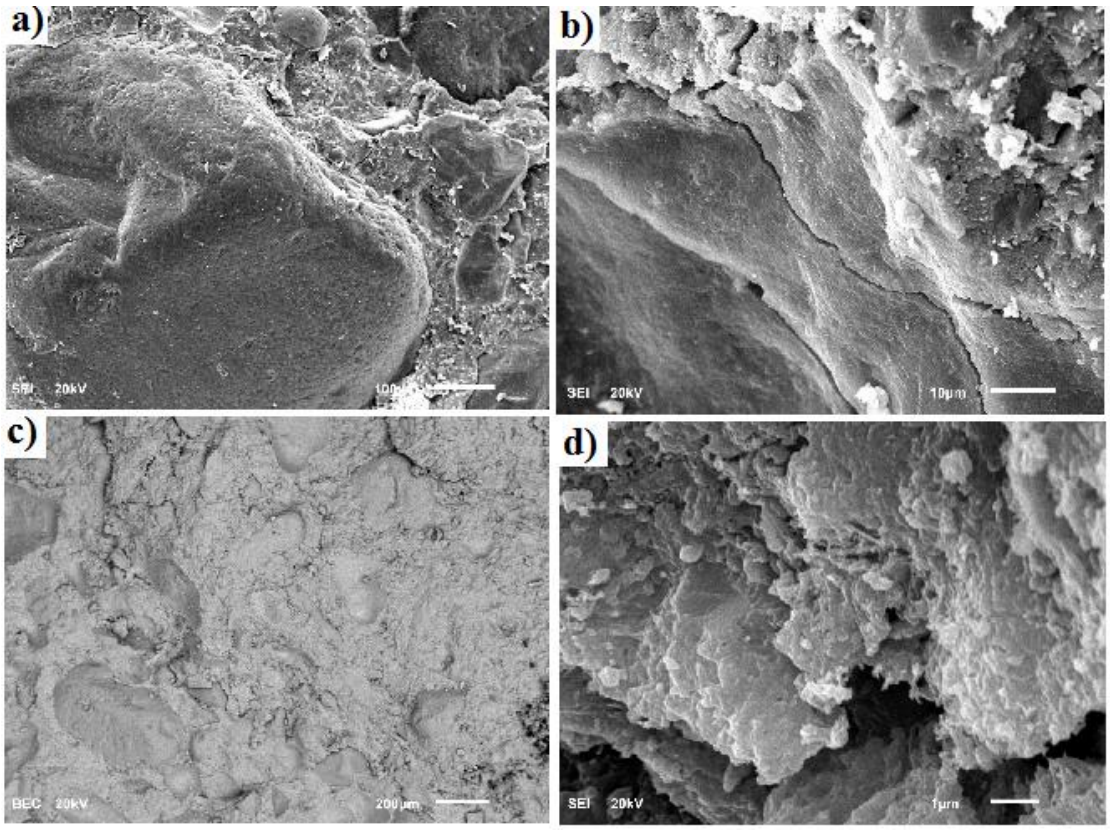

Figure 4.120: SEM and BEI images of 5%OA+5%NS concrete specimen.

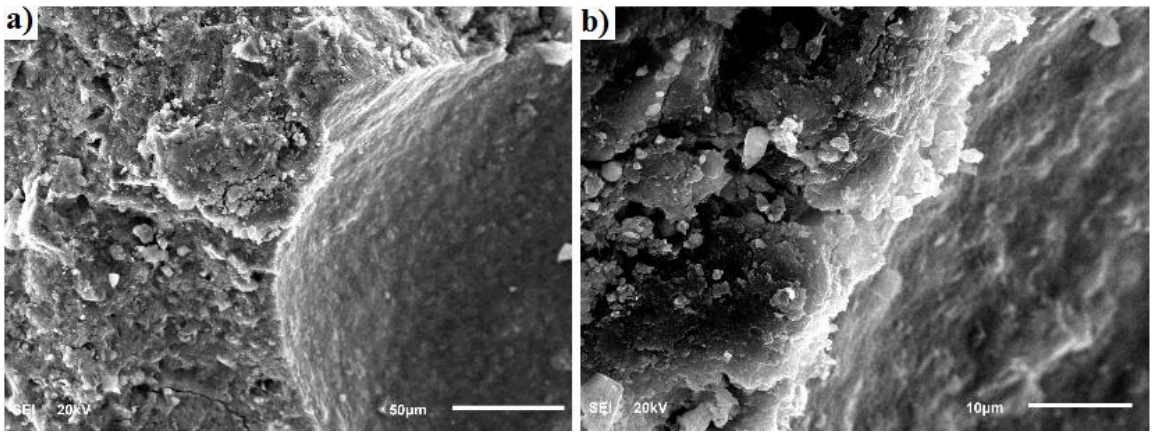

Figure 4.121: SEM of 10%OA+5%NS concrete specimen.

4.5.2.2 Mineralogical composition

The XRD spectra of 5%OA paste specimen showed less CH and more primary and secondary ettringite compared with that of OPC (Figure 4.122). The CH further decreased and the quartz increased in the spectra of 5%OA+5%NS paste specimen compared to that of 5%OA specimen (Figure 4.123). The XRD spectra of 5%OA+5%NS specimen exposed to the sodium sulfate solution showed more primary and secondary ettringite and less CH compared to the same specimen but cured in water (Figure 4.124). It can be noted from the spectra of specimen exposed to the magnesium sulfate solution that more gypsum and less CH and secondary ettringite are produced (Figure 4.125).

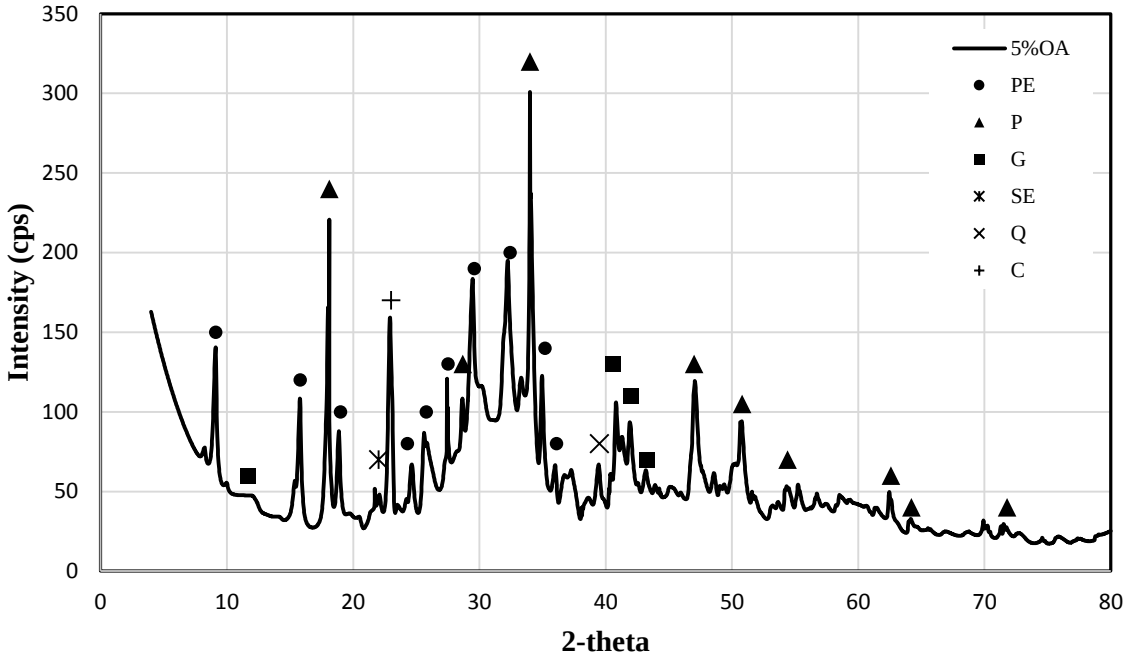

Figure 4.122: XRD spectra of 5%OA paste

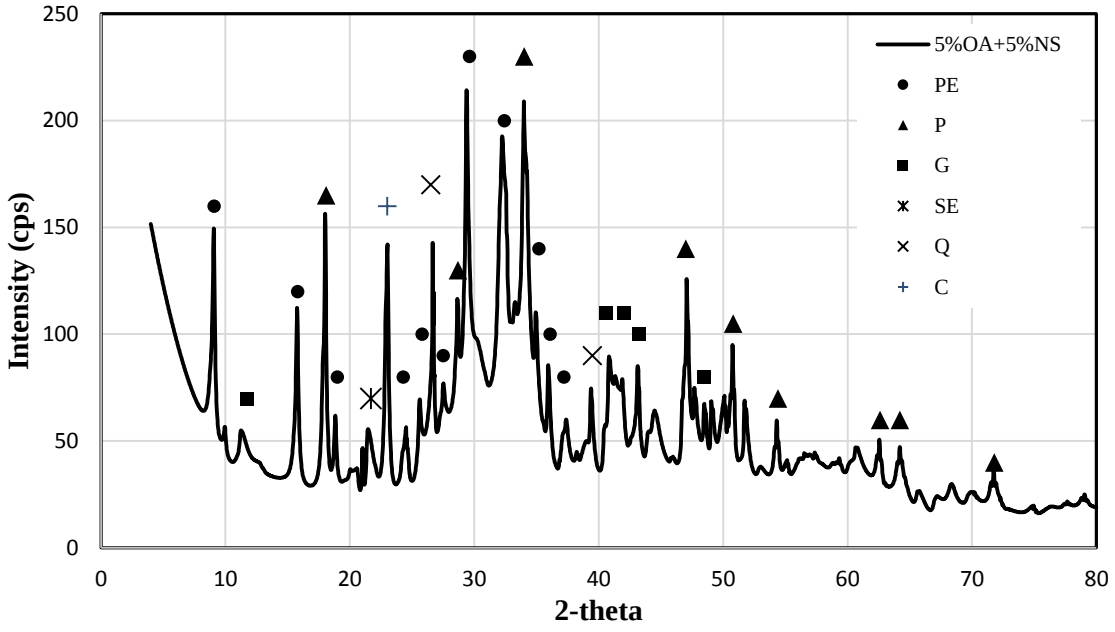

Figure 4.123: XRD spectra of 5%OA+5%NS paste

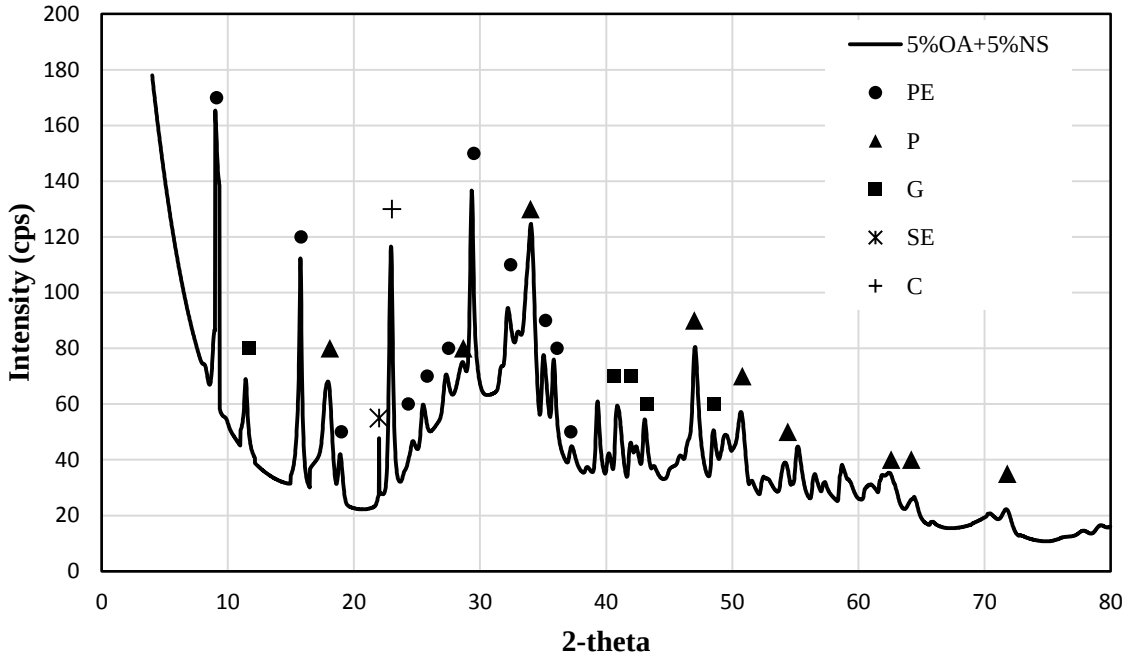

Figure 4.124: XRD spectra of 5%OA+5%NS paste exposed to sodium sulfate solution

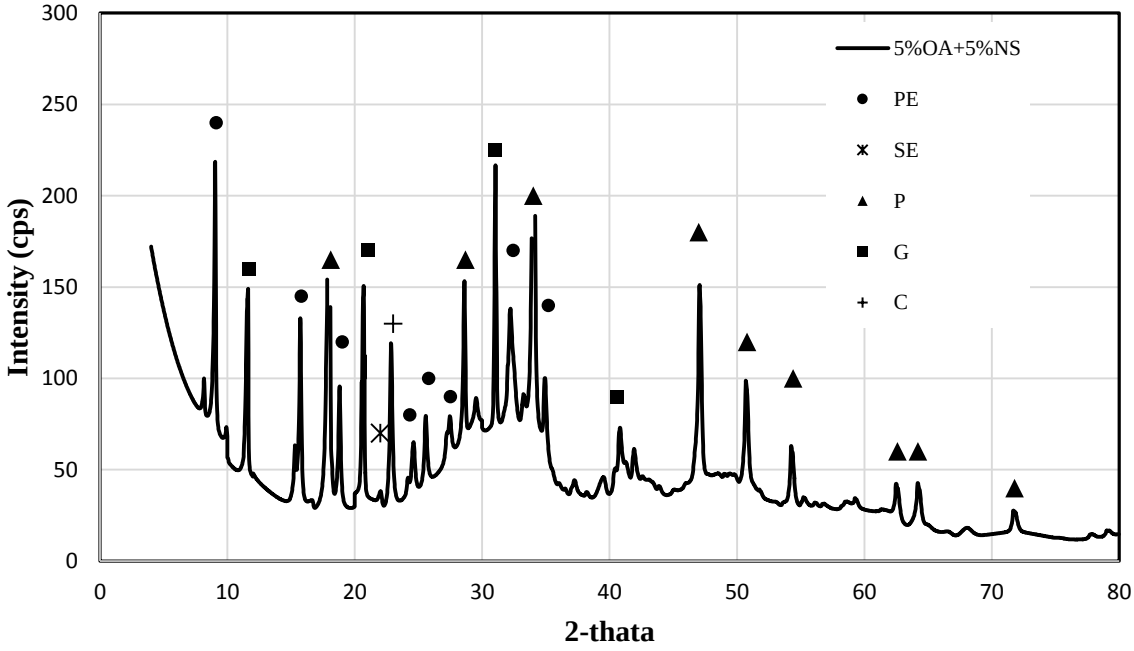

Figure 4.125: XRD spectra of 5%OA+5%NS paste exposed to the magnesium sulfate solution

4.5.3 Discussion of results

As stated earlier, specimens were prepared from four different mixes to evaluate the properties of OA concrete with and without NS. The early-age compressive strength of concrete with 5% and 10% OA was low, which may be attributed to the effect of ettringite which resulted from the reaction between sulfur as a constituent of OA with C_3A [77]. The XRD spectra for 5%OA specimen showed the secondary ettringite peak. At 28 days, the compressive strength of 5%OA specimen was slightly more than that of OPC. This may be attributed to the fact that OA does not have pozzolanic properties; as such the increase in strength may be attributed to the filling action of OA particles. At a dosage of 10% OA, the strength decreased, which may be attributed to the high OA content which negatively affected the ITZ, also the filling action of OA did not compensate the loss in strength resulting from the reduction in the quantity of cement. It was indicated in the literature [78] that the specimens with OA contained less quantity of $Ca(OH)_2$. However, due to the addition of NS, the strength increased which was due to the extra gel produced from the pozzolanic reaction and due to the physical action of NS. The XRD spectra of 5%OA+5%NS indicated less CH which agreed with the chemical action of NS. Due to the presence of secondary gel, more OA was incorporated as a filler which is evident from the high increase noted in the 10%OA+5%NS concrete compared to that of 5%OA+5%NS.

The flexural strength of 5%OA specimen increased compared to that of OPC, which may be attributed to the filling action of OA that resulted in a dense ITZ. At a dosage of 10% OA, the flexural strength decreased which may be attributed to the effect of extra OA particles in the ITZ, leading to its weakening. The combined use of NS and OA in concrete

increased the flexural strength, which may be attributed to the physical and chemical action of NS in producing a dense, uniform and compact ITZ.

The SEM images showed dense a CSH gel in OA concrete with NS. The dense microstructure resulted from the pozzolanic reaction between NS and CH as well as the filling action of NS. BEI and SEM images showed good bond between the aggregate and the mortar which was the reason behind the enhancement in the flexural strength.

The increase in the drying shrinkage of 10% OA specimen may be attributed to the evaporation of the free-water. The decrease in the shrinkage of 5%OA concrete may be attributed to the filling action of OA particles that makes the structure dense and does not allow the free-water to evaporate. Thus, the use of 5% OA in concrete, as a partial replacement of cement, increased the strength and decreased the drying shrinkage. The increase in the drying shrinkage of OA specimens with NS may be attributed to an increase in the hydration products, mainly secondary C-S-H gel. Thus, precautionary measures have to be adopted to avoid shrinkage cracking in this type of concrete.

The chloride permeability of 5%OA specimen decreased with respect to OPC, which may be attributed to the dense structure resulting from the replacement of 5% cement with OA. Thus, the use of 5% OA in concrete, as a partial replacement of cement, increased the strength and decreased the shrinkage. The chloride permeability of 10%OA specimen increased, which may be attributed to the bad dispersion of OA particles and to the reduction in the cement content. The reduction in cement content causes a reduction in the hydration products, mainly CSH gel that caused a reduction in the free-water. The significant reduction in the chloride permeability of OA specimens with NS may be attributed to the dense structure resulting from the chemical (production of more CSH gel)

and physical action (filling of the pores and act as a nuclei to the hydration products) of NS particles.

The corrosion potentials as well as the corrosion current density of specimen with 5% OA was less than that of OPC, which may be attributed to the physical effect of OA in making the microstructure dense. The I_{corr} and E_{corr} of 10%OA concrete was more than that of OPC which may be attributed to the reduction in the concrete quality due to a reduction in the quantity of cement. However, the concrete quality increased due to the use of NS. Although NS consumed CH in the pozzolanic reaction which decreased the pH of the pore solution, it produced more gel and filled the pores which compensated for the reduction in the alkalinity. The dense, compact, uniform microstructure delayed the chloride diffusion, increased the concrete resistivity, decreased the potential variation, and thereby decreased the corrosion current density.

The expansion due to sulfate attack decreased with the use of OA in the concrete, as a partial replacement of cement; this may be attributed to the reduction in the quantity of C_3A. The use of NS in OA concrete, as a partial replacement of cement, significantly decreased the expansion. The chemical and physical action of NS increased the concrete density and consumed CH, which is essential for the formation of secondary ettringite. The deterioration of the edges of OA paste specimens resulted from the production of magnesium hydroxide, which was produced due to the reaction between magnesium sulfate and calcium hydroxide. Magnesium hydroxide reduced the pH of the pore solution making the CSH unstable. However, negligible deterioration was noted in the OA+5%NS specimens. This may be attributed to their dense microstructure which delayed the diffusion of magnesium and sulfate ions. Also, deterioration was not noted in the specimens

exposed to sodium sulfate solution which can be attributed to the short period of exposure. The secondary ettringite which was noted in the spectra of specimens exposed to the sodium sulfate solution may be attributed to the reaction of CH and sulfate to produce gypsum which reacts with C_3A at high pH to produce secondary ettringite. While gypsum was formed in the specimens exposed to the magnesium sulfate solution, ettringite could not be produced due to the low alkalinity of the pore solution. Thus softening of the paste is noted in these specimens without any expansion.

4.6 Comparison between the effect of the IWMs on the properties of concrete

The cement in the developed high performance concrete was replaced with different dosages of IWMs (0%, 5%, 10%, 15%, and 20%) and NS (0% and 5%). The use of some of the selected enhanced the properties of concrete, while some had a negative effect. Table 4.1 shows the mechanical properties of concrete prepared with different dosages of IWMs and NS. The use of 5% IWMs in concrete, without NS, generally increased the 28-day compressive strength compared to OPC. The best increase in strength was noted in 5%EAFD specimen followed by 5%OA specimen. The flexural strength also increased at this level of replacement (5%), the optimum increase was noted in 5%LSP concrete. The increase in the strength of specimens with 5% IWMs may be attributed to the physical action of IWMs as well as to their chemical reaction mainly with CH. The resulting dense structure caused a reduction in the shrinkage compared to that of OPC through preventing the evaporation of the free-water. The maximum 120-day drying shrinkage was noted in

the specimens with 5%LSP while the lowest drying shrinkage was noted in the 5%OA. The dense structure of concrete due to the use of up to 5% IWM not only increased the strength but also decreased the drying shrinkage. Further, the use of 5%NS in conjunction with 5%IWMs further increased the strength; the optimum increase obtained in the 5%OA+5%NS concrete. However, the strength of 5%EAFD+5%NS was almost similar to that of 5%OA+5%NS. The flexural strength increased in all specimens with 5%IWMs and 5%NS, the maximum was achieved in 5%LSP+5%NS specimens. The use of NS in the specimens with 5%IWMs increased the strength further. This may be attributed to the dense microstructure and ITZ resulting from the chemical and physical action of NS. The increase in the flexural strength of 5%LSP specimens with and without NS may be attributed to the nucleation effect of LSP, in which LSP acted as a nuclei to CH crystals [74], which limited the growth of CH crystals and made the ITZ more uniform.

The durability characteristics of the developed high performance concrete are summarized in Table 4.2 and Table 4.3. The coefficient of chloride diffusion (D_e) of concrete prepared with 5%IWMs was less than that of OPC, the best enhancement in the chloride diffusion coefficient was obtained in 5%LSP concrete followed by 5%OA concrete. The use of NS along with the selected IWMs caused a significant reduction in the D_e, the optimum enhancement was obtained in 5%OA followed by 5%LSP. The rapid chloride permeability of concrete prepared with the selected IWMs can be classified as moderate to low while the chloride permeability of concrete with IWMS plus NS can be classified as very low. The I_{corr} decreased due to the use of 5%LSP and 5%OA concrete while it increased in 5%EAFD concrete compared to OPC. The I_{corr} significantly decreased in the concrete prepared with IWMs plus NS compared to those without NS, the lowest I_{corr} was obtained

in 5% EAFD concrete. The expansion, due to sulfate attack, in the concrete with 5%IWMs was less than that of OPC and it further decreased due to the addition of 5%NS.

Increasing the dosage of IWMs to 10% caused decreased the 28-day compressive strength compared to OPC. The 28-day compressive strength of 10%CKD, 10%OA, and 10%LSP concrete was almost close to each other, while the strength of 10%EAFD was the lowest. The reduction in the strength due to the use of 10% IWMs may be attributed to the bad dispersion of IWM particles that affected the ITZ. The flexural strength of 10% IWMs concrete decreased compared to that of 5%IWMS concrete, however, the flexural strength of 10%EAFD and 10%LSP was still more than that of OPC. The lowest flexural and compressive strength was measured in 10%OA that may be attributed to the negative effect of the very fine particles of OA on the ITZ. Since the density of the concrete structure decreased, the drying shrinkage further increased. The lowest drying shrinkage was obtained in 10%CKD specimen which may be attributed to the pozzolanic reactivity of CKD which is basically cement dust. The pozzolanic reactivity of CKD enhanced the density of concrete compared to other IWMs but it did not mask the negative effect of chloride, alkalis, and sulfate on the ITZ which caused a reduction in the strength compared to OPC. The use of 5%NS in conjunction with 10%IWMs enhanced the strength compared to only 10%IWMs. Among the IWMs investigated, maximum strength was measured in 10%CKD+5%NS specimen followed by 10%EAFD+5%NS. The flexural strength also increased due to the use of 5%NS in the IWMs. The ultimate flexural strength was obtained in 10%LSP+5%NS concrete while the strength of other specimens was close to each other. The drying shrinkage of concrete with IWMs and NS further increased due to the consumption of free water during the production of CSH gel. The lowest drying shrinkage

was found in the 10%CKD+5%NS specimen followed by 10%EAFD+5%NS. The trend of the drying shrinkage data is in line with the compressive strength results.

The coefficient of chloride diffusion (D_e) of 10%CKD, 10%OA, and 10%LSP concrete was more than that of OPC, while the D_e of 10%EAFD concrete was almost similar to that of OPC. Utilizing NS in 10%IWMs concrete significantly decreased the D_e compared to that of OPC. The D_e of 10%CKD+5%NS was the highest while the lowest D_e was obtained in 10%EAFD+5%NS concrete. The chloride permeability of concrete with 10%IWMs classified as low and moderate, while it was very low in the 10%IWMs concrete with NS. The I_{corr} of 10%CKD, 10%EAFD, and 10%LSP concrete were almost similar to that of OPC while it was more in 10%OA concrete. The I_{corr} of 10%IWMs concrete with NS was less than that of OPC, the lowest and highest I_{corr} was obtained in 10%EAFD+5%NS and 10%CKD+5%NS concrete, respectively. The expansion decreased in 10%IWMs concrete due to sulfate attack accept in 10%CKD concrete, it increased. The expansion in the IWMs concrete and NS decreases compared to the OPC and IWMs concrete. Although the expansion of 10%CKD+5%NS concrete was the highest among the IWMs+5%NS concrete, but it was less than that of OPC. The D_e and the expansion of 10%CKD concrete with and without NS was the highest among the 10%IWMS concrete with and without NS, which may be attributed to the high alkalinity, chloride and sulfate content, and alumina content.

The highest dosage of OA and EAFD used in this study was 10%. These dosages could not be increased due to their effect in delaying the setting time and workability (in case of oil ash). Utilizing 15% LSP and CKD in concrete further decreased the strength. The ultimate 28-day compressive strength was obtained in 15%CKD concrete which may be attributed

to the pozzolanic reaction of CKD while LSP acts as a filler. Utilizing NS simultaneously with 15% CKD and 15%LSP in concrete increased the strength compared to the strength of 15%CKD and 15% LSP concrete without NS. Although the cement content was reduced by 20% in the specimens with 15% CKD+5%NS and 15%LSP+5%NS, the strength in 15%CKD+5%NS was more than that of OPC and the strength of 15%LSP +5%NS was almost equal to that of OPC. The flexural strength of 15%LSP concrete was more than that of 15%CKD concrete and OPC. The drying shrinkage increased in the specimens with 15%CKD and 15%LSP and it further increased when 5%NS was utilized in 15%LSP and 15%CKD concrete. It was noted that the shrinkage of 15%CKD concrete was less than that of 15%LSP concrete. The combined effect of CKD and NS enhanced the density of the microstructure more than that of concrete with LSP and NS which was reflected in the compressive strength and drying shrinkage data.

The D_e of 15%CKD and 15%LSP concrete increased compared to OPC, while the D_e of 15%CKD+5%NS was almost similar to that of OPC and it decreased in the concrete with 15%LSP+5%NS. The I_{corr} of concrete with 15%CKD was almost similar to that of 15%LSP and less than that of OPC. Utilizing NS along with 15%LSP or 15%CKD decreased the I_{corr} compared to OPC. The expansion of 15%CKD specimens was more than that of OPC and 15%LSP specimens, while the expansion of 15%CKD+5%NS specimens was less than that of OPC. The expansion of mortar with 15%LSP was less than that of OPC.

Due to the pozzolanic reactivity of CKD, its dosage was increased to 20%. The 28-day compressive strength of 20%CKD further decreased compared to 15%CKD and OPC specimens, while the compressive strength of 20%+5%NS was slightly more than that of OPC. The flexural strength decreased compared to OPC which may be attributed to the

negative role of alkalis, chloride, sulfate, and CH on the ITZ. The drying shrinkage of 20%CKD with and without NS increased compared to that of 15%CKD specimens with and without NS. The I_{corr}, D_e, and the expansion increased in 20%CKD concrete compared to OPC. The coefficient of chloride diffusion of 20%CKD+5%NS was almost similar to that of OPC while the chloride permeability according to ASTM C1240 was very low. The I_{corr} of 20%CKD+5%NS decreased compared to OPC while the expansion increased.

Table 4.1: Effect of the IWMs and NS on the mechanical properties of concrete

IWM	Quantity of IWM, %	Quantity of NS, %	28-day compressive strength	The Flexural strength	Drying shrinkage	
					At 7 days	At 120 days
---	----	0%	58	4.19	345.1	670
---		5%	72.24	5.81	478.23	767
EAFD	5%	0%	63.96	4.76	343.7	612
LSP		0%	58.2	5.25	391.7	620
OA		0%	61.35	4.24	254	596
EAFD	5%	**5%**	69.27	4.9	433.1	710
LSP		**5%**	63.45	5.81	400.3	863
OA		**5%**	71.05	4.81	351.17	853.5
CKD	10%	0%	54.81	3.95	330	525.4
EAFD		0%	56.13	4.58	449.1	705
LSP		0%	55.53	5	462	830
OA		0%	49.5	3.39	469.35	850
CKD	10%	**5%**	70.23	4.83	463	619.2
EAFD		**5%**	66.42	4.8	509.4	740
LSP		**5%**	61.27	5.63	486.5	1000
OA		**5%**	62.52	4.67	480.3	950
CKD	15%	0%	54.08	3.76	379	629.36
LSP		0%	52.07	4.39	491.3	872.6
CKD	15%	**5%**	65.06	4.51	447	686.5
LSP		**5%**	58.32	4.95	530	1100
CKD	20%	0%	53.08	3.43	485	751.2
CKD	20%	**5%**	59.49	3.9	493	798.9

Table 4.2: Effect of IWMs and NS on the durability of concrete

IWM	Quantity of IWM, %	Quantity of NS, %	Coefficient of chloride diffusion, ($\times 10^{-8}$ cm²/s)	Chloride permeability	
				Coulombs	Rating
---		0	16.2	1711	Low
---		**5%**	6.21	294	Very low
EAFD	5%	0%	14.9	2094	Moderate
LSP		0%	11.95	2041	Moderate
OA		0%	13.44	2092	Moderate
EAFD	5%	**5%**	8.5	411	Very low
LSP		**5%**	8.29	296	Very low
OA		**5%**	5.27	332	Very low
CKD	10%	0%	21.78	1954	Low
EAFD		0%	16.8	1980	Low
LSP		0%	17.41	1891	Low
OA		0%	19.28	1172	Low
CKD	10%	**5%**	14.87	513	Very low
EAFD		**5%**	8.72	351	Very low
LSP		**5%**	8.95	495	Very low
OA		**5%**	7.62	252	Very low
CKD	15%	0%	24.8	2055	Moderate
LSP		0%	19.7	2228	Moderate
CKD	15%	**5%**	16.18	454	Very low
LSP		**5%**	10.07	503	Very low
CKD	20%	0%	29.86	2074	Moderate
CKD	20%	**5%**	16.96	757	Very low

Table 4.3: Effect of the IWMs and NS on the durability characteristics of concrete

IWM	Quantity of IWM, %	Quantity of NS, %	I_{corr} (μA/cm²)	Elongation due to sulfate attack (%)
---		0	0.69	0.15
---		**5%**	0.11	0.027
EAFD		0%	0.8	0.15
LSP		0%	0.54	0.14
OA	5%	0%	0.67	0.13
EAFD		**5%**	0.11	0.017
LSP	5%	**5%**	0.12	0.09
OA		**5%**	0.21	0.071
CKD		0%	0.64	0.62
EAFD		0%	0.6	0.11
LSP	10%	0%	0.67	0.13
OA		0%	0.96	0.11
CKD		**5%**	0.28	0.08
EAFD		**5%**	0.15	0.015
LSP	10%	**5%**	0.19	0.06
OA		**5%**	0.2	0.035
CKD		0%	0.84	0.68
LSP	15%	0%	0.86	0.13
CKD		**5%**	0.34	0.11
LSP	15%	**5%**	0.2	0.05
CKD	20%	0%	1.83	0.86
CKD	20%	**5%**	0.55	0.33

CHAPTER FIVE

EXPECTED SERVICE LIFE

Four IWMs were used in conjunction with NS to produce high performance concrete. The mechanical properties as well as the durability characteristics were enhanced due to the use of the selected IWMs in combination with NS. The results indicate that the use of IWMs and NS in concrete, as a partial replacement of cement, will lead to other benefits like reduction in the CO_2 emission and extending the service life of the structure. These aspects are discussed in the following sub-sections.

5.1 Reduction in CO_2 gas emission

Cement is the main component of concrete. Overall the world, 3300 million tons of cement is produced annually. Cement production contributes to the greenhouse gases in two ways, first contribution through production of CO_2 which results from the burning of the calcium carbonate in the kiln and the second contribution is through using the energy in the kiln especially if the energy resulted from fossil fuels. 5% of the global manmade CO_2 emission is produced from cement industries. The cement industries produce 900 kg of CO_2 for every 1000 kg of cement [79]. Cement is the main source of strength in concrete. Unfortunately, the production of cement increases the greenhouse gasses, so to conserve mineral resources and energy, other materials should replace the cement in producing the concrete. In this study, different local waste byproducts, such as cement kiln dust (CKD), limestone powder

(LSP), electric arc furnace dust (EAFD), and oil ash (OA) were utilized in the concrete as a partial replacement of cement. Due to partially replacing the cement with IWMs, the quantity of cement decreased which resulted in a reduction in the CO_2 gas emission. The reduction in the CO_2 emission due to the use of the selected IWMs in the concrete as a partial replacement of cement was evaluated and depicted in Figure 5.1. It is clear that as the dosage of IWMs increased, the CO_2 emission decreased.

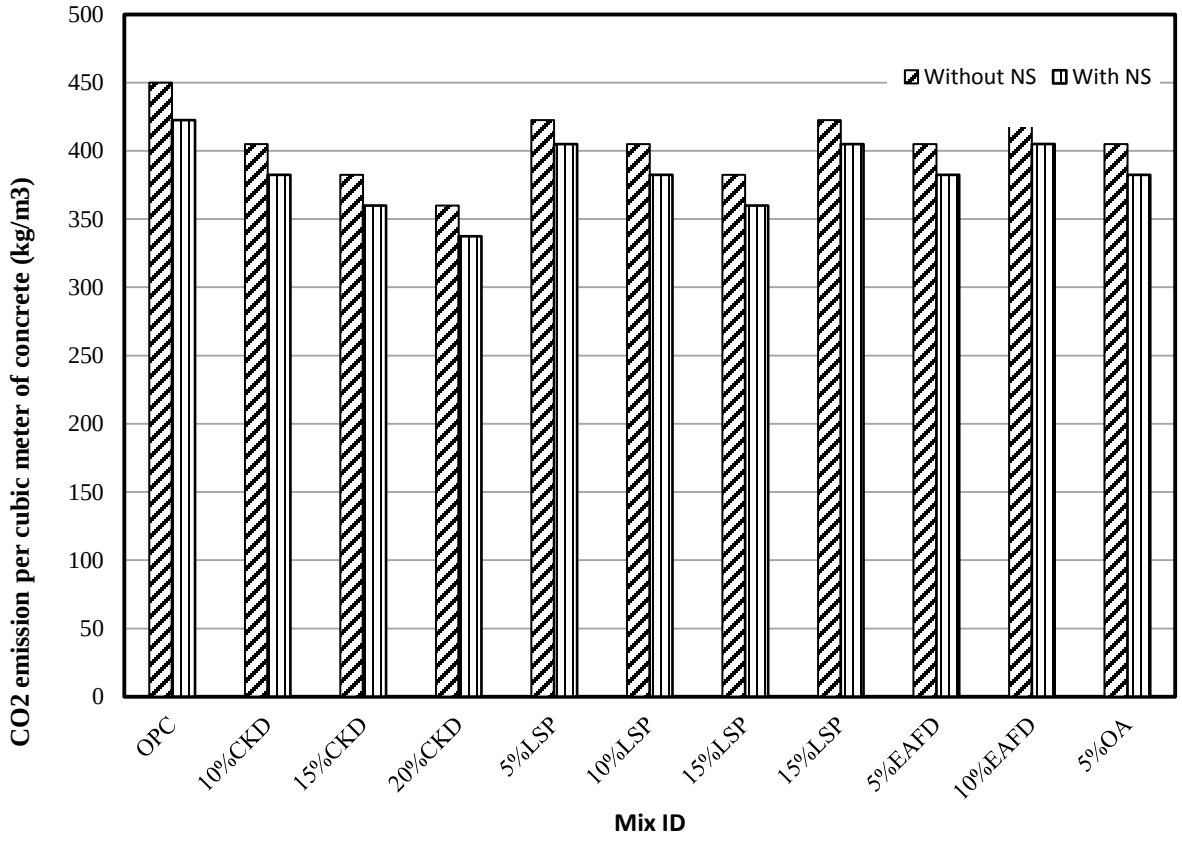

Figure 5.1: CO_2 emission in concrete due to the use of IWMs and NS.

5.2 Service life prediction

The increase in the service-life of concrete structures due to the use of the selected IWMs and NS was evaluated by assessing (i) Time to initiation of corrosion and the (ii) time to cracking.

a) Time of initiation corrosion

Since the corrosion resistance of concrete prepared with the selected IWMs and NS increased it is expected that the useful service-life will also increase. There are two different periods in deterioration resulting from corrosion. The first period is associated with the diffusion of CO_2 and chloride ions to the concrete-steel interface leading to the depassivation of steel. The second period is the period between corrosion initiation and concrete cracking (Figure 5.2).

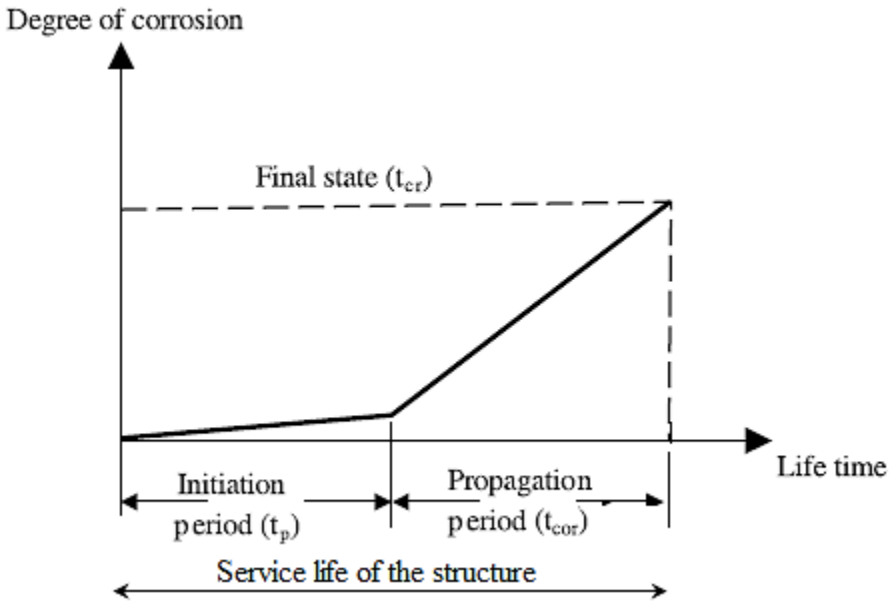

Figure 5.2: Stages of reinforcement corrosion.

So the time to initiation of corrosion is a function of the chloride threshold, cover thickness, surface chloride concentration, and chloride diffusion coefficient. All of these parameters are summarized in the following empirical equation [80]:

$$t_p = \frac{1}{12 D_{app}} \left[\frac{C_v}{1 - \left(C_{th} / C_s \right)^{0.5}} \right]^2 \qquad 5.1$$

where Cv = cover thickness (mm)

C_{th} = threshold chloride concentration (%)

C_s = chloride concentration at the concrete surface (%)

D_{app} = apparent diffusion coefficient for chloride (cm^2/s)

Equation 5.1 was utilized in predicting the time to initiation of corrosion of concretes prepared with the selected IWMs and NS (Figure 5.3). It is clear that utilizing NS in the concrete significantly delayed the time of initiation corrosion compared to the specimens prepared without NS. The use of 5% LSP, OA, and EAFD slightly increased the time to corrosion initiation compared to OPC, while utilizing other IWMs without NS caused a reduction in the time to depassivation. The lowest depassivation time was noted in the CKD concrete specimens, which may be attributed to the high chloride and sulfate concentration in the CKD. It can be noted that the depassivation time is directly proportional to the quality of concrete, as the concrete quality enhanced the time to initiation corrosion.

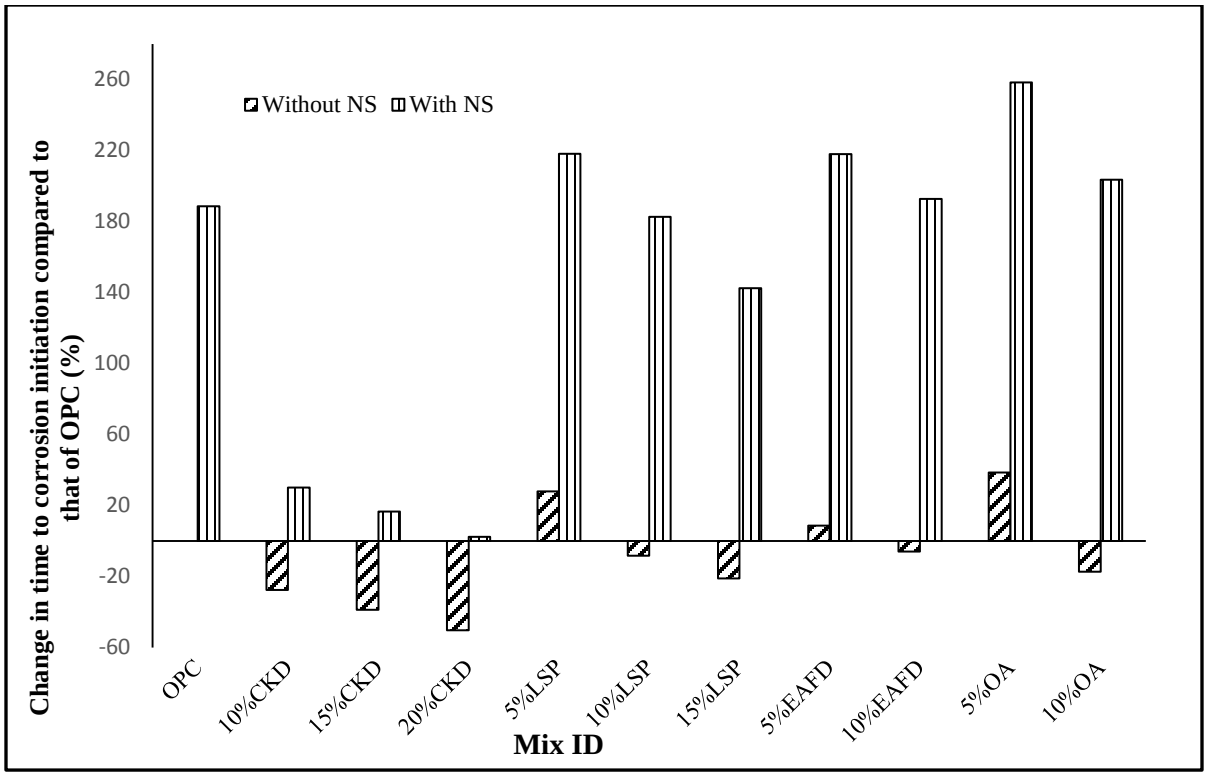

Figure 5.3: Time to corrosion initiation of the concrete mixtures

b) Time of corrosion cracking

After depassivation occurs, the corrosion will start if sufficient oxygen and moisture are available for the cathodic reaction. As the corrosion proceeds, the rust will form on the steel surface generating tensile stresses on the concrete. When the stress resulted from the rust formation exceeds the tensile strength capacity of the concrete, it cracks. The time from corrosion initiation up to concrete cracking is the time of corrosion cracking which can be estimated using the following empirical equation [81]:

$$Q_{cr} = 0.602 \left(1 + \frac{2C_v}{D}\right)^{0.85} D \qquad (5.2)$$

Where:

$Q_{cr\ is}$ the critical mass of corrosion products (10^{-4} g/cm^2).

C_v is the cover to the reinforcement (mm).

D is the diameter of reinforcing bar (mm).

The time of corrosion cracking is then given by:

$$t_{cr} = \frac{Q_{cr}}{J_r} \tag{5.3}$$

in which

$$J_r = \left(\frac{W}{F}\right) I_{corr} \tag{5.4}$$

W=27.925 g

Faraday's constant F=96487 Coulombs

J_r (g/cm^2/day) is the instantaneous corrosion rate

Equations 5.3 and 5.4 were utilized to estimate the time of concrete cracking (t_{cr}) (Figure 5.4). It can be noted that t_{cr} of NS concrete was significantly more than that of concrete without NS. The t_{cr} decreased as the dosage of IWMs was increased. This trend was noted in concrete with and without NS. However, the t_{cr} of 20%CKD+5%NS concrete specimen which has the lowest t_{cr} among the NS concrete specimens was more than that of OPC.

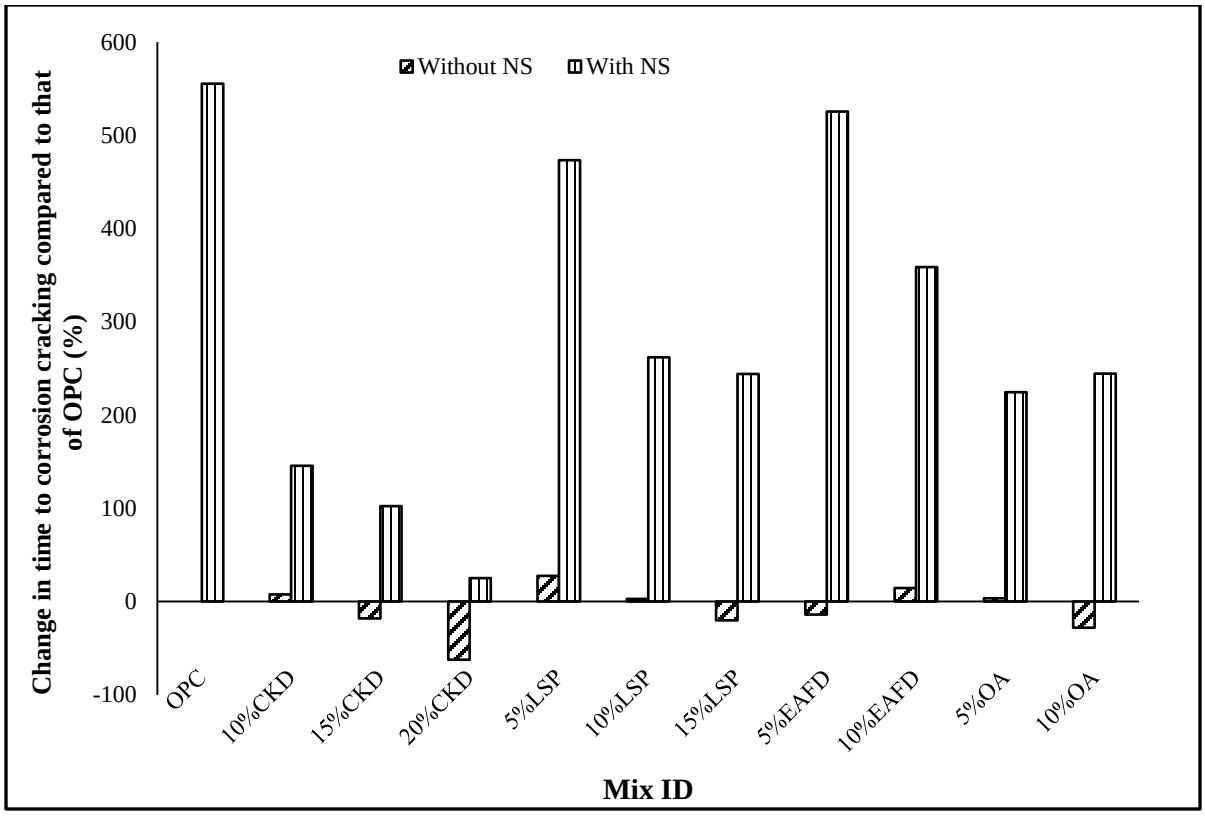

Figure 5.4: Time to corrosion cracking of the concrete mixtures

CHAPTER SIX

CONCLUSIONS AND FUTURE WORK

6.1 Conclusions

The following conclusions can be drawn based on the data developed in the reported study.

i. The compressive and flexural strength of concrete decreased due to the use of CKD (10%, 15%, and 20%), 10% EAFD, 10%OA, and (10% and 15%) LSP, as a partial replacement of cement while a marginal increase in the strength was noted in concrete incorporating 5% EAFD, OA, and LSP. However, the use of NS in conjunction with CKD, EAFD, LSP, and OA increased the strength of concrete.

ii. The use of NS in conjunction with the selected industrial waste materials increased the early strength of concrete. This may be attributed to the nucleation effect and due to the high surface area of NS that increased its reactivity. Also, the increased strength may be attributed to the production of additional C-S-H and the consumption of $Ca(OH)_2$.

iii. The drying shrinkage increased with increasing dosage of IWMs. The drying shrinkage further increased due to the use of NS. Consequently, preventive measures need to be taken to avoid drying shrinkage cracking in the developed HPC.

iv. The chloride permeability of concrete significantly decreased due to the conjoint use of the selected industrial waste materials and NS.

v. The coefficient of chloride diffusion of concrete increased due to the use of CKD (10%, 15%, and 20%), 10% EAFD, 10%OA, and (10% and 15%) LSP, as a partial replacement of cement while a decrease in the chloride diffusion coefficient was noted in the concrete incorporating 5% of EAFD, OA, and LSP. However, the use of nano-silica in conjunction with CKD, EAFD, LSP, and OA further decreased the coefficient of chloride diffusion.

vi. The corrosion current density, as well as corrosion potential, of concrete decreased due to the conjoint use of the selected industrial waste materials and NS. This may be attributed to the dense, compact, uniform structure which delayed the chloride diffusion and reinforcement corrosion.

vii. The expansion of the mortar decreased due to the use of EAFD, OA, and LSP, as a partial replacement of cement while an increase in the expansion was noted in the mortar incorporating CKD. However, using nano-silica with CKD, EAFD, LSP and OA significantly decreased the expansion.

viii. SEM images showed a uniform and compact microstructure in the specimens with the selected industrial waste materials and nano-silica compared to OPC concrete.

ix. X-ray diffraction spectra showed less CH in the concrete with NS, more gypsum in the specimens exposed to magnesium sulfate solution, and more secondary ettringite in the specimens exposed to the sodium sulfate solution.

x. The use of developed HPC (with the selected industrial waste materials and nano-silica) will lead to environmental, technical and economic benefits.

6.2 Recommendation

The durability of the developed high performance concrete can be classified into the following five groups (Figure 6.1).

i. Very low durability (20%CKD concrete)
ii. Low durability (Concrete with 10% and 15%CKD)
iii. Moderate durability (Concrete with IWMs except CKD)
iv. High durability (Concrete with high dosages of IWMs and NS)
v. Very high durability (concrete with Low dosage of IWMs and NS

Since the compressive strength of the developed HPCs is in the acceptable range of 50 to 60 MPa, the use of the developed concrete should be based on the durability as classified above. For examples, 20%CKD concrete should be selected for low durability requirements while concrete with low dosage of IWMs and NS should be preferred for very high durability requirements.

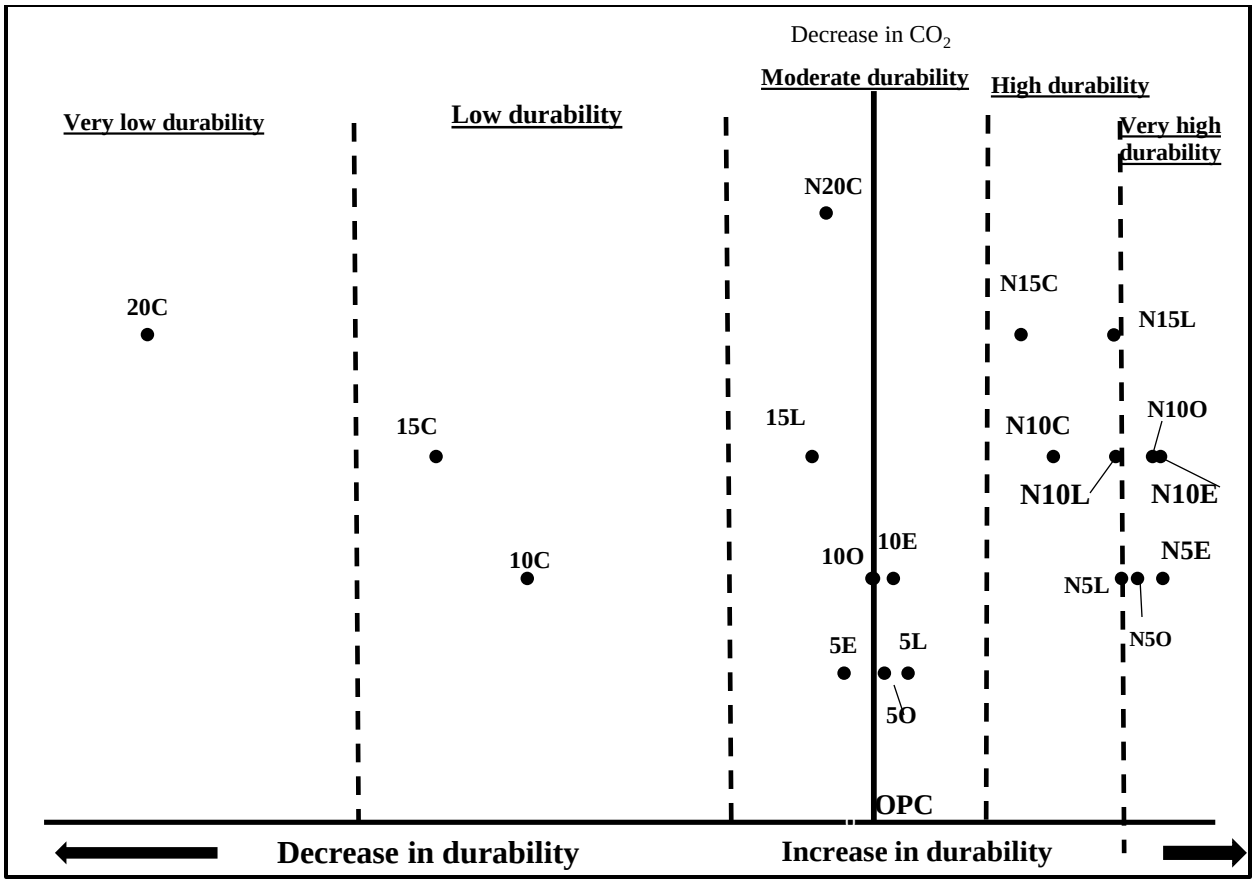

N: with 5%NS, L: LSP, E: EAFD, O: OA, C: CKD.

Figure 6.1: Durability classification of the developed HPC

6.3 Suggestions for future work

This study can be extended to:

- Investigate the possibility of producing self-compacted concrete utilizing NS and IWMs.
- Developing alkali activated binders using IWMs and NS.
- Assess the durability of the developed high performance concrete under different exposure conditions.

REFERENCES

1. Najamuddin, S.K., Production of medium to low strength concrete utilizing indigenous waste products. 2011, King Fahd University of Petroleum and Minerals (Saudi Arabia).
2. Moon, H.-Y., H.-S. Jung, and J.-P. Kim, Diffusion of chloride ions in limestone powder concrete. Journal of the Korea Concrete Institute, 2004. **16**(6): p. 859-865.
3. Jayapalan, A.R., B.Y. Lee, and K.E. Kurtis, Can nanotechnology be 'green'? Comparing efficacy of nano and microparticles in cementitious materials. Cement and concrete composites, 2013. **36**: p. 16-24.
4. Sanchez, F. and K. Sobolev, Nanotechnology in concrete–a review. Construction and building materials, 2010. **24**(11): p. 2060-2071.
5. Chanu, N.M. and T.K. Devi. Contribution of rice husk ash to the properties of cement mortar and concrete. in International Journal of Engineering Research and Technology. 2013. ESRSA Publications.
6. Morsy, M., S. Alsayed, and M. Aqel, Effect of nano-clay on mechanical properties and microstructure of ordinary Portland cement mortar. International Journal of Civil & Environmental Engineering IJCEE-IJENS, 2010. **10**(01): p. 23-27.
7. Shekari, A. and M. Razzaghi, Influence of nano particles on durability and mechanical properties of high performance concrete. Procedia Engineering, 2011. **14**: p. 3036-3041.
8. Brightson, P., G. Baskar, and S.B. Gnanappa, Strength and durability analysis of nano clay in concrete. Life Sci. J, 2013. **10**: p. 1172-1177.
9. Ji, T., Preliminary study on the water permeability and microstructure of concrete incorporating nano-SiO 2. Cement and Concrete Research, 2005. **35**(10): p. 1943-1947.
10. Khotbehsara, M.M., et al., Rheological, mechanical and durability properties of self-compacting mortar containing nano-TiO2 and fly ash. Journal of American Science, 2014. **10**(11): p. 222-228.
11. Nazari, A., et al., Improvement the mechanical properties of the cementitious composite by using TiO2 nanoparticles. Journal of American Science, 2010. **6**(4): p. 98-101.
12. Agarkar, S. and M. Joshi, Study of effect of Al2O3 nanoparticles on the compressive strength and workability of blended concrete. Int J Curr Res, 2012. **4**: p. 382-4.

13. Hou, P.-k., et al., Effects of colloidal nanosilica on rheological and mechanical properties of fly ash–cement mortar. Cement and Concrete Composites, 2013. **35**(1): p. 12-22.

14. Ltifi, M., et al., Experimental study of the effect of addition of nano-silica on the behaviour of cement mortars. Procedia Engineering, 2011. **10**: p. 900-905.

15. Jalal, M., et al., Mechanical, rheological, durability and microstructural properties of high performance self-compacting concrete containing SiO 2 micro and nanoparticles. Materials & Design, 2012. **34**: p. 389-400.

16. Said, A.M., et al., Properties of concrete incorporating nano-silica. Construction and Building Materials, 2012. **36**: p. 838-844.

17. Rong, Z., et al., Effects of nano-SiO 2 particles on the mechanical and microstructural properties of ultra-high performance cementitious composites. Cement and Concrete Composites, 2015. **56**: p. 25-31.

18. Quercia, G., et al., SCC modification by use of amorphous nano-silica. Cement and Concrete Composites, 2014. **45**: p. 69-81.

19. Lin, D., et al., Improvements of nano-SiO 2 on sludge/fly ash mortar. Waste management, 2008. **28**(6): p. 1081-1087.

20. Qing, Y., et al., Influence of nano-SiO 2 addition on properties of hardened cement paste as compared with silica fume. Construction and building materials, 2007. **21**(3): p. 539-545.

21. El-Baky, S.A., S. Yehia, and I.S. Khalil, Influence of nano-silica addition on properties of fresh and hardened cement mortar. NANOCON Brno, Czech Republic, EU, 2013. **10**: p. 16-18.

22. Veerendrakumar, C., M. Nuruddin, and B. Mohammad, Effects of Nano-silica modified self-compacted, high volume fly ash mortar on slump flow and compressive strength. Madridge J Nano Tec. Sci, 2016. **1**(3): p. 7-10.

23. Najigivi, A., A. Khaloo, and S.A. Rashid, Investigating the effects of using different types of SiO 2 nanoparticles on the mechanical properties of binary blended concrete. Composites Part B: Engineering, 2013. **54**: p. 52-58.

24. Fernández, J.M., et al., Influence of nanosilica and a polycarboxylate ether superplasticizer on the performance of lime mortars. Cement and concrete research, 2013. **43**: p. 12-24.

25. Morsy, M., S. Alsayed, and M. Aqel, Hybrid effect of carbon nanotube and nano-clay on physico-mechanical properties of cement mortar. Construction and Building Materials, 2011. **25**(1): p. 145-149.

26. Mohamed, A.M., Influence of nano materials on flexural behavior and compressive strength of concrete. HBRC Journal, 2016. **12**(2): p. 212-225.

27. Patel, K., The use of nanoclay as a constructional material. Int. J. Eng. Res. Appl.(IJERA), 2012. **2**(4): p. 1382-1386.

28. Oltulu, M. and R. Şahin, Effect of nano-SiO 2, nano-Al 2 O 3 and nano-Fe 2 O 3 powders on compressive strengths and capillary water absorption of cement mortar containing fly ash: a comparative study. Energy and Buildings, 2013. **58**: p. 292-301.

29. Salemi, N., K. Behfarnia, and S. Zaree, Effect of nanoparticles on frost durability of concrete. Asian Journal of Civil Engineering (BHRC), 2014. **15**(1): p. 411-420.

30. Nazari, A. and S. Riahi, Al 2 O 3 nanoparticles in concrete and different curing media. Energy and Buildings, 2011. **43**(6): p. 1480-1488.

31. Mahawish, A., et al., Effect of Adding Silicon Carbide and Titanium Carbide Nanoparticles on the Performance of the Cement Pastes. J Civil Environ Eng, 2017. **7**(277): p. 2.

32. Cao, B., et al., Cementitious Materials Modified with Hematite Nanoparticles for Enhanced Cement Hydration and Uranium Immobilization. Environmental Science: Nano, 2017.

33. Pathak, A. and A. Tiwari, Effect of Zinc Oxide Nanoparticle on Compressive Strength and Durability of Concrete. International Journal for Research in Applied Science & Engineering Technology (IJRASET), 2017. **5**(VIII).

34. Hosseini, P., A. Booshehrian, and S. Farshchi, Influence of nano-SiO2 addition on microstructure and mechanical properties of cement mortars for ferrocement. Transportation Research Record: Journal of the Transportation Research Board, 2010(2141): p. 15-20.

35. Jo, B.-W., et al., Characteristics of cement mortar with nano-SiO 2 particles. Construction and building materials, 2007. **21**(6): p. 1351-1355.

36. Saloma, A.N., I. Imran, and M. Abdullah, Experimental investigation on nanomaterial concrete. International Journal of Civil and Environmental Engineering, 2013. **13**(3).

37. Ozyildirim, C. and C. Zegetosky, Exploratory investigation of nanomaterials to improve strength and permeability of concrete. Transportation Research Record: Journal of the Transportation Research Board, 2010(2142): p. 1-8.

38. Nasution, A., I. Imran, and M. Abdullah, Improvement of Concrete Durability by Nanomaterials. Procedia Engineering, 2015. **125**: p. 608-612.

39. Nazari, A. and S. Riahi, The effects of SiO 2 nanoparticles on physical and mechanical properties of high strength compacting concrete. Composites Part B: Engineering, 2011. **42**(3): p. 570-578.

40. Sobolev, K., et al., Nanomaterials and nanotechnology for high-performance cement composites. Proceedings of ACI Sessions on Nanotechnology of Concrete: Recent Developments and Future Perspectives, 2006: p. 91-118.

41. Du, H., S. Du, and X. Liu, Durability performances of concrete with nano-silica. Construction and Building Materials, 2014. **73**: p. 705-712.

42. Zahedi, M., A.A. Ramezanianpour, and A.M. Ramezanianpour, Evaluation of the mechanical properties and durability of cement mortars containing nanosilica and rice husk ash under chloride ion penetration. Construction and Building Materials, 2015. **78**: p. 354-361.

43. Beigi, M.H., et al., An experimental survey on combined effects of fibers and nanosilica on the mechanical, rheological, and durability properties of self-compacting concrete. Materials & Design, 2013. **50**: p. 1019-1029.

44. Tobon, J.I., J. Payá, and O.J. Restrepo, Study of durability of Portland cement mortars blended with silica nanoparticles. Construction and Building Materials, 2015. **80**: p. 92-97.

45. Ibrahim, R.K., R. Hamid, and M.R. Taha, Fire resistance of high-volume fly ash mortars with nanosilica addition. Construction and Building Materials, 2012. **36**: p. 779-786.

46. Elboghdadi, A.S., et al., Coupled Effect of Nano Silica and Steel Fiber on Fresh and Hardened Concrete Properties.

47. Abreu, G.B.d., et al., Mechanical properties and microstructure of high performance concrete containing stabilized nano-silica. Matéria (Rio de Janeiro), 2017. **22**(2).

48. He, X. and X. Shi, Chloride permeability and microstructure of Portland cement mortars incorporating nanomaterials. Transportation Research Record: Journal of the Transportation Research Board, 2008(2070): p. 13-21.

49. Zhang, M.-h. and H. Li, Pore structure and chloride permeability of concrete containing nano-particles for pavement. Construction and Building Materials, 2011. **25**(2): p. 608-616.

50. Gaitero, J.J., I. Campillo, and A. Guerrero, Reduction of the calcium leaching rate of cement paste by addition of silica nanoparticles. Cement and Concrete Research, 2008. **38**(8): p. 1112-1118.

51. Sun, J., et al., Effect of Nano-SiO2 on the Early Hydration of Alite-Sulphoaluminate Cement. Nanomaterials, 2017. **7**(5): p. 102.

52. Niewiadomski, P., D. Stefaniuk, and J. Hoła, Microstructural Analysis of Self-compacting Concrete Modified with the Addition of Nanoparticles. Procedia Engineering, 2017. **172**: p. 776-783.

53. Zdeb, T., Ultra-high performance concrete - properties and technology. Bulletin of the Polish Academy of Sciences-Technical Sciences, 2013. **61**(1): p. 183-193.

54. Standard, A., ASTM C39 Standard Test Method for Compressive Strength of Cylindrical Concrete Specimens. ASTM International, 2015.

55. ASTM, C., Standard test method for flexural strength of concrete (using simple beam with third-point loading). Philadelphia, PA: American Society for Testing and Materials, 1999.

56. ASTM, C., 157,"Standard Test Method for Length Change of Hardened Hydraulic-Cement Mortar and Concrete," Annual Book of ASTM Standards, Vol. 4.02. 2005, American Society for Testing and Materials, West Conshohocken.

57. Astm, C., 1202-97. Standard test method for electrical indication of concrete's ability to resist chloride ion penetration. Annual book of ASTM standards, 1997. **4**(2): p. 639-644.

58. ASTM, C., 1556. Standard test method for determining the apparent chloride diffusion coefficient of cementitious mixtures by bulk diffusion. American Society for Testing and Materials, 2004.

59. Khan, M.U., Experimental investigation and numerical modeling of two-dimensional chloride diffusion in concrete. 2013, King Fahd University of Petroleum and Minerals (Saudi Arabia).

60. El-Mohsen, M.A., A.M. Anwar, and I.A. Adam, Mechanical properties of Self-Consolidating Concrete incorporating Cement Kiln Dust. HBRC Journal, 2015. **11**(1): p. 1-6.

61. El-Aleem, S.A., et al., Effect of cement kiln dust substitution on chemical and physical properties and compressive strength of Portland and slag cements. The Arabian Journal for Science and Engineering, 2005. **30**(2 B).

62. Kohlhaas, B., other authors, Cement Engineers' Handbook. Fourth English edition Bauverlag, 1983.

63. Bensted, J., Hydration of Portland cement, in Advances in cement technology. 1983, Elsevier. p. 307-347.

64. Neville, A.M., Properties of concrete. Vol. 4. 1995: Longman London.

65. Shoaib, M., M. Balaha, and A. Abdel-Rahman, Influence of cement kiln dust substitution on the mechanical properties of concrete. Cement and concrete research, 2000. **30**(3): p. 371-377.

66. Kacha, S.A.P.S., Effects of Cement Kiln Dust on the Properties of Pervious Concrete.

67. Castellote, M., et al., Radioactively contaminated electric arc furnace dust as an addition to the immobilization mortar in low-and medium-activity repositories. Environmental science & technology, 2004. **38**(10): p. 2946-2952.

68. Fares, G., et al., Performance of optimized electric arc furnace dust-based cementitious matrix compared to conventional supplementary cementitious materials. Construction and Building Materials, 2016. **112**: p. 210-221.

69. Yousuf, M., et al., The interfacial chemistry of solidification/stabilization of metals in cement and pozzolanic material systems. Waste management, 1995. **15**(2): p. 137-148.

70. Arliguie, G. and J. Grandet, Influence de la composition d'un ciment portland sur son hydration en presence de zinc. Cement and Concrete Research, 1990. **20**(4): p. 517-524.

71. Hamilton, I.W. and N.M. Sammes, Encapsulation of steel foundry bag house dusts in cement mortar. Cement and concrete research, 1999. **29**(1): p. 55-61.

72. Brehm, F.A., Adição de óxido de zinco (ZnO) em pastas de cimento visando viabilizar a reciclagem de pós de aciaria elétrica (PAE) na construção civil. 2004.

73. Yousuf, M., et al., An FTIR and XPS investigations of the effects of carbonation on the solidification/stabilization of cement based systems-Portland type V with zinc. Cement and Concrete Research, 1993. **23**(4): p. 773-784.

74. Erdoğ du, K., Hydration and properties of limestone incorporated cementitious systems. 2002, Middle East Technical University. Department of Civil Engineering.

75. Felekoğlu, B., et al., The effect of fly ash and limestone fillers on the viscosity and compressive strength of self-compacting repair mortars. Cement and concrete research, 2006. **36**(9): p. 1719-1726.

76. Rahhal, V. and R. Talero, Early hydration of Portland cement with crystalline mineral additions. Cement and Concrete Research, 2005. **35**(7): p. 1285-1291.

77. Paya, J., et al., Properties of Portland cement mortars incorporating high amounts of oil-fuel ashes. Waste Management, 1999. **19**(1): p. 1-7.

78. Camilleri, J., M. Anastasi, and A. Torpiano, The microstructure and physical properties of heavy oil fuel ash replaced Portland cement for use in flowable fill concrete and the production of concrete masonry units. Construction and Building Materials, 2013. **38**: p. 970-979.

79. Mahasenan, N., et al. The cement industry and global climate change: current and potential future cement industry CO2 emissions. in Greenhouse Gas Control Technologies-6th International Conference. 2003. Elsevier.

80. Bazant, Z.P., Physical model for steel corrosion in concrete sea structures-theory. ASCE J Struct Div, 1979. **105**(6): p. 1137-1153.

81. Morinaga, S., Prediction of service lives of reinforced concrete buildings based on rate of corrosion of reinforcing steel. Special report of Institute of Technology, Shimizu Corporation, 1988. **23**.

VITAE

Name	:	Anas Mohammad Ibrahim Alkhatib
Nationality	:	Palestinian
Date of Birth	:	20/Oct/1987
Email	:	anasalkhatib98@gmail.com
Address	:	KFUPM, Dhahran, Saudi Arabia, T.L:+966 590190540
Academic Background	:	Civil Engineering

- B.Sc. Degree from the Civil Engineering Department, College of Engineering, An-Najah National University"- Nablus, Palestine, August 2009.
- M.Sc. degree in Civil Engineering from the Civil Engineering Department, College of Engineering, King Fahd University of Petroleum and Minerals, Dhahran, Saudi Arabia, May 2015.
- PhD (Civil Engineering - Structure) from King Fahd University for Petroleum and Minerals (KFUPM), Dec 2018.